OPTOELECTRICAL STUDY OF NEURONAL CALCIUM NANODOMAINS

PhD thesis

Alberto Jesús González Hernández

October 2021

MOLCAN nanopdics

Universidad de La Laguna

Escuela de Doctorado y Estudios de Posgrado
Universidad de La Laguna

OPTOELECTRICAL STUDY OF NEURONAL CALCUM NANODOMAINS

Alberto Jesús González Hernández

Tesis doctoral presentada para aspirar al grado de Doctor con Mención Internacional por la Universidad de La Laguna

Programa de Doctorado en Ciencias de La Salud por la Universidad de La Laguna

Dirigida por:
Teresa Giráldez
Profesora titular de Fisiología
de la Universidad de La Laguna

Codirigida por:
Diego Álvarez de la Rosa
Catedrático de Fisiología
de la Universidad de La Laguna

Doctorado en Ciencias de la Salud
Universidad de La Laguna

This thesis has been funded by:

Research grants to Teresa Giraldez:

- *European Research Council, under Horizon 2020 Research and Innovation Programme Grant (ERC-CoG-2014 648936).*

PhD grants to Alberto J. Gonzalez-Hernandez:

- *Ministerio de Educación y Formación Profesional (MEFP). Professor training grant (FPU). (FPU15/02528).*
- *Research stay in Dr. Holmgren's lab in the National Institute for Neurological Disorders and Stroke (NINDS-NIH) funded by Cabildo de Tenerife and the Fostering Grads Mentoring program of the University of La Laguna and ECUSA (Españoles Científicos en USA).*

Dra. Teresa Giráldez Fernández, profesora titular del Departamento de Ciencias Médicas Básicas (Área de Fisiología) de la Universidad de La Laguna y directora de la presente tesis doctoral, así como Diego Álvarez de la Rosa Rodríguez, catedrático del mismo departamento y co-director de la tesis

Certificamos que:

El Graduado en Biología D. Alberto Jesús González Hernández ha realizado bajo nuestra supervisión la tesis titulada: 'Optoelectrical study of neuronal calcium nanodomains', que presenta para optar al grado de Doctor con Mención Internacional por la Universidad de La Laguna.

Para que conste y surta los efectos oportunos, firmamos el presente certificado en San Cristóbal de La Laguna a 2 de agosto de 2021.

Prof. Teresa Giráldez Fernández
Profesora titular de Fisiología

Prof. Diego Álvarez de la Rosa Rodríguez
Catedrático de Fisiología

"Research in neurophysiology is much more like paddling a small canoe on a mountain river. The river which is fed by many distant springs carries you along all right though often in a peculiar direction. You have to paddle quite hard to keep afloat. And sooner or later some of your ideas are upset and are carried downstream like an upturned canoe".

Sir Alan Hodgkin

(Speech at the Nobel Banquet in Stockholm, December 10, 1963).

Acknowledgements

Foremost, I would like to thank my mentor and supervisor Teresa Giraldez for her invaluable advice in all the stages of my scientific life, professionally and personally. Thanks for giving me the opportunity to start in your lab since I was studying my bachelor and being a constant *driving force* inside and outside the lab. Your motivation and care have been crucial to my personal development.

I would also like to thank my cosupervisor Diego Álvarez de la Rosa for his constant support and his endless molecular biology knowledge. Your guidance during my first steps in the lab was crucial in shaping my autonomy and critical scientific thinking.

To the former and current members of the lab, for the shared moments with them, the precious scientific and non-scientific conversations and the enjoyable moments outside of the lab. Specially, I would like to thank Belinda Rivero and David Bartolomé, for their personal advice and professional help in the molecular biology, biochemistry and imaging experiments of this thesis. Our valuable scientific discussions and their constant eagerness to help me have been crucial to reach this point. I would also like to acknowledge Aravind Kshatri for counting on me to be involved in the functional validation of the BK channel full-length structure (my first publication) and for teaching me how to face up the daily problems of an electrophysiology rig.

To Andrew Plested, for the opportunity to visit his lab twice and for the experimental design and helpful critical revision of the photocrosslinking experiments of this thesis. Thanks also to Marcus Wietstruk, Valentina Ghisi, Anahita Poshtiban and Héctor Salazar for their help in these experiments.

To Miguel Holmgren for kindly receiving me in his lab to learn how to do patch-clamp fluorometry in oocytes. Thanks also to Pablo Miranda for the patience training me in this process. I would like to thank both as well for the valuable discussions of my results.

And finally, I would like to thank Joshua Levitz for the help and training in the single molecule experiments, and most importantly, for giving me the opportunity to join his lab and continue my scientific career.

Abstract

In neurons, coupling between calcium influx and membrane voltage in presynaptic terminal is essential for neurotransmitter release, hyperpolarization and repolarization and shaping of Ca^{2+} dendritic spikes. In the functional context, these processes are fine-tuned and controlled by complexes called "nanodomains", which are formed by the tight association between calcium permeable channels and large conductance voltage- and calcium-gated potassium channels (BK). The structural mechanisms involved in the Ca^{2+} dependent activation of BK channels and deducing how these Ca^{2+} signals are integrated and converted into an outflux of potassium ions are intriguing questions that have to be comprehensively studied.

During this PhD, we aimed to advance our knowledge about the precise function of BK channels within the nanodomains as well as its structural roles in forming the complexes with N-methyl-D-aspartate glutamate receptors (NMDARs). In order to fulfil our aims, we used a combination of the most recent techniques developed in the field, including unnatural amino acids, self-labelling enzymes, superresolution microscopy and single molecule pull-down. This allowed us to study the specific structural rearrangements involved in the activation of this channel by Ca^{2+}, as well as to develop tools to study the protein-protein interactions between BK channel and NMDARs.

We demonstrated the existence of an intrasubunit bridge between the Ca^{2+} binding sites of BK channel as well as the crucial role of the intersubunit interfaces in the activation of the channel by this divalent cation. We reconstituted BK channel-NMDARs complexes in heterologous systems and studied the influence of GluN2 NMDAR composition in BK channel activation. Additionally, we constructed functional fusion proteins between self-labelling enzymes and BK channel, or NMDARs, and validated them under different microscopy approaches.

Index

Results

Outlook

Introduction

Ion channels

Ion channels are membrane-spanning proteins that mediate multiple cellular processes by controlling the flow of ions into and out of the cell. They are key physiological players controlling, among others, neuronal excitability and firing, muscle contraction, heart rate, hormone secretion, vision and hearing or cell homeostasis. There is an enormous variety of these proteins which is reflected in the high number of genes codifying for them: 330 in the human genome (HGNC database; consulted 03/06/21). They are present in all cell types, varying their expression patterns and function across the cells, i.e.: the same ion channel in different tissues behaves differently according to the environment stimuli and expressed regulatory proteins. All of them share some basic features: an aqueous cavity which forms a hydrophilic pore, a gate that controls the ion flow, the high-rate permeation of ions (>10^6 ions per second; Hille, 1992) through a selectivity filter and the pass of the ions passively down their electrochemical gradient. Hodgkin and Huxley pioneer works in the squid giant axon, where they proposed the existence of a high selectivity for ion fluxes across the membrane caused by a protein entity (Hodgkin and Huxley, 1952abcd; Hodgkin et al., 1953), were the basis for the ion channel search and study. Afterwards, the cloning and sequencing of the first ion channel in 1984, the electric eel Na+ channel (Noda et al., 1984) as well as the first structural works during the 1990s (Doyle et al., 1998) were pivotal to this exponentially expanding field. Nowadays, the high technical development is helping in the discovery of some of the most intriguing aspects of these proteins, isolated or in their physiological scenario (e.g.: cryo-EM structures; molecular dynamics simulations; chemical and genetic modification, etc).

In a highly simplified vision, an ion channel alternates between two functional states: closed (non-conducting) and open (conducting) (Scheme I).

$$\text{Closed} \underset{\beta}{\overset{\alpha}{\rightleftharpoons}} \text{Open}$$

Scheme I

This process is viewed as an equilibrium between both states which can be affected by different stimuli including voltage, ligands, modulatory molecules, or me-

chanical strength. Consistently, ion channels have been classically classified according to their most common activating stimulus (e.g.: voltage-gated ion channels [VGIC], ligand-gated ion channels [LGIC], mechanical-gated ion channels [MGIC]) together with the most permeable ions to their pores (e.g.: sodium channels, potassium channels, chloride channels, cationic channels) (IUPHAR; Catterall and Gutmann, 2005; Collingridge et al., 2009). Overall, ion channels should be considered as a continuum of many forms of activation and regulation, which intricately and excitingly interact to regulate the physiology of the cells.

The potassium channels superfamily

K^+ ions play crucial roles in cells, among others: setting the membrane potential, membrane repolarization and negative cell membrane potential maintenance in nonexcitable-cells (Giebisch 2001). Thus, channels permeating these ions represent a crucial superfamily. 90 genes in humans codify for potassium channel pore-forming (α) subunits (Tian et al., 2014). Channels belonging to this family show unique structures and gating mechanisms to exquisitely control potassium homeostasis.

A common feature of K^+ channels is their tetrameric association of an α subunit to form a functional channel. A large body of structure-function studies, together with the elucidation of the structure of the *Streptomyces lividans* potassium channel, KcsA, unveiled the basic features of permeation and pore cavity of K^+ channels (Doyle et al., 1998). This homotetrameric channel has two transmembrane domains per subunit and shares the signature sequence of the K^+ channel's selectivity filter (SF): TVGYG. Because of its simplicity, KcsA could represent the canonical *constriction block* for the pore of all K^+ channels. Two key findings from the structure were the dehydration of the K^+ ions to permeate through the selectivity filter and the specific binding-sites of K^+ ions inside the SF. This was relevant to explain the differential permeability between K^+ and Na+ channels.

The potassium channel superfamily includes three different classes according to their transmembrane topology of their pore-forming subunits: two transmembrane domains, also known as *inward rectifiers* or Kir; four transmembrane domains, referred as two-pore (K2P) channels; and six transmembrane domains, with a higher diversity in structures and gating mechanisms (Wei et al., 1996) (figure 1.1). Inside this last subgroup, we can distinguish among voltage regulated channels (voltage-gated

potassium channels, Kv channels; ether-a-go-go related gene, EAQ channels; and KvLQT channels) (Wei et al., 1996), cyclic-nucleotide regulated channels (cyclic nucleotide-gated channels, or CNG; and hyperpolarization-activated cyclic nucleotide modulated channels, or HCN) (Craver and Zagotta, 2006), Ca^{2+}-gated channels (small conductance calcium-gated potassium channels, or SK; intermediate conductance calcium-gated potassium channel, or IK; high conductance voltage and calcium-gated potassium channel, or BK), Na^+-gated channels (Slick and Slack channels) (Yuan et al., 2003) and pH regulated channels (Slo3) (Schreiber et al., 1998) .

Figure 1.1. Potassium superfamily classification

BK channel: the large conductance Ca^{2+} and voltage activated K^+ channel

Large conductance voltage- and Ca^{2+}-activated K^+ channels (BK, MaxiK channels, Slo1 or KCa1.1 channels) were first described in the early 1980s as calcium and voltage-activated potassium currents (Marty, 1981; Pallotta et al., 1981). A distinctive feature was their sensitivity to the scorpion toxins charybdotoxin (Miller et al., 1985) and iberiotoxin (Galvez et al., 1990). In comparison to other K^+ channels, BK channels exhibit an unusually large conductance ranging between 100 pS - 300 pS (Latorre et al., 2017). The BKα subunit is encoded by the gene KCNMA1 (also known as *Slowpoke*), which was cloned from *Drosophila* (Adelman et al., 1992; Atkinson et al., 1991), mice (Butler et al., 1993) and human (Dworetzky et al., 1994; McCobb et al., 1995). BK channels are synergistically activated by intracellular Ca^{2+} and membrane

depolarization. The channel's conductance (G) increases with voltage, analogously to other voltage-gated potassium channels; in addition, this G-V relationship is shifted towards negative voltages as Ca^{2+} concentration increases (figure 1.2). This complex kinetic behavior was elegantly described by the work of the Magleby (Magleby, 2003; McManus and Magleby, 1988; Rothberg and Magleby, 1999) and Aldrich (Cox et al., 1997; Horrigan and Aldrich, 1999; Horrigan et al., 1999) laboratories, leading to the widely accepted allosteric model of Horrigan and Aldrich (Horrigan and Aldrich, 2002). The physiological relevance of this activation mechanism is significant because of its wide dynamic range, covering voltage values from -200 mV to +300 mV and Ca^{2+} concentrations up to 10 mM (Magleby, 2003). Not surprisingly, BK channels constitute an essential link between membrane excitability and intracellular $[Ca^{2+}]$ signalling (Rothberg, 2012).

Figure 1.2. Macroscopic currents of BK channels. (A) Macroscopic currents of BK channels in response to a family of voltage pulses (schematized below the current traces) in the absence of Ca^{2+}. (B) Macroscopic currents of BK channels in response to increasing Ca^{2+} concentrations (color coded in the legend). (C) Increasing intracellular Ca^{2+} concentrations shift the voltage-dependent activation curves (G–V relations) towards more negative voltages. Ca^{2+} concentrations are color-coded as in B.

BK channel in neurons: location, functions, and interaction with other proteins

BK channels are localized throughout the dendrites, axon, soma and synaptic terminals of neurons in different brain regions, including cortex and hippocampus (Knaus et al., 1996;Grunnet and Kaufmann, 2004;Wang et al., 2014), where they play key roles in action potential duration, firing frequency and neurotransmitter release (for a recent review, see (Contet et al., 2016)). It should be noted that depending on the subcellular location where they are expressed, BK channel isoforms may exhibit different biophysical and trafficking properties, determined by the subunit composition (assembly with auxiliary subunits) and alternative splicing (Contet et al., 2016). At the synaptic terminals, it has been proposed that tight spatial coupling between BK channels and voltage-gated calcium channels (VGCCs) (Marrion and Tavalin, 1998) constitutes a molecular brake for neurotransmitter release, by the BK-mediated termination of action potentials (Bielefeldt and Jackson, 1993; Hu et al., 2001; Muller et al., 2007; Contet et al., 2016). In dendrites, this association is also relevant, contributing to regulation of the magnitude and duration of dendritic Ca^{2+} spikes to influence action potential output (Engbers et al., 2013; Indriati et al., 2013). BK channels have the ability to shape action potential waveforms and influence the frequency of firing in different ways. Pharmacological or genetic deletion of BK channels can increase or decrease the evoked or spontaneous firing frequency (Bielefeldt and Jackson, 1993; Nelson et al., 2003; Gu et al., 2007). Many studies have shown that blockade of BK channels using TEA, charybdotoxin or paxilline slows action potential repolarization and reduces the magnitude of the fast-duration after hyper polarization (fAHP) (Adams et al., 1982; Storm, 1987; Sah and McLachlan, 1992; Zhang and McBain, 1995; Faber and Sah, 2002). In the suprachiasmatic nucleus, BK channels contribute to spontaneous firing rate related to normal circadian behavioral rhythm (Meredith et al., 2006; Whitt et al., 2016; Whitt et al., 2018). Genetic ablation of the BKβ_4 subunit in neurons from the dentate gyrus (DG) augmented the fAHP amplitude, sharpened the action potential and increased spike frequency (Brenner et al., 2005). These findings support the idea that BK channels are not strictly excitatory or inhibitory but can be dynamically regulated to control neuronal excitability (Contet et al., 2016). Regulatory mechanisms include coupling to accessory subunits (Brenner et al., 2005;Whitt et al., 2016) and different sources of intracellular Ca^{2+} , as detailed below (Wang et al., 2016a;Whitt et al., 2018) (Gonzalez-Hernandez et al., 2021).

BK channels in pathophysiology

Even though this topic is outside the scope of my thesis, I would like to highlight the effect of deficient BK channels in different pathologies and symptoms, specially because the knowledge extracted from these mutations is key to understanding the functioning of the channel. A list of mutations encoding BK genes (α and β subunits) is presented in Table 1.1.

Human BK channel channelopathies are primarily associated with neurological conditions such as seizures, movement disorders, developmental delay, and intellectual disability (reviewed in Bailey et al., 2019). Gain-of-function (GOF) mutations in BK channels have been implicated in the development of neuronal excitability disorders. A single GOF mutation -D434G- increases the Ca^{2+} sensitivity of BK channels and causes autosomal dominant epilepsy with paroxysmal dyskinesias (Du et al., 2005). Similarly, another GOF mutation -N995S- was found to enhance the voltage dependence of BK channel activation and cause epilepsy (Li et al., 2018). Both of these mutations would enhance neuronal BK channel activity and therefore increase the fAHP of the action potential, ultimately leading to increased neuronal excitability. In addition to the BKα subunits, mutations in its accessory subunits have also been reported to cause idiopathic generalized epilepsy (IGE) (Lorenz et al., 2007). For instance, a deletion of base A450 in exon 4 of the β3 gene, results in a frame shift that alters three amino acids and truncates the protein by 18 amino acids (Hu et al., 2003). Functionally, this alteration causes a rapid inactivation of BK channels and also shifts the activation curve rightwards, which has been associated with reduced synaptic inhibition, and therefore increased neuronal excitability and seizure susceptibility (Hu et al., 2003). A recent study by (Du et al., 2020) identified a loss-of-function mutation in the selectivity filter of the BK channels (G354S) associated with progressive cerebellar degeneration, ataxia, and cognitive impairment. This mutation dramatically reduced BK single channel conductance and ion selectivity, leading to depolarization and mitochondrial dysfunction. Subsequently, this was associated with a reduction in cellular viability and cerebellar ataxia (Du et al., 2020).

The possible clinical treatments for these diseases are still poorly explored, nevertheless some BK channel modulators have been tested as plausible therapeutic approaches for certain diseases. For a recent review and discussion of therapeutic approaches on BK channels, see Kshatri et al., 2018 (*Annex III*).

TABLE 1.1 BK channelopathies, mutations and protein location, functional effects and reference (modified and updated from Gonzalez-Hernandez et al., 2021).

Gene/protein	Disease Phenotype	Mutation/ location in the protein	Functional effects	Reference
KCNMA1 / BKα	A, CI, tremor and hypertelorism	S351T/Pore	No current	(Liang et al., 2019)
KCNMA1 / BKα	A, CA, CI, E + PD, ID	G354S/Pore	Reduced current and slower activation kinetics	(Du et al., 2020)
KCNMA1 / BKα	A, CA, DD, H	G356R/Pore	No current	(Liang et al., 2019)
KCNMA1 / BKα	CA, CM, DD, E, ID, H,	G375R/S6	No current	(Liang et al., 2019)
KCNMA1 / BKα	A, CA, CM, DD, ID, H and strabismus	C413Y+N449fs/S6-RCK1 linker	Reduced current (G-V shift to depolarized potentials) (C413Y) + No current (N449fs)	(Liang et al., 2019)
KCNMA1 / BKα	E + PD	D434G/RCK1 domain	Gain-of-function mutation leading to enhanced Ca^{2+} sensitivity	(Du et al., 2005; Yang et al., 2010)
KCNMA1 / BKα	Non-described	H444Q/RCK1	Loss-of-function mutation (G-V shift to depolarized potentials, slower activation and faster deactivation).	(Moldenhauer et al., 2020)
KCNMA1 / BKα	A, CA, E + PD, DD, ID	R458Ter/S6-RCK1 linker	Truncation	(Yesil et al., 2018)
KCNMA1 / BKα	E (not directly linked to this mutation)	K518N/RCK1	No difference	(Li et al., 2018)
KCNMA1 / BKα	E (not directly linked to this mutation)	E656A/RCK1-RCK2 linker	No difference	(Li et al., 2018)
KCNMA1 / BKα	A, DD, ID, H and strabismus	I663V/RCK1-RCK2 linker	No current	(Liang et al., 2019)
KCNMA1 / BKα	E, DD, ID	Y676Lfs*7/RCK1-RCK2 linker	Truncation	(Tabarki et al., 2016)
KCNMA1 / BKα	CA, CI, DD, ID,	P805L/RCK2	Reduced current (G-V shift to depolarized potentials) and reduced expression	(Liang et al., 2019)
KCNMA1 / BKα	DD, ID, PD	E884K/RCK2	Not available	(Zhang et al., 2015b)
KCNMA1 / BKα	Non-described	D965V/RCK2	Loss-of-function mutation (G-V shift to depolarized potentials, slower activation).	(Moldenhauer et al., 2020)
KCNMA1 / BKα	CI, E, ID	D984N/RCK2	Not available	(Liang et al., 2019)
KCNMA1 / BKα	E	N995S or N999S or N1053S/RCK2 domain	De novo mutation Shifts the voltage dependence to more negative potentials without altering Ca^{2+} sensitivity	(Li et al., 2018; Plante et al., 2019)
KCNMA1 / BKα	Non-described	R1097H/RCK2 domain	Loss-of-function mutation (G-V shift to depolarized potential only at low $[Ca^{2+}]i$)	(Moldenhauer et al., 2020)
KCNMA1 / BKα	E (not directly linked to this mutation)	N1159S/C-terminal	No difference	(Li et al., 2018)
KCNMB1/ BKβ1	Diastolic hypertension	E65K/Extracellular loop connecting β1 two transmembrane segments.	Gain-of-function mutation rendering enhanced Ca^{2+} sensitivity	(Fernandez-Fernandez et al., 2004)
KCNMB3/ BKβ3	Idiopathic generalized epilepsy	Del A750/C-terminal region (truncation of 21 amino acids)	BK inactivation	(Hu et al., 2003; Lorenz et al., 2007)

A: ataxia; CA: cerebral/cerebellar atrophy; CI: cognitive impairment; CM: congenital malformations; DD: developmental delay; E: epilepsy; H: hypotonia; ID: intelectual disability; PD: paroxysmal dyskinesia.

Calcium nanodomains: BK channel Ca^{2+} sources

Unlike other members of the K_{Ca} family, BK channels are widely expressed in a variety of excitable and non-excitable cells (Latorre et al., 2017). In many cell types, BK activation relies on the local influx of Ca^{2+} to achieve micromolar levels (Fakler and Adelman, 2008) (figure 1.3). In neurons and smooth muscle cells, membrane depolarization provided by an action potential triggers Ca^{2+} influx through voltage-dependent Ca^{2+} channels (VGCCs) (Griguoli et al., 2016), coincidentally activating neighboring BK channels to repolarize the membrane and eventually closing VGCCs, terminating the Ca^{2+}signal (Marrion and Tavalin, 1998). This negative feedback mechanism enables BK channels as important regulators of many physiological processes including smooth muscle contraction (Meredith et al., 2004; Nelson et al., 1995; Semenov et al., 2011), insulin secretion (Houamed et al., 2010), neurotransmitter release (Lingle et al., 1996; Raffaelli et al., 2004; Robitaille et al., 1993), circadian rhythm (Meredith et al., 2006; Whitt et al., 2016), action potential termination (Montgomery and Meredith, 2012; Muller et al., 2007; Storm, 1987) and heart firing and pace (Lai et al., 2014).

Figure 1.3. Concepts of nanodomain and microdomain. The association between Ca2+ sources and their effectors is highly regulated and spatially restricted. According to the distances between these two proteins we can differentiate between microdomain (when effectors are between 50-200 nm) and nanodomain (when effectors are below 50 nm). BK channels have been usually found forming nanodomains with Ca2+ sources (e.g., VGCC).

Numerous studies have identified the VGCC subtypes mediating this coupling mechanism (Fakler and Adelman, 2008). These include Cav2.1 (Berkefeld and Fakler, 2008; Berkefeld et al., 2006; Edgerton and Reinhart, 2003; Womack et al., 2004), Cav2.2 (Berkefeld et al., 2006; Loane et al., 2007; Prakriya and Lingle, 1999), Cav1.2 (Berkefeld and Fakler, 2008; Berkefeld et al., 2006; Grunnet and Kaufmann, 2004; Prakriya and Lingle, 1999), Cav1.3 (Prakriya and Lingle, 1999; Vivas et al., 2017) and Cav3.2 (Gackiere et al., 2013; Rehak et al., 2013). Interestingly, although it was originally suggested that BK channels do not interact with Cav2.3 (Berkefeld et al., 2006; Cerrada et al., 2018), recent evidence suggests that functional association with these channels may occur in CA1 pyramidal neurons (Gutzmann et al., 2019). Additionally, accessory subunits of Cav channels have been proposed to interact independently with BK channels. Zou et al. (2008) demonstrated that interaction with Cavβ1 reduces Ca^{2+} sensitivity and slows down gating of the BK channel without affecting its relative membrane expression, although this finding remains to be shown in native tissues (Zou et al., 2008). Another recent finding suggests that high affinity interactions of the Cavα2δ1 subunit with the BK channel N-terminus result in reduced membrane expression of Cav2 channels. This mechanism has been proposed to be of physiological relevance, since the administration of a BK N-terminus peptide leads to decreased inflammatory and neuropathic pain in mice (Zhang et al., 2018a).

The functional association of BK to Ca^{2+} sources is quite versatile, not restricted to VGCC but including other Ca^{2+} sources, such as ryanodine (RyR) (Chavis et al., 1998; Irie and Trussell, 2017; Wang et al., 2016; Whitt et al., 2018; Yamamura et al., 2012) and inositol 1,4,5-triphosphate (InsP3R) receptors (Zhao et al., 2010 (Zhao et al., 2010). As mentioned above, Ca^{2+} influx through other non-selective cation-permeable channels, such as NMDAR or transient receptor potential (TRP) channels have been shown to activate BK channels. NMDARs associate with BK channels in the neuronal postsynaptic membrane where they modulate excitability (Isaacson and Murphy, 2001; Zhang et al., 2018b) and synaptic plasticity (Gómez et al., 2021, PNAS in press; *see below*). In the case of TRP channels, multiple subtypes of this large family of ion channels have been shown to form tight complexes with BK channels in a wide range of tissues. TRPV1 interacts with BK in dorsal root ganglion cells, where BK-mediated negative feedback has been proposed to modulate pain perception (Wu et al., 2013). In cerebral artery smooth muscle cells, TRPV4 has been proposed to activate BK channels via RyR-mediated Ca^{2+} release to induce artery relaxation (Earley et al., 2005; Liu et al., 2020; Szarka et al., 2018). In kidney podocytes, TRPC3 and TRPC6 physically interact with BK channels. These complexes have been proposed to be mechanically activated by glomeruli swelling, regulating glomerular filtration (Kim et al., 2009). Lastly, Ca^{2+} influx through menthol activated TRPM8 channels has been also shown to activate BK channel currents in glioblastoma cells, linking these Ca^{2+} signaling complexes to tumor invasion (Wondergem and Bartley, 2009). A summary of proteins proposed to interact with BK is shown in table 1.2.

The full functional picture of BK and its association to different calcium sources must take into account the regulation by auxiliary subunits and the characteristics of specific BK splice variants. Although the dynamics of these complexes has not been fully explored in all physiological settings, it is tempting to hypothesize that the fine-tuning of this combinatorial complexity constitutes the basis for a large diversity of physiological outputs. An example of such complexity has been shown in the brain suprachiasmatic nucleus (SCN), where BK coupling to different calcium sources and auxiliary subunits during day and night leads to distinct excitability patterns (Whitt et al., 2018).

In this thesis, I have focused on the study of NMDAR-BK channel interaction from the biophysical point of view, analyzing their crosstalk and developing tools for single molecule and super resolution microscopy.

TABLE 1.2. BK channel interacting proteins. *All the studies where reliable techniques for coassembly have been used were considered. In the case of GPCRs, most of the studies are functional through signalling pathways. However, the binding of $G_{\beta\gamma}$ and the coassembly with β2-AR opens the possibility of clustering with other receptors.*

Protein	Interaction part	Method	Reference(s)
Ion channels			
Cav1.2		Co-IP, F, MS	Berkefeld et al., 2006; Berkefeld and Fakler, 2008; Grunnet and Kaufmann, 2004.
Cav1.3		Co-IP, F, SRM	Grunnet and Kaufmann, 2004; Marcantoni et al., 2010; Vivas et al., 2017.
Cav2.1		Co-IP, F, MS	Berkefeld et al., 2006; Berkefeld and Fakler, 2008.
Cav2.2		Co-IP, F, MS	Berkefeld et al., 2006; Berkefeld and Fakler, 2008.
Cav.2.3		Co-IP, F	Gutzmann et al., 2019.
Cav3.2	N-terminal transmembrane region (S0)	Co-IP, F	Rehak et al., 2013.
Cavβ1	Calcium-bowl (884-936)	Co-IP, F	Zou et al., 2008.
Cavα2δ1	N-terminus (complete, aa's 1-86)	Co-IP, F	Zhang et al., 2018a.
NMDAR1	S0-S1 linker	Co-IP, F, PLA	Zhang et al., 2018b, Gomez et al., 2021.
TRPV1		Co-IP, F	Wu et al., 2013.
TRPV4		F	Feetham et al., 2015.
SOC	RCK1 (350-371) and RCK2 (720-814)	Co-IP, F	Wu et al., 2020.
RyR		F	Irie and Trussell, 2017.
Transporters			
GAT3		MS	Singh et al., 2016.
GPCR			
β2-adrenergic receptor	Third intracellular loop of β2-AR	Co-IP, F	Liu et al., 2004.
mGluR5		F (through signalling pathway)	Sala et al., 2005.
Melatonin		F (through $G_{\beta\gamma}$)	Niu et al., 2020.
Muscarinic 2		F	Guo et al., 2012.
MOR		F (through signalling pathway)	Baillie et al., 2015.
Scaffolding and synaptic vesicle proteins			
Dynamin-1		Co-IP	Gorini et al., 2010.
MAGI-1		Co-IP, F	Ridgway et al., 2010.
SNAP-25		Co-IP	Gorini et al., 2010.
VAMP-2		Co-IP	Gorini et al., 2010.
CSP-α	J-domain of CSP-α	Co-IP, F	Kyle et al., 2013; Ahrendt et al., 2014.
β-catenin	RCK2 (941-963)	Co-IP	Lesage et al., 2004; Bian et al., 2011.
AKAP79/150		Co-IP	Liu et al., 2004
RIM-BP	RBP2 FN3-domains and RCK1 or RCK2 domains (both)	Co-IP, F	Sclip et al., 2018.
Syntaxin 1A		Co-IP, F	Ling et al., 2003.
Adhesion molecules			
NCAM		Co-IP	Lee and Wu, 2010; Singh et al., 2016
LINGO1	LINGO1 tail (613-620)	Co-IP, F	Dudem et al., 2020.

Co-IP: Coimmunoprecipitation; F: functional (electrophysiology); PLA: proximity ligation assay; MS: Mass spectrometry; SRM: Superresolution microscopy.

N-methyl-D-aspartate receptors (NMDARs)

NMDA receptor: a key player in neuron physiology

Glutamate is the primary excitatory chemical transmitter in the mammalian central nervous system (CNS), where it is essential for neuronal viability, network function, and behavioural responses (Reiner & Levitz, 2018). Glutamate activates a variety of pre- and postsynaptic receptors, including ionotropic receptors (iGluRs) that form ligand-gated cation-permeable ion channels. The iGluR superfamily includes α-amino-3-hydroxy-5-methyl-4-isoxazolepropionic acid receptors (AMPARs), kainate receptors, and N-methyl-D-aspartate receptors (NMDARs), all of which form tetrameric assemblies that are expressed throughout the CNS (Traynelis et al., 2010).

NMDARs (figure 1.4) exhibit high sensitivity to glutamate (EC_{50} in the micromolar range) and voltage-dependent block by Mg^{2+} (Mayer et al., 1984; Nowak et al., 1984), slow gating kinetics (Lester et al., 1990), and high permeability to Ca^{2+} (MacDermott et al., 1986; Mayer and Westbrook, 1987) (for a review, see Paoletti et al., 2013). Together, these characteristics confer postsynaptic NMDARs with the ability to detect and decode coincidental activity of pre- and postsynaptic neurons: presynaptic glutamate release bringing about occupation of the agonist-binding site and AMPAR-driven postsynaptic depolarization removing voltage-dependent Mg^{2+} block. The coincidence of these two events leads to NMDAR activation and Ca^{2+} influx through the channel (Paoletti et al., 2013; Caporale and Dan, 2008), which initiates several forms of synaptic plasticity (Malenka and Nicoll, 1993; Markram et al., 1997).

NMDAR subunit composition tunes receptor function

General architecture of NMDARs is depicted in figure 1.4. Apart from the ligand's affinity, the different GluN composition of this receptor modulates the kinetics of activation and deactivation (Vicini et al., 1998; Paoletti et al., 2013). In the case of GluN1 subunit, its coding gene produces up to eight possible isoforms through alternative splicing. GluN1-a or GluN1-b are differentiated for the N-terminal exclusion or inclusion, respectively, of the exon 5, which affects dramatically the properties of the channel, including kinetics of deactivation or pharmacology (Rumbaugh et al., 2000; Paoletti et al., 2013). In addition, a or b GluN1s can be either 1, 2, 3 or 4, depending on the carboxy-terminal domain splicing, which largely mediates largely

the interaction with intracellular effectors as well as receptor trafficking (Horak and Wenthold, 2009; Vance et al., 2012).

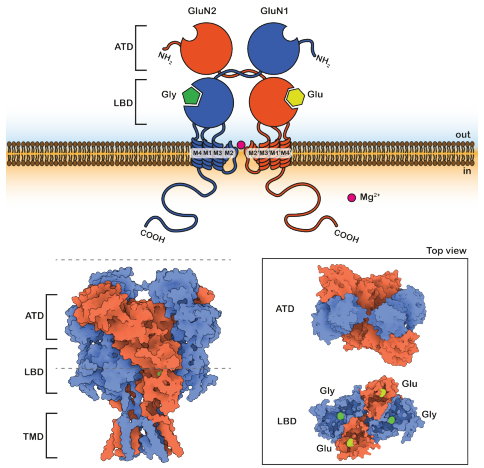

Figure 1.4. Architecture of NMDAR heterotetramers. Top Schematic diagram of NMDAR topology. Extracellular domain consists of two layers with four "clamshell" like subdomains each layer. Amino-terminal domains (ATD) possess multiple allosteric regulators binding sites different in 1 and 2 subunits. Just below, the ligand binding domains (LBD) bind glycine or glutamate and control the co-agonist activation of the channel just in presence of both ligands (Durham et al., 2020). These LBDs are constituted partly by the amino terminal sequence of the protein and M3-M4 linker of transmembrane domains. This extracellular domain is connected to the 4 α–helices (M1-M4) that constitute the transmembrane and pore domains. This basic body is highly conserved among all the subunits and has been thoroughly described by different groups (Paoletti et al., 2013). Bottom. Structure of a NMDAR formed by GluN1a and GluN2B with glycine and glutamate bound (PDB:4PE5). ATDs and LBDs top view depict the domain-swapped conformation and the multiple interaction surfaces at the two different levels. ATDs of both subunits interact with multiple allosteric modulators.

On the other side, GluN2 (A to D) and GluN3 (A or B) subunits are products of six different genes. GluN2A and GluN2B have a higher Ca^{2+} permeability than GluN2C and GluN2D and higher sensitivity to Mg^{2+} as well (Traynelis et al., 2010). Furthermore, they modify the unitary conductance, deactivation kinetics, open probability, and pharmacology (Paoletti et al., 2013). In this work we were focused in the GluN2A and GluN2B subunits because of their wide distribution throughout the

adult brain and specially in the hippocampus and cortex (Watanabe et al., 1992; Akazawa et al., 1994; Monyer et al., 1994; Paoletti et al., 2013). The abundance of GluN2A and GluN2B subunits in these regions points up their importance in key processes of the synaptic physiology and plasticity of the brain.

Ca^{2+} influx through non-selective cation-permeable channels, including NMDARs, has been shown to activate BK channels in granule cells from the olfactory bulb and dentate gyrus (Isaacson and Murphy, 2001; Zhang et al., 2018; Zorumski et al., 1989). In these neurons, Ca^{2+} entry through NMDARs opens BK channels in somatic and perisomatic regions, causing repolarization of the surrounding plasma membrane and subsequent closure of NMDARs. Because BK channel activation blunts NMDAR-mediated excitatory responses, it provides a negative feedback mechanism that modulates the excitability of these neurons (Isaacson and Murphy, 2001; Zhang et al., 2018). Thus, the same characteristics that make NMDARs key components in excitatory synaptic transmission and plasticity can paradoxically give rise to an inhibitory response when NMDARs are located in the proximity of BK channels. However, it is unclear whether functional NMDAR–BK coupling is relevant at dendrites and dendritic spines.

The barrel field area in the primary somatosensory cortex, also known as the barrel cortex (BC), processes information from peripheral sensory receptors for onward transmission to cortical and subcortical brain regions (Petersen, 2019; Erzurumlu and Gaspar, 2020). Sensory information is received in the barrel cortex from different nuclei of the thalamus. Among these nuclei, ventral posterior medial nucleus, ventrobasal nucleus, and posterior medial nucleus are known to directly innervate layer 5 pyramidal neurons (BC-L5PNs) (Agmon and Connors, 1992; Constantinople and Bruno, 2013; El-Boustani et al., 2020; Rodriguez-Moreno et al., 2020). In basal dendrites of BC-L5PN, coactivation of neighboring dendritic inputs can initiate NMDAR-mediated dendritically-restricted spikes characterized by large Ca^{2+} transients and long-lasting depolarizations (Schiller et al., 2000; Nevian et al., 2007; Polsky et al., 2009), providing the appropriate environment for BK activation.

To determine whether functional NMDAR–BK coupling plays a role in synaptic transmission, and potentially synaptic plasticity, as part of the work in this thesis we investigated the thalamocortical synapses at basal dendrites of BC-L5PNs. Work from the laboratory found that suppression of NMDAR activity by BK channels occurs in the basal dendrites of about 40% of BC-L5PNs, where NMDAR activation triggers strong negative feedback inhibition by delivering Ca^{2+} to nearby BK channels. This inhibition regulates the amplitude of postsynaptic responses and increases the threshold for induction of synaptic plasticity. Our findings thus unveil a calibration mechanism that can decode the amount and frequency of afferent synaptic inputs by selectively attenuating synaptic plasticity and providing input-specific synaptic diversity to a thalamocortical circuit (figure 1.5).

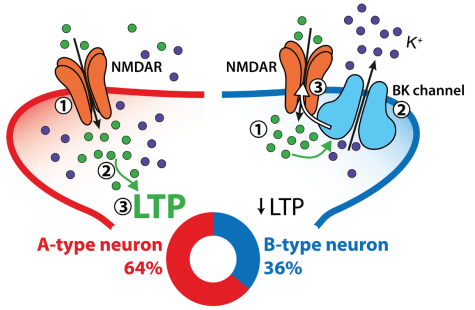

Figure 1.5. NMDAR–BK coupling controls dendrite-specific synaptic plasticity. Two populations of regular-spiking BC-L5PNs can be distinguished by the absence (A-type, left, red) or presence (B-type, right, blue) of NMDAR-BK functional association in basal dendrites. In B-type neurons (~36%), NMDAR–BK coupling provides a negative feedback mechanism whereby the entry of Ca^{2+} associated with NMDAR activation (1) opens neighbouring BK channels (2) that allow outward flow of K^+. The resultant membrane hyperpolarization (-Vm) reinstates voltage-dependent Mg^{2+} block of NMDARs (3), truncating Ca^{2+} entry and increasing the threshold for long-term synaptic plasticity (decreased LTP). We show that B-type BC-L5PNs exhibit a higher threshold for induction of t-LTP. On the other hand, A-type neurons (~64%) lacking the NMDAR–BK molecular break undergo long-term potentiation (3) associated with Ca^{2+} entry (2) via NMDARs (1). Our data reveal that A-type neurons reach saturation at a lower stimulation frequency than B-type, independent of the number of synaptic inputs.

BK channel structural and molecular determinants of voltage and Ca^{2+} sensing

BK channels have unique features that distinguish them from other members

of the calcium-gated and voltage-gated potassium channels families. BKα subunits show a modular structure (figure 1.6) consisting of a N-terminal domain embedded in the plasma membrane (TMD) and a large C-terminal cytosolic domain that encompasses about one-third of the channel protein (Yang and Cui, 2015). The TMD core is reminiscent of voltage-gated potassium channels, consisting of six transmembrane (TM) segments S1-S6 which include a conserved region (S1-S4) known as the voltage sensor domain (VSD), and a pore domain (PD) region formed by segments S5-S6, which constitutes the ion conducting pathway (figures 1.8 and 1.9). One striking feature of BK channels is their large conductance, which stands out within the potassium channels superfamily. Rather than differences in the sequence of the selectivity filter, which is highly conserved (Neyton and Miller, 1988), this characteristic is partly due to the presence of rings of negatively charged amino acids acting as an electrostatic bait to concentrate K^+ ions at the intracellular and extracellular cavities of the channel (Brelidze et al., 2003; Carvacho et al., 2008; Nimigean et al., 2003). Another relevant feature is the apparently large size of the inner cavity of around 8-10 Å, which results in inhibition by relatively large molecules (Tang et al., 2009; Wilkens and Aldrich, 2006) from the intracellular side (Li and Aldrich, 2004) and provides accessibility to MTS reagents (Zhou et al., 2011) (figure 1.9). In addition, BK has an extra TM segment S0, leading the NH_2 terminus of the protein to the extracellular side (figure 1.7). The function of this segment has been related to VSD function, as well as to interactions with the auxiliary subunits (Castillo et al., 2016; Koval et al., 2007; Wallner et al., 1996).

Full BK tetramers are embedded in the membrane with central PD regions forming a pore, surrounded by four VSDs and S0 segments at the periphery (figure 1.9). Similar to other members of the K_{Ca} family and bacterial Ca^{2+}-gated channels (MthK; Posson et al., 2013), it has been proposed that the gate of the BK channel that controls ion permeation is located near the selectivity filter and not at the cytosolic end of S6, although this issue remains controversial and is not fully answered by available structural data [for thorough analyses of this topic, see ((Latorre et al., 2017) and (Zhou et al., 2017)] (figure 1.9). Both movement of the VSD and Ca^{2+} binding to the C-terminal domain (see below) regulate the function of this gate.

Figure 1.6. BK channel topology and structure. BK channel presents a modular structure divided in a transmembrane domain, pore and gating domain and cytosolic domain (Human BK channel structure with Ca^{2+} and Mg^{2+} bound. PDB: 6V38).

Unlike other voltage-gated K^+ channels, the gating charges in BK's VSD are not confined to the S4 TM segment, but are distributed between the S2, S3 and S4 segments (Yang and Cui, 2015; figure 1.8). In fact, the voltage dependence of BK is relatively weak compared with Kv channels, (Horrigan and Aldrich, 1999; Rothberg and Magleby, 2000). It has been suggested that rather than undergoing a substantial movement of S4 as described in voltage-gated potassium channels, voltage-dependent gating in BK may involve small movements of S2, S3, and S4 (Ma et al., 2006; Pantazis et al., 2010). Additionally, interactions of the VSD with S0 (Koval et al., 2007) and the C-terminal domain (see below) modulate the unique VSD movements associated with channel activation (Ma et al., 2006; Pantazis et al., 2010). Unexpectedly, the cryo-EM structures of BK showed that, contrary to voltage-gated K^+ channels, the VSD is not domain-swapped, i.e. is located next to the PGD of the same subunit (Tao et al., 2017).

Figure 1.7. Transmembrane topology of S0 helix and S0-S1 linker. S0 helix makes the N-terminus of the protein face extracellular side. Its location is important to regulate interaction with β-subunits and voltage gating of the channel. S0-S1 linker is formed by an intrinsically disordered domain (unsolved in the structure) and two amphipatic helices (Shi et al., 2013). This region interacts with intracellular regulators of BK. In dark blue is D99, one of the residues which mediates Mg^{2+} coordination in the low-affinity site.

Figure 1.8. Voltage sensor domain of BK channel. In contrast to other voltage-gated potassium channels, the VSD of this channel is constituted by spread positive charges along S1-S4 helices. Arginines 207, 210 and 213, key in this voltage sensing (Tao et al., 2017), are depicted in blue (PDB: 6V38).

Figure 1.9. Pore and gating domain. Constituted by S5, S6 and the pore loop, this domain is the responsible of maintain an exquisite selectivity to K^+ ions with a high flux close to diffusion limit. Potassium channel selectivity filter signature TVGYG is in red. In the bottom part, glutamate sidechains of the residues hE386 (mE321) and hE389 (mE324) are in pale blue. These glutamates constitute two rings of negative charges whose maintain the cavity dimensions and allow the K^+ flow (Bottom).

The large cytosolic C-terminal domain of these channels contains two highly conserved domains known as Regulator of Conduction of K^+ (RCK1 and RCK2) (figure 1.10). Interestingly, RCK domains are also found in prokaryotic channels and other members of the Slo gene potassium channel family, playing a key role in gating and transporter activity (Giraldez and Rothberg, 2017). In the BK tetramer, four RCK tandems form a characteristic structure known as the *gating ring* (Hite et al., 2017; Tao et al., 2017; Wu et al., 2010; Yuan et al., 2011). This Ca^{2+}-sensing structural module contains distinct ion binding sites at the RCK1 and RCK2 domains (twelve in total in the full BK tetramer), which were identified in a large body of structure-function studies and account for the whole range of physiological Ca^{2+} concentrations activating the channel (Schreiber and Salkoff, 1997; Shi et al., 2002; Sweet and Cox, 2008; Xia et al., 2002; Zhang et al., 2010). The high calcium sensitivity of BK channels has been attributed to a binding site containing a cluster of acidic residues within RCK2, known as the *calcium bowl* (Schreiber and Salkoff, 1997; Schreiber et al., 1999; Wei et al., 1994). Two additional independent sites have been proposed to bind Ca^{2+} within the RCK1 domain, a high affinity site within the more N-terminal part of RCK1 and a low affinity site at the C-terminal lobe of RCK1 (Xia et al., 2002; Zhang et al., 2010). The latter has been proposed to be normally occupied by Mg^{2+} under physiological conditions (Latorre et al., 2017). Altogether, these three sites within the *gating ring* account for all of the Ca^{2+} sensitivity of the channel (figure 1.10). In fact, substitution of the C-terminal domain by that of the pH-gated channel Slo3 (Xia et al., 2004), or removal of the whole *gating ring* (Budelli et al., 2013) abolishes all of the Ca^{2+} and Mg^{2+} sensitivity of the channel, ruling out the possibility that other Ca^{2+} binding sites exist outside of the C-terminal domain. An intriguing question in the field relates to the cooperativity between Ca^{2+} binding sites. Several studies addressing this question arrived at different conclusions, although in all cases the level of cooperativity found was low (Qian et al., 2006; Sweet and Cox, 2008). Intriguingly, the cryo-EM structures suggest that interactions between sites may occur, paving the way for new functional studies (Hite et al., 2017; Zhou et al., 2017). In addition to Ca^{2+} and Mg^{2+}, other divalent cations can also activate BK channels including Sr^{2+}, Cd^{2+}, Mn^{2+}, Co^{2+}, and Ni^{2+} (Zeng et al., 2005). In addition, Ba^{2+} has been shown to activate the BK channel by binding to the *calcium bowl* (Zhou et al., 2012) (figure 1.11). BK channels can also be activated by protons binding to the RCK1 site (Hou et al., 2008).

Figure 1.10. Gating-ring and divalent cations binding sites. RCK1 is in blue and RCK2 in pink. The three different binding sites and the coordinating residues are depicted below. In RCK1 binding site, R514, S533 and S600 coordinate Ca^{2+} ion with the backbone carbonyl oxygen. In the RCK2 site or *calcium bowl*, the Q889 and D892 coordinates also with the backbone oxygen. All the other residues coordinate with the sidechain negative charge atom. (PDB: 6V38).

Figure 1.11. Divalent cations bind to different binding sites mainly depending on their size. Ionic radius is represented, and each circle size is proportional to this radius. Background inset is the *gating ring* of a monomer of BK channel with the three sites at each level of the channel (PDB: 6V38) (Modified from Zhou et al., 2012).

Understanding how the binding of calcium to the *gating ring* is mechanically transduced into pore opening constitutes an important question regarding BK channel function. Based on the structure of the *gating ring* from a bacterial Ca^{2+}-activated channel (Jiang et al., 2002), it was proposed that expansion of this region upon Ca^{2+}

binding would be transmitted to the PGD via a stretch of amino acids linking the RCK1 domain to the end of the S6 TM (known as the C-linker; (Niu et al., 2004)). Structural data showing no significant conformational changes in the C-linker upon calcium binding together with further functional studies seem to draw a more complex picture (Zhou et al., 2017). Thus, conformational changes of the *gating ring* could be partly transmitted to the PGD partly via the C-linker, in addition to noncovalent interactions between the C-terminal domain and the TMD (Lee and Cui, 2010). In fact, cryo-EM structures of full BK channels unveiled close associations of the *gating ring* with the TMD (Hite et al., 2017; Tao et al., 2017; Tao and MacKinnon, 2019), which is consistent with previous findings showing alterations in the voltage dependence

Figure 1.12. Interaction interfaces between RCKs. There are three main interesting surfaces of interactions between RCKs of the same and adjacent subunits. A. Intrasubunit RCK1-RCK2 interface and the residues involved. There are more hydrophobic interactions between RCK1 and RCK2 of the same subunit, however, no one has been demonstrated to be as critical in BK channel function as this one (see Kshatri et al., 2018). B. Intersubunit RCK1-RCK2 interaction through N449 coordinating residue. This was proposed by the structure (Tao et al., 2017) and its mutation produces a loss of Ca^{2+} sensitivity (Li et al., 2018). C. RCK2-RCK2 intersubunit interaction. This one is in the bottom part of the channel and selective mutations in this interface also affect channel function (Li et al., 2018).

of gating charge movements upon Ca^{2+} binding (Horrigan and Aldrich, 2002; Savalli et al., 2012). Recent functional studies further support the idea that the interaction between the calcium sensing domain and VSDs constitutes an important mechanism modulating voltage-dependent gating and pore opening in BK channels (Geng et al., 2020; Lorenzo-Ceballos et al., 2019; Miranda et al., 2018). Interestingly, some studies suggest that the two high affinity sites (RCK1 and Ca^{2+} bowl) may use distinct pathways leading to channel activation (Yang and Cui, 2015; Zhou et al., 2017). Evidence supporting this idea includes the identification of a number of residues that seem to participate in BK activation by Ca^{2+} binding to the RCK1 site but not the Ca^{2+} bowl (Bao et al., 2002; Yang et al., 2010). In addition, fluorescence studies have shown that RCK1 and RCK2 domains move independently when their specific binding sites are occupied (Miranda et al., 2016). Finally, both sites have shown different voltage sensitivities (Miranda et al., 2013; Savalli et al., 2012; Sweet and Cox, 2008).

The interfaces of the CTD

BK cryoEM structures unveiled the assembly interfaces of the *gating ring*. Considering the modular structure of BK channel, these interfaces are essential in the sensing-transduction to the pore process. As a tetramer of RCK dimers, BK channel would be expected to have several interfaces of interaction, intrasubunit and intersubunit, which would mediate the synergic activation of the channel. Within the same subunit, RCK1 and RCK2 extensively interact by a flexible interface composed of twin helix-turn-helix domains (one from RCK1 and the counterpart from RCK2) with hydrophobic residues that interact with each other (figure 1.12A; Yuan et al., 2010; Wu et al., 2012; Tao et al., 2017). These interactions would stabilize and transmit the stimuli to the upper parts of the channel in an intrasubunit pathway. It is noteworthy to mention the hR514, E902, Y904 bridge, being the clearest interaction between the two Ca^{2+} binding sites within each subunit. Hypothetically, this could be a transduction pathway of Ca^{2+} binding in the *calcium bowl*, influencing the RCK1 site occupancy.

Apart from the intrasubunit interface, there are two assembly interfaces in the *gating ring*. The adjacent subunits interact with each other in two clear points: one RCK1-RCK2' interface, with the N449 residue from RCK1 and the *calcium bowl* in the RCK2 (figure 1.12B); and one RCK2-RCK2' in the bottom part with electrostatic interaction of E955, R786 and R790 (figure 1.12C; Tao et al., 2017; Li et al., 2018). Mutations to alanine of the residues in both interfaces were demonstrated to dramatically

The development of unnatural amino acids (UAAs; also referred as non-canonical amino acids or ncAAs) provide a new dimension to this structure-function analysis studies by extending the range of variation. Besides that, it provides a high level of control for the introduced mutation. For instance, a charge can be introduced without modifying the steric characteristics of an amino acid. Moreover, fluorescent and photoactivatable amino acids have been also developed, increasing the side-chain functionalities. More than 230 UAAs (Swiss SideChain database; consulted: 13/06/21) have been synthesized and a diverse catalogue of functions to incorporate in proteins exists.

Different methods have been developed to site-specifically incorporate the UAA into the target proteins: (1) injection of tRNA-UAA conjugates into Xenopus oocytes, (2) in-vitro translation, (3) protein ligation and (4) the "genetic method" using engineered orthogonal synthetases. Among all, the genetic method has been the

Figure 1.13 Genetic method of BzF unnatural amino acid incorporation in BK channels (example with BK667YFP bakcbone construct, details in Methods). Cells are transfected with three different plasmids: a BK667YFP carrying the TAG mutation; the aminoacyl-tRNA synthetase (aaRS) coding plasmid; and tRNACUA synthesizing plasmid. 4-6 hours after transfection, culture media is replaced with a BzF enriched media. During the next 48 hours, the cell is going to synthesize the elements neccesary for the create the BK-BzF mutants: 1. aaRS recognizes specifically BzF and the region of the tRNACUA and aminoacylates the last one with the BzF. 2. The tRNA-BzF complex enters the ribosome and recognizes the TAG codon from the BK channel mRNA. 3. BK channel mutants, with the specific incorporation of BzF, are formed and inserted in the membrane by the inner cell machinery.

affect Ca^{2+} sensitivity of the channel (Li et al., 2018). These two intersubunit interfaces would mediate cooperativity between adjacent monomers and evoke the concerted activation of the BK channel.

Therefore, there is a dual role of these interfaces: Ca^{2+}-binding facilitation and signal transduction to the pore.

Deployment of unnatural amino acids approaches for the study of ion channels

As described above, the ion channels are a variable and versatile family of proteins whose activation mechanisms as well as their regulation can be really complex. Furthermore, the temporal scale of activation and deactivation of these proteins can be below microseconds. Therefore, the study of ion channels has classically needed the development of specific and high throughput techniques to answer the key questions of the field.

To deeply understand the function of ion channels and how the different domains of the proteins relate with each other, several mutagenesis approaches have been employed throughout the years. Until recently, structure-function studies have employed site-directed mutagenesis and amino acid substitution to evaluate the contribution of each residue in protein function. Alanine scanning mutagenesis has been the most used method in structure-function studies, substituting charged or sterically complex residues for alanine, a small and non-charged residue. Other modifications can also be performed using this method, such as the substitution of serine/threonine for charged glutamic or aspartic acid residues to induce phosphorylation effects. Altogether, this general approach provided a narrow analysis of indispensable residues in the active site of an enzyme or in the binding site of a ligand.

One could imagine numerous scientific questions that would be answered with experiments that substitute one amino acid for another; but how far could we go? The number of possibilities was restricted to the canonical repertoire of 20 amino acids, that is small even considering post-translational modifications (Walsh, Garneau-Tsodikova, and Gatto 2005).

most used in recent years due to its applicability to mammalian cells, among other advantages. This methodology consists of providing the cell with all the machinery necessary for UAA incorporation into the protein of interest. Three essential elements are needed: an UAA with desired characteristics, the tRNA that recognizes the codon where the UAA will be introduced and an aminoacyl-tRNA synthetase (aaRS) that recognizes the UAA and aminoacylates the tRNA with it (figure 1.13).

Table 1.3 shows the requirements of the UAA, the codon and the tRNA/aaRS pair needed for this system to work. To incorporate the UAA in the specific site of choice into the target protein, a codon must be used which does not encode any another amino acid. It was soon discovered that the STOP codons were the most appropriate to fulfil this role. Due to its lower frequency in mammalian proteins, the *amber* codon (UAG) has been the most widely used. Furthermore, the genetic code in some microorganisms uses this codon for encoding some amino acids, allowing the use of their machinery to suppress the mammalian STOP codon.

TABLE 1.3. Requirements of the UAA, Codon and aaRS/tRNA pair for effective UAA insertion.

UAA	Metabolic stability. Good bioavailability. Tolerated by EF-Tu and the ribosome. It should not be substrate of endogenous aaRS.
Codon	Recognized only by the exogenous tRNA (STOP codon).
aaRS/tRNA	UAA-specific. Functional in the host organism. Orthogonal in aaRS/tRNAs endogenous context.

Since UAAs are not present in the nature, engineering the aaRS and tRNA is necessary for the UAA to be recognized and aminoacylated. Many tRNA/aaRS pairs have been coevolved in different organisms (mainly bacteria and yeast) capable of UAA recognition and aminoacylation (Liu and Schultz 2010). A key point in the tRNA/aaRS pairs development is orthogonality. In other words, it is essential that the UAA-tRNA is not misaminoacylated by endogenous aaRSs, as well UAA-aaRS does not misaminoacylates endogenous tRNAs. This orthogonality is achieved directly or by engineering in different organisms (table 1.4).

Bacteria and yeast have shown high efficiencies for UAA incorporation. However, the genetic method has been more challenging in mammalian cells, requiring an extensive optimization of the tRNA/aaRS pairs. One example of this optimization is the *Bacillus stearothermophilus* (Bst) tRNATyr (BstRNATyr) and *Escherichia coli* TyrRS (EcTyrRS) pair coevolution. A human 5′-leader sequence was added to BstRNATyr to allow its use in mammalian cells. The resulting tRNA incorporates a tyrosine residue in UAG codons (these bacteria have an expanded genetic code and *amber* STOP codon does not exist). BstRNATyr / EcTyrRS pair has been the most used pair to incorporation of UAA in recent years. Directed mutagenesis of the synthetase has allowed aminoacylation of *BstRNATyr* with many different UAAs (Sakamoto et al. 2002; Liu et al. 2007; Wang et al. 2007; Ye et al. 2008; Klippenstein et al. 2018).

TABLE 1.4. Orthogonality in aaRS/tRNA pair development. (Modified with permission from Prof. Andrew Plested).

HOST for EVOLUTION and USAGE	DONOR: Bacteria	DONOR: Yeast / *Archaea*	DONOR: Eukaryote
Bacteria			
Yeast / *Archaea*	No way to evolve in eukaryotes		Need to engineer orthogonality
Eukaryote	No way to evolve in eukaryotes	No way to evolve in eukaryotes	

The chemistry of the sidechains of UAA have multiple functionalities: fluorescence, redox activity, NMR probes, infrared spectroscopy, protein evolution, bioconjugation, photocrosslinking, etc. (Liu and Schultz, 2010; Chin, 2014; Xiao and Schultz 2016; Debelouchina and Muir, 2017). Their small size and versatility allow their introduction in specific sites of the proteins to expand specifically the functionality of a domain of the protein and study their effects in the overall function. Therefore, this tool is quite attractive to use in ion channels, where some of the questions cannot be solved with the traditional approaches. Of special interest have been the light-sensitive amino acids (fluorescent or photoreactive), whose advantages and limitations were recently reviewed in Klippenstein et al., 2018.

Photoactivatable UAAs in the study of ion channels: p-benzo-L-phenylalanine (BzF)

Among all the UAAs, photoactivatable amino acids are one of the most used

BzF photocrosslinking reaction scheme is depicted in figure 1.14. Under UV irradiation (≈365 nm), the benzophenone adopts a triplet state. In this excited state, BzF reacts with accessible C-H group, normally from the Cα of the backbone, to abstract a hydrogen. The lifetime in the absence of this close hydrogen is around 80-120 μS, however it goes up to 100-fold faster in the presence of this partner. covalent bond (Dormán and Prestwich, 1994). Afterwards, there is a two-step reaction: hydrogen abstraction leads to alkyl and ketyl free radicals' creation and the posterior recombination that forms the covalent bond (Dormán and Prestwich, 1994; Ding and Horn, 2001). This UAA presents four characteristics that make it advantageous among other photocrosslinkers: (1) it is more stable than azides or diazo esters; (2) it can be easily manipulated in visible light and activated only under UV-A light 350-365 nm, causing reduced damage in aromatic residues of proteins; (3) it reacts with neighboring C-H groups from the protein backbone with higher reactivity than with other methylene groups of the side chains or lipids; (4) in the absence of a neighbor (≈3 Å) C-H group, the triplet state relaxes to the ground state, allowing multiple excitation cycles without losing the reactivity (Dorman and Prestwich, 1994). This last property is interesting for the use of BzF as an effective photocrosslinker, because it increases its yield of effective recombination. Despite the possibility of a photodestruction by oxidation, these effects are negligible (Horn et al., 2000).

BzF, and other photocrosslinkers as AzF, has been successfully incorporated in ion channels to answer different biological questions (Braun et al., 2020a). The Plested group demonstrated in AMPA receptors how the incorporation of BzF near the ligand-binding domain (LBD) inactivates the receptors following UV illumination (Klippenstein et al., 2014); the same group also mapped the gating and desensitization involved domains of these receptors (Poulsen et al., 2019). In NMDARs, despite BzF being succesfully introduced in the amino-terminal domain (ATD), there was no detectable UV effect, contrary to AzF, which allowed to unveil specific subunits interactions at this extracellular layer (Zhu et al., 2014). The study of protein-protein interaction with BzF revealed state-dependent interactions and stoichiometry between KCNQ1 potassium channel and its auxiliary subunit KCNE1 (Murray et al., 2016; Westhoff et al., 2017). The system has been also used in TRPV1, rendering functional channels ready for photocrosslinking experiments (Cabezas-Bratesco et al., 2018). Recently, BzF incorporation in a linker present in ASIC channels disclosed the role of this domain in desensitization and recovery (Rook et al., 2020). In the same channel, Braun et al. set a platform for high-throughput incorporation of BzF in hASIC1a and characterized the effects of different peptides on it (Braun et al., 2020b; preprint). It is important to mention that in the study of voltage sensor of Shaker potassium channel, a cysteine conjugated with a benzophenone was able to immobilize the move-

to date in ion channel studies. These UAAs can form covalent bonds with spatially close groups once they are irradiated with light (photocrosslinking). p-benzo-L-phenylalanine (BzF), together with L-azido-phenylalanine, is one of the most common photoactivatable UAAs (Grunbeck and Sakmar, 2013; Wang et al. 2007; Zhu et al. 2014; Klippenstein et al. 2018). Photoactivatable UAAs have assisted in the detailed study of protein function, identification of dimerization domains, study of desensitization and inactivation states of channels, mechanisms of allosteric modulators, etc. (Tanaka et al., 2008; Pless and Ahern, 2013; Klippenstein et al., 2018).

Benzophenone, the chemical active group of BzF, was early used in biology to study peptide-protein interactions and showed to serve as a probe that photoreact with glycine and covalently attach a peptide to a protein (Galardy et al., 1973; Kauer et al., 1986). Cornish et al. was the first one to use the genetic method to incorporate specifically the BzF *in vitro* into T4 lysozyme, however the resulting protein was non-functional (Cornish et al., 1994). Modifications and optimizations of ortholog aaRS and tRNAs allowed the insertion of this UAA in proteins of different organisms: bacteria (Chin et al., 2002); yeast (Chin et al., 2003); and mammals (Hino et al., 2005; Liu et al., 2007; Ye et al., 2008), allowing this tool to be versatile among different studies.

Figure 1.14. Photocrosslinking reaction of the BzF. (Modified from Ding and Horn, 2001).

ment of this domain, emphasizing the utility of this chemical group in photocrosslinking (Horn et al., 2000; Ding and Horn, 2001).

In this thesis, I exploited the advantages of BzF to study the structural rearrangements and the interfaces involved in the activation by Ca^{2+} of the BK channel.

Fluorescent tagging and labelling of ion channels

Tagging of proteins with small peptides and full proteins has its origin in 1980 by the β-galactosidase fusion to *E. coli* genes to purify them (Shuman et al., 1980). This milestone opened a huge range of opportunities to tag proteins of interest with the desired sequences for purification, specific cellular location, labelling and other applications (Kolodziej and Young, 1991). In the ion channel field, the first reported uses of these epitopes and fusion proteins were in Kv1.5 (Philipson et al., 1993) and acetylcholine receptors (Anand et al., 1993). Since these two works, multiple ion channels and positions of the same channel have been tagged with different epitopes according to the purposes of the studies (Maue, 2007). In this section I introduce the self-labelling enzyme advantages over FPs and the future perspectives.

Self-labelling enzymes (SLEs)

In the way to more versatile and specific fluorescent tagging of proteins, self-labelling enzymes (SLEs) are a recurrent tool. The concept behind the genetic engineering of these SLEs is the skill to react with a compound attached to a fluorophore and remain covalently attached to this fluorescent dye (figure 1.15). Therefore, using them as a fusion protein would render specific labelling of the protein of interest. Because the core or substrate of reaction is not in the fluorescent dye part of the compound, this module can be chemically fused to different fluorophores and other compounds of interest, having the same result of specific reaction with the SLE catalytic site. This greatly extends the possibilities of combinations with different chemical fluorescent dyes. Moreover, apart from the advantages of the use of chemical dyes, this system overcomes the problems of FPs with a smaller size and a flexible linker permission.

Currently, three SLEs have been thoroughly optimized for their use as fusion proteins: SNAPtag and CLIPtag (patented by New England Biolabs) and HaloTag

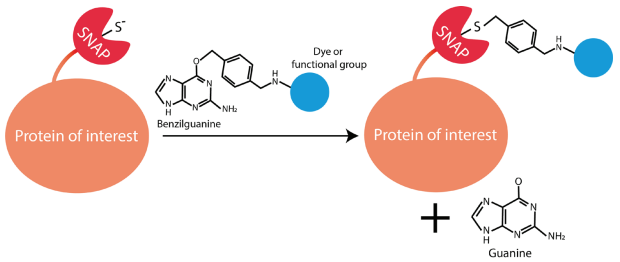

Figure 1.15. Example of SNAP-tag, a SLE. SLEs react with a core, in the case of SNAP, the benzylguanine, and the functional group coupled to it remains attached covalently to the enzyme.

(from Promega). SNAP and CLIPtag are 20 kD enzymes engineered from the O6-alkylguanine-DNA alkyltransferase, a DNA repair enzyme, which reacts with benzylguanine and benzylcytosine derivatives respectively (Keppler et al., 2003; Gautier et al., 2008). Because they possess orthogonality, the use of both enzymes can be used in the same set of experiments for multiple protein labelling with minimum crosstalk (Gautier et al., 2008). On the other hand, HaloTag comes from a haloalkane dehalogenase, an extremophile microorganism enzyme that converts haloalkanes as a source of carbon. This enzyme reacts with a chloroalkane linker fused to the group of interest (Los et al., 2008). These three enzymes represent multiple advantages over the FPs: (1) the fluorescence starts after addition of the compound and not directly after translation of the protein, allowing a time-resolved fluorescence which can be combined to discern newly synthesized proteins; (2) the same construct can be used with different dyes according to the desired application; (3) using non-permeable dyes, we can specifically isolate the plasma membrane population of a protein (special interest in ion channels and receptors); (4) the core of reaction can be conjugated with photostable and high quantum yield dyes, more resistant to photobleaching; (5) substrates are not only restricted to fluorophores but more complex chemical groups which allow photo reversible activation or blocking of the proteins with tethered ligands or blockers (see for example Levitz et al., 2017 and Royal et al., 2019).

Therefore, the use of these enzymes constitutes a qualitative advance over FPs for most applications. The modifications and optimizations of these enzymes have pointed towards a fast and specific labelling of our protein of interest. A recent study demonstrates differences in intensity and labelling efficacy between HaloTag and

Hypothesis & Aims

SNAPtag, demonstrating that the chosen enzyme and labelling strategy should be set up in each experimental condition and protein of interest (Erdmann et al., 2019). As in the FPs, insertion site of these tags can modify protein function, however, a smaller size and a more flexible interface (N and C-terminus are in different positions, compared to the β barrel of GFP with N and C terminus close to each other) seems to be favorable for them.

In ion channels and receptors, they have been used for localization and trafficking of voltage-gated sodium and potassium channels (Jensen et al., 2017; Akin et al., 2019; Kurakami et al., 2019), structure-function studies (Lecat-Guillet et al., 2017; Gutzeit et al., 2019; Vyklicky et al., 2021) or protein-protein interaction with FRET pair fluorophores (Maurel et al., 2008; Basu et al., 2018). Furthermore, this last application could be improved in the future with the use of split SNAP and CLIPtag enzymes, already developed but up to date not used in any complex formation (Mayasu et al., 2016).

In this work, I developed constructs with SNAP and CLIPtags fused to the BK channel and NMDAR1 subunit to study their interaction and complex formation dynamics. We validated them for their use in superresolution microscopy and single molecule studies.

Hypothesis and aims

BK channel regulation by Ca^{2+} is a key mechanism directly related to relevant physiological roles. Association to specific Ca^{2+} sources at distinct neuronal locations influences not only excitability and neuronal release, but critically regulates synaptic transmission and plasticity. Specifically, functional coupling of NMDARs and BK channels in the basal dendrites of somatosensory neurons modulates synaptic transmission and plasticity in thalamocortical circuits. At the molecular level, Ca^{2+} binding induces structural rearrangements leading to pore opening. Interaction between different domains of the protein upon Ca^{2+} binding is crucial for the transmission and coupling of the signal to channel activation. Within this context, this thesis has two differentiated parts:

PART 1: Ca^{2+}- INDUCED ACTIVATION MECHANISMS OF BK CHANNEL

The activation of BK channel by Ca^{2+} is mediated by a set of complex and concerted structural rearrangements in the gating-ring with an involvement of pivotal residues in coordination and coupling. The intra and intersubunit interfaces between the functional domains of BK channel play a crucial role in the cooperation between the two chemically different high affinity Ca^{2+} binding sites and in the transduction of the signal to the gate.

Aim 1. To study the molecular mechanisms underlying coupling of Ca^{2+} binding to pore opening.

- *Subaim 1.1.* To evaluate, in the human BK channel, the role of newly described residues from the *Aplysia* structure involved in Ca^{2+} coordination and its coupling to channel activation.
- *Subaim 1.2.* To generate a library of mutants for insertion of the UAA BzF in different regions of the BK channel that are relevant for activation by Ca^{2+}.
- *Subaim 1.3.* To functionally evaluate BzF-inserted BK channels undergoing real-time photocrosslinking.
- *Subaim 1.4.* To model the role of the studied regions in BK activation mechanisms by Ca^{2+}.

Materials & Methods

PART 2: BK CHANNEL FUNCTIONAL AND PHYSICAL ASSOCIATION WITH NMDARs

BK channels assemble with NMDARs in dendrites to mediate synaptic plasticity. This physical association is solely dependent in the presence of both proteins, and it is potentially dependent on the NMDAR subunit composition.

Aim 2. To investigate the effect of NMDARs as Ca^{2+} sources modulating BK function

- *Subaim 2.1.* To characterize the functional assembly of BK channels and NMDARs in heterologous systems.
- *Subaim 2.2.* To characterize the potentially distinct influence of GluN2A- or GluN2B-containing NMDARs in BK channel function.
- *Subaim 2.3.* To develop tools to study this paradigm under superresolution microscopy, single molecule tracking and single molecule pulldown.
- *Subaim 2.4.* To set up single molecule approaches including single molecule tracking and analysis, subunit counting (stoichiometry) and smFRET to characterize BK channel interaction with physiological partners. As a proof of concept, we aim to quantify NMDAR and BK stoichiometry, as well as NMDAR-BK association stoichiometry.

Plasmids and molecular biology

The different plasmids used during this thesis and the cloning strategies followed for their obtention are explained in this section. All the vector maps, as well as the primers used, are described in Annex I.

Human BK channel

The full-length human BK channel construct (GenBank accession number U11058) as well as the fluorescent derivatives BK667YFP and BK860YFP were selected from a library previously available in the lab (Giraldez et al., 2005; Miranda et al, 2013; Miranda et al., 2016; Miranda et al., 2018). All the inserts were in a mammalian expression with ampicillin resistance vector under a CMV promoter (pBNJ13).

BzF aminoacyl-tRNA synthetase and amber supressor tRNA

Plasmids expressing the orthogonal pair of BzF specific aminoacyl-tRNA synthetase (aaRS) ad *amber*-supressor tRNA were kindly gifted by Dr. Thomas Sakmar (Rockefeller University, New York, USA). These constructs were previously designed and validated to be used in mammalian cell lines (Ye et al., 2008; Ye et al., 2009).

BzF-aaRS was modified from *Escherichia coli* tyrosine-aaRS with three-point mutations (Y37G, D182G, and L186A) to accommodate and recognize the bulkier amino acid BzF. This modified gene was cloned in the commercial vector pcDNA3.1 with ampicillin resistance and contained a C-terminal FLAG epitope. BzF-aaRS was able to recognize its cognate tRNA and aminoacylate it with BzF. The tRNA coding sequence was cloned for expression in a pSVBpUC. This tyrosine-tRNA of *Bacillus stearothermophilus* has in its anticodon loop the nucleotides CUA, recognizing the codon UAG (Amber STOP codon in mammals) and suppressing it with the specific insertion of BzF.

NMDA receptors

Bacteria strains, transformation and plasmid purification

Bacteria strains and competent cell preparation

E. coli strain TOP10 (#C404010; Thermo Fisher Scientific, Massachusetts, USA) were homemade prepared to be competent using RbCl2 method (Hanahan, 1983; Hanahan et al., 1991). This strain was used for the conventional cloning reaction transformations and plasmid purification, with the only exception of site-directed mutagenesis. XL-10 Gold Ultracompetent cells (#200314; Agilent Technologies, California, USA) were used for site-directed mutagenesis. Transformation in this case was performed following the manufacturer instructions.

Bacteria transformation, growing and storage

Transformation was as follows: 1 to 3 μL of plasmid was added to TOP10 cells and gentle mixed pipetting up and down. Mixture was incubated in ice for 5 minutes. After that, they were heat-shocked during 45 seconds at 42ºC and incubated on ice again for 2 minutes. 300μL of 37ºC pre-warmed SOC-medium (table 3.2) was added afterwards and cells were incubated at 37ºC in an orbital shaker (200 rpm) for 1 hour to ensure antibiotic resistance gene expression. After this, cells were plated in LB+agar plates (table 3.3) with the specific antibiotics for each plasmid and incubated overnight at 37ºC. Each colony was grown in 5 ml of liquid LB medium + antibiotic (table 3.3). Plasmids were purified using a commercial kit (Macherey-Nagel, Dueren, Germany) and sent for DNA sequencing (Ez-Seq, Macrogen Spain, Madrid, Spain).

Table 3.2. Super Optimal Broth medium with Catabolite repression (SOC)

Name	Final concentration
Tryptone	2 %
Yeast extract	0.5 %
NaCl	10 mM
KCl	2.5 mM
$MgCl_2$	10 mM (added after autoclave)
Glucose	20 mM (added after autoclave)
Adjusted to pH 7	
0.22 μM PVDF filtered and aliquoted	

Plasmids for expression of *Rattus norvergicus* N-methyl-D-aspartate receptors (GluN) subunits 1a (pEYFP-NR1a), 2A (pEGFP-NR2A) and 2B (pEGFP-NR2B) were a gift from Stefano Vicini (Addgene; Table 3.1). These constructs had the fluorescent proteins inserted in the N-terminal domain of the protein (extracellular).

Table 3.1. NMDAR constructs

Name	Addgene reference	Insert	Origin	Vector	Depositing lab
pEYFP-NR1a	17928	GluN1-1a	*R. norvergicus* (rat)	pcDNA3.1	Stefano Vicini (Luo et al., 2002)
pEGFP-NR2A	17924	GluN2A	*R. norvergicus* (rat)	pcDNA3.1	Stefano Vicini (Luo et al., 2002)
pEGFP-NR2B	17925	GluN2B	*R. norvergicus* (rat)	pRK5	Stefano Vicini (Luo et al., 2002)

These plasmids were further modified in the lab for different applications according to the experiment. To avoid undesirable effects of the presence of fluorescent proteins during the imaging experiments in the NMDAR heterodimer, GFP was removed from GluN2A-GFP and GluN2B-GFP using the specific restriction enzymes sites flanking the GFP (SacII and ApaI respectively).

Original NR1a yellow fluorescent protein (YFP) was replaced with CLIP-tag self labelling enzyme, in the N-terminal domain (section *SNAP and CLIP cloning*).

SNAPf and CLIPf

Vector for subcloning of SNAPf and CLIPf fusion proteins were a gift from Prof. Joshua Levitz (Weill Cornell Medicine, New York). From now on, they will be called SNAP and CLIP, referring to the SNAPf and CLIPf commercial variants from New England Biolabs (vectors pSNAPf, #N9183S; pCLIPf, #N9215S).

mGluR2 receptors

mGluR2 modified expression vectors HA-mGluR2-SNAP and FLAG-mGluR2-CLIP were also kindly provided by Prof. Joshua Levitz (Weill Cornell Medicine, New York, USA). These constructs were used as controls in imaging experiments.

Table 3.3. Lysogeny Broth (LB) liquid medium and LB-agar plates

To 1 liter in H_2O

Name	Amount to add
Tryptone	10 g
Yeast extract	5 g
NaCl	10 g
Agar (for solid LB)	7.5 g
Adjusted to pH 7 and autoclaved	
Ampicillin was added (only for resistance selection) after cooling down to ≈ 55ºC to a final concentration of 50 μg/ml	

Positive clones of the new constructs were stored in the laboratory Bacteria Stock. 500 μL of overnight grown cultures were mixed with 500 μL of LB+30% glycerol to a final storage concentration of glycerol of 15%.

Plasmid purification

Bacterial cells were growth in different volumes of LB media (generally 5 ml for mini-prep extraction and 100 ml for midi-prep) with antibiotic shaking at 250 rpm and 37ºC overnight for plasmid extraction. Plasmid purifications for cloning procedures or mammalian cell lines transfection were performed using high-yield column-based commercial kits NucleoSpin Plasmid Mini Kit and NucleoBond Xtra Midi kit, respectively (#740727 & #740410; Macherey-Nagel, Dueren, Germany) following usage protocols. The latter possessed high endotoxin removal yield, needed for mammalian cell transfection. Final concentration of plasmids was measured using NanoDrop 2000 spectrophotometer (Thermo Fisher Scientific, Massachusetts, USA).

Site-directed mutagenesis

A scheme of the mutagenesis workflow is shown in figure 3.1. All mutagenesis was was performed with the QuickChange Lightning Site-directed Mutagenesis kit (#210519, Agilent Technologies, California, USA) following the manufacturer protocol based in an overlapping PCR.

Figure 3.1. Scheme of the mutagenesis process (modified from manufacturer protocol).
1. Forward and reverse pair of primers carrying the mutation (in pink) were added together with the backbone plasmid to be mutated.
2. Overlapping PCR amplification was carried in the thermocycler for both DNA strands during 30 cycles. Punctual mutations were incorporated in the newly synthesized strands and original vector was used as backbone for the mutagenesis again in the next cycle (2*).
3. After mutagenesis, residual backbone vector was digested with DpnI to reduce the background transformation. The resulting products were transformed in E. coli XL-10 Gold ultracompetent strain cells and plated overnight in ampicillin agar plates at 37ºC.

SNAP and CLIP cloning

In order to develop versatile constructs for their use in a wide range of microscopy and electrophysiology experiments, including single molecule, superresolution microscopy or patch-clamp fluorometry (PCF) among others, we inserted SNAP and CLIP self-labeling enzymes in the BK channel and GluN1.

In the case of the BK channel, SNAP was inserted in three different positions along the coding sequence (figure 3.2). Human BK channel WT construct was used as the backbone for these insertions. Two of the selected sites were extracellular in order to achieve the specific isolation of the plasma membrane channel subpopulation with the use of non-permeable dyes. BK-N-SNAP and BK-S1S2-SNAP were cloned using *In Fusion* cloning (#102518, Takara Bio, Kusatsu, Japan) following the manufacturer guidelines. BK667SNAP construct was made substituting the fluorescent protein YFP from the original BK667YFP construct using restriction enzyme sites flanking the YFP cassette. Restriction sites were added at both sides of SNAP by PCR and YFP was replaced with conventional cloning methods. Insert orientation was checked by sequencing. BK-N-CLIP construct variant was made by inserting CLIP instead of

SNAP using the same cloning protocol and primers (SNAP and CLIP share high sequence homology and identical ends).

Figure 3.2. BK channel and GluN1 SNAP (and CLIP insertions). (A) SNAP and CLIP were inserted in the N-terminus and between S1 and S2 extracellular loop (position 140). (B) Intracellular SNAP was inserted in a previous tested position for fluorescent protein insertion (Giraldez et al., 2005) (A&B: Protein concatenation between human BK channel EDTA-Ca^{2+} free structure, PDB: 6V3G and SNAPtag bound to benzylguanine, PDB: 3KZZ). (C) In GluN1 subunit, SNAP and CLIP were inserted in the N-terminus replacing the original YFP from the commercial acquired vector (GluN1 PDB: 4PE5).

To promote appropiate membrane insertion and cell surface expression of the BK-Nt-SNAP and BK-Nt-CLIP constructs, the endoplasmic reticulum export signal sequence from mGluR5 was inserted before the SNAP/CLIP sequences (description in *Results*). For single molecule experiments, the original N-terminal FLAG epitope of all BK constructs was substituted by a hemagglutinin (HA) epitope.

GluN1-SNAP and GluN1-CLIP were designed to have the enzyme placed in the N-terminal domain, just after its native signal sequence (figure 3.2). YFP was substituted from the original construct GluN1-YFP using the same strategy that for BK channel (overlapping PCR *In Fusion* cloning). The variant GluN1-SNAP was constructed substituting the CLIP by In Fusion cloning and HA epitope was added.

Amplification of SNAP and CLIP fragments was performed by PCR with PfuUltra II Hotstart polymerase (#600850, Master Mix 2X; Agilent Technologies, California, USA).

A large part of the work presented in this thesis involved the validation and optimization of these molecular tools. Therefore, the strategies and optimization protocols testing the ion channel functionality and labelling efficiencies are thoroughly described in the *Results* section.

Cell culture

Buffers and solutions

Culture medium

Cell lines were growth in complete Dulbecco's Modified Eagles Medium (DMEM). DMEM High-glucose (4500 mg/l), with stable-glutamine and sodium pyruvate (L0103), was supplemented with 10% fetal bovine serum (FBS) (S1300) and 1% penicillin/streptomycin (L0014). These components were purchased from Biowest (Nuaillé, France). Complete DMEM was occasionally supplemented with MycoZap™ Prophylactic (0.2%) (#VZA-2031; Lonza, Basel, Switzerland) to prevent mycoplasma contamination.

UAA supplemented DMEM media

P-benzoyl-l-phenylalanine supplemented complete DMEM was freshly made before changing the medium after transfection. To obtain DMEM supplemented with 1 mM BzF, 4 mg of BzF (MW: 269.3; #4017646; Bachem, Bubendorf, Switzerland) were dissolved in 300 μL of HCl (1M). The dissolved BzF was immediately added to 15 mL of 37 ºC pre-warmed complete DMEM and pH was adjusted to 7.4 with NaOH. This standard protocol was extensively used and optimized before in Hino et al. (2006), Ye et al. (2009), Klippenstein et al. (2014) and Poulsen et al., (2019) among others.

In order to increase membrane expression of the BK-BzF channels, enriched medium was supplemented with the molecular chaperone sodium 4-phenylbutyrate (10 mM 4-PBA, MW: 186.18, sc-200652A; Santa Cruz Biotechnology, California, USA)

(Rubenstein et al., 1997). All this process was done under low-light conditions to prevent nonspecific photoreactivity of the UAA. The supplemented medium was filtered through a 0.22 μm PVDF membrane and added to the cells after washing transfection reagent (4-6 hours post-transfection). Experiments were performed between 48- and 72-hours post-transfection.

NMDAR-transfected cells culture media

When the cells were transfected with GluN receptors, medium was replaced 4 hours post-transfection with Opti-MEM (#L0106; Thermo Fisher, France) supplemented with 5% FBS and antibiotics. The absence of L-glutamine prevented the non-desirable activation of the receptors (Sands and Barish, 1997; Vyklicky et al., 2021). Reversible competitive antagonists of GluN1 (5,7-dichlorokynurenic acid or DCKA) and GluN2 ((2R)-amino-5-phosphonovaleric acid or APV) were added to the pre-warmed media (20 μM and 200 μM final concentration, respectively) to temporarily block GluN receptors and prevent from Ca^{2+} entry into the cell and cytotoxicity (Chazot et al., 1999).

Extracellular solution and SNAP or CLIP labelling

Extracellular solution (EX) (table 3.4) was a saline buffer used for labelling SNAP and CLIP fusion proteins with their specific BG or BC fused dyes as well as for the washing steps. Each fluorophore (table 3.5) was used at a 5 μM final concentration in EX. Cells expressing SNAP or CLIP fusion proteins were incubated during 45 min at 37 °C or 4 ºC for labelling.

Table 3.4. Extracellular solution (EX)

Name	Final concentration
NaCl	135 mM
KCl	5.4 mM
HEPES	10 mM
$CaCl_2$	2 mM
$MgCl_2$	1 mM

Adjusted to pH 7.4

In the cases where GluN1-SNAP or GluN1-CLIP were cotransfected to form

functional NMDARs with GluN2 subunits, the EX medium contained 50 μM DCKA and 400 μM APV to prevent their activation by residual glutamate during labelling.

Table 3.5. SNAP and CLIP fluorophores purchased from New England Biolabs and used in this study.

Name	Excitation/emission peaks	Reference
SNAP-Cell® 647-SiR	645/661	S9102S
SNAP-Surface® Alexa Fluor® 546	558/574	S9132S
SNAP-Surface® Alexa Fluor® 647	652/670	S9136S
CLIP-Surface™ 488	506/526	S9232S
CLIP-Surface™ 547	554/568	S9233S
CLIP-Surface™ 647	660/673	S9234S

Cell culture

For most of the experiments, HEK293T cells (ATCC® CRL-11268) between 3 and 25 passages after nitrogen retrieval were used. HEK293T cells were maintained in complete DMEM at 37ºC and 5% CO2. For passages, ≈90% confluent cells were first rinsed with sterile PBS and incubated with Trypsin-EDTA (0.4%) (L0930; Biowest, Nuaillé, France) for 5 min at 37ºC. Trypsin was then inactivated with 5 mL of complete DMEM medium and detached cells were collected and centrifuged at 300xg for 4 min. Pelleted cells were immediately resuspended in 5 mL of fresh complete DMEM media and plated in new flasks for maintenance at a 1:15 dilution.

HeLa (ATCC® CRM-CCL-2) cell line was used for BK SNAP constructs expression characterization. The splitting and seeding protocols were equivalent to HEK293T cells ones.

Cell seeding for electrophysiology experiments

For electrophysiology, HEK293T cells were seeded in Ø13 mm glass covers-

lips (VWR, Pennsylvania, USA). Coverslips were previously cleaned by sonication and sterilized by autoclave and flame. Once cleaned and sterilized, they were placed into Ø35 mm dishes (Thermo Fisher Scientific, Massachusetts, USA) and coated with 0.01% poly-L-lysine solution (# P4832; Merck-MilliporeSigma, Munich, Germany) for at least 1 hour at 37ºC (generally overnight). After this, coverslips were thoroughly rinsed with sterile water and dried. Cells were plated in these dishes in different dilutions ranging from 1:50 to 1:200, depending on the experimental requirements.

Cell seeding for imaging

In this case, Ø18 mm glass coverslips (VWR, Pennsylvania, USA) were used. For transfection, we introduced the coverslips in 12-well plates and treated with poly-L-lysine as described above. For live-cell imaging, the day of the experiment coverslips with cells were placed in a "quick-release" low-profile imaging chamber (RC-41LP, Warner Instruments), designed for fast solution exchange with maximum imaging surface. EX buffer was added to the chamber for live cell imaging.

Cell seeding for Single-Molecule Pull-down

The procedure for this preparation was similar to the ones described above for whole-cell imaging but with a higher density of cells in order to have enough membrane extracts for the following steps.

DNA transfection

Cells were chemically transfected with jetPrime (Polyplus™, Strasbourg, France) following manufacturer recommendations. This reagent yielded high transfection efficiency (up to 70%) and high cell viability. Culture media with transfection reagent was replaced with fresh media between 4-6 hours after transfection. If needed, replacing media were supplemented with UAAs or NMDARs blockers, as previously described.

Transfection ratios

For most of the experiments performed, there was more than one plasmid

transfected into the cell. Optimization of the plasmid ratio for transfection was done in order to ensure the best expression of all the proteins of interest.

BK channel and GFP.

Plasmid expressing a cytosolic and soluble GFP was cotransfected with BK wild type and mutants in 1:5 ratio to mark transfected cells and facilitate electrophysiology experiments.

BzF incorporation in BK channel

For these experiments, a 1:1:1 ratio was used between aaRS (specific for each UAA), $tRNA^{CUA}$ and BK-TAG mutant plasmids.

BK channel coexpression with NMDARs

In this case, BK channel was coexpressed with a GluN1 and GluN2A or 2B subunit to reconstitute the whole complex. The ratio used was 1:1:1 respectively (low amounts of total DNA were maintained in the imaging experiments for proper NDMAR membrane expression).

Biochemistry

Cell-lysis, protein purification and concentration determination

Cells were collected in PBS after 24-, 48- or 72-hours post-transfection, depending on the requirements. After pelleting by centrifugation, cells were resuspended in TENT lysis buffer (table 3.6) supplemented with cOmplete™ Mini-EDTA free protease inhibitor cocktail (11836170001; Roche, Manheim, Germany). Lysates were incubated 5 min on ice and centrifuged 10 min - 14000 x g at 4ºC. Supernatant was kept on ice and pellet was discarded.

Protein extracts were quantified using the bicinchoninic acid (BCA) assay (Smith

et al., 1985). After quantification, Laemmli loading buffer (table 3.7) was added, and the samples were stored at -20ºC until loading them in the electrophoresis gel.

Table 3.6. TENT lysis buffer

Name	Final concentration
Tris-HCl (pH7.5)	50 mM
NaCl	150 mM
EDTA	5 mM
Triton X-100	1 %

Table 3.7. Laemmli protein loading buffer (Laemmli, 1970)

Name	Final concentration
Tris base	62.5 mM
Sodium dodecyl sulfate (SDS)	70 mM
Glycerol	10 %
β-mercaptoethanol	1 mg/ml

Adjusted to pH 6.8 and aliquoted

In vivo photocrosslinking experiments

Cells were exposed to UV to achieve *in vivo* photocrosslinking of the unnatural amino acid BzF and correlate the electrophysiology experiments with biochemical confirmation of intersubunit crosslinking. For these experiments, HEK293T cells were plated in Ø 100 mm dishes and transfected with up to 15 μg of DNA (5 μg of each of the BK-TAG mutant, the tRNA and aaRS; in the case of WT transfection, 5 μg of BK667YFP was transfected). BzF supplemented medium was added to the cells 4 hours post transfection.

Forty-eight hours later, cells were washed once with PBS and replaced with PBS containing 40 mM N-Ethylmaleimide (NEM; MW: 125.13, #E3876, Sigma-Aldrich, St Louis, USA), a cysteine-reducing agent that prevents unspecific crosslinking of cysteine amino acids. In the indicated conditions, cells were exposed to UV with an open 4 W, 365 nm UV-lamp (#VL-4.L; Vilber-Lourmat, Collégien, France) for different times, ranging from 15 to 90 min. Light was applied inside a homemade dark chamber and dishes were placed on ice to avoid overheating. Afterwards, cells were collected with the help of a scraper, centrifuged and lysed as described above. BK were then recovered from the lysate with an anti-FLAG antibody (table 3.8) and

PureProteome™ Protein G Magnetic Beads (#LSKMAGG02; Merck-MilliporeSigma, Munich, Germany) following manufacturer protocol.

Table 3.8. Antibodies used in this study

Name	Host and type	Reference	Working concentration
Anti-Maxi Potassium channel α/SLO antibody [L6/60]	Mouse monoclonal	Abcam (ab192759)	WB: 1/1000
Anti-Maxi Potassium channel α/SLO antibody	Rabbit polyclonal	Abcam (ab3586)	WB: 1/1000
Anti-SNAP-tag® Antibody	Rabbit polyclonal	New England Biolabs (P9310S)	WB: 1/1000
Anti-NMDAR1	Goat polyclonal	Novus (NB100-41105)	WB: 1/2000
Anti-mouse HRP conjugated	Goat polyclonal	Dako (P0447)	WB: 1/25000
Anti-rabbit HRP conjugated	Goat polyclonal	Abcam (ab6721)	WB: 1/25000
Anti-goat HRP conjugated	Donkey polyclonal	Abcam (ab97110)	WB: 1/10000
Anti-HA biotin	Rabbit polyclonal	Abcam (ab26228)	WB: 1/1000; SP: 1/500
Anti-FLAG M2	Mouse monoclonal	Sigma (F3165)	WB: 1/1000 IC: 1/1000
Anti-mouse Alexa 594	Goat polyclonal	Invitrogen (R37121)	IC: 1/200

WB: Western blot; SP: Single-molecule pulldown; IC: Immunocytochemistry.

SDS-PAGE and Western blot

SDS-PAGE was performed in Mini-PROTEAN® TGX Stain-Free™ Precast gels (10%) (BioRad, California, USA). The Stain-Free system allowed *in situ* protein photo activation on the gel after electrophoresis for total protein load visualization, quantification and normalization when needed. Proteins were transferred to a PVDF membrane using a Trans-Blot® Turbo™ Transfer Starter System (PVDF) for Western Blot analysis (BioRad, California, USA).

Proteins were specifically detected in PVDF membranes using primary and sec-

ondary-HRP conjugated antibodies (table 3.8).

In order to detect the signals, chemiluminescent Clarity™ Western ECL Blotting Substrate (BioRad, California, USA) was used and protein bands were visualized in an ImageQuant™ LAS500 (GE Healthcare, Illinois, USA).

Electrophysiology

Setup

Electrophysiology recordings as well as fluorescence intensity measurements and photoactivation of BzF unnatural amino acid were performed using the experimental setup schematized in figure 3.3.

Figure 3.3. Setup for electrophysiology and photoactivation.

For voltage-clamp and current measurements, a silver chloride electrode was inserted into the holder coupled to CV-203BU headstage and connected to an Axopatch 200B amplifier and a Digidata 1550A digitizer (Molecular Devices, USA). Digitizer

was controlled through a conventional PC. Fluorescent cells were illuminated with a multicolor Spectra X LED engine (Lumencor, Oregon, USA) and captured under a Nikon Eclipse Ti-U (Nikon, Tokyo, Japan) inverted microscope with an emCCD camera (iXon Ultra 888, Oxford Instruments Andor, UK). Microscope LED, and camera were synchronized and controlled using μManager (Image J, USA) with a Z440 workstation (Hewlett-Packard, California, USA).

Photocrosslinking

Photoactivation of the UAAs was achieved with a 365 nm wavelength UV LED (Thorlabs, USA) remotely controlled through the electrophysiology computer and digitizer with TTL pulses. A dichroic mirror T400lp (Chroma Technology, Vermont, USA) mounted on Nikon adapter filter cube was used for total LED reflection to the focal plane.

Recording solutions

Symmetrical potassium recording solution

For the recording of BK channel currents, a symmetrical potassium solution the following was used (table 3.9). The amounts of calcium to obtain the desired Ca^{2+} free concentrations into bath solutions were calculated using WebMaxC Standard calculator (UC David, California, USA: https://somapp.ucdmc.ucdavis.edu/pharmacology/bers/maxchelator/webmaxc/webmaxcS.htm). In the case of concentrations of 100 μM Ca^{2+} or larger, no chelator was added. Available Ca^{2+} free concentrations were corroborated using a Ca^{2+} electrode (Orion, Thermo Fisher Scientific, Massachusetts, USA).

Inside-out GluN+BK solutions

In order to distinguish the contribution of GluN receptors to the Ca^{2+} mediated activation of BK in heterologous systems, during the recording of GluN+BK channel currents in inside-out excised patches, two different solution systems were used. One of them contained symmetrical potassium concentrations (table 3.9).The other contained potassium concentrations closer to the physiological range in the bath and the pipette (table 3.10). In both cases, pipette solutions were supplemented with 0.01 mM of glycine and 0.2 mM of NMDA, to activate GluN receptors.

Table 3.9. Symmetrical K^+ recording solution

	Concentration in mM	
Reagent	Bath	Pipette
$KMeSO_3$*	80	80
NMDG-$MeSO_3$*	60	60
HEPES	20	20
KCl	2	2
$MgCl_2$	-	2
HEDTA	1	-
$CaCl_2$	To desired concentration	-

*$KMeSO_3$ and NMDG-$MeSO_3$ salts were prepared from KOH and NMDG and titrated with $MeSO_3$ to pH 7.4.

Table 3.10. NMDA recording solution.

	Concentration in mM	
Reagent	Bath	Pipette
NaCl	5	140
KCl	10	2.69
$KMeSO_4$	135	-
HEPES-K	10	-
KH_2PO_4	-	1.25
$MgSO_4$	-	2
$NaHCO_3$	-	26
Glucose	-	10
$CaCl_2$	-	2
Ascorbic acid	-	0.4
Glycine	-	0.01
NMDA	-	0.2
HEDTA	1	-

pH 7.4

Recordings

Data was acquired using the setup described above and Clampex acquisition software (pClamp suite, Molecular Devices, California, USA) at 10.000 Hz acquisition rate and 5 kHz low pass filter.

Pipettes and configurations

Pipettes were pulled using a flaming micropipette P-97 puller (Sutter Instruments) to give them the desired shape and resistance. Fire polishing was applied after pulling to finish the tip. Resistance of the pipettes ranged between 2 and 5 MΩ depending on the configuration and application used. Pipettes were filled with recording solution and place on the setup electrode.

Among the different patch-clamp configurations, inside-out was extensively used during this thesis due to the cytosolic orientation of the Ca^{2+} binding sites in BK channel. Therefore, inside-out was employed for most of the BK channel experiments where quick exchange of different Ca^{2+} concentrations was needed. The whole-cell configuration was used in some of the GluN-BK channel interaction experiments to have control over the NMDA or glutamate concentration to activate the GluN receptor. Configurations used are specified in each experiment throughout the *Results and Discussion* section.

Data analysis

Data was firstly analyzed in Clampfit 11 (pCLAMP11, Molecular Devices, USA) to measure current traces (peaks and averages) as well as activation and deactivation kinetics. Current traces were exported from the software and plotted using Prism 9 (Analysis and figure edition software).

Conductance vs voltage analysis

Conductance vs. voltage (G-V) analysis was obtained by normalizing tail current value at - 80 mV (I) to the highest current value (Imax) obtained under the maximum Ca^{2+} concentration condition (mainly 100 μM Ca^{2+}) and represented versus voltage (figure 3.4).

Conductance versus voltage (G-V) curves were generated from tail current amplitudes normalized. The resultant curves were fitted with the Boltzmann equation:

$$\frac{G}{G_{max}} = \frac{1}{1+\exp\, zF\frac{Vm-V_{1/2}}{RT}}$$

where, $V_{1/2}$ is the voltage of the half-maximum activation, z is the slope of the curve, Vm is the test potential and G_{max} is the maximal conductance.

Ca^{2+} sensitivity was measured as the change in $V_{1/2}$ in response to different Ca^{2+} concentrations ($\Delta V_{1/2}$). This value was obtained mainly comparing 0 μM Ca^{2+} with the other different Ca^{2+} concentrations (figure 3.3).

$$\Delta V_{1/2} = V_{1/2}\, in\ 0\ \mu M - V_{1/2}\, in\ 100\ \mu M\ Ca^{2+}$$

To express the direct effect of Ca^{2+} on the channel we measured the changes in the Gibbs free energy (ΔG_0) in the closed and open states at 0 mV, as previously reported (Zhou et al., 2011; Chowdhury and Chanda, 2012). Slope (z) and $V_{1/2}$ were obtained from the Boltzmann fit values and ΔG_0 was calculated using:

$$\Delta G_0 = 0.2389\, zFV_{1/2}$$

where F is the Faraday constant. ΔG_0 has the units of energy (kJ / mol). The change in ΔG_0 in the presence of Ca^{2+} was calculated using:

$$\Delta\Delta G_0\,(Ca^{2+}) = \Delta G_0\,(Ca^{2+}) - \Delta G_0\,(Ca^{2+}\ free)$$

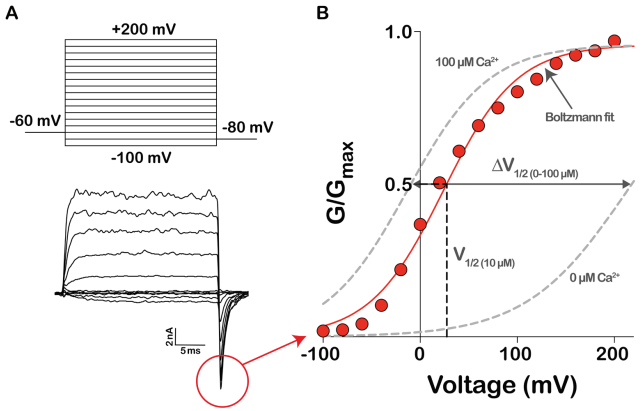

Figure 3.4. G-V analysis. (A) Voltage-step protocol elicited were measured and the tail current was normalized to the maximum tail current under different Ca^{2+} concentrations (in this example, current traces of human BK wt under 10 μM Ca^{2+} is depicted). (B) Normalized values were plotted against voltage and a Boltzmann equation was fitted. From the curves described by this equation, important values like the slope (z), $V_{1/2}$ and $\Delta V_{1/2}$ were obtained.

The percent reduction of $\Delta\Delta G_0$ was then calculated as follows:

$$\%\ reduction = \frac{\Delta\Delta G_{0_{WT(100\ \mu M\ Ca^{2+})}} - \Delta\Delta G_{0_{mutant(100\ \mu M\ Ca^{2+})}}}{\Delta\Delta G_{0_{WT(100\ \mu M\ Ca^{2+})}}}$$

All the data correspond to the mean ± SEM. For z and $V_{1/2}$ values, all the experiments were analyzed individually, and averages were calculated.

Statistical significance was assessed with one-way ANOVA followed by post-hoc analysis (Bonferroni) for multiple comparison test (*Annex II*).

Photocrosslinking evaluation

To evaluate the effect of photocrosslinking in overall function of BK channel, different protocols of UV application and recording were applied, as indicated in the results. Due to the limited availability of the UAA, the expected effect of its photocrosslinking should describe an exponential effect of current reduction or potentiation. The photocrosslinking effects were measured as a change in the steady-state current at the end of an activating depolarizing pulse of +100 mV along the cumulative exposure to UV. For all the mutants that presented this exponential effect (decrease or increase), a single exponential was fitted, as previously reported (Ding and Horn, 2001). The current was normalized to the average of the baseline before UV application for comparison among patches $(\frac{I_t}{I_{baseline\ average}})$

Imaging

Confocal imaging

Imaging of fixed or live cells was done under a TCS SP8 (Leica, Wetzlar, Germany) confocal microscope using LASX Leica control software. 63X or 100X oil immersion objectives were used for all the experiments.

Live imaging

Coverslips with live cells were mounted in a Quick Exchange Chamber (World

Precision Instruments, USA) with extracellular solution (see cell culture buffers and solutions) previously warmed to 37ºC if needed. For longer time experiments under physiological conditions the microscope chamber was pre-heated and stabilized to 37ºC.

Acceptor photobleaching FRET (FRET-AB)

Acceptor photobleaching FRET constitutes a straightforward method to easily and quickly evaluate the proximity between two fluorophores and estimate a distance between proteins. It is based in the partial quenching of the donor intensity by its energy transfer to the acceptor. If there is FRET between two fluorophores, photobleaching of the acceptor under a high-power laser dequenches the donor, increasing its intensity.

FRET between subunits of a same protein or between different proteins was assessed under the confocal microscope using the FRET-AB LASX software module, selecting donor and acceptors parameters in concordance with the conditions and fluorophores used. Photobleaching of the acceptor was done with an output laser power of 95% and subsequently checked by post bleaching imaging. Donor intensity (D) was measured in the same region of interest (ROI) before and after bleaching and FRET efficiency was calculated as:

$$E_{FRET} = \frac{D_{post} - D_{pre}}{D_{post}}$$

ROIs from non-bleached adjacent parts of the same cell and background were measured simultaneously for each experiment to ensure the specificity of the bleaching in the selected zone of the cell. When FRET was addressed in the membrane, measurement ROIs were defined to that portion of the cell.

Fluorescence Recovery After Photobleaching (FRAP)

Evaluation of protein dynamics and diffusion rates was assessed with Fluorescence Recovery After Photobleaching (FRAP). This technique allows to estimate global diffusion rates of the proteins of a membrane by measuring the recovery of fluorescence of a small region of membrane after a previous photobleaching on the fluorophores occupying this region (figure 3.5). Because molecules diffuse in two dimensions in the membrane and the initial fluorophores of the bleached region bleached are permanently off, the recovery of fluorescence in this region is proportional to the new molecules of the surrounding regions diffusing and occupying the bleached region (figure 3.5A). Theoretically, the faster this recovery of fluorescence occurs, the quicker diffusion kinetics of the molecules of interest. Furthermore, FRAP can be partial or total, determining the existence of an immobile fraction (figure 3.5B).

Figure 3.5. FRAP method. (A) Cells are locally bleached (ROI in white dashed circle). The area (t=0) is occupied by the diffusion of the surrounding molecules (t>0). (B) Example of a FRAP measurement (BK-Nt-SNAP+GluN1-CLIP/2B). The obtained recovery measurements (empty dots) were fitted to an exponential (teal curve). The plateau of this fitting determined the mobile and immobile fractions.

For FRAP measurements of BK channel - GluN dynamics in membranes, live cells expressing BK and GluN channels in different combinations were imaged using the FRAP module of the LASX software. In all the cases, the bleached fluorophore was attached to BK-Nt-SNAP construct (Surface Alexa Fluor 647). Because we used a fluorophore which is non-permeant, only the cell surface population was considered and effects of membrane insertion of newly synthesized protein was avoided. The protocol of FRAP was as follows: 10 frames at 0.5 Hz (baseline), high laser power bleaching of a region in the membrane, 200 frames at 1 Hz for fluorescence recovery tracking and 10 frames at 0.03 Hz to test the behavior after the recovery and calculate the plateau and immobile fraction. Recovery rates were calculated fitting an exponential function.

TIRF microscopy

Total Internal Reflection Fluorescence (or TIRF) microscopy allows visualization of membrane proteins by illumination of just a small portion of the sample close to the bottom of the glass surface where the sample is attached. The physical principle behind this is the regulation of the angle of the incident laser beam and the different refraction indexes of the materials to reach a total reflection of the light once hits the glass surface. The total reflection angle is called the *critical angle*. This phenomenon will create an evanescent wave of illumination, variable in depth depending on the laser and materials, but with a maximum depth of approximately 200 nm. Therefore, only fluorophores that are close enough to the glass surface are excited and membrane and surrounding environment, like endoplasmic reticulum or membrane-attached cytoskeleton, can be seen. For single molecule pull-down (SiMPull) and single molecule tracking experiments, a motorized Nikon Eclipse Ti microscope with a 100x (1.49NA) immersion objective. A laser unit with a DPSS 488 laser and fiber 647 nm was used. Stochastic Optical Reconstruction Microscopy (STORM) modules were coupled for superresolution microscopy (Nikon, Tokyo, Japan). Images were acquired with an Orca Flash 4.0 CMOS camera (Hamamatsu, Shizuoka, Japan) (figure 3.6).

Figure 3.6. TIRF and STORM superresolution microscope.

ments to find the critical angle for each wavelength. This setup was used in two different sets of experiments: STORM superresolution microscopy and single molecule pull-down.

STORM superresolution microscopy

STORM imaging was done using the microscope described above and a protocol previously set up and validated in our lab. Fixation and fluorescence reduction were done as previously described (Kshatri et al., 2020) without adding antibodies, since labelling made use of SNAPtag and CLIPtag. The imaging buffer used is described in table 3.11.

Table 3.11. STORM imaging buffer

Name	Final concentration
Tris pH 8	50 mM
NaCl	10 mM
Glucose	10%
β-mercaptoethylamine	100 mM
Glucose-oxidase	0.56 mg/ml
Catalase	34 µg/ml

Reconstructed images with Gaussian representation were generated from 2.5 x 104 acquired frames using NIS-Elements software (Nikon).

Single molecule Pulldown (SiMPull)

To study protein interactions at the single molecule level, as well as stoichiometries of association between BK channel and GluN receptors, we took advantage of the SiMPull approach coupled to step-photobleaching counting (Jain et al., 2011; Gutzeizt et al., 2019; Lee et al., 2020). It combines pull-down of protein complexes immobilized in a glass surface with single-particle resolution to be imaged under TIRF microscopy.

To perform these experiments, microfluidic chambers were homemade and ensembled the day of the experiment as follows (figure 3.7):

First step is to drill holes at both sides of the slide (figure 3.7, top view) with

a Dremel 3000 instrument and 0.75 diamond drill bits (#1-0500; Kingsley North,). After that, coverslips and slides glass surfaces were cleaned with a mixture of KOH, methanol and acetone under a sonication bath. After this process, coverslips and slides were treated with (3-Aminopropyl)-trimethoxysilane (APTMES) (#281778, Merck-MilliporeSigma, Munich, Germany) to functionalize the glass surface. To prevent non-specific interaction of molecules, the internal sides of the coverslip and slide, which are the ones that are going to face each other and form the channels of the microfluidic chamber, were passivated. Passivation consisted in the addition of mPEG (#MPEG-SVA-5000-1g; Laysan Bio Inc, Alabama, USA) to the surface of the slide to make it uncharged, avoiding unspecific interaction with proteins. Together with mPEG, PEG-biotin (#Biotin-PEG-SVA-5000-1g; Laysan Bio Inc, Alabama, USA) was added in a low proportion (1:40 approximately). A powder mixture of mPEG and PEG-biotin was dissolved in sodium bicarbonate solution (10 mM) and immediately added to the surfaces, putting coverslip on top of the slide and avoiding bubble formation. Reaction was incubated overnight in darkness. The result is that some sparsely molecules of biotin are facing up in the slide surface (figure 3.7). Coverslips were thoroughly washed with double distilled water, dried with filtered compressed air and storaged in a dessicator at -20 ºC up to 1 month after the preparation.

Figure 3.7. Single molecule pulldown workflow.

The day of the experiment, a chamber was assembled with double-sided tape to form the different channels and side sealed with two-components epoxy glue. Each channel was tested with T50 buffer (table 3.12) and after that, NeutrAvidin (#31000; Thermo Fisher Scientific, Massachusetts, USA) was added for 2 minutes to each channel. NeutrAvidin is a homotetramer with four binding sites for biotin. Therefore, when loaded in the chamber, it binds specifically biotin molecules from PEG-biotin. After incubation, each channel was washed with T50 three times.

Table 3.12. T50 buffer

Name	Final concentration
Tris pH 8	10 mM
NaCl	50 mM

A specific biotin-fused antibody against the bait protein (in our experiments we used anti-HA biotin antibody from Abcam, ab26228; table 3.8) was incubated into the channels at a 1/500 dilution in T50 buffer during 30 min (one channel was left without antibody for non-specific binding control). To remove unbound antibody, three washes with T50 were done per channel. The chamber was ready for imaging under

TIRF microscopy.

Cells were transfected with SNAP and CLIP-tag fused constructs the day before the experiment and labeled during 45 minutes in EX solution with specific dyes before the start of the chamber assembly protocol. The labelling was quickly checked under an epifluorescence microscope and cells were collected in PBS and centrifuged. Pellets were resuspended in a mild lysis buffer (table 3.13) and incubated in darkness during 1 hour at 4ºC in a nutating rocker. Afterwards, lysates were centrifuged 20 min (4ºC) at 13000 rpm and supernatant was kept as the sample for imaging. These samples were diluted with dilution buffer (1% lysis working buffer in EX) and loaded in the chambers starting from a more diluted condition and testing the particle density. Once optimal density was achieved, several washes with EX were performed to discard unbound particles.

Table 3.13. Lysis buffer stock *

Name	Final concentration
Tris pH 8	10 mM
NaCl	150 mM
EDTA	1 mM

* For 1 mL of working buffer (prepared fresh before the lysis):
987 μL Lysis buffer stock
1 μL Protease inhibitor (1000 x)
12 μL of IGEPAL (=1.2%)

Imaging was done under TIRF illumination and with the 100X oil immersion objective using the perfect focus system (PFS) from Nikon microscope (figure 3.6) to prevent particles from getting out of focus during the recording. Laser power was adjusted to each fluorophore to prevent fast photobleaching. 256x256 pixels movies were acquired at 200 Hz frequency (50 ms per frame) during 800 frames. Each movie consisted in a baseline dark period of 10 seconds and afterwards a laser illuminated period up to the end of the movie. In the cases of two-color conditions, the fluorophore with the longer excitation wavelength was recorded first to avoid any non-radiative energy transfer from a donor to acceptor pair.

Step photobleaching counting and analysis

Step-photobleaching relies on the random bleaching of fluorophores along time when they are excited. Because this randomness applies to each individual fluorophore, multiple fluorophores in an oligomeric protein (for example, the homotetramer of BK channel) will undergo multiple bleaching steps at different time points. Hence, representation of fluorescence intensity against time of each particle shows an "staircase" shape, where each step represents a bleaching event. In an ideal situation, with a close to a 100% percent of labelling efficiency of SNAP and CLIP constructs, the number of bleaching steps is directly proportional to the number of molecules that constitute the immobilized particle. Under two-color SiMPull, stoichiometries of association of two different proteins can be estimated (in our case, BK channels with GluN receptors).

Analysis of the recorded movies was done using a LabView (NI, Texas, USA) based analysis software provided by Prof. Joshua Levitz (Weill Cornell Medicine, New York, USA). In this program, each particle can be selected, fluorescence intensity traces can be analysed (with background subtraction) and the number of steps for each particle can be counted manually. A report of the particles from each movie, including the number of bleaching steps and coordinates of each particle, was exported to Prism (GraphPad, USA) where statistical analysis was performed. Representative traces of particles were also exported and graphed in the same software. Averages of the first 5 frames of illuminated spots were done in Image J and used as representative images.

Statistical analysis

Statistical analysis was performed using Prism 9 (Graphpad, California, USA). T-tests and ANOVA were used to extract the significance of the difference between two or more conditions respectively. Post-hoc tests were applied following the software recommendation to assess the significance values of the desired comparisons. A p-value <0.05 was considered statistically significant. In all figures *, **, *** indicate a $p < 0.05$, 0.01, 0.001 respectively. All the statistical methods selected, the comparisons performed, the level of significance and the output are described in the table A.II of *Annex II*.

Results & Discussion

Figure edition softwares

Prism 9 (GraphPad, California, USA) was used to plot graphs and current traces extracted from Clampfit (.

Chimera software, from Resource for Biocomputing, Visualization, and Informatics at the University of California, San Francisco (supported by NIH P41 RR-01081), was used for protein visualization, in silico unnatural amino acid mutagenesis (with SwissSideChain plugin; Gfeller et al., 2013) and distance calculations. Protein imager (Tomasello et al., 2020; https://3dproteinimaging.com/protein-imager/) was employed for protein representation.

Microscopy images and analysis were done in Image J (Fiji, USA). SiMPull was analysed using a LabView (NI, Texas, USA) based own-built program kindly gifted by Prof. Joshua Levitz (Weill Cornell Medicine, New York, USA).

Adobe Illustrator 2021 (Adobe, California, USA) was used to draw vectorially all the original schemes and diagrams of this work, as well as to mount and align the final figures.

PART 1: Ca^{2+}- INDUCED ACTIVATION MECHANISMS IN THE BK CHANNEL

Chapter 1: New insights on the molecular basis of Ca^{2+}-activation in the BK channel.

In this chapter of the thesis, we studied the activation mechanisms of the BK channel by Ca^{2+} ions. First, we studied the functional role of specific residues newly described in the full-length *Aplysia* (aBK) cryoEM structure (Tao et al., 2017; Hite et al., 2017) that were proposed to be involved in BK activation by Ca^{2+}. Secondly, we characterized the role of residues at protein-protein interfaces proposed to orchestrate channel activation by Ca^{2+} binding.

Our results unveil residues that had not been functionally characterized before in the human BK channel, showing an important contribution to channel activation. In addition, we demonstrate the relevance for the Ca^{2+} activation mechanism of an intrasubunit non-covalent interaction between two high-affinity Ca^{2+}-binding sites.

In order to avoid confusion and overweight the text, all the numerical results of fittings of this part are summarized in table 4.1. Main results and their interpretations are described.

Characterization of key residues in Ca^{2+} coordination and BK channel activation

In general, Ca^{2+} ions are coordinated by oxygen-containing side chains, carbonyl groups of amino acids backbones as well as water molecules. Consistent with this theory, the available structures from isolated *gating rings* as well as the full-length aBK[1] structure showed Ca^{2+} ions bound to oxygen atoms of amino acids at the Ca^{2+} bowl and RCK1 Ca^{2+} binding sites (Wu et al., 2010; Yuan et al., 2012; Tao et al., 2017). Among these, new residues were identified including aR503, aG523 and aE591 (hR514, hS533 and hS600) (figure 4.1) in the RCK1 site that had not been extensively studied in hBK. In the aBK structure, these residues coordinate Ca^{2+} through the main chain carbonyl oxygen atoms. We began our investigation by mutating all of these residues to alanine and tested the effects of increasing Ca^{2+} from 0 μM to 100 μM.

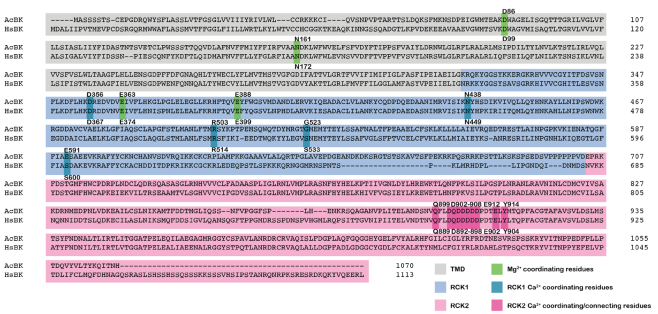

Figure 4.1. Ca^{2+} modulating residues of the BK channel. Comparison of sequence alignments between Aplysia californica (aBK) and Human (hBK) BK channels.

Coordinating residues N449 and R514 exert important roles in Ca^{2+} activation

Figure 4.2 shows representative current recordings from patches containing hBKα channels (BKwt) and the different mutants generated in this study, corresponding to voltage pulses ranging from -100 mV to +100 mV in 20 mV increments at different Ca^{2+} concentrations. The summary G-V curves are shown in Figure 4.3. The $V_{1/2}$ and slope values obtained for all mutants at various Ca^{2+} concentrations are listed in Table 4.1. As previously shown for wild-type hBKα channels (Latorre et al., 2017; Wei et al., 1994; Xia et al., 2002; Giraldez et al., 2005; Miranda et al., 2013; Webb et al., 2015), increasing Ca^{2+} from 0 to 100 μM led to larger outward K^+ currents due to a leftward shift in the $V_{1/2}$ (Figure 2A). We next evaluated the role of the hS533 and hS600A mutations in coordinating Ca^{2+} at the RCK1 site. As shown in Figures 4.2 and 4.3A,C-D, the Ca^{2+} sensitivity of the mutations hS533A and hS600A was undistinguishable from that of WT hBKα channels, indicating that the side chains of these two non-conserved residues are not involved in coordinating the Ca^{2+} ion in the human BK channel.

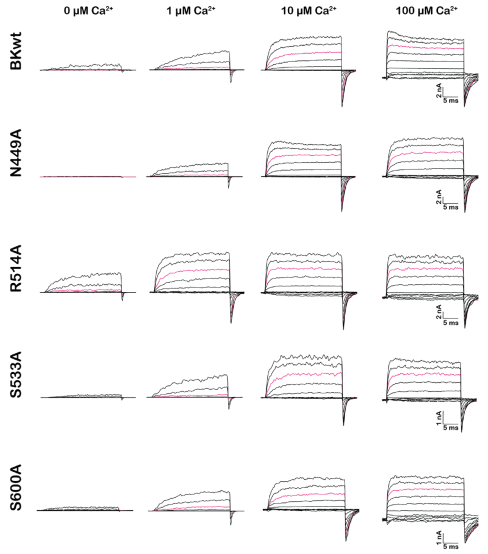

Figure 4.2. Representative current recordings of wild type hBKα and various mutations of proposed Ca^{2+} coordinating sites. The current traces were recorded after depolarizing the membrane to voltages ranging from −100 mV to +100 mV in 20 mV increments at different Ca^{2+} concentrations (1 μM, 10 μM and 100 μM). The mutation of serine residues (hS533A and hS600A) did not affect the Ca^{2+} sensitivity of the channels significantly compared to the BKα channels. However, the hN449 activated at more positive voltages in low Ca^{2+} (> +100mV) hR514A channels activated at less positive voltages (<+40 mV) compared to BKα channels. Currents recorded at +60 mV are highlighted in pink. Data corresponding to hR514A, hS533A and hS600A are published in Kshatri et al., 2018, see *Annex III.*

1 aBK: *Aplysia californica* BK channel; hBK: human BK channel. Residues labels referring to different BK channels are preceded by the letter of the species (e.g. hN449: human asparagine 449). If there is no specification, the labelling refers to human BK channel by default.

As shown in Figure 4.2A, the WT hBKα channels began to activate at around +80 mV in 0 Ca^{2+} ($V_{1/2}$ = 207 ± 3 mV, n=19). N449A, in contrast, exhibited a reduction in the voltage dependence of activation in the absence of calcium ions, as well as a shift to more positive potentials at lower Ca^{2+} concentrations (shallow slope in 0 μM Ca^{2+} and shifted curves for 0, 0.5 and 1 μM Ca^{2+}, Table 4.1, figure 4.3). Higher Ca^{2+} concentrations (5, 10 and 100 μM) were non-significantly rightward shifted. This results in an increased $\Delta V_{1/2}$ between 0 and 100 μM Ca^{2+}, indicating higher Ca^{2+} sensitivity of this mutant (figure 4.3B, F-G). In this Thesis, we further studied the relevance of this residue in the RCK-RCK2 intersubunit interaction using the photocrosslinker BzF experimental approach (see *Chapter 2: Photoactivation and crosslinking of residues to study Ca^{2+} activation*).

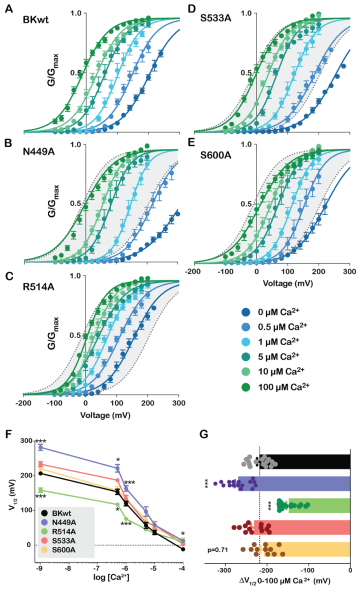

Figure 4.3. N449A and R514A altered Ca^{2+} sensitivity in opposite ways. (A-E) Mean conductance-voltage (G-V) relationships for various alanine mutations. (F) Summary of $V_{1/2}$ for the WT and the mutations at different Ca^{2+} concentrations. (G) Mean $\Delta V_{1/2}$ produced by 100 μM Ca^{2+} for all mutations.

Interestingly, the R514A mutation led to activation of the channels at voltages below +40 mV (figure 4.2, $V_{1/2}$ = 158 ± 6 mV, n=16, p<0.001). Although this mutant is still sensitive to increasing Ca^{2+} concentrations, the apparent Ca^{2+} sensitivity in higher Ca^{2+} (5 μM - 100 μM) was significantly reduced compared to the WT hBKα channels as is noticeable from its compressed G-V relationship and the mean $\Delta V_{1/2}$ summary (figure 4.3A,C&G). The R514A mutant left shifted the $V_{1/2}$ in 0 Ca^{2+} and decreased the Ca^{2+} sensitivity to higher Ca^{2+} concentrations without affecting the slope of G-V curves significantly (Table 4.1).

Is the hR514A mutation affecting the Ca^{2+} sensitivity of the RCK1 site directly or the RCK2 Ca^{2+} bowl site indirectly?

The magnitude of the shift in the $V_{1/2}$ induced by high Ca^{2+} concentrations (5 μM–100 μM) was significantly reduced in the R514A mutation (figure 4.4A–C). To precisely distinguish the region that is affected by mutating the R514 residue, we used a double mutation approach. One assumption is that, if R514A is acting independently of the RCK1 high-affinity Ca^{2+}-binding site, mutation of an additional residue in this site, such as D367, should have additive effects; if they were both part of the same Ca^{2+}-binding site (RCK1), the effect of both mutations would not be additive. To test this hypothesis, we mutated D367 to alanine (RCK1 Ca^{2+} binding site, [Xia et al., 2002]) in combination or not with R514A. Consistent with previous studies (Zhang et al., 2010; Bao et al., 2002), the single mutation D367A lowered Ca^{2+} sensitivity of BKα channels by approximately 50% (figure 4.4D). Double mutant D367A+R514A exerted effects that are comparable to single mutant D367A. The double mutant showed an apparent tendency towards higher sensitivity to lower [Ca^{2+}] and lower sensitivity to higher [Ca^{2+}] than the D367A construct (figure 4.4E). However, statistical analysis of the data shows no significant differences between the apparent shifts induced by 100 μM Ca^{2+} in D367A and D367A + R514A ($\Delta V_{1/2}$ =–89 ± 5 mV and $\Delta V_{1/2}$= –78 ± 7 mV, respectively), whereas both were significantly different to the WT hBKα channels ($\Delta V_{1/2}$ = 218 ± 6 mV; figure 4.4F). To further test our hypothesis, we next mutated the RCK2 Ca^{2+} bowl to alanine (D894 through D899, mutant 5D5A) in combination or not with the R514A mutation. If R514A affects only the RCK1 binding site, as suggested by the previous experiment, we would expect that the combination of both mutations (R514A + 5D5A) would additively reduce the Ca2+ response. Figure 4.4G displays the effect of increasing Ca^{2+} on the 5D5A mutation. In agreement with previous studies (Bao et al., 2002), this mutation diminished the Ca^{2+} sensitivity at lower μM ranges

Figure 4.4. Mutation of R514A affects the RCK1 Ca2+ dependent response. (A–C), Effects of the R514A mutation on hBKα channels. Only the shift in $V_{1/2}$ induced by 5 µM–100 µM Ca^{2+} is significantly reduced in this mutation. (D-E) G-V curves for the D367A and D367A+R514A mutations. The non-additive effects of this mutation suggest that they both are part of the same Ca^{2+} binding site. (G-H) Effects of mutations 5D5A and R514A + 5D5A. The double mutation lowers the Ca^{2+} sensitivity in an additive manner. (F) Average $V_{1/2}$ as a function of $[Ca^{2+}]$ for all the mutations (I) $\Delta V_{1/2}$ at 100 µM Ca^{2+}. *(Modified from Kshatri et al., 2018).*

(0 µM–1 µM) whereas at the intermediate and higher µM Ca^{2+} ranges (5-100 µM) Ca^{2+} sensitivity was only partially affected. Interestingly, the double mutation, R514A + 5D5A (figure 4.4H) reduced the hBKα Ca^{2+} sensitivity considerably more than either of the mutations alone. In fact, this double mutant showed almost no response to Ca^{2+} between 5 µM–100 µM and also its $V_{1/2}$ appeared left-shifted similar to the other RCK1 site mutations (figure 4.4I). The $\Delta V_{1/2}$ value in 100 µM Ca^{2+} for this mutation was significantly reduced by 60% (−87 ± 5 mV, n = 9 vs. −218 ± 6 mV, n = 17 in hBKα), which was significantly higher than the 32% ($\Delta V_{1/2}$ = −148 ± 6 mV, n = 16) and 22% ($\Delta V_{1/2}$ = 169 ± 6 mV, n =3) reduction in the R514A and 5D5A mutants respectively (figure 4.4F). Taken together, these results suggest that R514A affects BK Ca^{2+} sensitivity by directly disrupting the RCK1 binding site.

Mutation of the R514-E902-Y904 bridging-residues selectively diminish the Ca^{2+} response mediated by the RCK1 site

We then examined the effects of mutating two residues hE902 and hY904, which in the full-length aBK structure are shown to interact directly with the side chain of the R514 residue at the RCK1 site, and indirectly with the Ca^{2+} bowl site via the loop (Tao et al., 2017) (figure 4.5A). The resulting summary G-V relationships are shown in figure 4.5B-I. The mutation of E902A failed to alter the effects of Ca2+ at all concentrations tested (figure 4.5D, H & I). In contrast, the Y904A mutation significantly reduced the Ca^{2+} sensitivity of the channel at 100 µM Ca^{2+} (figure 4.5E & I). Moreover, this mutation also affected the voltage dependence of the channel similarly to hR514A ($V_{1/2}$ = 158 ± 6 mV, n =16). In this case, $V_{1/2}$ at 0 Ca^{2+} is significantly left-shifted ($V_{1/2}$ = 162 ± 4 mV, n = 6) when compared to WT hBKα channels ($V_{1/2}$ = 207 ± 4 mV, n = 19). Interestingly, the reduction in the Ca^{2+} response of Y904A mutant was further enhanced with the double mutation E902A + Y904A (figure 4.5F). Moreover, the G-V curves appear more compressed than the individual mutations (figure 4.5D-E) as well as the WT (figure 4.5B). The $\Delta V_{1/2}$ in 100 µM Ca^{2+} was reduced approximately by 50% compared to WT hBKα channels (figure 4.5I). Remarkably, the triple mutation involving R514A + E902A + Y904A (figure 4.5G) induced a moderately lower reduction that was not statistically significant (p =0.36, Student's t-test) to that of E902A + Y904A channels. The $V_{1/2}$ vs. $[Ca^{2+}]$ dependence was also identical for these mutations (figure 4.5H), suggesting that these residues are part of the same transduction pathway involving the RCK1 site.

It is important to remark that the cation-π interaction described in the structure between R514 and Y904 seems to be crucial in this bridge stabilization because Y904A causes an effect of its own which is not seen in the E902A. This was the main reason why we decided to explore deeper and modify this interaction through cation-π amino acid substitutions.

Figure 4.5. The side chains of E902, Y904 & R514 are essential for Ca^{2+} sensing in the RCK1 site. (A) Position of residues R514-E902-Y904 residues in the human BK channel structure (Tao et al., 2019; PDB:6V38). Mean G-V curves determined for (B) BKα (C) R514A (D) E902A (E) Y904A (F) E902A +904A (G) R514A+ E902A + Y904A. The double mutation E902A + Y904A additively reduced the response to Ca^{2+}. The addition of R514A to this double mutation did not further decrease the Ca^{2+} response. (H) Mean $V_{1/2}$ summary as a function of $[Ca^{2+}]$. (I) Shift in $V_{1/2}$ induced by 100 μM Ca^{2+}. (*Modified from Kshatri et al., 2018*).

Effects of the mutations on free energy

Our results show that some of the mutations studied reduce the Ca^{2+} dependence of activation of the hBK channel. These effects could be due to alterations in the Ca^{2+} binding/transduction pathway or to a modification in voltage sensing. To distinguish more precisely which of these effects may be affected, we evaluated the free energies ($\Delta\Delta G_0$) from the Boltzmann fits to the data (see *Materials and Methods*). The mean $\Delta\Delta G_0$ in response to 100 μM Ca^{2+} and the relative percent reduction for the Ca^{2+} sensitivity-reducing mutations is shown in figure 4.6. The $\Delta\Delta G_0$ (100 μM Ca^{2+}) in WT hBKα was 13.11 ± 0.63 kJ/mol (n =17). Consistent with the reduced $\Delta V_{1/2}$, the R514A mutation also significantly reduced the free energy difference by 30%. The $\Delta\Delta G_0$ of the double mutation, D367A+R514A was not additive, suggesting that these sites are not influencing each other. However, the R514A + 5D5A mutant displayed strict additivity (% reduction: R514A - 32%, 5D5A - 27%, R514A + 5D5A - 64%) indicating that both regions are acting independently in sensing Ca^{2+}. Interestingly, the E902 + Y904A double mutant also showed an additive effect, ($\Delta\Delta G_0$ ~ 40%), whereas the effect on $\Delta\Delta G_0$ of the triple mutation (R514A + E902A + Y904A) was identical to the double E902A + Y904A mutation. Taken together, these data indicate that the reduction in Ca^{2+}-induced $V_{1/2}$ of the mutations is potentially due to an alteration in the Ca2+ binding/transduction pathway/s of the channel.

Figure 4.6. Energetic effects of the mutations. (Left) $\Delta\Delta G_0$ of mutations in response to 100 μM Ca^{2+}. (Right) Positioning of the mutants in the structure did not show any pattern related to the changes in energy (color code in the legend. All mutations with the exception of E902A and Y904A displayed significant reductions in $\Delta\Delta G_0$. Only the double mutations R514A+-5D5A and E902A+Y904A are quantitatively additive in reducing the $\Delta\Delta G_0$ of 100 μM Ca^{2+}. (*Modified from Kshatri et al., 2018*).

Figure 4.7F-G shows $\Delta V_{1/2}$ and $\Delta\Delta G_0$ values calculated these mutants. Not surprisingly, $\Delta V_{1/2}$ was significantly altered in the R514K and Y904W mutants. However, in the case of $\Delta\Delta G_0$, only the latter showed a significant reduction, linking the mutation effect to a Ca^{2+} binding impairment (possibly in the transduction pathway to pore opening). R514K showed a trend towards reduced values. The statistical analysis rendered a p-value close to a standard significance threshold of $p<0.05$ ($p\approx0.07$), but the small number of experiments (n=4) was not sufficient to conclude a strong effect on free energy.

A cation-π interaction between R514 and Y904 is crucial for the intrasubunit communication between both high-affinity Ca^{2+} binding sites

Encouraged by our previous results showing that the cation-π interaction between R514 and Y904 was important in the Ca^{2+} transduction pathway, we decided to mutate sequentially these two residues to those that can be involved in cation-π interactions in proteins (cation: lysine, K; aromatic residue: phenylalanine, F; tryptophan, W (Gallivan and Dougherty 1999; Dougherty, 2007). Theoretically, arginine to lysine mutation (R to K) modifies completely the guanidinium group from arginine (NH-(NHR)NH2) to a terminal amino group. In both residues there is a protonation under physiological pH. In the specific case of the BK channel, we hypothesized that R514K limits the interaction with E902 or Y904 producing an impaired channel function. In concordance with this hypothesis, R514K showed a striking overall shift to more negative voltages than the WT and R514A (figures 4.7B,E-F). This would match with a premise where a weaker interaction in this interface would lead to faster activation of the channel but reduced Ca^{2+} sensitivity, which constitutes a plausible negative intrasubunit cooperativity mechanism (see *Discussion*).

In the case of tyrosine to phenylalanine mutation (Y904F), the π-electron cloud would be homogenous and more stable in the phenylalanine in comparison to the tyrosine, where oxygen higher electronegativity pulls the electron cloud density towards this part of the ring. This mutant had little effect in the Ca^{2+} sensitivity of the channel ($V_{1/2}$ vs Ca^{2+} almost overlaps with that of the WT channel, figure 4.7C,E). In contrast, we observed an apparently strong effect in slowing down the deactivation (tail currents) of the channel in higher Ca^{2+} concentrations (figure 4.7C). This mutant also showed slightly slower activation kinetics that were not significantly different from the WT (data not shown). This data suggested that this change of the cation-π interaction does not alter the Ca^{2+} binding of the channel but its transduction to the pore, stabilizing the open conformation of the channel.

Lastly, the double aromatic ring of tryptophan makes its unlocalized electron cloud larger, and consequently, the Y904W mutation, in combination with the guanidinium group (from the arginine), would strengthen the interaction between 514 and 904 residues. In fact, it evoked a slight shift of the voltage dependence to more negative voltages in the absence of Ca^{2+} but a dramatic reduction on the Ca^{2+} sensitivity (figure 4.7D-F).

Table 4.1. Boltzmann fit parameters for the BKα and mutant channels. For $V_{1/2}$ and z, mean ± SEM is represented.

$[Ca^{2+}]_i$	Mutant	$V_{1/2}$	z	N
0 μM Ca^{2+}	BKwt	207 ± 5 mV	0.59 ± 0.02	19
	D367A	167 ± 2 mV	0.80 ± 0.05	10
	5D5A	210 ± 2 mV	0.63 ± 0.06	5
	N449A	282 ± 6 mV	0.61 ± 0.02	16
	R514A	159 ± 2 mV	0.62 ± 0.02	16
	S533A	257 ± 3 mV	0.61 ± 0.03	13
	S600A	224 ± 5 mV	0.62 ± 0.04	12
	E902A	234 ± 4 mV	0.64 ± 0.05	6
	Y904A	166 ± 2 mV	0.57 ± 0.04	6
	D367A + R514A	127 ± 2 mV	0.73 ± 0.03	5
	R514A + 5D5A	174 ± 2 mV	0.76 ± 0.03	9
	E902A + Y904A	152 ± 2 mV	0.7 ± 0.04	7
	R514A + E902A + Y904A	131 ± 3 mV	0.73 ± 0.06	7
	R514K	129 ± 7 mV	0.7 ± 0.08	4
	Y904F	186 ± 10 mV	0.7 ± 0.05	6
	Y904W	156 ± 5 mV	0.77 ± 0.05	7
0,5 μM Ca^{2+}	BKwt	147 ± 2 mV	0.67 ± 0.02	9
	D367A	134 ± 1 mV	0.83 ± 0.06	5
	5D5A	174 ± 2 mV	0.68 ± 0.07	4
	N449A	218 ± 3 mV	0.66 ± 0.04	9
	R514A	112 ± 2 mV	0.59 ± 0.03	10
	S533A	189 ± 2 mV	0.61 ± 0.06	7
	S600A	156 ± 3 mV	0.79 ± 0.04	12
	E902A	158 ± 4 mV	0.64 ± 0.05	6
	Y904A	98 ± 3 mV	0.58 ± 0.04	6
	D367A + R514A	99 ± 3 mV	0.72 ± 0.05	5
	R514A + 5D5A	143 ± 2 mV	0.78 ± 0.03	9
	E902A + Y904A	96 ± 4 mV	0.61 ± 0.04	4
	R514A + E902A + Y904A	78 ± 2 mV	0.71 ± 0.04	7
	R514K	102 ± 11 mV	0.73 ± 0.1	3
	Y904F	165 ± 10 mV	0.6 ± 0.05	6
	Y904W	133 ± 9 mV	0.74 ± 0.03	6
1 μM Ca^{2+}	BKwt	101 ± 3 mV	0.7 ± 0.05	9
	D367A	113 ± 2 mV	0.83 ± 0.06	10
	5D5A	149 ± 2 mV	0.76 ± 0.07	4
	N449A	148 ± 3 mV	0.83± 0.02	14
	R514A	74 ± 2 mV	0.66 ± 0.03	13
	S533A	125 ± 3 mV	0.76 ± 0.05	10
	S600A	117 ± 3 mV	0.78 ± 0.06	12
	E902A	113 ± 3 mV	0.73 ± 0.07	6
	Y904A	62 ± 3 mV	0.65 ± 0.04	6
	D367A + R514A	77 ± 2 mV	0.83 ± 0.05	5
	R514A + 5D5A	119 ± 3 mV	0.89 ± 0.04	7
	E902A + Y904A	68 ± 4 mV	0.69 ± 0.05	7

Figure 4.7. R514K and Y904W mutants showed diminished Ca^{2+} sensitivity. (A-D) Representative current traces from -100 to +100 mV and summary mean G-V relationship for the WT and the three different mutants. Currents recorded at +60 mV are highlighted in pink. (E) Mean $V_{1/2}$ summary as a function of $[Ca^{2+}]$. (F) Shift in $V_{1/2}$ induced by 100 μM Ca^{2+}. (G) Energetic effect of the mutants. R514K and Y904W caused a noticeably effect in the Ca^{2+} sensitivity. Y904F overlapped with the WT, however, its deactivation kinetics seems to be slower than the WT (A vs C).

	R514A + E902A + Y904A	61 ± 2 mV	0.96 ± 0.04	5
	R514K	68 ± 9 mV	0.8 ± 0.09	2
	Y904F	123 ± 13 mV	0.68 ± 0.05	5
	Y904W	117 ± 2 mV	0.75 ± 0.02	7
5 μM Ca^{2+}	BKwt	56 ± 3 mV	0.74 ± 0.02	19
	D367A	97 ± 3 mV	0.84 ± 0.04	5
	5D5A	108 ± 3 mV	0.72 ± 0.07	4
	N449A	84 ± 2 mV	0.77 ± 0.06	7
	R514A	50 ± 3 mV	0.62 ± 0.04	8
	S533A	68 ± 3 mV	0.72 ± 0.05	6
	S600A	72 ± 4 mV	0.77 ± 0.05	12
	E902A	75 ± 3 mV	0.90 ± 0.07	7
	Y904A	25 ± 4 mV	0.83 ± 0.07	6
	D367A + R514A	74 ± 2 mV	0.9 ± 0.07	7
	R514A + 5D5A	98 ± 3 mV	0.86 ± 0.04	7
	E902A + Y904A	41 ± 3 mV	0.68 ± 0.06	4
	R514A + E902A + Y904A	44 ± 3 mV	0.85 ± 0.05	7
	R514K	46 ± 16 mV	0.65 ± 0.15	4
	Y904F	66 ± 5 mV	0.67 ± 0.03	4
	Y904W	123 ± 8 mV	0.72 ± 0.03	7
10 μM Ca^{2+}	BKwt	32 ± 3 mV	0.69 ± 0.02	16
	D367A	86 ± 2 mV	0.91 ± 0.04	10
	5D5A	82 ± 2 mV	0.8 ± 0.06	5
	N449A	57 ± 2 mV	0.7 ± 0.03	11
	R514A	31 ± 3 mV	0.72 ± 0.04	14
	S533A	41 ± 3 mV	0.65 ± 0.03	10
	S600A	49 ± 3 mV	0.72 ± 0.03	12
	E902A	53 ± 3 mV	0.86 ± 0.06	6
	Y904A	8 ± 4 mV	0.82 ± 0.06	5
	D367A + R514A	72 ± 2 mV	0.88 ± 0.04	5
	R514A + 5D5A	91 ± 2 mV	0.99 ± 0.03	7
	E902A + Y904A	36 ± 3 mV	0.78 ± 0.03	7
	R514A + E902A + Y904A	37 ± 3 mV	0.85 ± 0.04	7
	R514K	20 ± 5 mV	0.6 ± 0.08	7
	Y904F	46 ± 5 mV	0.73 ± 0.06	8
	Y904W	99 ± 7 mV	0.7 ± 0.05	7
100 μM Ca^{2+}	BKwt	-13 ± 5 mV	0.72 ± 0.02	17
	D367A	78 ± 2 mV	0.83 ± 0.02	10
	5D5A	33 ± 2 mV	0.88 ± 0.07	6
	N449A	12 ± 5 mV	0.72 ± 0.02	16
	R514A	7 ± 2 mV	0.8 ± 0.03	16
	S533A	2 ± 5 mV	0.66 ± 0.01	13
	S600A	18 ± 7 mV	0.73 ± 0.02	12
	E902A	12 ± 5 mV	0.85 ± 0.08	6
	Y904A	-18 ± 6 mV	0.85 ± 0.05	6
	D367A + R514A	69 ± 2 mV	0.87 ± 0.08	5
	R514A + 5D5A	88 ± 2 mV	0.92 ± 0.03	9
	E902A + Y904A	29 ± 4 mV	0.81 ± 0.05	7
	R514A + E902A + Y904A	26 ± 4 mV	0.95 ± 0.03	7
	R514K	-33 ± 9 mV	0.52 ± 0.04	5
	Y904F	-3 ± 4 mV	0.7 ± 0.09	6
	Y904W	65 ± 8 mV	0.77 ± 0.04	6

Chapter 1: Discussion

Structure determination of proteins is essential for understanding the molecular and atomistic basis underlying their function. The ion channel field is experiencing a revolution after cryo-EM appearance, which, overcoming X-ray crystallography problems with membrane protein structure determination, has exponentially unveiled numerous structures of ion channels during the last years under different activation, inactivation and blocking conditions. However, the validation of these structures and correlation with functional data is extremely important for two key reasons: (1) most of the structures are obtained in extreme conditions to ensure a major proportion of certain states (e.g. unliganded or liganded channels) and represent snapshots of the total number of rearrangements that could happen in a protein; (2) in the structure determination there is no voltage applied, which represents a clear limitation to understand the mechanisms underlying voltage gated ion channels' function.

In this study, we have validated in the hBK channel the functionality of the high affinity Ca^{2+} binding sites identified in the aBK channel cryo-EM structure (Tao et al., 2017; Hite et al., 2017). Although the aBK channel sequence is only ≈60% similar to that of human BK, our functional data suggest that the conserved Ca^{2+} binding sites are essentially identical in both species. This was corroborated by the publication of the full-length human BK channel structures in both Ca^{2+}-free and Ca^{2+}-bound states, (Tao et al., 2019). These structures show that, at the RCK1 site, Ca^{2+} ion is coordinated by five residues, two of which are not conserved. In the presence of the Ca^{2+} ions, the side chains of conserved residues hD367, hR514 and hE535 tilt inwards towards the Ca^{2+} binding site to cradle the ion (Zhou et al., 2017; Tao et al., 2019). At the Ca^{2+} bowl site, the side chain of hD897 changes its conformation significantly providing a binding site for the Ca^{2+} ion. Interestingly, the hN449 barely moves from its position pointing to this binding-site, whereas the α-helix where this residue is integrated rotates and moves up after Ca^{2+} binding, serving hN449 residue a pivotal position

for this movement (Zhou et al., 2017; Tao et al., 2019). Additionally, the side chain of hY904 moves closer to the RCK1 site in the presence of Ca^{2+} (Hite et al., 2017; Tao et al., 2019). In the human BK channel, the side chains of two non-conserved serine residues (hS533 and hS600) did not appear to have a functional role in Ca^{2+} sensing. However, our results do not discard the possibility that they coordinate Ca^{2+} with their backbone carbonyl oxygens, as showed by the structure.

N449 exerts a key function coordinating Ca^{2+} in the Ca^{2+} bowl and transducing the signal to the pore

The N449 residue is located at the interface of RCK1 and the *calcium bowl* of the adjacent subunit and proposed to coordinate Ca^{2+} (Wu et al., 2010; Yuan et al., 2012; Tao et al., 2017). Vouga and Rothberg proposed a role of this residue in the mouse BK as an intersubunit connecting residue between the RCK1 and RCK2 Ca^{2+} binding sites (Vouga and Rothberg, 2017). When mutated to alanine, this residue reduced the Ca^{2+} sensitivity at all the Ca^{2+} concentrations tested. However, in the absence of Ca^{2+}, the G-V activation curve was comparable to WT. Li et al. (2018, in collaboration with Rothberg group) reported that in the human BK channel, the same point mutation, N449A, produced no significant changes in Ca^{2+} sensitivity but a rightward shift for all the Ca^{2+} concentrations tested. With this result, they concluded that N449 has a role in Ca^{2+} coordination but does not mediate Ca^{2+} sensitivity (Li et al., 2018). In agreement with Li et al., in our hands the N449A showed a clear shift to positive potentials for all the Ca^{2+} concentrations tested. However, in the absence of Ca^{2+} and contrary to their data, we observed a significantly larger shift ($V_{1/2}$: WT = 207 ± 5 mV; N449A = 282 ± 6 mV). This led us to conclude that the Ca^{2+} sensitivity was increased (figure 4.3G). Therefore, N449 is not only important as a coordinating residue but also seemed to mediate the Ca^{2+} sensitivity and the interface assembly between RCK1 and RCK2′ (in the adjacent subunit). The importance of this residue and the interface assembly in the overall function of the BK channel was further studied using unnatural amino acid photocrosslinkers (see *Chapter 2: Photoactivation and crosslinking of residues to study Ca^{2+} activation*).

R514 coordinates Ca^{2+} in the RCK1 site and serves as an intrasubunit connection between Ca^{2+} binding sites

Using molecular modelling, Zhang et al. proposed the backbone carbonyl goup oxygen of the R514 residue coordinates the Ca^{2+} ion on the RCK1 site (Zhang et al., 2010). This was confirmed by the full-length aBK structure (Tao et al., 2017). However, Zhang et al. did not provide functional data about the gating behavior of the R514 mutation due to the fact that only its main-chain carbonyl oxygen atom participates in Ca^{2+} coordination, so no large effectes on Ca^{2+} sensitivity were expected. Bukiya et al. (2014) reported that hR514 is an important residue for ethanol sensing, since it provides net positive charge to favor ethanol-BK interaction. Additionally, that study showed that R514N mutation increased the NPo of the channels, leftward shifted the G-V curves and significantly reduced the sensitivity to 100 μM Ca^{2+} (Bukiya et al., 2014). Our results with the R514A are consistent with their study since neutralizing the positive charge also shifted the G-V curves leftwards. In addition, R514A displayed a significant reduction in the Ca^{2+}-dependence response between 5 μM - 100 μM Ca^{2+}) as can be inferred by the compressed G-V relationships presented in our study. The G-V compression observed in R514A mutant could be mainly attributed to altered Ca^{2+} binding but not voltage-sensing due to the following reasons: (1) the steepness of G-V curves in the absence and presence of Ca^{2+} (table 4.1) is not significantly different when compared to WT hBKα; (2) the mutation decreased the $\Delta\Delta G_0$ in higher Ca^{2+} by > 30%, suggesting that either a reduction in Ca^{2+} binding affinity or number of Ca^{2+} binding sites has occurred. However, we cannot rule out the possibility that this mutation destabilizes the RCK1 Ca^{2+} binding site, exerting a similar role than its neighbouring residue hM513, which was proposed to maintain the structural integrity of the RCK1 site (Wu et al., 2010). A direct biochemical approach, using a $^{45}Ca^{2+}$ gel overlay to BKα and hR514A mutant channels would give more information about Ca^{2+} binding to the RCK1 site using this assay (Bao et al., 2002; Bian e t al., 2001; Braun and Sy, 2001).

We confirmed the structural insight that R514 is connected with E902 and Y904, mediating an intrasubunit connection between both Ca^{2+} binding sites. This connection is conserved in *Aplysia* and human structures (figure 4.1; Hite et al., 2017; Tao et al., 2019). Bao et al (2004) previously reported that E902A and Y904A did not alter the Ca^{2+} response, assessed by comparing the G-V shifts induced by 10 μM Ca^{2+} (Bao et al., 2004). Our data is in agreement with this study, since we did not observe any alteration in that concentration (table 4.1). However, disruption of the cation-π interaction between R514 and Y904 significantly reduced the response to 100 μM Ca^{2+} (figure 4.5). This effect showed an additive reduction in the E902A+Y904A double mutant that was not further increased in the triple R514A+E902A+Y904A. Our results

support the hypothesis raised by Hite et al. suggesting that this interaction constitutes a structural mechanism underlying cooperativity between the RCK1 Ca^{2+} binding site and the Ca^{2+} bowl regions (Hite et al., 2017).

Fine-tuning of the cation-π interaction between R514 and Y904 corroborated a clear importance of this interaction in the Ca^{2+} activation mechanism of the BK channel. Interestingly, neutralization of one of the arginine charges in the R514K mutant speeded up the activation kinetics of the channel at 100 μM Ca^{2+} and significantly leftward shifted all the G-V relationships (figure 4.7). In the case of Y904F, where a more unlocalized electron cloud density was expected, the G-Vs were comparable to WT, however, the deactivation kinetics were slowed down (figure 4.7). Even more interesting was the result with the Y904W mutant: a drastically reduced Ca^{2+} sensitivity as well as a shift to the left in lower Ca^{2+} to achieve an almost flat $V_{1/2}$ vs log [Ca^{2+}] relationship (figure 4.7E). In this case, a stronger cation-π interaction is expectable according to the tryptophan double ring structure. Overall, these data suggest that the stronger the cation-π interaction, the smaller the Ca^{2+} sensitivity (case of Y904W). Additionally, weakening this connection (R514K and Y904F), the kinetics of the channel were altered towards higher activation. Thus, it is tempting to think that this interaction could underlie a negative intrasubunit cooperativity between both Ca^{2+} binding sites, which would be in agreement with Sweet and Cox and Savalli et al. works (Sweet and Cox, 2008; Savalli et al., 2012). Nevertheless, previous studies have shown that the interpretation of cation-π mutagenesis within protein structures is complex, due to tangled hydration, electrophilic and hydrophobic microenvironments close to the residues involved. Moreover, a cation-π interaction only takes place in the case of a suitable perpendicular interface between the aromatic ring and the cation (Dougerthy, 1996; Dougerthy et al., 1999), forcing us to consider the reorientation caused by the punctual mutations used in these experiments. Therefore, while we can convincingly argue that these data brought out the importance of R514-Y904 interaction, unveiling a crucial functional interaction, we are aware that these results should be interpreted with caution. We are currently finishing the kinetics experiments of this last part and the adjustment to the H-A model of the data to conclude the constants affected by these intriguing mutants.

Chapter 2: Photoactivation and crosslinking of residues to study Ca^{2+} activation

To study the structural rearrangements of the BK channel involved in activation by Ca^{2+} as well as the interfaces of interaction between domains playing a role in this process, we implemented in the lab the unnatural amino acid approach for incorporation of photoactivatable BzF. This allowed us to perform *in vivo* crosslinking between these domains.

We generated a library of 14 mutants including the Amber codon (see *Methods*) on two background plasmids, BK667YFP and BK860YFP. These constructs are fluorescent protein fusions previously characterized (Giraldez et al., 2005; Miranda et al., 2013; Miranda et al., 2016; Miranda et al., 2018). This allowed us to quickly assess the Amber suppression by BzF incorporation. Locations for insertion of photocrosslinkable amino acids was rationally designed. Two positions (F160TAG and Y163TAG) were located into the VSD to potentially lock its movement and isolate the Ca^{2+} transduction pathway to pore opening in a voltage independent manner. The other residues were selected in the different interaction interfaces between RCK domains or RCK with transmembrane domains. Therefore, F223TAG, Y332TAG, Y336TAG, H379TAG, H394TAG and F395TAG were selected to study activation pathway through S6-RCK1 or VSD-RCK1 αB helix interfaces. F315TAG was selected due to its location in the pore cavity in order to generate a mutant that could selectively alter the pore function without disturbing directly its permeability. On the other hand, N449TAG-Y450TAG and R786TAG-R790TAG were selected to generate an intersubunit crosslinking between RCK domains in the different RCK1-RCK2′ and RCK2-RCK2′[2] interfaces respectively described by the structure. Finally, H667TAG was used as a negative control because is a residue that would point outside the protein and in principle would not generate huge effects under photocrosslinking (as it did not do under fluorescent protein insertion, Giraldez et al., 2005; Miranda et al., 2013; Miranda et al., 2016; Miranda et al., 2018) (figure 4.8A; H667 is not shown because it was not solved in the structure).

2 RCK2′ is used here to clarify the intersubunit interaction between RCK1 or RCK2 from one subunit and the RCK2 from the adjacent subunit.

BK-TAG mutants exhibited specific insertion of BzF amino acid and retained most of the WT features

From the 14 mutants of the library, 12 of them showed full length protein recovery (figure 4.8B), under BzF-incubated conditions, indicating a specific and high yield incorporation of the photocrosslinker. F160BzF and F315BzF did not show protein expression and were not further studied.

The 12 mutants were expressed. All of them were validated for function and most of them for Ca^{2+} sensitivity, two crucial elements to rely on our mutants as a tool to study the mechanisms of activation by this divalent cation. Successfully, all of them showed outward potassium currentswith Ca^{2+} sensitivity. Interestingly, insertion of BzF produced a dramatic effect in the G-V curves slopes of some constructs, as well as in their Ca^{2+} sensitivity (figure 4.9B-C, Y163BzF, F223BzF). This suggests a role of these residues in activation mechanisms of the BK channel, where the insertion of a bulkier and chemically different amino acid alters the overall function of the channel. Figure 4.9C summarizes the $V_{1/2}$ vs log[Ca^{2+}] relationships for the Ca^{2+} concentrations tested for the WT and four representative mutants (two altered and two similar to WT).

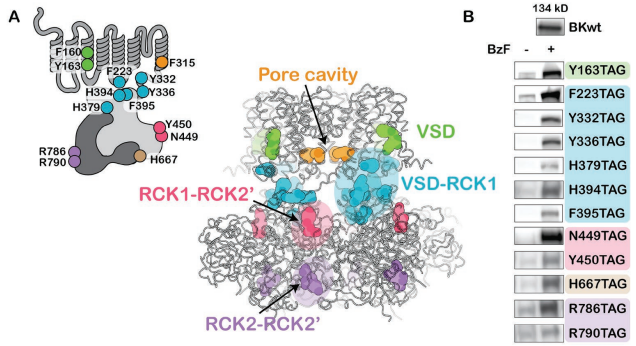

Figure 4.8. BK-BzF mutants rendered full-length proteins only under BzF incubated conditions. (A) Schematic diagram and structure location of the different residues selected for this study. (B) Western blot of the Amber suppression and full-length protein recovery in presence of BzF. F160TAG and F315TAG did not show protein expression.

Out of the 12 mutants generated, N449BzF, Y450BzF, R786BzF and R790BzF exhibited functional effects under UV light (figure 4.9B,D). Therefore, we decided to study in depth the role of these residues in the intersubunit interfaces of the BK channel under different protocols and Ca^{2+} concentrations.

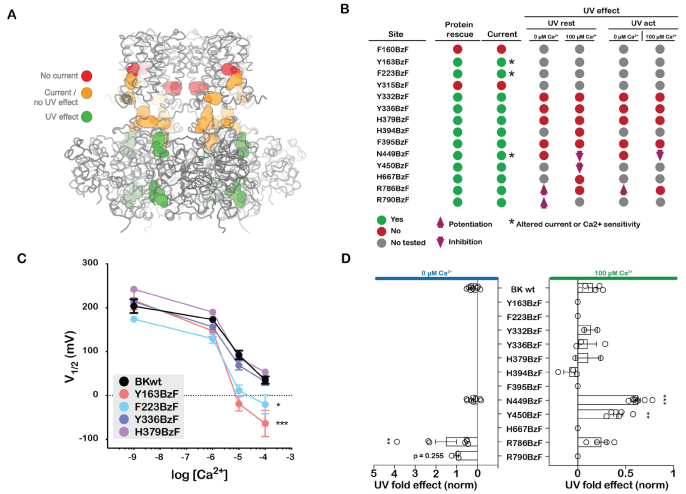

Figure 4.9. Summary of BK-BzF mutants function and UV-specific effects. (A) Location of the residues in the BK channel. Only in the intersubunit interfaces between RCKs a UV-specific effect was observed. (B) Summary table of mutants characterization. (C) Mean $V_{1/2}$ vs log[Ca^{2+}] of two non-altered and two altered representative mutants. (D) Summary of the UV fold effect in 0 and 100 μM Ca^{2+} for the conditions and mutants tested in this work.

N449BzF evoked UV-specific Ca^{2+} dependent slow reduction of the maximum steady state current

N449BzF, located in the intersubunit interface of RCK1 and adjacent subunit *calcium bowl* (RCK1-RCK2'; figure 4.10A), showed a dramatic reduction in Ca^{2+} sensitivity, with a compression of the G-V curves (figure 4.10B-C). Surprisingly, despite the N449 residue was proposed to be coordinating the *calcium bowl* site (the one with higher affinity), the effect of introducing this bulkier residue is specially striking in the absence of Ca^{2+} and in the highest Ca^{2+} concentration (100 μM) and almost unaf-

fected in intermediate Ca^{2+} concentrations (figure 4.10C-D). This result is consistent with the role of RCK1-site occupancy to position N449 in the *calcium bowl* highlighting the interconnection of Ca^{2+} binding sites between adjacent subunits (see *Discussion*).

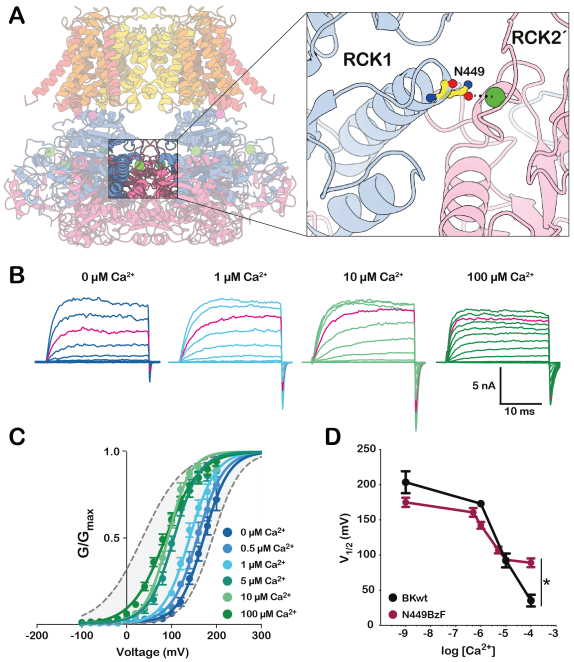

Figure 4.10. Functional characterization of N449BzF mutant. (A) N449 residue belongs to RCK1 but it has been proposed to coordinate Ca^{2+} in the adjacent RCK2 domain. (B) Representative current traces from -100 to +100 mV in the different Ca^{2+}. (C) Mean G-V summary for the mutant. (D) $V_{1/2}$ vs log[Ca^{2+}].

Despite the altered Ca^{2+} sensitivity, we validated N449BzF as a tool to study the coupling mechanisms at the interface because it still sensed the changes between low and high calcium concentrations. We then evaluated the role of this residue in BK channel activation by Ca^{2+} under four different conditions: with and without saturating Ca^{2+} (100 μM) combined with hyperpolarization (-60 mV) or depolarization (+100 mV). The protocols applied and changes in steady-state current evaluation were performed as mentioned in *Methods*. To compare the effects under the different conditions, we represented the normalized current vs sweep number in a kymogram (figure 4.11). A cartoon of the condition where UV was applied, as well as representative traces of the baseline and at the end of UV application are shown together with the corresponding time-course. WT (BK667YFP background) was included as a control for non-specific UV effects in other parts of the channel.

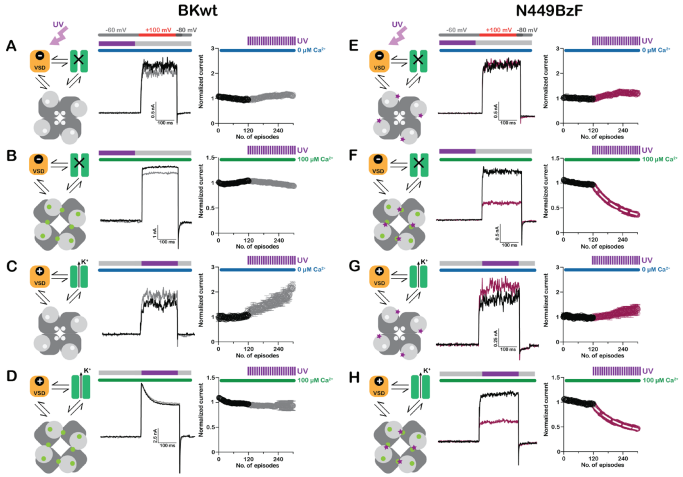

Figure 4.11. N449BzF experienced UV-dependent current reduction only in saturating Ca^{2+} conditions. (A-D) BKwt non-specific effect under UV light in the absence and presence of Ca^{2+} and applying UV in -60 mV or +100 mV. (E-H) N449BzF effect under UV light. Only under 100 μM Ca^{2+} an exponential current reduction is seen regardless voltage applied during UV exposure.

N449BzF showed a Ca^{2+} dependent and voltage independent reduction of current under UV light. Only under 100 μM Ca^{2+}, the N449BzF mutant showed a UV-dependent exponential decay both in UV rest or UV act conditions (figure 4.11F,H). The linear decay rate is similar (UV rest $\tau \approx 93$ episodes vs UV act $\tau = 108$ episodes; Table 4.2), and the estimated total effect had no significant differences between both conditions (UV rest plateau ≈ 0.26 vs UV act plateau ≈ 0.35; Table 4.2). This would mean a current reduction of ≈74% and ≈65% respectively. In the absence of Ca^{2+} there was no specific effect (figure 4.11E,G). A possible explanation of this effect is that the photocrosslinking causes a stabilization of the closed conformation of the channel in high calcium concentration, independently of the voltage sensor position. This would mean that BzF found a partner close enough to photocrosslink when Ca^{2+} is present in both Ca^{2+} sites, saturating the channel.

The BzF photocrosslinking reaction only happens if it finds a closer partner during its triplet state, being able to go back to the basal state if there was no reaction. Therefore, to discard the possibility that crosslinking in 0 μM Ca^{2+} was not rendering any effect in the measured current, we performed an experiment applying UV (UV rest condition) in the absence of Ca^{2+} and afterwards changed to 100 μM Ca^{2+} while light pulses were applied (figure 4.12A-B, WT vs N449BzF). We could see how just when 100 μM Ca^{2+} period started, an exponential current reduction happened at a slower rate than the previous experiments ($\tau \approx 232$ episodes) but with a striking effect in reduction comparable to the previous experiments. This experiment gave us crucial information: the BzF is not reacting during 0 μM, causing a "non-measurable" effect on the channel. In contrast, it has no close partner under this condition, otherwise, little effect would be seen in 100 μM Ca^{2+}. Thus, N449BzF is close enough to react just during Ca^{2+} saturation, and this position is moved apart in the absence of Ca^{2+}, where it did not find any close partner. Additionally, we confirmed that this effect is highly UV specific (figure 4.12C).

Interestingly, WT channels experienced linear potentiation of current under UV light in the absence of Ca^{2+} (figure 4.11A,C). This interesting output was not further explored in this thesis, but it could be explained by different reasons: aromatic residues photoxidation (improbable due to the absorption peaks in UVB or UVC wavelengths), cystine disruption, oxidation of other residues (like methionine) via ROS generation, etc., as previously reported (Middendorf et al., 2000; Fricke et al., 2019).

Because N449 residue is located at the RCK1 domain while pointing to the *calcium bowl* (RCK2) of the adjacent subunit one, next questions were: is this crosslinking ocurring intersubunit? Are the Ca^{2+} binding sites needed for the observed effects?

Figure 4.12. The N449BzF observed current reduction is Ca^{2+} and UV dependent. (A) BK WT was exposed to UV at 0 μM Ca^{2+} and afterwards at 100 μM Ca^{2+}. There is no UV specific effect observed during the experiment. A non-specific linear rundown was observed under 100 μM Ca^{2+}. (B) N449BzF experienced a UV driven exponential decay only in 100 μM Ca^{2+}. This corroborated that in 0 μM Ca^{2+}, BzF is not reacting with any close partner. (C) Alternating dark and UV light periods we observed that N449BzF effect is specific under UV light.

N449BzF reduced current is due to intersubunit crosslinking

One of the limitations of the use of these genetically encoded photocrosslinkers is the lack of control and knowledge about the specific location of the crosslinking partner prior to the experiment (only definable by mass spectrometry). However, according to the structure this position is in the intersubunit interface of RCK1 and adjacent RCK2. Therefore, a logical situation would be an intersubunit crosslinking. To test this, we performed protein biochemistry applying UV directly to the cells expressing our N449BzF mutant. In the case of the existence of a covalent bond between adjacent subunits, in a denaturing western blot, higher order oligomers should appear (dimers, trimers and/or tetramers). This is clearly seen in figure 4.13-right: bands corresponding to dimers and trimers appeared specifically after application of UV light.

As a comparison, the use of another photocrosslinker, azidophenylalanine (or AzF), with a lower yield and a faster exhaustion by photoactivaction, was included. Comparing both residues, the BzF showed, as expected, a higher density of oligomer bands. These bands are faint compared to the monomer because of the low efficiency of this approach, no intracellular Ca^{2+} control and bulk UV irradiation to the whole cell. This low yield was comparable to the previously reported intersubunit studies with this UAA (Klippenstein et al., 2014).

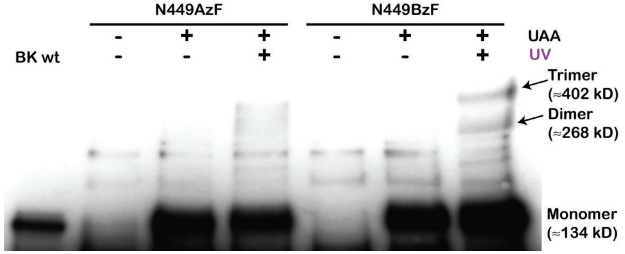

Figure 4.13. N449BzF showed bands corresponding to oligomeric states only under UV light. This result strongly suggests an intersubunit photocrosslinking.

RCK1 site integrity is needed for the UV driven effect

To test the independent contribution of Ca^{2+} binding sites in the photocrosslinking of N449BzF, we performed on top of this construct the mutagenesis to obtain Ca^{2+} insensitive mutants of the RCK1 (D367A), *calcium bowl* site (5D5A) or both (D367A+5D5A). These three mutants were evaluated under saturating (100 μM) calcium concentration and, because voltage influence was irrelevant for this effect, the experiments were done in the 'UV rest' condition. Interestingly, the result clearly pointed to the requirement of RCK1 Ca^{2+} coordination to allow photocrosslinking: under RCK1-D367A mutation, the exponential photorreduction disappeared (figure 4.14B). This effect was not seen in the RCK2-5D5A mutation, where an exponential decay was still present (to a lesser extent, $\tau \approx 219.4$ episodes) (figure 4.14C). As expected from the D367A mutation, in the case of the double mutant D367A+5D5A, the result was not further increased, showing no current reduction either (figure 4.14D).

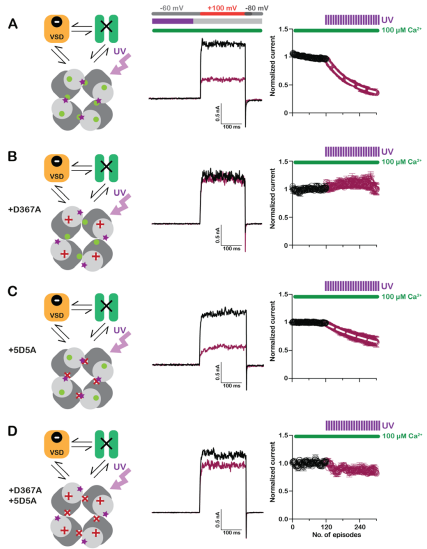

Figure 4.14. Prevention of Ca^{2+} binding to the RCK1 site abolished the N449BzF effect. (B-D) Effect of the different mutants under UV light. D367A containing mutants abolished the effect. 5D5A still showed a UV-dependent current reduction.

Altogether, this data suggest that the RCK1 site is mandatory for N449 function. N449BzF needs Ca^{2+} in this region to photocrosslink with a closer partner. Translated into BK channel function, it is alluring to conclude that the proposed role of N449 on *calcium bowl* seems to be relevant only after full occupancy of RCK1 by Ca^{2+} (see Discussion).

Photorreduction occurs selectively at the RC1-RCK2′ interface

It could be argued that the observed effect is not specific of the RCK1-RCK2′ intersubunit interface; in this case, a similar effect would be expected to happen after mutation of residues within the RCK2-RCK2′ interface (Tao et al., 2017; Li et al., 2018) To address this question I first chose to insert BzF into Y450, adjacent to N449. Time-dependent current photorreduction was observed in saturating Ca^{2+} conditions in the Y450BzF mutant (figure 4.9D; τ = 196 episodes). This effect, while modest compared to N449BzF (≈61% of total reduction in the plateau), suggests that the effect is consistent for this interface. However, the mutant R786BzF ,a position at the RCK2-RCK2 interface, did not show a significant current decrease under UV light at 100 μM Ca^{2+} (figure 4.15F,H). Overall, these data suggest that the RCK1-RCK2′ intersubunit interfaces are closer when the Ca^{2+} binding sites are saturated at 100 μM Ca^{2+} compared to the RCK2-RCK2 interfaces.

Photocrosslinkers in the RCK2-RCK2′ interface mediate a potentiation of the BK current in the absence of Ca^{2+} free condition

In the absence of Ca^{2+}, and contrary to the RCK1-RCK2′ interface, where no effect was observed, residue R786BzF rendered a ≈ 2-fold potentiation under UV illumination (figure 4.15E,G). This potentiation is again voltage independent and Ca^{2+} dependent. The rate of the effect in this case is faster than the measured for the N449BzF in 100 μM Ca^{2+} (UV rest $\tau \approx 31$ vs 93 episodes; UV act $\tau \approx 17$ vs 108 episodes), which indicates a closer and favorable crosslinking partner in this environment, as well as a more accentuated effect in BK channel function. Furthermore, this potentiation is evidently different from the linear potentiation observed for the WT channel in the absence of Ca^{2+} (figure 4.15A,C vs E,G), discarding the possibility of a non-specific effect.

A possible interpretation would be that , the immobilization of the lower region of the tetramer produces a 'stabilization' of the open conformation of the channel. Importantly, this potentiation is only seen during the depolarization step to +100 mV and not during the hyperpolarizing period at -60 mV (there are no openings in this part of the protocol). This points a misbalance towards a more open conformation in one of the allosteric coupling factors with the pore, more than just a lock in an 'open channel' conformation (see Discussion).

Taking into consideration all these results, we concluded that we have elicited Ca^{2+} dependent dynamics of the *gating ring* in the intersubunit interfaces which are independent from voltage sensors motions and definitely affects the overall function of the channel in two different positions. We are currently modeling this data and finishing some key experiments which would lead us to conclude where the effect is coming from and how this can explain the activation rearrangements induced by Ca^{2+} in the BK channel.

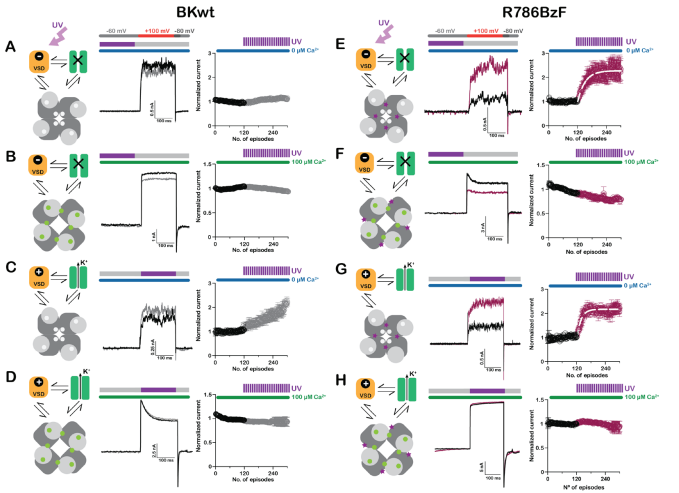

Figure 4.15. In the absence of Ca^{2+}, RCK2 mutant R786BzF exerted a potentiation of the current under UV light. (A-D) BKwt effects under UV light repeated here for comparison. (E-H) R786BzF showed a fast Ca^{2+} dependent and voltage independent potentiation of the current that reaches ≈2 times the baseline current.

Table 4.2. Summary of the BzF mutants under UV light.

Construct	UV application potential (mV)	[Ca^{2+}] (μM)	N	Crosslinking effect	τ (episodes)	Cumulative UV exposure at τ (s)	Plateau
BK wt (667YFP)	-60	0	9	None			
	-60	100	5	None			
N449BzF	-60	0	8	None			
	100	0	3	None			
	-60	100	7	Current reduction	93	37.2	0.26
	100	100	5	Current reduction	108	43.2	0.35
N449BzF + D367A	-60	100	4	None			
N449BzF + 5D5A	-60	100	3	Current reduction	219	87.6	0.4
N449BzF + D367A + 5D5A	-60	100	5	None			
Y450BzF	-60	100	5	Current reduction	196	78.4	0.39
R786BzF	-60	0	7	Current potentiation	31	12.4	2.3
	-60	100	6	None			
	100	0	4	Current potentiation	17	6.8	2.2
	100	100	3	None			
R790BzF	-60	0	4	Current potentiation	101	40.4	2

Chapter 2: Discussion

Unnatural amino acid incorporation has emerged as a polyvalent tool for expanding the side chain chemistry of proteins. In ion channels, these tools have been extensively used to study the atomic mechanistic insights and interacting domains (for a recent review see Klippenstein et al., 2018). One of the most extended used UAAs in ion channels are photocrosslinkers (Braun et al., 2020), which allow a finely controlled and specific crosslinking in comparison with other methods (e.g. cysteines).

Effective incorporation of photocrosslinkable UAA BzF in the BK channel

In this study we have successfully incorporated the unnatural amino acid BzF in different domains of the BK channel using the genetic method (Ye et al., 2008). This is, to our knowledge, the first study on this ion channel using unnatural amino acid incorporation in mammalian cells. A previous work from Tian et al. showed effective Amber suppression in the BK channel by conjugated tRNAs in Xenopus oocytes (Tian et al., 2016). Differently, in this case we have used the orthogonal aminoacyl-tRNA synthetase and tRNA coding plasmids for BzF together with the mutated BK channel to specifically incorporate this photocrosslinker. We have obtained full-length and functional channels in 12 of the 14 positions tested, a good efficiency, considering some of the selected positions and the bulkiness of the BzF. The size of the macroscopic currents in most of these residues is high enough to ensure that mutant channels conserved a high conductance as well as good membrane expression (figure of 449 currents). Moreover, most of these channels showed Ca^{2+} sensitivity similar to WT, which mapped certain positions where there were no highly steric or electrostatic limitations for the insertion of an exogenous amino acid. Unfortunately, among all these promising candidates for photocrosslinking, only 4 mutants showed a UV driven effect. This efficiency is comparable to the previously reported one for other proteins (e.g. AMPA receptors in Poulsen et al., 2019).

Altogether these characterization data validated the Amber suppression system in BK channel for different positions. This will allow future studies not only for incorporation of the BzF but for other UAAs of interest (e.g. fluorescent UAAs, photo-switchable UAAs…).

The suppression of N449TAG mutant with BzF rendered channels with altered Ca^{2+} sensitivity

The solely insertion of a bulkier residue like the photoactivatable UAA BzF in the N449 position produced BK channels with reduced Ca^{2+} sensitivity, as denoted by the compression of the curves in its G-V relationship (figure 4.10C-D). In the absence of Ca^{2+} this curve is significantly leftward shifted, which explains that neutralization of the asparagine charge and substitution by a bulkier residue is able to evoke a functional disturbance in the activation of the channel. This effect matches with the previous reported N449A mutant (previous chapter): disruption of this position already

produces an effect under Ca^{2+} free conditions, which is remarkably considering that this residue was previously proposed to be involved in RCK2 Ca^{2+} coordination but is connecting two different domains of two different subunits. Thus, N449 seems to be important for interfaces assembly and, in a higher order, for tetramerization of the BK channel RCK domains. Furthermore, in higher Ca^{2+} there is almost no Ca^{2+} sensitivity, with overlapping curves in 5 to 100 μM Ca^{2+} Due to this important insight, where a photocrosslinking would give us useful information about the interface interaction, we decided to continue using this mutant despite of its affected function and considering that the shift between 0 and 100 μM Ca^{2+} was still measurable.

N449BzF Ca^{2+} dependent slow photocrosslinking rely on RCK1 site occupancy by Ca^{2+} ions

Interestingly N449BzF produced a UV-dependent current reduction only under saturating Ca^{2+} conditions independently from voltage applied. This effect is slow in comparison to previously reported trapping effects in potassium channels (Ding and Horn, 2001) and did not reach a plateau during the experimental window (although could be estimated by the fitting; Table 4.2) . Hence, under structural rearrangements in the absence and presence of 100 μM Ca^{2+} there is a change in the distance where BzF finds a partner for photocrosslinking. Furthermore, this effect is specific from this RCK1-RCK2′ interface, as insertion in the Y450 position also produces a similar effect which is not seen in the other interfaces studied (figure 4.9B,D). This data suggests that locking the protein conformation in the position where Ca^{2+} binding sites are fully occupied produces a current reduction. Figure .A summarizes all the conditions in which an effective photocrosslinking was observed. One concern about these results could be that in the absence of Ca^{2+}, BzF could be crosslinking with another partner without effect on the overall function of the channel. However, we can firmly conclude that there is little crosslinking in the absence of Ca^{2+} according to control experiments in figure 4.12.B, demonstrating that BzF is not reacting before the saturating calcium condition exists.

The current reduction caused by N449BzF photocrosslinking can be explained by two possibilities: (1) the crosslinking impedes a further movement needed for activation that is not transmitted to the pore domain, stabilizing a 'pre-opening' conformation; (2) the interaction of this RCK1-RCK2′ interface at saturating Ca^{2+} condition produce a negative effect between the RCK2 Ca^{2+} binding site and adjacent

subunit-RCK1 domain, thus the locking of this interface in this extreme condition induces a reduction of channel activity by reducing the coupling of Ca^{2+} binding to pore opening.

Additionally, we showed that this recombination is produced only in the cases where the RCK1 site is occupied by a Ca^{2+} ion. In the absence of this divalent cation in the RCK1 site (0 μM Ca^{2+} or '+D367A' mutants), N449BzF is out of the range to find a partner for photocrosslinking, which demonstrates that the structural rearrangement caused by the occupancy of this site is the one that reaches the photocrosslinking distance and would be mediating the distance of N449 to RCK2 site. It can be argued that the N449 role cannot be relevant just under 100 μM Ca^{2+}, because in the absence of Ca^{2+}, there is a shift in the voltage dependence of the N449A mutant where no Ca^{2+} is present in any of the sites. Thus, considering these experiments we could think in a simultaneous movement of the RCK1 and RCK2 interfaces after Ca^{2+} binding which would use the N449 position as a center of rotation and it changes its interacting residues from one state to the other. Unfortunately, the structures in Ca^{2+} free and Ca^{2+} bound conditions (Tao et al., 2019) did not show any residue close enough to interact with N449 in Ca^{2+} free nor Ca^{2+} bound conditions. One of the limitations of the use of photocrosslinkers is that we cannot control in advance the crosslinking partner. To explore the residues close enough to experiment photocrosslinking, we did an in silico analysis in the published human structures of the BK channel (Tao et al., 2019). We mutated the N449 to BzF using the SwissSideChain database and selecting the rotamer with the highest probability. Afterwards, we measured the distances between the carbon from the ketone reactive group of BzF and the C-α carbons closer to it (from RCK2′ *calcium bowl* region) (figure 4.16A1). A comparison between the Ca^{2+} free and Ca^{2+} bound structures showed a clear hotspot for photocrosslinking around Q889 residue (figure 4.16A2), being the only point where a distance slightly below the maximum ideal 3.1Å (Dormán and Prestwich, 1994) is reached.

In a study about intra and intersubunit cooperativity between the two different high-affinity Ca^{2+} binding sites, Qian et al. proposed that intrasubunit interface between RCK1 and RCK2 is more important for Ca^{2+} mediated activation of the BK channel (Qian et al., 2006). According to their data combining the mutations of Ca^{2+} binding sites and the proportions of them injected in oocytes (combining the two mutations in the same subunit or in alternate subunits), the Ca^{2+} activation was more potent if both Ca^{2+} binding sites were present within the same subunit. They concluded that a model of flexible intrasubunit RCK1-RCK2 interface and fixed intersubunit

RCK1-RCK2′ interface is more favorable to activation by Ca^{2+} of the BK channel. They based their conclusions in assumptions by the homology between BK and MthK channel, where fixed and flexible interfaces alternate in the RCK octamer (Jiang et al,. 2002), a fact corroborated by a recent structure of the MthK channel in the closed and open states (Fan et al., 2020). However, similar to a posterior study on MthK (Dong et al., 2005), our data suggest that in BK channel RCK1-RCK2′ intersubunit interface has some degree of flexibility. In the human BK channel structures Ca^{2+}-free and Ca^{2+}-bound states (Tao et al., 2019) this flexibility can be observed in two rearrangements: the *calcium bowl* formation and the upward movement of the αD helix where N449 is included.

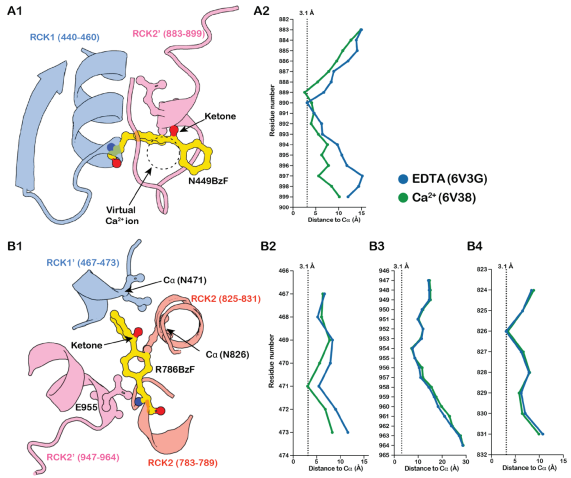

Figure 4.16. In silico analysis of the potential distances for photocrosslinking showed a hotspot in the N449BzF but not in R786BzF.

We are currently modelling the kinetics of these effects to conclude how they are mediating a closure of the BK channel.

Photocrosslinking in the RCK2-RCK2′ interfaces produces a potentiation of the channel activity

BK channels with BzF incorporated in the 786 position (R786BzF) showed under UV illumination a fast potentiation that reaches ≈2 fold the levels of current observed during the baseline recording (table 4.2). This effect, contrarily to N449BzF, was recorded in the absence of Ca^{2+} and the potentiation was not trapping the open conformation because no 'leak' increase was observed during the recording (figure 4.15E,G), going back the channels to the closed conformation. Interestingly, this effect was not observed at 100 μM Ca^{2+}. R786 is forming part of an electrostatic interaction with E955 together with R790 (Li et al., 2018; Tao et al., 2019). However, the distances between these three residues remains similar in the absence and presence of Ca^{2+} (Li et al., 2018; Tao et al., 2017; Tao et al., 2019), for that reason, a clear position in the absence of Ca^{2+} where the crosslinking could happen is not easily hinted. Doing the same in silico analysis, for N449BzF we discovered that BzF insertion in R786BzF has three different domains close enough to photocrosslink. Surprisingly, the furthest one was the loop where E955 is located (figure 4.16B1,B3) and which forms part of the RCK2-RCK2′ interface. The other close residues to photocrosslink are the N471 on the RCK1′ (figure 4.16B1-B2) and the N826 in the same RCK2 (figure 4.16.B1,B4). Interestingly, the only one that suits the situation of 0 μM Ca^{2+} and below 3.1 Å is the N826. We have to keep in mind that this analysis is based on the most probable rotamer by using the 'Rotamer' tool of Chimera software which has some limitations regarding the local reorganizations in the backbone by insertion of the mutated amino acid, only considering the side chain. This analysis was useful to explore the environment surrounding the R786 position, however, in this case we could not extract more information. We are currently working to refine this prediction and do some simulations to obtain a better understanding of this effect.

Trapping the protein conformation in two different states and regions produced antagonistic effects

The crosslinking of N449BzF and R786BzF occur in antagonistic situations (presence and absence of Ca^{2+} respectively; figure 4.17), thus, we can conclude that we are mapping two movements of the *gating ring* that are directly transmitted to the pore, voltage independent and directly linked with Ca^{2+} activation mechanisms. We are currently performing the G-V analysis of R786BzF mutant, as well as noise-anal-

ysis to measure the conductance before and after the potentiation and modelling this mutant together with N449BzF to obtain a dynamic map of these two interaction interfaces in the *gating ring* of the BK channel.

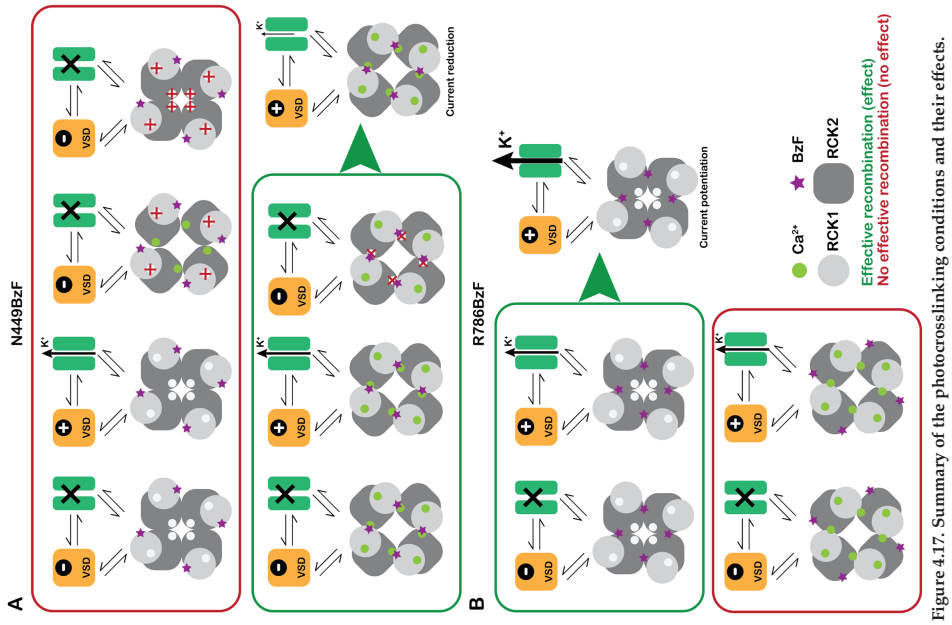

Figure 4.17. Summary of the photocrosslinking conditions and their effects.

PART 2: BK CHANNEL FUNCTIONAL AND PHYSICAL ASSOCIATION WITH NMDARs

In this second part we aimed to explore in depth the interaction of BK channels with the ionotropic glutamate receptors NMDARs. Under the hypothesis of a physical and functional association between these two ion channels, we studied the contribution of NMDAR Ca^{2+} flux in BK channel activation in heterologous systems to better understand this interaction. We compared the effects between the two most abundant GluN2 subunits in the adult brain: GluN2A and GluN2B. In parallel, we developed and validated new tools for studying this interaction with single molecule approaches and super resolution microscopy techniques.

The association between NMDAR and BK channels contains interesting open questions, because in the plasticity scenario and postsynaptic dynamics, this association finely tunes the neuronal outputs. For example, differences in the ability to form complexes with BK of GluN2A or 2B subunit containing NMDARs have not been evaluated yet. Therefore, it is quite relevant to study this interaction in depth. While the coupling between these two channels has been described in different neuron types (Isaacson and Murphy, 2001; Zhang et al., 2018), biophysical characterization of the interaction remains elusive. Integration of NMDAR and BK channels in complexes, where both proteins are tightly coupled, may alter the biophysical properties of individual channels, e.g. inducing synergistic effects in activation and deactivation kinetics, or their mobility along the membrane. Thus, the understanding of the basis of this interaction is crucial to understand the physiological role of these complexes.

Both GluN2A- and GluN2B-containing NMDARs can functionally couple to BK channels

This work was done in collaboration with Dr. David Bartolomé-Martín and Dr. Belinda Rivero Pérez, members of the lab and is part of the publication "NMDA receptor–BK channel coupling regulates synaptic plasticity in the barrel cortex" (Gómez et al., 2021; Annex 2).

Because GluN2 subunits determine the deactivation kinetics and ion conductance of NMDARs (Vicini et al., 1998), we reasoned that the molecular composition of NMDARs might affect NMDAR–BK coupling efficiency. We first tested whether BK preferentially associates with specific NMDAR subunit combinations using a proximity ligation assay (PLA). In agreement with our pharmacological data (Gómez et al., 2021; figure 1F), positive PLA signals were observed for HEK293T cells co-expressing BK and either GluN1/GluN2A or GluN1/GluN2B NMDARs (Figure 4.18A), without any preference between GluN2A and GluN2B subunits (Figure 4.18B).

Having confirmed that NMDARs and BK channels are located in close proximity in the plasma membrane when co-expressed in HEK293T cells, we characterized functional coupling between specific channel/subunit combinations. By using the inside-out configuration of the patch-clamp technique, we were able to monitor channel function while controlling 'intracellular' Ca^{2+} concentration in the bath solution (Giraldez et al., 2005). NMDARs were activated by including 200 μM NMDA and 10 μM glycine in the 'extracellular' pipette solution. Under these conditions, desensitization of NMDAR is significantly reduced (Lerma et al., 1992). The relative conductance (G) of BK channels exposed to different intracellular Ca^{2+} concentrations (from 0 to 100 μM) in patches from cells expressing BK channels but no NMDARs (Figure 4.18C) corresponded to typical Ca^{2+}-dependent activation curves for these channels (Kshatri et al., 2018; Horrigan and Aldrich, 2002). We reasoned that addition of Ca^{2+} to the intracellular side of the patch through a Ca^{2+} source such as NMDARs would result in a leftward shift of the BK activation curve in zero Ca^{2+} bath solution. This would be favoured if the channels were closely located, allowing Ca^{2+} to activate BK before being diluted in the large Ca^{2+}-free bath solution (following an analogous reasoning than the experiments using chelators above). Indeed, co-expression of BK channels with either GluN1/GluN2A or GluN1/GluN2B NMDARs produced a significant leftward shift of the BK activation curve (Figure 4.18D). Interestingly, the shift resulted in an activation curve comparable to that recorded with 10 μM intracel-

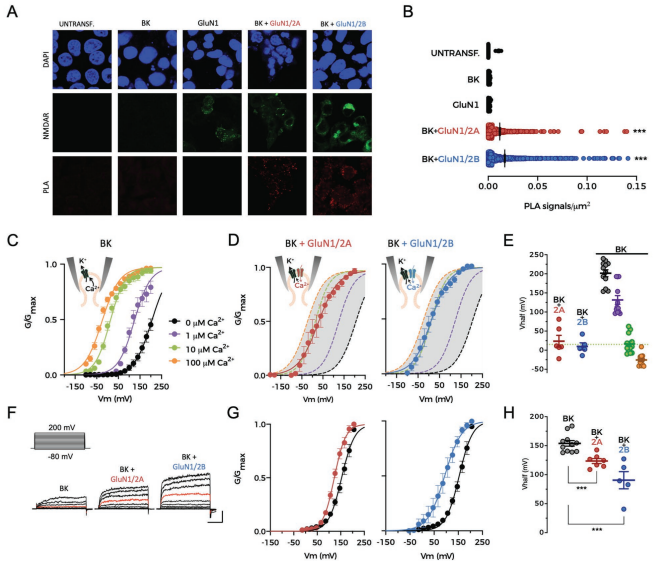

Figure 4.18. Both GluN2A- and GluN2B-containing NMDARs can functionally couple to BK channels. (A) Representative confocal microscopy images of PLA experiments in HEK293 cells expressing the protein combinations indicated at the top of the images. Each row corresponds to an imaging channel (top, DAPI, blue; middle, NMDAR, green; bottom, PLA, red). (B) Average PLA signals/μm2 for all conditions shown in (A). Data points represent individual measurements. Four independent experiments were performed for each condition. Black lines represent mean ± SEM. ***p<0.001 vs. untransfected cells (UNTRANSF), BK alone (BK), and GluN1 alone (GluN1). (C) Normalized conductance-voltage (G-V) relationships obtained from excised inside-out patches expressing BK channels alone (n = 12) in the presence of different intracellular Ca2+ concentrations in symmetrical K+ solutions. Data points represent mean ± SEM. Lines represent the best fit of a Boltzmann equation to the data. Ca2+ concentrations are color-coded as indicated in the legend. (D) Normalized G-V relationships from excised inside-out patches co-expressing BK channels with GluN1/GluN2A (left; n = 6) or GluN1/GluN2B (right; n = 5) in the absence of intracellular Ca2+, with 200 μM NMDA/10 μM Glycine in the pipette. Data points represent mean ± SEM. Lines represent the best fit of a Boltzmann equation to the data. (E) Vhalf values obtained from experiments depicted in (C) and (D). Data points represent individual measurements and lines represent mean ± SEM. (F) Representative current traces recorded in physiological Na+ solutions from excised inside-out patches containing BK alone (left), BK+GluN1/GluN2A (middle), and BK+GluN1/GluN2B (right). Scale bars represent 30 ms and 2000 pA. Currents recorded at +140 mV are highlighted in red. (G) Normalized G-V relationships from excised inside-out patches containing BK and GluN1/GluN2A (left, red; n = 6) or GluN1/GluN2B (right, blue; n = 5) in solutions containing

physiological concentrations of Na+ (see methods). Black traces in both graphs correspond to G-V curves for BK channels expressed alone (n = 11). Data points represent mean ± SEM. Lines represent the best fit of a Boltzmann equation to the data. (H) Summary of Vhalf values from experiments in (G). Data points represent individual measurements and lines represent mean ± SEM. ***p<0.001 vs. BK alone.

lular Ca^{2+} in patches expressing BK alone (Figure 4.18E). Of note, the reduction of the driving force for Ca^{2+} at very positive voltages was not paralleled by diminished values in the G-V curves, as is commonly observed in VGCC-BK coupling experiments (Berkefeld et al., 2006), probably due to increased permeation of K^+ through NMDAR (Ichinose et al., 2003). These results suggest that NMDAR activation increases Ca^{2+} concentration in the close vicinity of BK channels, favouring their activation.

NMDARs are non-selective cation channels that are permeable to Na^+, K^+, and Ca^{2+} (Traynelis et al., 2010; Paoletti et al., 2013). Under physiological conditions, the proportion of NMDAR current carried by Ca^{2+} corresponds to 10-15% of the total current (Garaschuk et al., 1996; Plant et al., 1997; Burnashev et al., 1995). However, because the above-mentioned inside-out patch experiments were performed in the absence of Na^+, inward current through NMDARs could only be due to Ca^{2+} ions, whose permeability is increased as extracellular Na^+ concentration is reduced (Mayer et al., 1987). We may therefore be overestimating the effects of NMDAR-dependent Ca^{2+} activation on BK channels in our zero Na^+ experimental conditions. Nevertheless, activation of GluN1/GluN2A or GluN1/GluN2B NMDARs in excised inside-out patches using physiological concentrations of Na^+ still produced a leftward shift in the BK activation curve (Figures 4.18F–H). Interestingly, GluN1/GluN2B produced larger shifts than GluN1/GluN2A.

Taken together, these results demonstrate that both GluN2A- and GluN2B-containing NMDARs can provide sufficient Ca^{2+} for BK activation, consistent with our data from BC-L5PN basal dendrites (Gómez et al., 2021 - figure 1F).

However, because of the intrinsic limitations of the PLA approach, where only shows interactions with resolutions above 40 nm, and motivated by the experiments in mice slices where using Ca^{2+} chelators we estimated the distance between these two proteins of ≈ 25 nm (Gomez et al., 2021; figure 2), we decided to refine this result and obtain a better resolution of the distance between BK channel and NMDAR in complexes.

GluN2B containing NMDARs tends to be closer to BK channel than GluN2A containing ones

In order to quickly obtain an estimation to the possibility of a closer distance of these complexes, we took advantage of our GluN1-YFP subunit and BK-N-terminal FLAG epitope whose insertions are both in the extracellular side. We labelled the cells in vivo with an anti-FLAG conjugated to Alexa 555 for 30 minutes at 37ºC and imaged immediately after. Because YFP can act as a donor and Alexa 555 as an acceptor of FRET, we performed acceptor photobleaching FRET experiments under confocal microscopy. In GluN2B containing NMDARs the FRET efficiency significantly trends to a modest increase in the efficiency if we compare the bleached part of the cell with the unbleached one (paired-test, figure 4.19). This effect is not the case in the GluN2A containing ones or in the absence of GluN2 subunits (negative control). This experiment, although was not accurate enough due to an antibody faint labelling, clearly showed that GluN1/2B combination tends to be the tighter coupled. No more calculations were performed on this experiment, but an estimated distance by using the R0 of the FRET pair EGFP-Alexa Fluor 555 (≈6.3 nm) would give us a distance close to the FRET limit of 10 nm.

This result motivated us to reach a better signal and proper measurements of this distance. Hence, we aimed to develop constructs with BK and NMDARs tagged with self-labelling enzymes (SLEs) in the extracellular side of the membrane. This strategy permitted us to isolate membrane expressed receptors as well as use brighter and more stable fluorophores. Furthermore, the versatility of the SLEs would allow us to use the same constructs in a wide range of experiments.

Figure 4.19. FRET-AB experiments on BK-NMDARs complexes showed a trend of GluN2B containing NMDARs to be closer to BK channel. (Scale bar = 10 μm)

SNAPtag and CLIPtag fusion to BK channel: construct strategy and validation

SNAP-tag has a great advantage for the study of ion channels and other membrane proteins: the use of non-permeable dyes allows to isolate and only label the membrane population. Then, we decided to introduce SNAP-tag in the extracellular domains of the BK channel: one in the N-terminus and other in the position 140 (S1-S2 linker). These constructs were named as BK-Nt-SNAP and BK-S1S2-SNAP, respectively. In addition, we decided to put SNAP-tag in one of the positions tested before to be functional after fluorescent protein insertion, H667 (construct name: BK-667-SNAP; Giraldez et al., 2005). The expression of the three constructs as well as the SNAP-tag labelling ability were checked by surface and intracellular labelling (with non-permeant and cell-permeant dyes respectively).

One challenge of this fusion protein design was that, to our knowledge, only one successful N-terminal fusion of tag-protein in BK channel was reported before this work, the Fluorogen Activating Protein or FAP (Pratt et al., 2017); and the membrane insertion and expression efficiency is tag dependent, as N-terminus fusion of GFP variants did not render any functional BK in the plasma membrane (Giraldez et al., 2005). In fact, in the first trials, the BK-Nt-SNAP showed low membrane expression (figure 4.20B-middle).

The BK channel lacks endogenous signal sequence in its native gene, because of this, the proper folding and trafficking of this new construct to the membrane could be compromised. Therefore, we improved this construct by the addition of the native metabotropic glutamate receptor 5 (mGluR5) signal sequence (MVLLLILSVLLLKEDVRGSAQSTRPV) just 5' to the sequence of HA-epitope and SNAPtag (figure 4.20A). This endogenous sequence from mGluR5 was previously fused to other GPCRs and ensures the ER-mediated trafficking to the membrane apart from a better folding efficiency (Doumazane et al., 2011; Levitz et al., 2016). In general, signal sequences has been previously validated to improve membrane secretion and membrane insertion in a wide variety of proteins (Owji et al., 2018), and this strategy was used before in the FAP-BK fusion (Pratt et al., 2017). This modification greatly increased the membrane expression of the BK-Nt-SNAP construct (labelled with Surface Alexa Fluor-647; figure 4.20B middle vs right), evident not only in the increased intensity of the cells (figure 4.20C) but in the number of cells showing expression of

the construct. As a control, I transfected mGluR2-SNAP construct, which included the same mGluR5 signal sequence in the N-terminus and was previously validated (Levitz et al., 2016; Levitz et al., 2017). BK-Nt-ss+SNAP showed a similar pattern to the mGluR2-SNAP construct (figure 4.20B-C). The only insertion of the exogenous signal sequence improved the expression up to 2-fold in terms of intensity and with a higher proportion of transfected cells. To simplify, from now on, our improved construct BK-Nt-ss-SNAP will be called just BK-Nt-SNAP.

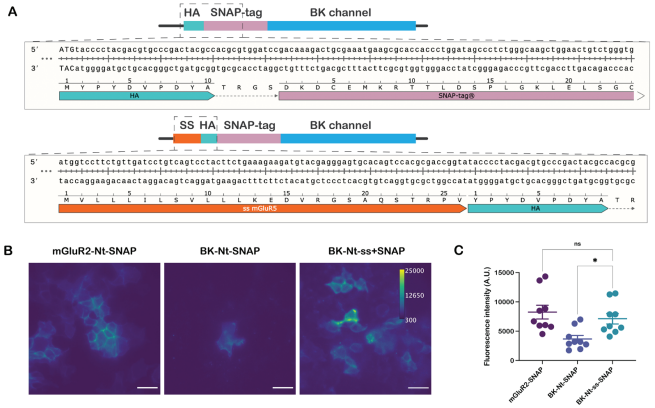

Figure 4.20. Signal sequence insertion in the BK-Nt-SNAP N-terminus yielded better membrane expressed constructs. (A) Signal sequence of mGluR5 was inserted before the HA epitope of the BK-Nt-SNAP construct. (B) Representative image of fluorescence intensity between mGluR2-SNAP, BK-Nt-SNAP and BK-Nt-ss+SNAP (Scale bar = 20 μm). (C) Quantification of the images in (B).

Next, we interrogated which are the membrane and intracellular proportions of BK-Nt-SNAP and BK-S1S2-constructs as well as which is the localization of BK-667-SNAP in the cells. We chose the HeLa cell line this time because of its bigger size and cytoplasm area. We sequentially labelled the cells first with the non-permeant dye Surface Alexa Fluor 546 and secondly with the permeable one SNAP-Cell SiR 647. Only in the cells transfected with BK-Nt-SNAP, a clear membrane labelling was achieved (figure 4.21, second row). In the case of BK-S1S2-SNAP, the construct was not expressed, as no detectable labelling was achieved with the fluorophores. Because we had BK-Nt-SNAP construct good results, we decided to exclude this construct from latter characterizations. BK-667-SNAP expressed well in the cells although membrane expression was indistinguishable from the inner population because the SNAPtag was located intracellularly. Both constructs were functionally validated, and they rendered an activation similar to the WT (G-V curves, figure 4.21, bottom). Not surprisingly, BK-Nt-SNAP and BK-667-SNAP monomers produced proteins of the expected size for the approximate fusion of SNAPtag to this ion channel (≈ 145 kD; figure 4.22). After the good result of BK-Nt-SNAP, we immediately developed the CLIPtag version (BK-Nt-CLIP) under the same backbone to increase the versatility of our experiments.

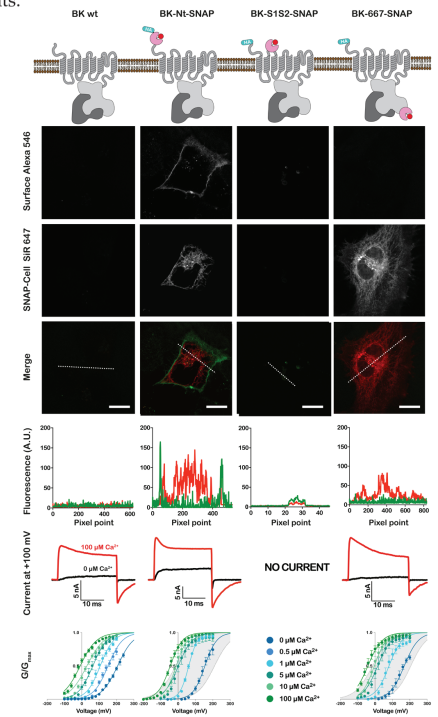

Figure 4.21. BK-Nt-SNAP and BK-667-SNAP rendered functional constructs able to be labelled by commercial SNAP dyes. White dashed line plot profile below each image. (Scale bar = 10 μm).

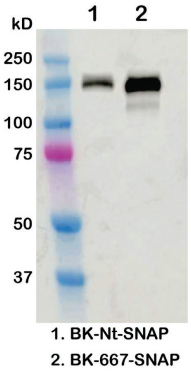

Figure 4.22. BK-SNAP insertions rendered proteins of the expected size (≈145 kD).

CLIPtag fusion to GluN1 rendered functional and specifically labelled NMDARs that coassemble with BK-Nt-SNAP

At the beginning and in parallel with BK channel fusion we designed GluN1 subunit tagging with the homologous SNAPtag enzyme CLIPtag. In this case we substituted YFP from the original plasmid (pEYFP-NR1), inserted in the N-terminus, and replaced by amplified CLIPtag by conventional cloning techniques. Unlike BK channel, GluN1 subunit possesses endogenous signal-sequence, thus, GluN1-CLIP was designed to conserve this endogenous feature (construct called GluN1-CLIP).

It has been reported before that expression of NMDARs in heterologous systems is challenging because their permeability to Ca^{2+} and activation by residual glutamate and glycine on the culture media would lead to Ca^{2+} influx into the cells causing cytotoxicity and cell death (Chazot et al., 1999). Therefore, a great part of the last year of this thesis was invested in optimization of the expression of GluN1-CLIP construct in HEK cells. We have used specific blockers and glutamine free media (Opti-MEM, details in Methods) after transfection, different transfection amounts and labelling strategies at different temperatures (4, RT or 37 ºC). Among all the trials and conditions tested, we achieved good conditions for correct NMDARs expression: (1) transfection in OptiMEM + 5% FBS with low amounts of plasmids for these receptors (≈ 66 ng*subunit/cm2); (2) replace media 4 hrs after transfection with the same medium complemented with 200 μM APV and 20 μM DCKA, (3) expression up to 24-28 hrs; (4) labelling at room temperature in the continuous presence of blockers.

To test whether this construct was properly trafficking to the membrane we cotransfected it with GluN2A-GFP and labelled with CLIP surface DY547 (figure 4.23A-B). Although a colocalization in the membrane was achieved (figure 4.23B, asterisks), the CLIP labelling efficiency was low.

Complementarily we performed the labelling at the same time on BK-Nt-CLIP. Under the same conditions (labelled with CLIP Surface DY547), GluN1-CLIP (+2A) expressed and labelled worse than BK-Nt-CLIP, being the former fainter and poorly expressed in the cells (figure 4.24).

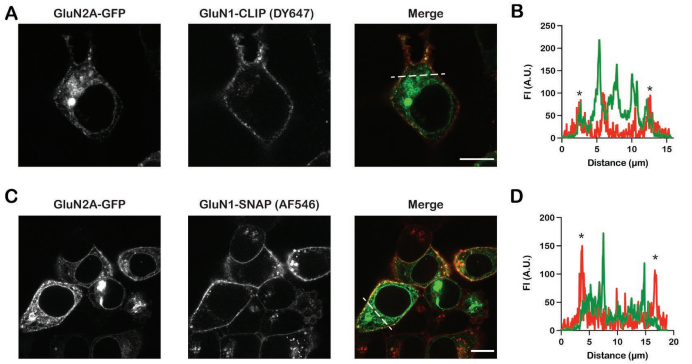

Figure 4.23. GluN1-CLIP and GluN1-SNAP coexpressed with the GluN2A-GFP subunit in the membrane of the cells. GluN1-CLIP showed a fainter labelling due to a lower expression than GluN1-SNAP (asterisks for plotted profile membrane reference). (Scale bar = 10 μm).

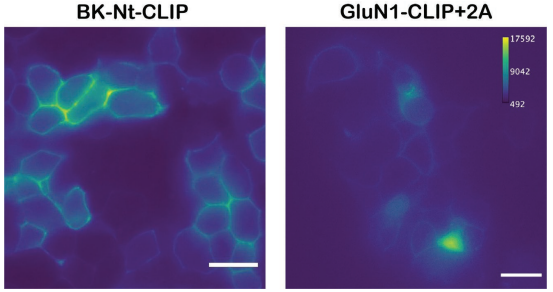

Figure 4.24. GluN1-CLIP showed faint labelling and lower number of labelled cells than BK-Nt-CLIP labelled under the same conditions with Surface CLIP DY547. (Scale bar = 20 μm)

Despite its lower expression, we decided to contransfect it with BK-Nt-SNAP as well as test the GluN1-CLIP function. In whole-cell configuration and under a brief pulse of glutamate (1s) at -40 mV, GluN1-CLIP+2A showed an inward current with a peak of ≈ 150 pA (figure 4.25C-top). Furthermore, when cotransfected with BK-Nt-SNAP, we could differentially label them (figure 4.25A-B) and in response to the same brief pulse of glutamate and at 0 mV, we recorded an inward current (corresponding to NMDAR evoked one) immediately followed by an outward current (activation of BK channel by the influx of Ca^{2+} into the cell). This current behavior resembled previously described ones in neurons, where BK channel and NMDARs were functionally coupled (Introduction; Gomez et al., 2021; Zhang et al., 2018). Therefore, although this construct needed to be optimized, the ability to form complexes with the BK channel was retained despite the insertion of SNAP and CLIP tags.

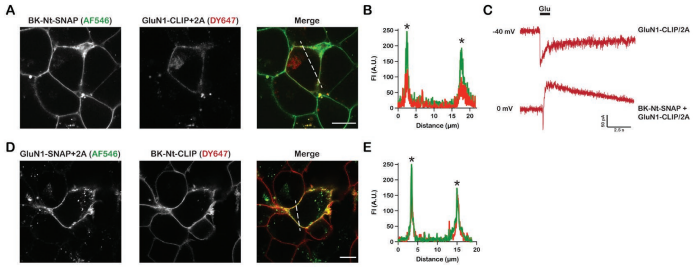

Figure 4.25. Coexpression of SNAP and CLIP tag fused BK and GluN1 (together with 2A) rendered membrane colocalization and functional coupling. GluN1-SNAP shower a higher ability to be labelled and a better expression in the membrane (E) compared to GluN1-CLIP (B) when cotransfected with BK channel. (C) GluN1-CLIP was functional and could functionally coassembly with BK-Nt-SNAP. (Scale bar = 10 μm).

After these promising results of functional coupling, we decided to perform FRAP experiments with BK-Nt-SNAP in absence and in combination with NMDARs to test the interaction of the BK channel with these receptors in live cells (next section).

In parallel to the FRAP experiments, we decided to swap the tags between NMDAR (GluN1-SNAP) and BK channel (BK-Nt-CLIP) to balance between a good membrane expression and a good labelling of the enzyme. GluN1-SNAP showed a better membrane colocalization with GluN2-GFP than GluN1-CLIP (figure 4.23C-D). This was probably due to better membrane trafficking as well as coassembly with

GluN2-GFP to form functional heterotetramers. When cotransfected with BKNt-CLIP, GluN1-SNAP+2A rendered better labelling of both enzymes simultaneously than the GluN1-CLIP+BK-Nt-SNAP (figure 4.25D-E vs A-B). Consequently, we have decided to use this combination for future experiments.

GluN1/2B-BK channel complexes diffused slower in the membrane

One of the hypotheses regarding the transient interaction between two proteins in the membrane is that, if this interaction is happening, the diffusion coefficient of the molecules is slower because this oligomerization would lead to less movement or confinement.

We took advantage of FRAP to quickly assess this question. BK-Nt-SNAP was labelled with non-permeant Alexa Fluor-647 during 45 min at 37ºC and imaged under the confocal microscope at 25ºC. A ROI of constant diameter was selected for all the conditions. BK-Nt-SNAP+GluA2, a Ca^{2+} permeable AMPA receptor (unedited Q; kindly gifted by Prof. Andrew Plested), was included in the experiment as a control. Previous work from the lab demonstrated that the BKwt+GluA2 combination had no functional coupling by electrophysiology (data not shown), thus, we expected no physical interaction for this condition. In figure 4.26A, a representative time-lapse of the three test conditions is shown. All the conditions elicited no significant difference in the recovery rate from photobleaching (≈50-70 s). However, in the case of BK-Nt-SNAP+GluN1-CLIP+2B, there was a trend to slower rates but a high variability of the data did not cause any significance under the statistical analysis (figure 4.26B-bottom left). Nonetheless, the mobile fraction of the BK-Nt-SNAP+GluN1-CLIP+2B (≈ 60%) was significantly less than the other combinations (figure 4.26B-bottom right: comparing BK-Nt-SNAP+GluA2 or BK-Nt-SNAP+GluN1-CLIP/2A —> # ≈ 0.037; *** = 0,0004). This result matches with the idea of a complex formation and less mobile BK-Nt-SNAP+GluN1-CLIP/2B hubs.

densities and distributions as was previously reported in our lab for BK-FMRP interaction (Kshatri et al., 2020).

Figure 4.27. BK-Nt-SNAP labelled with Surface Alexa Fluor 647 showed a sharp and defined particle localization under STORM superresolution microscopy which makes it suitable for this microscopy technique.

Single-molecule pull down allowed us to effectively count the stoichiometry of BK channel

Another fundamental question regarding a complex formation between proteins is the stoichiometry of association. To extract information about these interactions we set up Single Molecule Pull Down (SiMPull) in collaboration with Prof. Joshua Levitz (Weill Cornell Medicine, New York). One of the first goals was to set the capability of this technique to record BK-Nt-SNAP and BK-667-SNAP homotetramers. To do that, we counted the number of photobleaching steps for 8 movies per condition (figure 4.28A-B). BK-Nt-SNAP labelled with Alexa Fluor 546 showed a distribution with a majority of 4-bleaching steps. This was a clearly indicative of a homotetramer immobilization (figure 4.28A-right). However, in the case of the BK-667-SNAP construct labelled with the permeant dye Janelia Fluor 646, the distribution completely changed to a 2-step preponderance, although 4-step also showed a high proportion of the total population (figure 4.28B). These differences were attributed to the differences in the Alexa Fluor 546 and Alexa Fluor 647 stability, quantum yield

Figure 4.26. BK-Nt-SNAP diffused significantly slower along the membrane in the presence of GluN2B containing NMDARs. (A) BK-Nt-SNAP (labelled with SNAP Surface Alexa Fluor 546) alone recovered fast from photobleaching (top panels) as so do in the presence of GluN1-CLIP/2A (middle). In the presence of GluN1-CLIP/2B, the bleached region of BK-Nt-SNAP did not recover fully during the experiment time frame. (B) Fluorescence recovery vs time showed a clear difference in the GluN2B containing condition (more immobile fraction). (C) The recovery rates are not significantly different for all the conditions. (D) However, the mobile fraction is significantly lower for BK-Nt-SNAP+GluN1-CLIP/2B condition.

BK-Nt-SNAP construct constitutes an excellent candidate for superresolution microscopy

In order to validate our BK-Nt-SNAP tool even further, we took advantage of the possibilities of STORM superresolution microscopy. Our desirable goal is to see clusters and complexes formation between BK and NMDARs. It represents an advantage of the use of these self-labelling enzymes for microscopy, not only for restriction of labelling to proteins inserted in the plasma membrane, but also because we can avoid the use of antibodies and the specificity of the location of the molecules is higher. We expressed BK-Nt-SNAP and labeled it with SNAP-Alexa Fluor 647. This construct showed a good membrane expression as was demonstrated by normal epifluorescence and under TIRF (figure 4.27-left top and bottom panels respectively). STORM superresolution particle localization produced sharp and well-defined points under Gaussian representation, indicating a good localization efficiency and validating our construct for these experiments (figure 4.27-middle and right panels). In the ideal situation, together with GluN1-CLIP/2A or 2B combinations, this will let us to assert a quantitative vision of these cluster formations, evaluating their different

and lifetime (source: ThermoFisher data sheet:

https://www.thermofisher.com/es/es/home/references/molecular-probes-the-handbook/tables/fluorescence-quantum-yields-and-lifetimes-for-alexa-fluor-dyes.html). Therefore, preferentially use of Alexa Fluor 546 is desirable for 1-color SiMPull experiments.

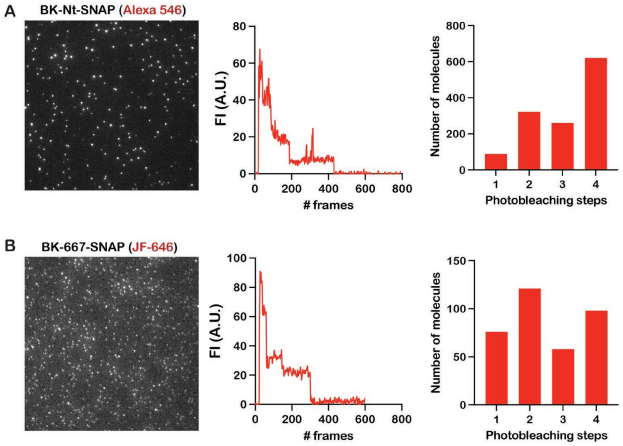

Figure 4.28. 1-color SiMPull was effective to immobilize and count the homotetramer stoichiometry of BK channels under two different SNAPtag fusion proteins. (A) BK-Nt-SNAP showed preponderant 4 photobleaching steps. (B) BK-667-SNAP showed a mixture of 2 and 4-steps. These differences were attributed to the different fluorophores used.

Nevertheless, as a proof of concept in two-color SiMPull we decided to use Alexa Fluor 647 for the BK-Nt-SNAP (with high labelling efficiency demonstrated) and the cyanine derivative DY-547 for GluN1-CLIP to balance fluorophore quality and labelling efficiency in our experimental framework. We could copulldown GluN1-CLIP/2B receptor with BK-Nt-SNAP (figure 4.29A-C). In the colocalized spots (≈6.8% of total BK-Nt-SNAP molecules) the number of steps varied widely for different combinations from 1:1 to 4:4, with a preponderance of 4:2 ratio (figure 4.29D). Considering that BK can be labelled in up to 4 subunits per full channel and NMDAR only in two (GluN1-CLIP), this result pointed towards a 1:1 stoichiometry of association (one full BK channel associates with one full NMDAR).

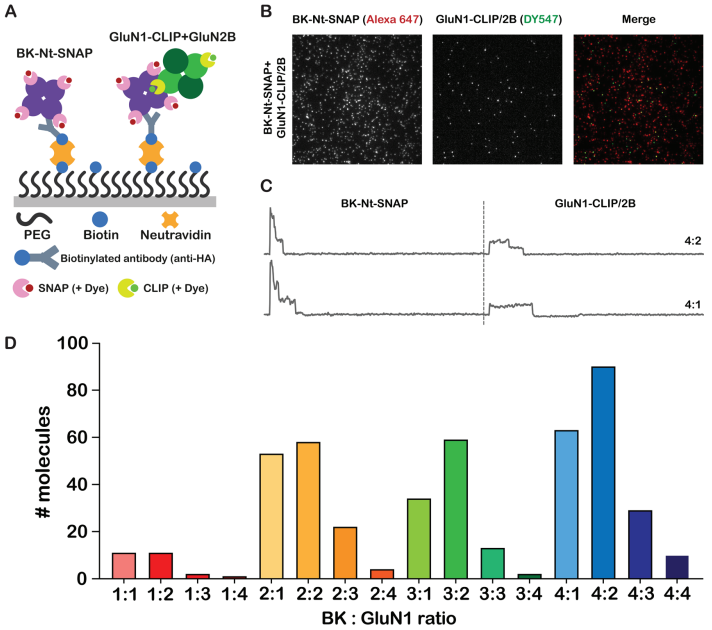

Figure 4.29. Two-color SiMPull of membrane extracts of cells expressing BK channel and GluN2B containing NMDAR showed copulldown of the two proteins as well as the effective counting of an estimated stoichiometry.

We are currently setting the SiMPull technique in our lab and ensuring the proper conditions of detergent, fluorophore, imaging buffer, etc. for our experiments. In our first trials, we have successfully pulled down BK-Nt-SNAP labelled with Surface Alexa Fluor 647 using biotinylated HA-antibody (figure 30A). This immobilization was specific as in conditions without antibody, the number of spots is negligible (figure 4.30B). Despite the experiments showing a high number of 4-step photobleaching, the highest number of steps was 2. This is comparable to the previous results with the use of a far red fluorophore (JF-646 in BK-667-SNAP). All our efforts are now in improving the quality of our samples, ensuring proper expression of the GluN1-CLIP construct as well as formuling an imaging buffer which extends the

photostability of these fluorophores to properly address the question of BK-NMDAR stoichiometry.

Figure 4.30. BK-Nt-SNAP (labelled with Surface Alexa Fluor 647) 1 color SiMPull rendered a majority of 2 photobleaching steps due to the lower photostability of this fluorophore. (A-B) Immobilization is highly specific and depends on the presence of the antibody in the microfluidic chamber. (C) Example of 4 photobleaching steps form the spot red circled in A. (D) Total quantification of three different days of experiments. (Experiments performed in our lab).

PART II: Discussion

BK channel functionally coassembly with NMDAR and these complexes are reconstituted in heterologous systems

We have recently described the functional association of NMDARs and BK channels, and the role of this coupling in synaptic function, in the basal dendrites of a population of regular-spiking BC-L5PNs (Gómez et al., 2021). NMDAR activation and subsequent Ca^{2+} entry promotes BK opening, which repolarizes the cell membrane and halts NMDAR activity. Both GluN2A- and GluN2B-containing NMDARs can activate BK channels, although our data suggest that GluN2B-containing NMDARs are more efficient. Functional coupling of NMDARs and BK channels in the basal dendrites of this specific BC-L5PN population modulates synaptic transmission and produces an increase in the threshold for induction of synaptic plasticity, indicating that NMDAR–BK association critically influences how specific neuronal types integrate afferent synaptic inputs. In fact, NMDAR–BK functional coupling bestows B-type BC-L5PNs with the ability to work as high-pass filters of incoming inputs, depending on the number and frequency of afferent stimuli.

In this work, we used a low frequency STDP protocol to induce LTP. Under these experimental conditions, it has been proposed that GluN1/GluN2B NMDARs make a larger contribution to the total charge transfer than GluN1/GluN2A NMDARs (Erreger et al., 2005), as expected from the slower deactivation rates of GluN2B-containing NMDARs (Vicini et al, 1998). Taking this into account, GluN2B-containing NMDARs should conduct more Ca^{2+} than GluN1/GluN2A channels in our experimental conditions, activating BK more efficiently. That being the case, Ca^{2+} entry through GluN2B-containing NMDARs would be the main contributor to BK activation and thus the inhibitory mechanism underlying modulation of synaptic transmission and LTP. This notion corresponds with our heterologous expression experiments using physiological concentrations of extracellular Na^{+}, in which GluN1/GluN2B NMDARs produced a larger leftward shift in the BK activation curve than GluN1/GluN2A (figure 4.18F-H). It also correlates with our observations in basal dendrites of BC-L5PNs, where specific blockade of GluN2B-containing NMDARs produced a larger reduction in the NMDA-evoked outward current. In summary, we have demonstrated that GluN2A- and GluN2B-containing NMDARs are able to activate BK channels in both heterologous expression systems and the

basal dendrites of BC-L5PNs. Furthermore, the GluN2B containing NMDARs tended to be closer and slowed down the BK channel diffusion in the membrane as shown in our FRET-AB (figure 4.19) and FRAP (figure 4.26) experiments. This supports the hypothesis of a tighter complex between BK-GluN1/2B. Whether BK channel coassemble with a combination of GluN1/GluN2A and GluN1/GluN2B heteromers, or GluN1/GluN2A/GluN2B triheteromers (Paoletti et al., 2013) in neurons, requires further investigation, a question that we plan to address with the new fluorescent tools that we have developed in the lab.

Another open research by this study is to elucidate which are the domains of interaction. Based on the work done by Zhang et al. where they proposed that the domains of interaction between BK channel and GluN1 comprises the S0-S1 linker of the BK channel (Zhang et al., 2018), we have designed new constructs with partial or total deletions of this domain to test this hypothesis in our experiments. This domain has been proposed to be intrinsically disordered between amino acids 58 and 93 (Peng et al., 2014; Shi et al., 2013), thus is a versatile region which could interact transiently with NMDARs. We plan to extend this study to the complex CTD of GluN1 subunit.

SLEs attached to BK and NMDARs are useful tools for study the interaction between these two proteins

The SNAP-tag and CLIP-tag have been extensively used for superresolution microscopy and single molecule techniques as versatile tags for simultaneous labelling of proteins (Liss et al., 2015; Erdmann et al., 2019; Bosch et al., 2014; Hansen et al., 2016; Lee et al., 2020). Here we have set out for the first time a BK channel with a SLE fused in two different positions. We overcame the problems of tag fusion in the N-terminus of this ion channel and validate this construct as a powerful tool for superresolution microscopy and single molecule approaches. On the other hand we could successfully tag GluN1 with the SNAP and CLIPtag. During the last steps of validation of these tools, a similar N-terminal GluN1-SNAP construct was reported in the literarure. This construct was used in smFRET experiments on the NMDAR activation conformational dynamics (Vyklicky et al., 2021). We also pulled down BK channel and NMDARs with single molecule resolution. This confirmed the capability of BK channel to interact physically with these glutamate receptors that was previously reported in the literature by co-IP (Zhang et al., 2018). With our tools validated, we are planning to open new pathways of research and collaborations (see *Outlook*).

Outlook

Structural rearrangements of the *gating ring* induced by Ca^{2+}

BK channel exhibits a kinetic complex behavior to integrate voltage and Ca^{2+} stimuli and transduce it to the spatially distant gate (Lee and Cui, 2011). Despite great efforts have been done to understand all the structural rearrangements that concert the opening of this channel (for review see Zhou et al., 2017; Latorre et al., 2017), we are just starting to understand its functioning and allosteric modulation. In this direction, the publication of the full-length BK structures of *Aplysia* (Tao et al., 2017; Hite et al., 2017) and human complexed with regulatory subunit β4 (Tao et al., 2019) have contributed significantly to this goal. In this work, we aimed to understand which the roles of the new residues are described by these structures in the Ca^{2+} sensing mechanisms as well as how RCKs interact with each other and mediate the activation of the channel. We extracted interesting information about a intrasubunit bridge (R514+E902+Y904) and two intersubunit interfaces that rearranged with the presence or absence of Ca^{2+} (RCK1-RCK2' and RCK2-RCK2'). We plan to perform kinetics experiments with the R514K, Y904F and Y904W mutants to puzzle out which constant parameters of the H-A model (Horrigan and Aldrich, 2002) are these mutants affecting, as they showed singular characteristics among them.

We also aim to finish the experiments with R786BzF, characterizing its G-V relationship, performing biochemical assays to unveil the most plausible photocrosslinking partners and analyzing the noise variance in the traces pre- and post-UV. This latter would lead us to determine if there was a change in the single channel conductance induced by the photocrosslinking. Another interesting experiment would be to combine the two UV positive mutants (N449BzF and R786BzF) in the same construct. As they showed antagonistic effects, we would expect that in the absence of Ca^{2+}, R786BzF would exert its effect and, in the presence of 100 μM Ca^{2+}, N449BzF would be the one leading to the current reduction. Together with different Ca^{2+} application in specific time frames would allow us to map the two movements we are currently studying and reveal their connection to orchestrate the BK channel activation.

Additionally, all the extracted information for the characterization of the TAG mutants will allow us to expand the unnatural amino acid insertions to different domains of the proteins to insert other side chain chemistries (e.g., fluorescent amino acids or reactive groups by cycloaddition) where we know they would not disrupt the proper BK channel function.

SLEs in ion channels are versatile tools for fluorescent labelling and optopharmacology

SLEs are powerful tools for the specific labelling of fusion proteins with different purposes that include, among others, single and multiple fluorescent labelling (Liss et al., 2015; Erdmann et al., 2019), protein purification (Deplus et al., 2013; Mickolajczyk et al., 2020) and optopharmacology (Broichhagen et al., 2015; Farrants et al., 2018). In this thesis, we aimed to develop tools based on this technology for its use in different sets of single molecule resolution experiments: single molecule pulldown, single molecule tracking and superresolution microscopy. We have successfully developed the tools and validated their functionality and labelling capability. Therefore, we can now address some questions regarding the interaction of BK channel and NMDARs. In collaboration with Prof. Joshua Levitz (Weill Cornell Medicine, New York, USA), we plan to use our tools in SiMPull experiments to estimate the stoichiometry between these two proteins. One intriguing question about these complexes is the GluN2 composition and what happens in the previously reported heterotrimeric receptors. To answer this, we aim to expand our tools fusing SNAP-tag and Halo-Tag (Promega) to GluN2 subunits and combine them with untagged or tagged GluN1 subunits and BK-Nt-CLIP. This would allow us to scale up our experiments up to three colors for STORM superresolution microscopy and SiMPull experiments. One hypothesis is that GluN2B containing NMDARs interact better with BK channel. As a proof of this, one of the SiMPull experiments will be to cotransfect BK-Nt-CLIP+GluN1+GluN2A-SNAP+GluN2BHalo and compare the proportions of SNAP and Halo tagged GluN2. If our hypothesis is correct, a high number of GluN2B containing NMDARs should colocalize with BK-Nt-CLIP spots.

In parallel, we are setting in the lab the conditions to insert SNAP and CLIPtags in endogenous BK and NMDARs in neurons through CRISPR technology. This will let us to label endogenous proteins and study the existence of these complexes in their natural setup.

In collaboration also with Prof. Levitz and Dr. Johanness Broichhagen (Leibniz Institute for Molecular Pharmacology, Berlin, Germany), we plan to attach to the SNAPtag in BK-Nt-SNAP construct a photoswitchable blocker that would selectively block and relieve the pore of BK channel under different wavelengths. This can be achieved with the use of azobenzene based compound that constitutes a flexible arm with a biologically active molecule (ligands, allosteric modulators or blockers) in one side and a benzylguanine (the SNAPtag reacting core) in the other (Broichhagen et al., 2015; Royal et al., 2019; Donthamsetti et al., 2019; Acosta-Ruiz et al., 2020). In preliminary experiments, we used BGAQ12 (EP3146981A1, European Patent Office), where a TEA molecule was fused to the terminus of the compound (figure O.1A). We labelled BK-Nt-SNAP with this compound as shown by the ineffectiveness of Alexa Fluor 546 to label this construct (figure O.1B-C). In gap-free experiments at - 40 mV holding potential and 100 μM Ca^{2+}, alternating light pulses of 385 and 525 nm showed a modest 2 % of current variation (figure O.1D). We plan to optimize this tool in heterologous systems and deploy it in cultured neurons and slices to study the function of BK channel in diverse scenarios using patterned light stimulation under different temporal resolution.

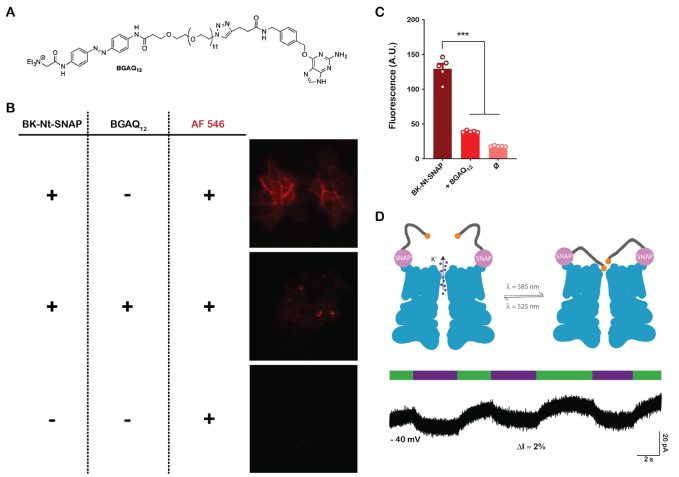

Figure O.1. Photoswitchable control of BK channel activation by genetic mediated tagging with BGAQ12 compound. (A) BGAQ12 (EP3146981A1, European Patent Office) is an azobenzene-based compound with a quaternary ammonium (TEA) as the reactive molecule in one end (left) and a benzylguanine to react with SNAPtag in the other end (right). (B) Successful labelling with BGAQ12. In the middle panel we labelled with the compound and after 45 minutes we added Alexa 546. As expected from a high-yield reaction of the great majority of SNAPtags fused to BK channel, a faint labelling with the fluorophore was achieved after they reacted with BGAQ12. (C) Quantification of the experiment in (B). Fluorescence intensity was significantly different between conditions without and with BGAQ12. (D) Reversible blocking effect in the BK channel current at -40 mV and 100 μM Ca^{2+} caused by BGAQ12.

Other tags and future directions

There are some limitations and trends in the use of fluorescent labels in the study of ion

Conclusions

channels. The smaller the tag, the less disruption of the normal protein function. To achieve this goal, one of the strategies has been to use the click chemistry. The first use of this nature was described by Roger Tsien and coworkers using a tetracysteine tag (CCXXCC) fused to an α helix (Griffin et al., 1998). Named as FlAsH, this technology provided small steric effect and a non-covalent binding to a biarsenical dye. However, these dyes can react with endogenous cysteines in the proteins where two or more cysteines exist, giving a high background signal, and the toxicity of the biarsenical dyes is sometimes high (Griffin et al., 1998). In ion channels it has been also used the cysteine tagging (Cha and Bezanilla, 1997). In this case a residue mutated to cysteine in the site where the fluorophore would like to be located reacts with a MTS or maleimide fused fluorophore, labelling the protein covalently. However, they are restricted to positions in contact with solvent and they can label other cysteines from the protein of interest and others, lacking specificity and increasing the background (Braun et al., 2020a). Maybe one of the most solid strategies is the modification of proteins with UAAs. As explained before, this method has some limitations but rely on the use of an amino acid specific aaRS and a tRNA specific for the suppression of TAG Amber STOP codon, what sometimes could be challenging. However, the use of intrinsically fluorescent UAAs or chemically incorporation by bioorthogonal chemistry in reactive UAAs has been established as a versatile, specific and potentially accessibility-unrestricted technique to use in conformational and localization studies. In structure-function studies of ion channels. ANAP fluorescent UAAs has been used widely in nicotinic receptors (Pantoja et al., 2009), Shaker (Kalstrup and Blunck, 2013; Kalstrup and Blunck, 2018), GlyRα1 (Sho et al., 2017), TRPV1 (Zagotta et al., 2016), ASIC1a (Wulf and Pless, 2018) and KATP channels (Puljung et al., 2019; Usher et al., 2020) among other channels. Other fluorescent UAAs have been used as well as coumarin-tyrosine (Steinberg et al., 2017). On the other hand, the use of reactive UAAs has also demonstrated as a powerful tool for labelling residues in ion channels and study their conformational changes (see for example Dolino et al., 2015 in NMDARs or Gupta et al., 2019 in Shaker). These two approaches and more alternatives to small and specific labelling of ion channels have been thoroughly reviewed in Young and Schultz, 2018; Lee et al., 2019 and Braun et al., 2020.

Altogether, these state-of-the-art approaches allow to expand the available tools for studying the variety of ion channel behaviors. The developed tools and constructs and the experience gained in the use of UAAs allow us to use these tools in the next future and to study BK channel structural dynamics, untangling the complexity of this channel. Furthermore, we can employ these in neurons tagging environmental sensitive epitopes (Kang et al., 2018; Arsic et al., 2021), and combine with SLEs, as recently reported (Bessa-Neto et al., 2021).

Based on our results, we can conclude that:

1. We have evaluated in human BK the role of residues involved in gating by Ca^{2+}, recently proposed in the Aplysia structures (which had not been previously studied in human BK).
2. Functional data from the human BK channel support an interaction between residues R514 (RCK1 site), E902 & Y904 (Ca^{2+}-bowl site).
3. Amino acid substitutions of the cation-π interaction suggest that R514 and Y904 interact, which would support the hypothesis of a structural bridge underlying the cooperative mechanism of Ca^{2+} sensing in the BK channel proposed by Tao et al. (Tao et al., 2017).
4. We have demonstrated that BzF insertion in our BK-TAG mutants renders functional proteins.
5. Our results suggest an intersubunit and state dependent photocrosslinking of BzF in N449BzF and R786BzF mutants.
6. While both GluN2A- and GluN2B-containing NMDARs can functionally couple to BK channels, GluN2B containing ones seem to couple functionally and physically better to BK channels.
7. SNAPtag and CLIPtag fusion in BK and GluN1 rendered well expressed and functional proteins. They can be labeled with their specific substrates with a high yield. These tools are powerful to isolate plasma membrane inserted channels and analyze their behavior and complex formation under different experimental frameworks.

References

Acosta-Ruiz, Amanda, Vanessa A. Gutzeit, Mary Jane Skelly, Samantha Meadows, Joon Lee, Puja Parekh, Anna G. Orr, et al. 2020. "Branched Photoswitchable Tethered Ligands Enable Ultra-Efficient Optical Control and Detection of G Protein-Coupled Receptors In Vivo." *Neuron* 105 (3): 446-463.e13. https://doi.org/10.1016/j.neuron.2019.10.036.

Adelman, John P., Ke Zhong Shen, Michael P. Kavanaugh, Robin A. Warren, Yan Na Wu, Armando Lagrutta, Chris T. Bond, and R. Alan North. 1992. "Calcium-Activated Potassium Channels Expressed from Cloned Complementary DNAs." *Neuron* 9 (2): 209–16. https://doi.org/10.1016/0896-6273(92)90160-F.

A. Agmon, B. W. Connors, Correlation between intrinsic firing patterns and thalamocortical synaptic responses of neurons in mouse barrel cortex. *The Journal of neuroscience : the official journal of the Society for Neuroscience* **12**, 319-329 (1992).

Ahrendt, Eva, Barry Kyle, Andrew P. Braun, and Janice E.A. Braun. 2014. "Cysteine String Protein Limits Expression of the Large Conductance, Calcium-Activated K+ (BK) Channel." *PLoS ONE* 9 (1): 1–9. https://doi.org/10.1371/journal.pone.0086586.

Anand, René, Lynn Bason, Volodymyr Gerzanich, Xiao Peng, Jon Lindstrom, and Mohammad S. Saedi. 1993. "Reporter Epitopes: A Novel Approach To Examine Transmembrane Topology of Integral Membrane Proteins Applied to the A1 Subunit of the Nicotinic Acetylcholine Receptor." *Biochemistry* 32 (38): 9975–84. https://doi.org/10.1021/bi00089a013.

Arsic, Aleksandra, Cathleen Hagemann, Nevena Stajkovic, Timm Schubert, and Ivana Nikic-Spiegel. 2021. "Minimal Genetically Encoded Tags for Fluorescent Protein Labeling in Living Neurons." *BioRxiv*, 1–33. https://doi.org/10.1101/2021.01.14.426692.

Atkinson, Nigel S., Gail A. Robertson, and Barry Ganetzky. 1991. "A Component of Calcium-Activated Potassium Channels Encoded by the Drosophila Slo Locus." *Science* 253 (5019): 551–55. https://doi.org/10.1126/science.1857984.

Bailey, Cole S, Hans J Moldenhauer, Su Mi Park, Sotirios Keros, and Andrea L Meredith. 2019. "KCNMA1-Linked Channelopathy" 151 (10).

Baillie, Landon D., Helmut Schmidhammer, and Sean J. Mulligan. 2015. "Peripheral μ-Opioid Receptor Mediated Inhibition of Calcium Signaling and Action Potential-Evoked Calcium Fluorescent Transients in Primary Afferent CGRP Nociceptive Terminals." *Neuropharmacology* 93: 267–73. https://doi.org/10.1016/j.neuropharm.2015.02.011.

Bao, Lin, Christina Kaldany, Ericka C. Holmstrand, and Daniel H. Cox. 2004. "Mapping the BKCa Channel's 'Ca2+ Bowl': Side-Chains Essential for Ca^{2+} Sensing." *Journal of General Physiology* 123 (5): 475–89. https://doi.org/10.1085/jgp.20409052.

Bao, Lin, Anne M. Rapin, Ericka C. Holmstrand, and Daniel H. Cox. 2002. "Elimination of the BKCa Channel's High-Affinity Ca^{2+} Sensitivity." *Journal of General Physiology* 120 (2): 173–89. https://doi.org/10.1085/jgp.20028627.

147–61. https://doi.org/10.1085/jgp.200709862.

Chavis, Pascale, Fabrice Ango, Jean Marie Michel, Joel Bockaert, and Laurent Fagni. 1998. "Modulation of Big K+ Channel Activity by Ryanodine Receptors and L-Type Ca^{2+} Channels in Neurons." *European Journal of Neuroscience* 10 (7): 2322–27. https://doi.org/10.1046/j.1460-9568.1998.00243.x.

Chazot, Paul L., Miroslav Cik, and F. Anne Stephenson. 1995. "An Investigation into the Role of N-Glycosylation in the Functional Expression of a Recombinant Heteromeric NMDA Receptor." *Molecular Membrane Biology* 12 (4): 331–37. https://doi.org/10.3109/09687689509072435.

Chin, Jason W. 2014. "Expanding and Reprogramming the Genetic Code of Cells and Animals." *Annual Review of Biochemistry* 83: 379–408. https://doi.org/10.1146/annurev-biochem-060713-035737.

Chin, Jason W., T. Ashton Cropp, J. Christopher Anderson, Mridul Mukherji, Zhiwen Zhang, and Peter G. Schultz. 2003. "An Expanded Eukaryotic Genetic Code." *Science* 301 (5635): 964–67. https://doi.org/10.1126/science.1084772.

Chin, Jason W., Andrew B. Martin, David S. King, Lei Wang, and Peter G. Schultz. 2002. "Addition of a Photocrosslinking Amino Acid to the Genetic Code of Escherichia Coli." *Proceedings of the National Academy of Sciences of the United States of America* 99 (17): 11020–24. https://doi.org/10.1073/pnas.172226299.

Collingridge, Graham L., Richard W. Olsen, John Peters, and Michael Spedding. 2009. "A Nomenclature for Ligand-Gated Ion Channels." *Neuropharmacology* 56 (1): 2–5. https://doi.org/10.1016/j.neuropharm.2008.06.063.

C. M. Constantinople, R. M. Bruno, Deep cortical layers are activated directly by thalamus. *Science* **340**, 1591-1594 (2013).

Contet, C., S. P. Goulding, D. A. Kuljis, and A. L. Barth. 2016. *BK Channels in the Central Nervous System. International Review of Neurobiology*. 1st ed. Vol. 128. Elsevier Inc. https://doi.org/10.1016/bs.irn.2016.04.001.

Cornish, V. W., D. R. Benson, C. A. Altenbach, K. Hideg, W. L. Hubbell, and P. G. Schultz. 1994. "Site-Specific Incorporation of Biophysical Probes into Proteins." *Proceedings of the National Academy of Sciences of the United States of America* 91 (8): 2910–14. https://doi.org/10.1073/pnas.91.8.2910.

Craven, Kimberley B., and William N. Zagotta. 2006. "CNG and HCN Channels: Two Peas, One Pod." *Annual Review of Physiology*. https://doi.org/10.1146/annurev.physiol.68.040104.134728.

Debelouchina, Galia T., and Tom W. Muir. 2017. "A Molecular Engineering Toolbox for the Structural Biologist." *Quarterly Reviews of Biophysics* 50. https://doi.org/10.1017/S0033583517000051.

Deplus, Rachel, Benjamin Delatte, Marie K. Schwinn, Matthieu Defrance, Jacqui Méndez, Nancy Murphy, Mark A. Dawson, et al. 2013. "TET2 and TET3 Regulate GlcNAcylation and H3K4 Methylation through OGT and SET1/COMPASS." *EMBO Journal* 32 (5): 645–55. https://doi.org/10.1038/emboj.2012.357.

Ding, S., and R. Horn. 2001. "Slow Photo-Cross-Linking Kinetics of Benzophenone-Labeled Voltage Sen-

Basu, Srinjan, Lisa Maria Needham, David Lando, Edward J.R. Taylor, Kai J. Wohlfahrt, Devina Shah, Wayne Boucher, et al. 2018. "FRET-Enhanced Photostability Allows Improved Single-Molecule Tracking of Proteins and Protein Complexes in Live Mammalian Cells." *Nature Communications* 9 (1). https://doi.org/10.1038/s41467-018-04486-0.

Berkefeld, Henrike, and Bernd Fakler. 2008. "Repolarizing Responses of BKCa-Cav Complexes Are Distinctly Shaped by Their Cav Subunits." *Journal of Neuroscience* 28 (33): 8238–45. https://doi.org/10.1523/JNEUROSCI.2274-08.2008.

Berkefeld, Henrike, Claudia A Sailer, Wolfgang Bildl, Volker Rohde, Jörg-oliver Thumfart, Silke Eble, Norbert Klugbauer, et al. 2006. "BK Ca -Cav Channel Complexes." *Science*, no. October: 615–21.

Bessa-Neto, Diogo, Alexander Kuhlemann, Gerti Beliu, Valeria Pecoraro, Sören Doose, Natacha Retailleau, Nicolas Chevrier, David Perrais, Markus Sauer, and Daniel Choquet. 2021. "Bioorthogonal Labeling of Transmembrane Proteins with Non-Canonical Amino Acids Allows Access to Masked Epitopes in Live Neurons." *BioRxiv*, 2021.02.27.433189. https://doi.org/10.1101/2021.02.27.433189.

Bian, Shumin, Jun Ping Bai, Hannah Chapin, Cathy Moellic, Huiping Dong, Michael Caplan, Fred J. Sigworth, and Dhasakumar S. Navaratnam. 2011. "Interactions between β-Catenin and the HSlo Potassium Channel Regulates HSlo Surface Expression." *PLoS ONE* 6 (12). https://doi.org/10.1371/journal.pone.0028264.

Braun, N., Z. P. Sheikh, and S. A. Pless. 2020. "The Current Chemical Biology Tool Box for Studying Ion Channels." *Journal of Physiology* 598 (20): 4455–71. https://doi.org/10.1113/JP276695.

Braun, Nina, Søren Friis, C Ihling, A Sinz, J Andersen, and Stephan Alexander Pless. 2020. "High-Throughput Characterization of 309 Photocrosslinker-Bearing ASIC1a Variants Maps Residues Critical for Channel Function and Pharmacology." *Biorxiv*, 1–32.

Brelidze, Tinatin I., Xiaowei Niu, and Karl L. Magleby. 2003. "A Ring of Eight Conserved Negatively Charged Amino Acids Doubles the Conductance of BK Channels and Prevents Inward Rectification." *Proceedings of the National Academy of Sciences of the United States of America* 100 (15): 9017–22. https://doi.org/10.1073/pnas.1532257100.

Broichhagen, Johannes, Arunas Damijonaitis, Joshua Levitz, Kevin R. Sokol, Philipp Leippe, David Konrad, Ehud Y. Isacoff, and Dirk Trauner. 2015. "Orthogonal Optical Control of a G Protein-Coupled Receptor with a SNAP-Tethered Photochromic Ligand." *ACS Central Science* 1 (7): 383–93. https://doi.org/10.1021/acscentsci.5b00260.

Budelli, Gonzalo, Yanyan Geng, Alice Butler, Karl L. Magleby, and Lawrence Salkoff. 2013. "Properties of Slo1 K+ Channels with and without the Gating Ring." *Proceedings of the National Academy of Sciences of the United States of America* 110 (41): 16657–62. https://doi.org/10.1073/pnas.1313433110.

Butler, Alice, Susan Tsunoda, David P. McCobb, Aguan Wei, and Lawrence Salkoff. 1993. "MSlo, a Complex Mouse Gene Encoding 'Maxi' Calcium-Activated Potassium Channels." *Science* 261 (5118): 221–24. https://doi.org/10.1126/science.7687074.

Carvacho, Ingrid, Wendy Gonzalez, Yolima P. Torres, Sebastian Brauchi, Osvaldo Alvarez, Fernando D. Gonzalez-Nilo, and Ramon Latorre. 2008. "Intrinsic Electrostatic Potential in the BK Channel Pore: Role in Determining Single Channel Conductance and Block." *Journal of General Physiology* 131 (2):

sors of Ion Channels." *Biochemistry* 40 (35): 10707–16. https://doi.org/10.1021/bi010709y.

Dolino, Drew M., David Cooper, Swarna Ramaswamy, Henriette Jaurich, Christy F. Landes, and Vasanthi Jayaraman. 2015. "Structural Dynamics of the Glycine-Binding Domain of the N-Methyl-D-Aspartate Receptor." *Journal of Biological Chemistry* 290 (2): 797–804. https://doi.org/10.1074/jbc.M114.605436.

Donthamsetti, Prashant C., Johannes Broichhagen, Vojtech Vyklicky, Cherise Stanley, Zhu Fu, Meike Visel, Joshua L. Levitz, Jonathan A. Javitch, Dirk Trauner, and Ehud Y. Isacoff. 2019. "Genetically Targeted Optical Control of an Endogenous G Protein-Coupled Receptor." *Journal of the American Chemical Society* 141 (29): 11522–30. https://doi.org/10.1021/jacs.9b02895.

Dormán, György, and Glenn D. Prestwich. 1994. "Benzophenone Photophores in Biochemistry." *Biochemistry* 33 (19): 5661–73. https://doi.org/10.1021/bi00185a001.

Doyle, Declan A, Morais Cabral, Richard A Pfuetzner, Anling Kuo, Jacqueline M Gulbis, Steven L Cohen, Brian T Chait, and Roderick Mackinnon. 1998. "The Structure of the PotassiumChannel: Molecular Basis of K." *Science* 280 (April): 1–9. papers2://publication/uuid/054C4FA3-F61C-4B97-92F6-7707970FA7F6.

Du, Wei, Jocelyn F. Bautista, Huanghe Yang, Ana Diez-Sampedro, Sun Ah You, Lejin Wang, Prakash Kotagal, et al. 2005. "Calcium-Sensitive Potassium Channelopathy in Human Epilepsy and Paroxysmal Movement Disorder." *Nature Genetics* 37 (7): 733–38. https://doi.org/10.1038/ng1585.

Du, Xiaofei, Joao L. Carvalho-De-Souza, Cenfu Wei, Willy Carrasquel-Ursulaez, Yenisleidy Lorenzo, Naileth Gonzalez, Tomoya Kubota, et al. 2020. "Loss-of-Function BK Channel Mutation Causes Impaired Mitochondria and Progressive Cerebellar Ataxia." *Proceedings of the National Academy of Sciences of the United States of America* 117 (11): 6023–34. https://doi.org/10.1073/pnas.1920008117.

Dudem, Srikanth, Roddy J. Large, Shruti Kulkarni, Heather McClafferty, Irina G. Tikhonova, Gerard P. Sergeant, Keith D. Thornbury, Michael J. Shipston, Brian A. Perrino, and Mark A. Hollywood. 2020. "LINGO1 Is a Regulatory Subunit of Large Conductance, Ca^{2+}-Activated Potassium Channels." *Proceedings of the National Academy of Sciences of the United States of America* 117 (4): 2194–2200. https://doi.org/10.1073/pnas.1916715117.

Dworetzky, S. I., Trojnacki, J. T., & Gribkoff, V. K. (1994). "*Cloning and expression of a human large-conductance calcium-activated potassium channel*". *Molecular Brain Research*, *27(1)*, *189–193*. doi:10.1016/0169-328x(94)90203-8

Earley, Scott, Thomas J. Heppner, Mark T. Nelson, and Joseph E. Brayden. 2005. "TRPV4 Forms a Novel Ca^{2+} Signaling Complex with Ryanodine Receptors and BKCa Channels." *Circulation Research* 97 (12): 1270–79. https://doi.org/10.1161/01.RES.0000194321.60300.d6.

S. El-Boustani *et al.*, Anatomically and functionally distinct thalamocortical inputs to primary and secondary mouse whisker somatosensory cortices. *Nature communications* **11**, 3342 (2020).

Engbers, Jordan D.T., Dustin Anderson, Gerald W. Zamponi, and Ray W. Turner. 2013. "Signal Processing by T-Type Calcium Channel Interactions in the Cerebellum." *Frontiers in Cellular Neuroscience* 7 (NOV): 1–15. https://doi.org/10.3389/fncel.2013.00230.

Erdmann, Roman S., Stephanie Wood Baguley, Jennifer H. Richens, Rebecca F. Wissner, Zhiqun Xi, Edward S. Allgeyer, Sheng Zhong, et al. 2019. "Labeling Strategies Matter for Super-Resolution Microscopy: A Comparison between HaloTags and SNAP-Tags." *Cell Chemical Biology* 26 (4): 584-592.e6. https://doi.org/10.1016/j.chembiol.2019.01.003.

Erreger, Kevin, Matthew T. Geballe, Anders Kristensen, Philip E. Chen, Kasper B. Hansen, C. Justin Lee, Hongjie Yuan, et al. 2007. "Subunit-Specific Agonist Activity at NR2A-, NR2B-, NR2C-, and NR2D-Containing N-Methyl-D-Aspartate Glutamate Receptors." *Molecular Pharmacology* 72 (4): 907–20. https://doi.org/10.1124/mol.107.037333.

Eun, Young Kim, Claudia P. Alvarez-Baron, and Stuart E. Dryer. 2009. "Canonical Transient Receptor Potential Channel (TRPC) 3 and TRPC6 Associate with Large-Conductance Ca^{2+}-Activated K + (BK ca) Channels: Role in BK ca Trafficking to the Surface of Cultured Podocytes." *Molecular Pharmacology* 75 (3): 466–77. https://doi.org/10.1124/mol.108.051912.

Faber, E. S.Louise, and Pankaj Sah. 2002. "Physiological Role of Calcium-Activated Potassium Currents in the Rat Lateral Amygdala." *Journal of Neuroscience* 22 (5): 1618–28. https://doi.org/10.1523/jneurosci.22-05-01618.2002.

Fakler, Bernd, and John P. Adelman. 2008. "Control of KCa Channels by Calcium Nano/Microdomains." *Neuron* 59 (6): 873–81. https://doi.org/10.1016/j.neuron.2008.09.001.

Feetham, C. H., N. Nunn, R. Lewis, C. Dart, and Richard Barrett-Jolley. 2015. "TRPV4 and KCa Ion Channels Functionally Couple as Osmosensors in the Paraventricular Nucleus." *British Journal of Pharmacology* 172 (7): 1753–68. https://doi.org/10.1111/bph.13023.

Gackière, Florian, Marine Warnier, Maria Katsogiannou, Sandra Derouiche, Philippe Delcourt, Etienne Dewailly, Christian Slomianny, et al. 2013. "Functional Coupling between Large-Conductance Potassium Channels and Cav3.2 Voltage-Dependent Calcium Channels Participates in Prostate Cancer Cell Growth." *Biology Open* 2 (9): 941–51. https://doi.org/10.1242/bio.20135215.

Galardy, R.E., L.C. Craig, and M.P. Printz. 1973. "Benzophenone Triplet: A New Photochemical Probe of Biological Ligand-Receptor Interactions." *Nat. Phys. Sci.* 241: 20.

Galvez, A., G. Gimenez-Gallego, J. P. Reuben, L. Roy-Contancin, P. Feigenbaum, G. J. Kaczorowski, and M. L. Garcia. 1990. "Purification and Characterization of a Unique, Potent, Peptidyl Probe for the High Conductance Calcium-Activated Potassium Channel from Venom of the Scorpion Buthus Tamulus." *Journal of Biological Chemistry* 265 (19): 11083–90. https://doi.org/10.1016/s0021-9258(19)38560-6.

Gautier, Arnaud, Alexandre Juillerat, Christian Heinis, Ivan Reis Corrêa, Maik Kindermann, Florent Beaufils, and Kai Johnsson. 2008. "An Engineered Protein Tag for Multiprotein Labeling in Living Cells." *Chemistry and Biology* 15 (2): 128–36. https://doi.org/10.1016/j.chembiol.2008.01.007.

Geng, Yanyan, Zengqin Deng, Guohui Zhang, Gonzalo Budelli, Alice Butler, Peng Yuan, Jianmin Cui, Lawrence Salkoff, and Karl L. Magleby. 2020. "Coupling of Ca^{2+} and Voltage Activation in BK Channels through the AB Helix/Voltage Sensor Interface." *Proceedings of the National Academy of Sciences*

poration of a Photoreactive Amino Acid." *Nature Methods* 2 (3): 201–6. https://doi.org/10.1038/nmeth739.

Hite, Richard K., Xiao Tao, and Roderick MacKinnon. 2017. "Structural Basis for Gating the High-Conductance Ca^{2+}-Activated K+ Channel." *Nature* 541 (7635): 52–57. https://doi.org/10.1038/nature20775.

Hodgkin, A. L., and A. F. Huxley. 1952. "A Quantitative Description of Membrane Current and Its Application to Conduction and Excitation in Nerve." *The Journal of Physiology* 117 (4): 500–544. https://doi.org/10.1113/jphysiol.1952.sp004764.

Horak, Martin, and Robert J. Wenthold. 2009. "Different Roles of C-Terminal Cassettes in the Trafficking of Full-Length NR1 Subunits to the Cell Surface." *Journal of Biological Chemistry* 284 (15): 9683–91. https://doi.org/10.1074/jbc.M807050200.

Horn, Richard, Shinghua Ding, and Hermann J. Gruber. 2000. "Immobilizing the Moving Parts of Voltage-Gated Ion Channels." *Journal of General Physiology* 116 (3): 461–75. https://doi.org/10.1085/jgp.116.3.461.

Horrigan, Frank T., and Richard W. Aldrich. 1999. "Allosteric Voltage Gating of Potassium Channels I: MSlo Ionic Currents in the Absence of Ca^{2+}." *Journal of General Physiology* 114 (2): 277–304. https://doi.org/10.1085/jgp.114.2.277.

Horrigan, Frank T., and Aldrich, Richard W. 2002. "Coupling between Voltage Sensor Activation, Ca^{2+} Binding and Channel Opening in Large Conductance (BK) Potassium Channels." *Journal of General Physiology* 120 (3): 267–305. https://doi.org/10.1085/jgp.20028605.

Hou, Shangwei, Rong Xu, Stefan H. Heinemann, and Toshinori Hoshi. 2008. "The RCK1 High-Affinity Ca^{2+} Sensor Confers Carbon Monoxide Sensitivity to Slo1 BK Channels." *Proceedings of the National Academy of Sciences of the United States of America* 105 (10): 4039–43. https://doi.org/10.1073/pnas.0800304105.

Hu, H., Li Rong Shao, Sorush Chavoshy, Ning Gu, Maria Trieb, Ralf Behrens, Petter Laake, et al. 2001. "Presynaptic Ca^{2+}-Activated K+ Channels in Glutamatergic Hippocampal Terminals and Their Role in Spike Repolarization and Regulation of Transmitter Release." *Journal of Neuroscience* 21 (24): 9585–97. https://doi.org/10.1523/jneurosci.21-24-09585.2001.

Indriati, Dwi Wahyu, Naomi Kamasawa, Ko Matsui, Andrea L. Meredith, Masahiko Watanabe, and Ryuichi Shigemoto. 2013. "Quantitative Localization of Cav2.1 (P/Q-Type) Voltage-Dependent Calcium Channels in Purkinje Cells: Somatodendritic Gradient and Distinct Somatic Coclustering with Calcium-Activated Potassium Channels." *Journal of Neuroscience* 33 (8): 3668–78. https://doi.org/10.1523/JNEUROSCI.2921-12.2013.

Irie, Tomohiko, and Laurence O. Trussell. 2017. "Double-Nanodomain Coupling of Calcium Channels, Ryanodine Receptors, and BK Channels Controls the Generation of Burst Firing." *Neuron* 96 (4): 856-870.e4. https://doi.org/10.1016/j.neuron.2017.10.014.

Isaacson, Jeffry S., and Gabe J. Murphy. 2001. "Glutamate-Mediated Extrasynaptic Inhibition: Direct Coupling of NMDA Receptors to Ca^{2+}-Activated K+ Channels." *Neuron* 31 (6): 1027–34. https://doi.org/10.1016/S0896-6273(01)00428-7.

of the United States of America 117 (25): 14512–21. https://doi.org/10.1073/pnas.1908183117.

Giebisch, G. 2001. "Renal Potassium Channels: Function, Regulation, and Structure." In *Kidney International*, 60:436–45. https://doi.org/10.1046/j.1523-1755.2001.060002436.x.

Gorini, Giorgio, Olga Ponomareva, Kevin S. Shores, Maria D. Person, R. Adron Harris, and R. Dayne Mayfield. 2010. "Dynamin-1 Co-Associates with Native Mouse Brain BKCa Channels: Proteomics Analysis of Synaptic Protein Complexes." *FEBS Letters* 584 (5): 845–51. https://doi.org/10.1016/j.febslet.2009.12.061.

Grigoli, Marilena, Martina Sgritta, and Enrico Cherubini. 2016. "Presynaptic BK Channels Control Transmitter Release: Physiological Relevance and Potential Therapeutic Implications." *Journal of Physiology* 594 (13): 3489–3500. https://doi.org/10.1113/JP271841.

Grunnet, Morten, and Walter A. Kaufmann. 2004. "Coassembly of Big Conductance Ca^{2+}-Activated K+ Channels and L-Type Voltage-Gated Ca^{2+} Channels in Rat Brain." *Journal of Biological Chemistry* 279 (35): 36445–53. https://doi.org/10.1074/jbc.M402254200.

Gu, Ning, Koen Vervaeke, and Johan F. Storm. 2007. "BK Potassium Channels Facilitate High-Frequency Firing and Cause Early Spike Frequency Adaptation in Rat CA1 Hippocampal Pyramidal Cells." *Journal of Physiology* 580 (3): 859–82. https://doi.org/10.1113/jphysiol.2006.126367.

Guo, Chang Kai, Yi Wang, Tao Zhou, Hong Yu, Wen Juan Zhang, and Wei Jia Kong. 2012. "M2 Muscarinic ACh Receptors Sensitive BK Channels Mediate Cholinergic Inhibition of Type II Vestibular Hair Cells." *Hearing Research* 285 (1–2): 13–19. https://doi.org/10.1016/j.heares.2012.02.003.

Gupta, Kanchan, Gilman Es Toombes, and Kenton J. Swartz. 2019. "Exploring Structural Dynamics of a Membrane Protein by Combining Bioorthogonal Chemistry and Cysteine Mutagenesis." *ELife* 8: 1–28. https://doi.org/10.7554/eLife.50776.

Gutzeit, Vanessa A., Jordana Thibado, Daniel Starer Stor, Zhou Zhou, Scott C. Blanchard, Olaf S. Andersen, and Joshua Levitz. 2019. "Conformational Dynamics between Transmembrane Domains and Allosteric Modulation of a Metabotropic Glutamate Receptor." *ELife* 8: 1–29. https://doi.org/10.7554/eLife.45116.

Gutzmann, Jakob J., Lin Lin, and Dax A. Hoffman. 2019. "Functional Coupling of Cav2.3 and BK Potassium Channels Regulates Action Potential Repolarization and Short-Term Plasticity in the Mouse Hippocampus." *Frontiers in Cellular Neuroscience* 13 (February): 1–14. https://doi.org/10.3389/fncel.2019.00027.

Hicks, Gareth A., and Neil V. Marrion. 1998. "Ca^{2+}-Dependent Inactivation of Large Conductance Ca^{2+}-Activated K+ (BK) Channels in Rat Hippocampal Neurones Produced by Pore Block from an Associated Particle." *Journal of Physiology* 508 (3): 721–34. https://doi.org/10.1111/j.1469-7793.1998.721bp.x.

Hille, B. (2001). "Ion channels of excitable membranes". Sunderland, Mass: Sinauer.

Hino, Nobumasa, Yuko Okazaki, Takatsugu Kobayashi, Akiko Hayashi, Kensaku Sakamoto, and Shigeyuki Yokoyama. 2005. "Protein Photo-Cross-Linking in Mammalian Cells by Site-Specific Incor-

Jiang, Youxing, Alexander Pico, Martine Cadene, Brian T Chait, and Roderick Mackinnon. 2001. "Structure of the RCK Domain from the E. Coli K+ Channel and Demonstration of Its Presence in the Human BK Channel" 29: 593–601.

Kauer, J. C., S. Erickson-Viitanen, H. R. Wolfe, and W. F. DeGrado. 1986. "P-Benzoyl-L-Phenylalanine, a New Photoreactive Amino Acid. Photolabeling of Calmodulin with a Synthetic Calmodulin-Binding Peptide." *Journal of Biological Chemistry* 261 (23): 10695–700. https://doi.org/10.1016/s0021-9258(18)67441-1.

Keppler, Anije, Susanne Gendreizig, Thomas Gronemeyer, Horst Pick, Horst Vogel, and Kai Johnsson. 2003. "A General Method for the Covalent Labeling of Fusion Proteins with Small Molecules in Vivo." *Nature Biotechnology* 21 (1): 86–89. https://doi.org/10.1038/nbt765.

Klippenstein, Viktoria, Laetitia Mony, and Pierre Paoletti. 2018. "Probing Ion Channel Structure and Function Using Light-Sensitive Amino Acids." *Trends in Biochemical Sciences* 43 (6):436–51. https://doi.org/10.1016/j.tibs.2018.02.012.

H. G. Knaus *et al.*, Tremorgenic indole alkaloids potently inhibit smooth muscle high-conductance calcium-activated potassium channels. *Biochemistry* **33**, 5819-5828 (1994).

Knaus, Hans Günther, Christoph Schwarzer, Robert O.A. Koch, Andreas Eberhart, Gregory J. Kaczorowski, Hartmut Glossmann, Frank Wunder, Olaf Pongs, Maria L. Garcia, and Günther Sperk. 1996. "Distribution of High-Conductance Ca^{2+}-Activated K^+ Channels in Rat Brain: Targeting to Axons and Nerve Terminals." *Journal of Neuroscience* 16 (3): 955–63. https://doi.org/10.1523/jneurosci.16-03-00955.1996.

Kolodziej, Peter A., and Richard A. Young. 1991. "Epitope Tagging and Protein Surveillance." *Methods in Enzymology* 194 (C): 508–19. https://doi.org/10.1016/0076-6879(91)94038-E.

Koval, Olga M., Yun Fan, and Brad S. Rothberg. 2007. "A Role for the S0 Transmembrane Segment in Voltage-Dependent Gating of BK Channels." *Journal of General Physiology* 129 (3): 209–20. https://doi.org/10.1085/jgp.200609662.

Kshatri, Aravind, Alejandro Cerrada, Roger Gimeno, David Bartolomé-Martín, Patricio Rojas, and Teresa Giraldez. 2020. "Differential Regulation of BK Channels by Fragile X Mental Retardation Protein." *The Journal of General Physiology* 152 (6). https://doi.org/10.1085/jgp.201912502.

Kshatri, Aravind S., Alberto Gonzalez-Hernandez, and Teresa Giraldez. 2018. "Physiological Roles and Therapeutic Potential of Ca^{2+} Activated Potassium Channels in the Nervous System." *Frontiers in Molecular Neuroscience* 11 (July): 1–18. https://doi.org/10.3389/fnmol.2018.00258.

Kyle, Barry D., Eva Ahrendt, Andrew P. Braun, and Janice E.A. Braun. 2013. "The Large Conductance, Calcium-Activated K+ (BK) Channel Is Regulated by Cysteine String Protein." *Scientific Reports* 3: 29–32. https://doi.org/10.1038/srep02447.

Latorre, Ramon, Karen Castillo, Willy Carrasquel-Ursulaez, Romina V. Sepulveda, Fernando Gonzalez-Nilo, Carlos Gonzalez, and Osvaldo Alvarez. 2017. "Molecular Determinants of BK Channel Functional Diversity and Functioning." *Physiological Reviews* 97 (1): 39–87. https://doi.org/10.1152/physrev.00001.2016.

Lecat-Guillet, Nathalie, Carine Monnier, Xavier Rovira, Julie Kniazeff, Laurent Lamarque, Jurriaan M. Zwier, Eric Trinquet, Jean Philippe Pin, and Philippe Rondard. 2017. "FRET-Based Sensors Unravel Activation and Allosteric Modulation of the GABA B Receptor." *Cell Chemical Biology* 24 (3): 360–70. https://doi.org/10.1016/j.chembiol.2017.02.011.

Lee, Jihye, and Chun Fang Wu. 2010. "Orchestration of Stepwise Synaptic Growth by K+ and Ca^{2+} Channels in Drosophila." *Journal of Neuroscience* 30 (47): 15821–33. https://doi.org/10.1523/JNEUROSCI.3448-10.2010.

Lee, Joon, Hermany Munguba, Vanessa A. Gutzeit, Melanie Kristt, Jeremy S. Dittman, and Joshua Levitz. 2020. "Defining the Homo- and Heterodimerization Propensities of Metabotropic Glutamate Receptors." *Cell Reports* 31 (5): 107605. https://doi.org/10.1016/j.celrep.2020.107605.

Lee, Kyung Jin, Deokhee Kang, and Hee Sung Park. 2019. "Site-Specific Labeling of Proteins Using Unnatural Amino Acids." *Molecules and Cells* 42 (5): 386–96. https://doi.org/10.14348/molcells.2019.0078.

Lesage, F., H. Hibino, and A. J. Hudspeth. 2004. "Association of β-Catenin with the α-Subunit of Neuronal Large-Conductance Ca^{2+}-Activated K+ Channels." *Proceedings of the National Academy of Sciences of the United States of America* 101 (2): 671–75. https://doi.org/10.1073/pnas.0307681100.

Li, Qin, Yingxin Li, Hua Wei, Hao Min Pan, Alexandre G. Vouga, Brad S. Rothberg, Yunkun Wu, and Jiusheng Yan. 2018. "Molecular Determinants of Ca^{2+} Sensitivity at the Intersubunit Interface of the BK Channel Gating Ring." *Scientific Reports* 8 (1): 1–9. https://doi.org/10.1038/s41598-017-19029-8.

Li, Weiyan, and Richard W. Aldrich. 2004. "Unique Inner Pore Properties of BK Channels Revealed by Quaternary Ammonium Block." *Journal of General Physiology* 124 (1): 43–57. https://doi.org/10.1085/jgp.200409067.

Li, Xia, Sibylle Poschmann, Qiuyun Chen, Walid Fazeli, Nelly Jouayed Oundjian, Francesca M. Snoeijen-Schouwenaars, Oliver Fricke, Erik Jan Kamsteeg, Marjolein Willemsen, and Qing Kenneth Wang. 2018. "De Novo BK Channel Variant Causes Epilepsy by Affecting Voltage Gating but Not Ca^{2+} Sensitivity / 631/378/1689/178 / 631/443/376 / 631/208/737 Article." *European Journal of Human Genetics* 26 (2): 220–29. https://doi.org/10.1038/s41431-017-0073-3.

Liang, Lina, Xia Li, Sébastien Moutton, Samantha A. Schrier Vergano, Benjamin Cogné, Anne Saint-Martin, Anna C.E. Hurst, et al. 2019. "De Novo Loss-of-Function KCNMA1 Variants Are Associated with a New Multiple Malformation Syndrome and a Broad Spectrum of Developmental and Neurological Phenotypes." *Human Molecular Genetics* 28 (17): 2937–51. https://doi.org/10.1093/hmg/ddz117.

Ling, Shizhang, Jian Zhong Sheng, Janice E.A. Braun, and Andrew P. Braun. 2003. "Syntaxin 1A Co-Associates with Native Rat Brain and Cloned Large Conductance, Calcium-Activated Potassium Channels in Situ." *Journal of Physiology* 553 (1): 65–81. https://doi.org/10.1113/jphysiol.2003.051631.

Liss, Viktoria, Britta Barlag, Monika Nietschke, and Michael Hensel. 2015. "Self-Labelling Enzymes as Universal Tags for Fluorescence Microscopy, Super-Resolution Microscopy and Electron Microscopy." *Scientific Reports* 5 (November): 1–13. https://doi.org/10.1038/srep17740.

Liu, Chang C., and Peter G. Schultz. 2010. "Adding New Chemistries to the Genetic Code." *Annual Review of Biochemistry* 79: 413–44. https://doi.org/10.1146/annurev.biochem.052308.105824.

Liu, Na, Jilin Wu, Yunxia Chen, and Jianhua Zhao. 2020. "Channels That Cooperate with TRPV4 in the Brain." *Journal of Molecular Neuroscience*. https://doi.org/10.1007/s12031-020-01574-z.

Loane, David J., Pedro A. Lima, and Neil V. Marrion. 2007. "Co-Assembly of N-Type Ca^{2+} and BK Channels Underlies Functional Coupling in Rat Brain." *Journal of Cell Science* 120 (6): 985–95. https://doi.org/10.1242/jcs.03399.

Lorenzo-Ceballos, Yenisleidy, Willy Carrasquel-Ursulaez, Karen Castillo, Osvaldo Alvarez, and Ramon Latorre. 2019. "Calcium-Driven Regulation of Voltage-Sensing Domains in BK Channels." *ELife* 8: 1–24. https://doi.org/10.7554/eLife.44934.

Luo, J. H., Z. Y. Fu, G. Losi, B. G. Kim, K. Prybylowski, B. Vissel, and S. Vicini. 2002. "Functional Expression of Distinct NMDA Channel Subunits Tagged with Green Fluorescent Protein in Hippocampal Neurons in Culture." *Neuropharmacology* 42 (3): 306–18. https://doi.org/10.1016/S0028-3908(01)00188-5.

Ma, Zhongming, Xing Jian Lou, and Frank T. Horrigan. 2006. "Role of Charged Residues in the S1-S4 Voltage Sensor of BK Channels." *Journal of General Physiology* 127 (3): 309–28. https://doi.org/10.1085/jgp.200509421.

Magleby, Karl L. 2003. "Gating Mechanism of BK (Slo1) Channels: So near, yet so Far." *Journal of General Physiology* 121 (2): 81–96. https://doi.org/10.1085/jgp.20028721.

Marty, Alain. 1981. "Ca-Dependent K Channels with Large Unitary Conductance in Chromaffin Cell Membranes." *Nature* 291: 497–500.

Maue, Robert A. 2007. "Understanding Ion Channel Biology Using Epitope Tags: Progress, Pitfalls, and Promise." *Journal of Cellular Physiology* 213 (3): 618–25. https://doi.org/10.1002/jcp.21259.

Maurel, Damien, Laëtitia Comps-Agrar, Carsten Brock, Marie Laure Rives, Emmanuel Bourrier, Mohammed Akli Ayoub, Hervé Bazin, et al. 2008. "Cell-Surface Protein-Protein Interaction Analysis with Time-Resolved FRET and Snap-Tag Technologies: Application to GPCR Oligomerization." *Nature Methods* 5 (6): 561–67. https://doi.org/10.1038/nmeth.1213.

McCobb, D. P., N. L. Fowler, T. Featherstone, C. J. Lingle, M. Saito, J. E. Krause, and L. Salkoff. 1995. "A Human Calcium-Activated Potassium Channel Gene Expressed in Vascular Smooth Muscle." *American Journal of Physiology - Heart and Circulatory Physiology* 269 (3 38-3). https://doi.org/10.1152/ajpheart.1995.269.3.h767.

Meera, P, M Wallner, Z Jiang, and L Toro. 1996. "A Calcium Switch for the Functional Coupling between α (Hslo) and β (K(V,Ca)β) of Maxi K Channels." *FEBS Letters*. https://doi.org/10.1016/0014-5793(96)83884-1.

Meredith, Andrea L., Steven W. Wiler, Brooke H. Miller, Joseph S. Takahashi, Anthony A. Fodor, Norman F. Ruby, and Richard W. Aldrich. 2006. "BK Calcium-Activated Potassium Channels Regulate Circadian Behavioral Rhythms and Pacemaker Output." *Nature Neuroscience* 9 (8): 1041–49. https://doi.org/10.1038/nn1740.

Mickolajczyk, Keith J., Paul Dominic B. Olinares, Yiming Niu, Nan Chen, Sara E. Warrington, Yusuke Sasaki, Thomas Walz, Brian T. Chait, and Tarun M. Kapoor. 2020. "Long-Range Intramolecular Allostery and Regulation in the Dynein-like AAA Protein Mdn1." *Proceedings of the National Academy of Sciences of the United States of America* 117 (31): 18459–69. https://doi.org/10.1073/pnas.2002792117.

Miller, Christopher, Edward Moczydlowski, Ramon Latorre, and Marcia Phillips. 1985. "Charybdotoxin, a Protein Inhibitor of Single Ca^{2+}-Activated K^+ Channels from Mammalian Skeletal Muscle" 313: 316–18.

Miranda, Pablo, Jorge E. Contreras, Andrew J.R. Plested, Fred J. Sigworth, Miguel Holmgren, and Teresa Giraldez. 2013. "State-Dependent FRET Reports Calcium- and Voltagedependent Gating-Ring Motions in BK Channels." *Proceedings of the National Academy of Sciences of the United States of America* 110 (13): 5217–22. https://doi.org/10.1073/pnas.1219611110.

Miranda, Pablo, Teresa Giraldez, and Miguel Holmgren. 2016. "Interactions of Divalent Cations with Calcium Binding Sites of BK Channels Reveal Independent Motions within the Gating Ring." *Proceedings of the National Academy of Sciences of the United States of America* 113 (49): 14055–60. https://doi.org/10.1073/pnas.1611415113.

Miranda, Pablo, Miguel Holmgren, and Teresa Giraldez. 2018. "Voltage-Dependent Dynamics of the BK Channel Cytosolic Gating Ring Are Coupled to the Membrane-Embedded Voltage Sensor." *ELife* 7: 1–18. https://doi.org/10.7554/eLife.40664.

Moldenhauer, Hans J., Su Mi Park, and Andrea L. Meredith. 2020. "Characterization of New Human KCNMA1 Loss-of-Function Mutations." *Biophysical Journal* 118 (3): 114a. https://doi.org/10.1016/j.bpj.2019.11.767.

Moss, Brenda L., and Karl L. Magleby. 2001. "Gating and Conductance Properties of BK Channels Are Modulated by the S9-S10 Tail Domain of the α Subunit: A Study of MSlo1 and MSlo3 Wild-Type and Chimeric Channels." *Journal of General Physiology* 118 (6): 711–34. https://doi.org/10.1085/jgp.118.6.711.

Nelson, Alexandra B., Claudia M. Krispel, Chris Sekirnjak, and Sascha Du Lac. 2003. "Long-Lasting Increases in Intrinsic Excitability Triggered by Inhibition." *Neuron* 40 (3): 609–20. https://doi.org/10.1016/S0896-6273(03)00641-X.

T. Nevian, M. E. Larkum, A. Polsky, J. Schiller, Properties of basal dendrites of layer 5 pyramidal neurons: a direct patch-clamp recording study. *Nature neuroscience* **10**, 206-214 (2007).

Nimigean, Crina M., Joshua S. Chappie, and Christopher Miller. 2003. "Electrostatic Tuning of Ion Conductance in Potassium Channels." *Biochemistry* 42 (31): 9263–68. https://doi.org/10.1021/bi0348720.

Niu, Longgang, Yan Li, Pengyu Zong, Ping Liu, Yuan Shui, Bojun Chen, and Zhao-Wen Wang. 2020. "Melatonin Promotes Sleep by Activating the BK Channel in C. Elegans." *Proceedings of the National Academy of Sciences*, 202010928. https://doi.org/10.1073/pnas.2010928117.

Niu, Xiaowei, Xiang Qian, and Karl L. Magleby. 2004. "Linker-Gating Ring Complex as Passive Spring and Ca^{2+}-Dependent Machine for a Voltage- and Ca^{2+}-Activated Potassium Channel." *Neuron* 42

(5): 745–56. https://doi.org/10.1016/j.neuron.2004.05.001.

Noda, Masaharu, Shin Shimizu, Tsutomu Tanabe, Toshiyuki Takai, Toshiaki Kayano, Takayuki Ikeda, Hideo Takahashi, et al. 1984. "Primary Structure of Electrophorus Electricus Sodium Channel Deduced from CDNA Sequence." *Nature* 312 (5990): 121–27. https://doi.org/10.1038/312121a0.

Pallotta, Barry S., K. L. Magleby, and John N. Barrett. 1981. "Single Channel Recordings of Ca^{2+}-Activated K+ Currents in Rat Muscle Cell Culture." *Nature* 293: 471–74.

Pantazis, Antonios, Vadym Gudzenko, Nicoletta Savalli, Daniel Sigg, and Riccardo Olcese. 2010. "Operation of the Voltage Sensor of a Human Voltageand Ca $^{2+}$-Activated K+ Channel." *Proceedings of the National Academy of Sciences of the United States of America* 107 (9): 4459–64. https://doi.org/10.1073/pnas.0911959107.

Pantoja, Rigo, Erik A. Rodriguez, Mohammed I. Dibas, Dennis A. Dougherty, and Henry A. Lester. 2009. "Single-Molecule Imaging of a Fluorescent Unnatural Amino Acid Incorporated into Nicotinic Receptors." *Biophysical Journal* 96 (1): 226–37. https://doi.org/10.1016/j.bpj.2008.09.034.

Paoletti, Pierre, Camilla Bellone, and Qiang Zhou. 2013. "NMDA Receptor Subunit Diversity: Impact on Receptor Properties, Synaptic Plasticity and Disease." *Nature Reviews Neuroscience* 14 (6): 383–400. https://doi.org/10.1038/nrn3504.

Peng, Zhenling, Yoshihisa Sakai, Lukasz Kurgan, Bernd Sokolowski, and Vladimir Uversky. 2014. "Intrinsic Disorder in the BK Channel and Its Interactome." *PLoS ONE* 9 (4). https://doi.org/10.1371/journal.pone.0094331.

Philipson, Louis H., Andrew Malayev, Andrey Kuznetsov, Christine Chang, and Deborah J. Nelson. 1993. "Functional and Biochemical Characterization of the Human Potassium Channel Kv1.5 with a Transplanted Carboxyl-Terminal Epitope in Stable Mammalian Cell Lines." *BBA - Biomembranes* 1153 (1): 111–21. https://doi.org/10.1016/0005-2736(93)90282-5.

Pless, Stephan A., and Christopher A. Ahern. 2013. "Unnatural Amino Acids as Probes of Ligand-Receptor Interactions and Their Conformational Consequences." *Annual Review of Pharmacology and Toxicology* 53: 211–29. https://doi.org/10.1146/annurev-pharmtox-011112-140343.

A. Polsky, B. Mel, J. Schiller, Encoding and decoding bursts by NMDA spikes in basal dendrites of layer 5 pyramidal neurons. *The Journal of neuroscience : the official journal of the Society for Neuroscience* **29**, 11891-11903 (2009).

Poulsen, Mette H., Anahita Poshtiban, Viktoria Klippenstein, Valentina Ghisi, and Andrew J.R. Plested. 2019. "Gating Modules of the AMPA Receptor Pore Domain Revealed by Unnatural Amino Acid Mutagenesis." *Proceedings of the National Academy of Sciences of the United States of America* 116 (27): 13358–67. https://doi.org/10.1073/pnas.1818845116.

Qian, Xiang, Xiaowei Niu, and Karl L. Magleby. 2006. "Intra- and Intersubunit Cooperativity in Activation of BK Channels by Ca^{2+}." *Journal of General Physiology* 128 (4): 389–404. https://doi.org/10.1085/jgp.200609486.

Rehak, Renata, Theodore M. Bartoletti, Jordan D.T. Engbers, Geza Berecki, Ray W. Turner, and Gerald W. Zamponi. 2013. "Low Voltage Activation of KCa1.1 Current by Cav3-KCa1.1 Complexes." *PLoS ONE* 8 (4). https://doi.org/10.1371/journal.pone.0061844.

Reiner, Andreas, and Joshua Levitz. 2018. "Glutamatergic Signaling in the Central Nervous System: Ionotropic and Metabotropic Receptors in Concert." *Neuron* 98 (6): 1080–98. https://doi.org/10.1016/j.neuron.2018.05.018.

J. Rodriguez-Moreno *et al.*, Area-Specific Synapse Structure in Branched Posterior Nucleus Axons Reveals a New Level of Complexity in Thalamocortical Networks. *The Journal of neuroscience : the official journal of the Society for Neuroscience* **40**, 2663-2679 (2020).

Rothberg, Brad S. 2012. "The BK Channel: A Vital Link between Cellular Calcium and Electrical Signaling." *Protein & Cell* 3 (12): 883–92. https://doi.org/10.1007/s13238-012-2076-8.

Rothberg, Brad S., and Karl L. Magleby. 1999. "Gating Kinetics of Single Large-Conductance Ca^{2+}-Activated K+ Channels in High Ca^{2+} Suggest a Two-Tiered Allosteric Gating Mechanism." *Journal of General Physiology* 114 (1): 93–124. https://doi.org/10.1085/jgp.114.1.93.

Royal, Perrine, Alba Andres-Bilbe, Pablo Ávalos Prado, Clément Verkest, Brigitte Wdziekonski, Sébastien Schaub, Anne Baron, et al. 2019. "Migraine-Associated TRESK Mutations Increase Neuronal Excitability through Alternative Translation Initiation and Inhibition of TREK." *Neuron* 101 (2): 232-245.e6. https://doi.org/10.1016/j.neuron.2018.11.039.

Rubenstein, Ronald C., Marie E. Egan, and Pamela L. Zeitlin. 1997. "In Vitro Pharmacologic Restoration of CFTR-Mediated Chloride Transport with Sodium 4-Phenylbutyrate in Cystic Fibrosis Epithelial Cells Containing ΔF08-CFTR." *Journal of Clinical Investigation* 100 (10): 2457–65. https://doi.org/10.1172/JCI119788.

Rumbaugh, Gavin, Kate Prybylowski, Jian Feng Wang, and Stefano Vicini. 2000. "Exon 5 and Spermine Regulate Deactivation of NMDA Receptor Subtypes." *Journal of Neurophysiology* 83 (3): 1300–1306. https://doi.org/10.1152/jn.2000.83.3.1300.

Sah, Pankaj, and Elspeth M. McLachlan. 1991. "Ca^{2+}-Activated K+ Currents Underlying the Afterhyperpolarization in Guinea Pig Vagal Neurons: A Role for Ca^{2+}-Activated Ca^{2+} Release." *Neuron* 7 (2): 257–64. https://doi.org/10.1016/0896-6273(91)90264-Z.

Sala, Carlo, Gautier Roussignol, Jacopo Meldolesi, and Laurent Fagni. 2005. "Key Role of the Postsynaptic Density Scaffold Proteins Shank and Homer in the Functional Architecture of Ca^{2+} Homeostasis at Dendritic Spines in Hippocampal Neurons." *Journal of Neuroscience* 25 (18): 4587–92. https://doi.org/10.1523/JNEUROSCI.4822-04.2005.

Sands, Steven B., and Michael E. Barish. 1989. "NMDA Receptor Activition by Residual Glutamate in Glutamine Preparations: A Cautionary Note Regarding Weak NMDA Receptor Agonists." *Brain Research* 495 (1): 193–97. https://doi.org/10.1016/0006-8993(89)91237-7.

Savalli, Nicoletta, Antonios Pantazis, Taleh Yusifov, Daniel Sigg, and Riccardo Olcese. 2012. "The Contribution of RCK Domains to Human BK Channel Allosteric Activation." *Journal of Biological Chemistry* 287 (26): 21741–50. https://doi.org/10.1074/jbc.M112.346171.

J. Schiller, G. Major, H. J. Koester, Y. Schiller, NMDA spikes in basal dendrites of cortical pyramidal neurons. *Nature* **404**, 285-289 (2000).

Schreiber, Matthew, and Lawrence Salkoff. 1997. "A Novel Calcium-Sensing Domain in the BK Channel." *Biophysical Journal* 73 (3): 1355–63. https://doi.org/10.1016/S0006-3495(97)78168-2.

Schreiber, Matthew, Aguan Wei, Alex Yuan, Joseph Gaut, Mitsuyoshi Saito, and Lawrence Salkoff. 1998. "Slo3, a Novel PH-Sensitive K+ Channel from Mammalian Spermatocytes." *Journal of Biological Chemistry* 273 (6): 3509–16. https://doi.org/10.1074/jbc.273.6.3509.

Sdip, Alessandra, Claudio Acuna, Fujun Luo, and Thomas C Südhof. 2018. " RIM -binding Proteins Recruit BK-channels to Presynaptic Release Sites Adjacent to Voltage-gated Ca 2+ -channels ." *The EMBO Journal* 37 (16): 1–14. https://doi.org/10.15252/embj.201798637.

Shi, Jingyi, and Jianmin Cui. 2001. "Intracellular Mg2+ Enhances the Function of BK-Type Ca2+ -Activated K+ Channels." *J. Gen. Physiol* 115891700 (118): 589–605. http://www.jgp.org/cgi/content/full/118/5/589.

Shi, Pan, Dong Li, Chaohua Lai, Longhua Zhang, and Changlin Tian. 2013. "Intracellular Segment between Transmembrane Helices S0 and S1 of BK Channel α Subunit Contains Two Amphipathic Helices Connected by a Flexible Loop." *Biochemical and Biophysical Research Communications* 437 (3): 408–12. https://doi.org/10.1016/j.bbrc.2013.06.091.

Shuman, H. A., T. J. Silhavy, and J. R. Beckwith. 1980. "Labeling of Proteins with β-Galactosidase by Gene Fusion. Identification of a Cytoplasmic Membrane Component of the Escherichia Coli Maltose Transport System." *Journal of Biological Chemistry* 255 (1): 168–74. https://doi.org/10.1016/s0021-9258(19)86280-4.

Singh, H., M. Li, L. Hall, S. Chen, S. Sukur, R. Lu, A. Caputo, A. L. Meredith, E. Stefani, and L. Toro. 2016. "MaxiK Channel Interactome Reveals Its Interaction with GABA Transporter 3 and Heat Shock Protein 60 in the Mammalian Brain." *Neuroscience* 317: 76–107. https://doi.org/10.1016/j.neuroscience.2015.12.058.

Steinberg, Ximena, Marina A. Kasimova, Deny Cabezas-Bratesco, Jason D. Galpin, Ernesto Ladron-de-Guevara, Federica Villa, Vincenzo Carnevale, Leon Islas, Christopher A. Ahern, and Sebastian E. Brauchi. 2017. "Conformational Dynamics in TRPV1 Channels Reported by an Encoded Coumarin Amino Acid." *ELife* 6: 1–18. https://doi.org/10.7554/eLife.28626.

Sweet, Tara Beth, and Daniel H. Cox. 2008. "Measurements of the BK Ca Channel's High-Affinity Ca 2+ Binding Constants: Effects of Membrane Voltage." *Journal of General Physiology* 132 (5): 491–505. https://doi.org/10.1085/jgp.200810094.

Tabarki, Brahim, Nabil AlMajhad, Amal AlHashem, Ranad Shaheen, and Fowzan S. Alkuraya. 2016. "Homozygous KCNMA1 Mutation as a Cause of Cerebellar Atrophy, Developmental Delay and Seizures." *Human Genetics* 135 (11): 1295–98. https://doi.org/10.1007/s00439-016-1726-y.

Tang, Qiong Yao, Xu Hui Zeng, and Christopher J. Lingle. 2009. "Closed-Channel Block of BK Potassium Channels by Bbtba Requires Partial Activation." *Journal of General Physiology* 134 (5): 409–36. https://doi.org/10.1085/jgp.200910251.

Tao, Xiao, Richard K. Hite, and Roderick MacKinnon. 2017. "Cryo-EM Structure of the Open High-Conductance Ca^{2+} -Activated K+ Channel." *Nature* 541 (7635): 46–51. https://doi.org/10.1038/nature20608.

Tao, Xiao, and Roderick Mackinnon. 2019. "Molecular Structures of the Human Slo1 K+ Channel in Complex with B4." *ELife* 8: 1–27. https://doi.org/10.7554/eLife.51409.

Tian, C., Zhu, R., Zhu, L., Qiu, T., Cao, Z., & Kang, T. (2014). Potassium channels: structures, diseases, and modulators. *Chemical biology & drug design*, *83*(1), 1–26. https://doi.org/10.1111/cbdd.12237

Tian, Meilin, and Shixin Ye. 2016. "Allosteric Regulation in NMDA Receptors Revealed by the Genetically Encoded Photo-Cross-Linkers." *Scientific Reports* 6 (February): 1–12. https://doi.org/10.1038/srep34751.

Tomasello, Gianluca, Ilaria Armenia, and Gianluca Molla. 2020. "The Protein Imager: A Full-Featured Online Molecular Viewer Interface with Server-Side HQ-Rendering Capabilities." *Bioinformatics* 36 (9): 2909–11. https://doi.org/10.1093/bioinformatics/btaa009.

Traynelis, Stephen F., Lonnie P. Wollmuth, Chris J. McBain, Frank S. Menniti, Katie M. Vance, Kevin K. Ogden, Kasper B. Hansen, Hongjie Yuan, Scott J. Myers, and Ray Dingledine. 2010. "Glutamate Receptor Ion Channels: Structure, Regulation, and Function." *Pharmacological Reviews* 62 (3): 405–96. https://doi.org/10.1124/pr.109.002451.

Vance, Katie M., Kasper B. Hansen, and Stephen F. Traynelis. 2012. "GluN1 Splice Variant Control of GluN1/GluN2D NMDA Receptors." *Journal of Physiology* 590 (16): 3857–75. https://doi.org/10.1113/jphysiol.2012.234062.

Vicini, Stefano, Jian Feng Wang, Jin Hong Li, Wei Jian Zhu, Yue Hua Wang, Jian Hong Luo, Barry B. Wolfe, and Dennis R. Grayson. 1998. "Functional and Pharmacological Differences between Recombinant N- Methyl-D-Aspartate Receptors." *Journal of Neurophysiology* 79 (2): 555–66. https://doi.org/10.1152/jn.1998.79.2.555.

Vivas, Oscar, Claudia M. Moreno, Luis F. Santana, and Bertil Hille. 2017. "Proximal Clustering between BK and Cav1.3 Channels Promotes Functional Coupling and BK Channel Activation at Low Voltage." *ELife* 6: 1–18. https://doi.org/10.7554/eLife.28029.

Vyklicky, Vojtech, Cherise Stanley, Chris Habrian, and Ehud Y. Isacoff. 2021. "Conformational Rearrangement of the NMDA Receptor Amino-Terminal Domain during Activation and Allosteric Modulation." *Nature Communications* 12 (1). https://doi.org/10.1038/s41467-021-23024-z.

Wallner, Martin, Pratap Meera, and Ligia Toro. 1996. "Determinant for β-Subunit Regulation in High-Conductance Voltage-Activated and Ca^{2+}-Sensitive K+ Channels: An Additional Transmembrane Region at the N Terminus." *Proceedings of the National Academy of Sciences of the United States of America* 93 (25): 14922–27. https://doi.org/10.1073/pnas.93.25.14922.

Wang, Bin, David B. Jaffe, and Robert Brenner. 2014. "Current Understanding of Iberiotoxin-Resistant BK Channels in the Nervous System." *Frontiers in Physiology* 5 (OCT): 1–11. https://doi.org/10.3389/fphys.2014.00382.

Acids into Functional G Protein-Coupled Receptors Using Unnatural Amino Acid Mutagenesis." *Journal of Biological Chemistry* 283 (3): 1525–33. https://doi.org/10.1074/jbc.M707355200.

Yeşil, Gözde, Ayşe Aralaşmak, Enes Akyüz, Dilara İçağasıoğlu, Türkan Uygur Şahin, and Yavuz Bayram. 2018. "Expanding the Phenotype of Homozygous Kcnma1 Mutations; Dyskinesia, Epilepsy, Intellectual Disability, Cerebellar and Corticospinal Tract Atrophy." *Balkan Medical Journal* 35 (4): 336–39. https://doi.org/10.4274/balkanmedj.2017.0986.

Young, Douglas D., and Peter G. Schultz. 2018. "Playing with the Molecules of Life." *ACS Chemical Biology* 13 (4): 854–70. https://doi.org/10.1021/acschembio.7b00974.

Yuan, Alex, Celia M Santi, Aguan Wei, Zhao-Wen Wang, Kelly Pollak, Michael Nonet, Leonard Kaczmarek, C Michael Crowder, and Lawrence Salkoff. 2003. "The Sodium-Activated Potassium Channel Is Encoded by a Member of the Slo Gene Family." *Neuron* 37: 765–73. https://ac.els-cdn.com/S0896627303000965/1-s2.0-S0896627303000965-main.pdf?_tid=cafb37be-0d04-461e-87c6-f05a244381a6&acdnat=1543264737_b4afe8d9e112b0b0d893b1a9208b1c71.

Yuan, Peng, Manuel D. Leonetti, Yichun Hsiung, and Roderick MacKinnon. 2012. "Open Structure of the Ca^{2+} Gating Ring in the High-Conductance Ca^{2+}-Activated K + Channel." *Nature* 481 (7379): 94–98. https://doi.org/10.1038/nature10670.

Zeng, Xu Hui, Xiao Ming Xia, and Christopher J. Lingle. 2005. "Divalent Cation Sensitivity of BK Channel Activation Supports the Existence of Three Distinct Binding Sites." *Journal of General Physiology* 125 (3): 273–86. https://doi.org/10.1085/jgp.200409239.

Zhang, Fang Xiong, Vinicius M. Gadotti, Ivana A. Souza, Lina Chen, and Gerald W. Zamponi. 2018. "BK Potassium Channels Suppress Cav2δ2 Subunit Function to Reduce Inflammatory and Neuropathic Pain." *Cell Reports* 22 (8): 1956–64. https://doi.org/10.1016/j.celrep.2018.01.073.

Zhang, Guohui, Sheng You Huang, Junqiu Yang, Jingyi Shi, Xiao Yang, Alyssa Moller, Xiaoqin Zou, and Jianmin Cui. 2010. "Ion Sensing in the RCK1 Domain of BK Channels." *Proceedings of the National Academy of Sciences of the United States of America* 107 (43): 18700–705. https://doi.org/10.1073/pnas.1010124107.

Zhang, Jiyuan, Xin Guan, Qin Li, Andrea L. Meredith, Hui Lin Pan, and Jiusheng Yan. 2018. "Glutamate-Activated BK Channel Complexes Formed with NMDA Receptors." *Proceedings of the National Academy of Sciences of the United States of America* 115 (38): E9006–14. https://doi.org/10.1073/pnas.1802567115.

Zhang, L., and C. J. McBain. 1995. "Potassium Conductances Underlying Repolarization and After-hyperpolarization in Rat CA1 Hippocampal Interneurones." *The Journal of Physiology* 488 (3): 661–72. https://doi.org/10.1113/jphysiol.1995.sp020998.

Zhou, Yu, Xiao Ming Xia, and Christopher J. Lingle. 2011. "Cysteine Scanning and Modification Reveal Major Differences between BK Channels and Kv Channels in the Inner Pore Region." *Proceedings of the National Academy of Sciences of the United States of America* 108 (29): 12161–66. https://doi.org/10.1073/pnas.1104150108.

Zhou, Yu, Huanghe Yang, Jianmin Cui, and Christopher J. Lingle. 2017. "Threading the Biophysics of Mammalian Slo1 Channels onto Structures of an Invertebrate Slo1 Channel." *Journal of General*

Wei, Aguan, Christopher Solaro, Christopher Lingle, and Lawrence Salkoff. 1994. "Calcium Sensitivity of BK-Type KCa Channels Determined by a Separable Domain." *Neuron* 13 (3): 671–81. https://doi.org/10.1016/0896-6273(94)90034-5.

Whitt, Joshua P., Beth A. McNally, and Andrea L. Meredith. 2018. "Differential Contribution of Ca^{2+} Sources to Day and Night BK Current Activation in the Circadian Clock." *Journal of General Physiology* 150 (2): 259–75. https://doi.org/10.1085/jgp.201711945.

Whitt, Joshua P., Jenna R. Montgomery, and Andrea L. Meredith. 2016. "BK Channel Inactivation Gates Daytime Excitability in the Circadian Clock." *Nature Communications* 7: 1–13. https://doi.org/10.1038/ncomms10837.

Wilkens, Christina M., and Richard W. Aldrich. 2006. "State-Independent Block of BK Channels by an Intracellular Quaternary Ammonium." *Journal of General Physiology* 128 (3): 347–64. https://doi.org/10.1085/jgp.200609579.

Wondergem, Robert, and Jeremy W. Bartley. 2009. "Menthol Increases Human Glioblastoma Intracellular Ca^{2+}, BK Channel Activity and Cell Migration." *Journal of Biomedical Science* 16 (1): 1–7. https://doi.org/10.1186/1423-0127-16-90.

Wu, Ying, Yongfeng Liu, Panpan Hou, Zonghe Yan, Wenjuan Kong, Beiying Liu, Xia Li, et al. 2013. "TRPV1 Channels Are Functionally Coupled with BK(MSlo1) Channels in Rat Dorsal Root Ganglion (DRG) Neurons." *PLoS ONE* 8 (10): 1–12. https://doi.org/10.1371/journal.pone.0078203.

Wu, Yunkun, Yi Yang, Sheng Ye, and Youxing Jiang. 2010. "Structure of the Gating Ring from the Human Large-Conductance Ca^{2+}-Gated K+ Channel." *Nature* 466 (7304): 393–97. https://doi.org/10.1038/nature09252.

Wulf, Matthias, and Stephan Alexander Pless. 2018. "High-Sensitivity Fluorometry to Resolve Ion Channel Conformational Dynamics." *Cell Reports* 22 (6): 1615–26. https://doi.org/10.1016/j.celrep.2018.01.029.

Xia, Xiao Ming, Xuhui Zeng, and Christopher J. Lingle. 2002. "Multiple Regulatory Sites in Large-Conductance Calcium-Activated Potassium Channels." *Nature* 418 (6900): 880–84. https://doi.org/10.1038/nature00956.

Xiao, Han, and Peter G. Schultz. 2016. "At the Interface of Chemical and Biological Synthesis: An Expanded Genetic Code." *Cold Spring Harbor Perspectives in Biology* 8 (9). https://doi.org/10.1101/cshperspect.a023945.

Yang, Huanghe, Guohui Zhang, and Jianmin Cui. 2015. "BK Channels: Multiple Sensors, One Activation Gate." *Frontiers in Physiology* 6 (FEB): 1–16. https://doi.org/10.3389/fphys.2015.00029.

Yang, Junqiu, Gayathri Krishnamoorthy, Akansha Saxena, Guohui Zhang, Jingyi Shi, Huanghe Yang, Kelli Delaloye, David Sept, and Jianmin Cui. 2010. "An Epilepsy/Dyskinesia-Associated Mutation Enhances BK Channel Activation by Potentiating Ca^{2+} Sensing." *Neuron* 66 (6): 871–83. https://doi.org/10.1016/j.neuron.2010.05.009.

Ye, Shixin, Caroline Köhrer, Thomas Huber, Manija Kazmi, Pallavi Sachdev, Elsa C.Y. Yan, Aditi Bhagat, Uttam L. RajBhandary, and Thomas P. Sakmar. 2008. "Site-Specific Incorporation of Keto Amino

Annex I

Physiology 149 (11): 985–1007. https://doi.org/10.1085/jgp.201711845.

Zhou, Yu, Xu Hui Zeng, and Christopher J. Lingle. 2012. "Barium Ions Selectively Activate BK Channels via the Ca^{2+}-Bowl Site." *Proceedings of the National Academy of Sciences of the United States of America* 109 (28): 11413–18. https://doi.org/10.1073/pnas.1204444109.

Zhu, Shujia, Morgane Riou, C. Andrea Yao, Stéphanie Carvalho, Pamela C. Rodriguez, Olivier Bernsaude, Pierre Paoletti, and Shixin Ye. 2014. "Genetically Encoding a Light Switch in an Ionotropic Glutamate Receptor Reveals Subunit-Specific Interfaces." *Proceedings of the National Academy of Sciences of the United States of America* 111 (16): 6081–86. https://doi.org/10.1073/pnas.1318808111.

Zou, Shengwei, Smita Jha, Young Kim Eun, and Stuart E. Dryer. 2008. "The B1 Subunit of L-Type Voltage-Gated Ca^{2+} Channels Independently Binds to and Inhibits the Gating of Large-Conductance Ca^{2+}-Activated K^+ Channels." *Molecular Pharmacology* 73 (2): 369–78. https://doi.org/10.1124/mol.107.040733.

Table A.I. Oligos used in this study. *Color code: Yellow: alanine and point mutation mutagenesis; Green: unnatural amino acid insertion mutagenesis to TAG; Orange: SNAP and CLIP cloning, epitope changes, vector linearization… with In Fusion cloning; Blue: sequencing primers.*

Number	Name	Sequence (5'-3')
1	Fw-N449A	TCTCCATAAAGGCCTACCATCCGAAGATAAG
2	Rv-N449A	CTTATCTTCGGATGGTAGGCCTTTATGGAGA
3	Fw-R514A	CTTCTCCATGGCGTCATTCATAAAGATTGAG
4	Rv-R514A	CTCAATCTTTATGAATGACGCCATGGAGAAG
5	Fw-S533A	TACTTGGAAGGAGTCGCAAATGAAATGTACACAGAA
6	Rv-S533A	TTCTGTGTACATTTCATTTGCGACTCCTTCCAAGTA
7	Fw-S600A	AGGATTTTTCATCGCAGCTGATCCCAAAGAAGTTAA
8	Rv-S600A	TTAACTTCTTTGGGCATCAGCTGCGATGAAAAATCCT
9	Fw-D367A	TTTCTGCACAAGGCCCCGGATGACGTCAAT
10	Rv-D367A	ATTGACGTCATCCCGGGCCTTGTGCAGAAA
11	Fw-5D5A	GTTCAGTTTTTGGACCAAGCCGCTGCTGCTGCCCCTGATACAG
12	Rv-5D5A	AAACTGTATCAGGGGCAGCAGCAGCGGCTTGGTCCAA AAACTGAAC
13	Fw-E902A	GACCCTGATACAGCACTGTACCTCACGCAGCCC
14	Rv-E902A	GGGCTGCGTGAGGTACAGTGCTGTATCAGGGTC
15	Fw-Y904A	GACCCTGATACAGAACTGGCCCTCACGCAGCCC
16	Rv-Y904A	GGGCTGCGTGAGGGCCAGTTCTGTATCAGGGTC
17	Fw-R514K	GCCAACCTCTTCTCCATCAAGTCATTCATAAAGATTG
18	Rv-R514K	CAATCTTTATGAATGACTTCATGGAGAAGAGGTTGGC
19	Fw-Y904F	CTGATACAGAACTGTTCCTCACGCAGCCCTTTG
20	Rv-Y904F	CAAAGGGCTGCGTGAGGAACAGTTCTGTATCAG
21	Fw-Y904W	CTGATACAGAACTGTGGCTCACGCAGCCCTTTG
22	Rv-Y904W	CAAAGGGCTGCGTGAGCCACAGTTCTGTATCAG
23	Fw-F160TAG	CTTTCAACGTGTTCTAGCTTCTCTACTTTGGCTT
24	Rv-F160TAG	AAGCCAAAGTAGAGAAGCTAGAAACACGTTGAAAG
25	Fw-Y163TAG	TGTTCTTCCTTCTCTAGTTTGGCTTGCGGTTT
26	Rv-Y163TAG	AAACCGCAAGCCAAACTAGAGAAGGAAGAACA
27	Fw-F223TAG	TTCAGAAATTTTGCAGTAGCTGAATATTCTTAAAACAAG
28	Rv-F223TAG	CTTGTTTTAAGAATATTCAGCTACTGCAAAATTTCTGAA
29	Fw-F315TAG	GGACTGGCCATGTAGGCCAGCTACGTCC
30	Rv-F315TAG	GGACGTAGCTGGCCTACATGGCCAGTCC
31	Fw-Y332TAG	GGAAACCGCAAGAAATAGGGGGGCTCCTATAGTGCGG
32	Rv-Y332TAG	CCGCACTATAGGAGCCCCCCTATTTCTTGCGGTTTCC
33	Fw-Y336TAG	CGCAAGAAATACGGGGGCTCCTAGAGTGCGGTTAGTGGAAG
34	Rv-Y336TAG	CTTCCACTAACCGCACTCTAGGAGCCCCCGTATTTCTTGCG
35	Fw-H379TAG	TGTGGAGATCGTTTTTCTTTAGAACATCTCCCCCAACCTGG
36	Rv-H379TAG	CCAGGTTGGGGGAGATGTTCTAAAGAAAACGATCTCCACA
37	Fw-H394TAG	GCTCTGTTCAAACGATAGTTTACTCAGGTGGAATTTTATCAGG G
38	Rv-H394TAG	CCCTGATAAAATTCCACCTGAGTAAACTATCGTTTGAACAGA GC

85	TAGseqprimer1	GCTCTCAGCATCGGTGCACTT
86	TAGseqprimer2	TGGTGGAGAATTCAGGGGAC
87	TAGseqprimer3	TGGAAAGAAGGTGATGACGCA
88	Sequencing primer 2265	CTCCGTGCCAGCAACTTTCATTACCATG
89	primer_CMV	GGGCGGTAGGCGTGTACGGT

39	Fw-F3951TAG	GCTCTGTTCAAACGACATTAGACTCAGGTGGAATTTTATCAGG G
40	Rv-F3951TAG	CCCTGATAAAATTCCACCTGAGTCTAATGTCGTTTGAACAGA GC
41	Fw-N449TAG	AGTAATCTCCATAAAGTAGTACCATCCGAAGATAAGAAT
42	Rv-N449TAG	ATTCTTATCTTCGGATGGTACTACTTTATGGAGATTACT
43	Fw-Y450TAG	AGTAATCTCCATAAAGAACTAGCATCCGAAGATAAGAAT
44	Rv-Y450TAG	ATTCTTATCTTCGGATGCTAGTTCTTTATGGAGATTACT
45	Fw-H667TAG	CTCGCCTAAGCTGATGAGGTAGGACCCCTTGTTAATTCCTG
46	Rv-H667TAG	CAGGAATTAACAAGGGGTCCTACCTCATCAGCTTAGGCGAG
47	Fw-R786TAG	CTGGTACGCCATTAAGTTAGGCTGATTTAAGGGCTG
48	Rv-R786TAG	CAGCCCTTAAATCAGCCTAACTTAATGGCGTACCAG
53	Fw-R790TAG	GTCGGGCTGATTTATAGGCTGTCAACATCAACCTCTG
54	Rv-R790TAG	CAGAGGTTGATGTTGACAGCCTATAAATCAGCCCGAC
55	F-SNAP inf	GACGATGGCGCGCCTATGGACAAAGACTGCGAAATG
56	R-SNAP inf	GATGATGAGCGCATCGGCGCGCCTACCCAG
57	F-N'BK	GATGCGCTCATCATCCCGGTG
58	R-C'BK	AAGCTTTTCAAATGCTTCGC
59	F-pBNJ13	GCATTTGAAAAGCTTACTAGTGATGCATATTCTATAG
60	R-pBNJ13	AGGCGCGCCATCGTCGTCGTCCTTGTAGTC
61	F-SNAP S1S2	AATAGAAGGCGCGCCTATGGACAAAGACTGCGAAATG
62	R-SNAP S1S2	GCAGGAGGCGCGCCTACCCAGCCCAGGCTTGCCC
63	F-BK S1S2	AGGCGCGCCTCCTGCCAGAATTTCTAC
64	R-pBNJ13 S1S2	AGGCGCGCCTTCTATTGGGTTTGATGAATC
65	Fw-HA-BK-NtSNAP	CTACGACGTGCCCGACTACGCCACGCGTGGATCCGACAAAG
66	Rv-HA-BK-NtSNAP	TCGGGCACGTCGTAGGGGTATACCGGTCGCCGTGGACTG
67	Fw-HA-BK667SNAP	CTACGACGTGCCCGACTACGCCGATGCGCTCATCATCCCGG
68	Rv-HA-BK667SNAP	TCGGGCACGTCGTAGGGGTACACCATGGTACCTGCAGGC
69	Fw-ss-NR1CLIP	GCCCGCGCGGATCCTATGGTCCTTCTGTTG
70	Rv-ss-NR1CLIP	GCAGTCTTTGTCCATTCGCGTGGACTGTGC
71	Fw-vec-NR1CLIP	GCACAGTCCACGCCAATGGACAAAGACTGC
72	Rv-vec-NR1CLIP	CAACAGAAGGACCATAGGATCCGCGCGGGC

167

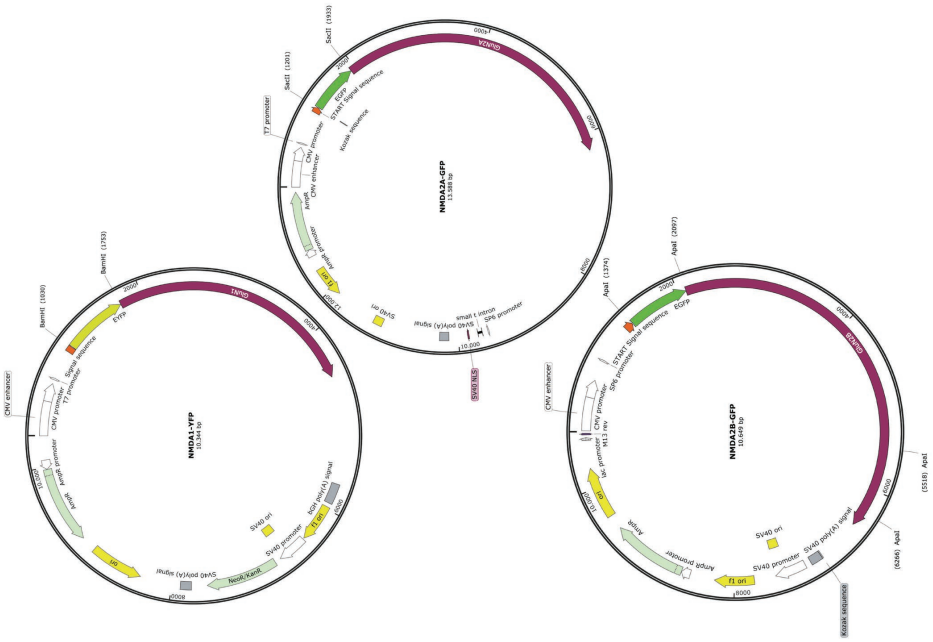

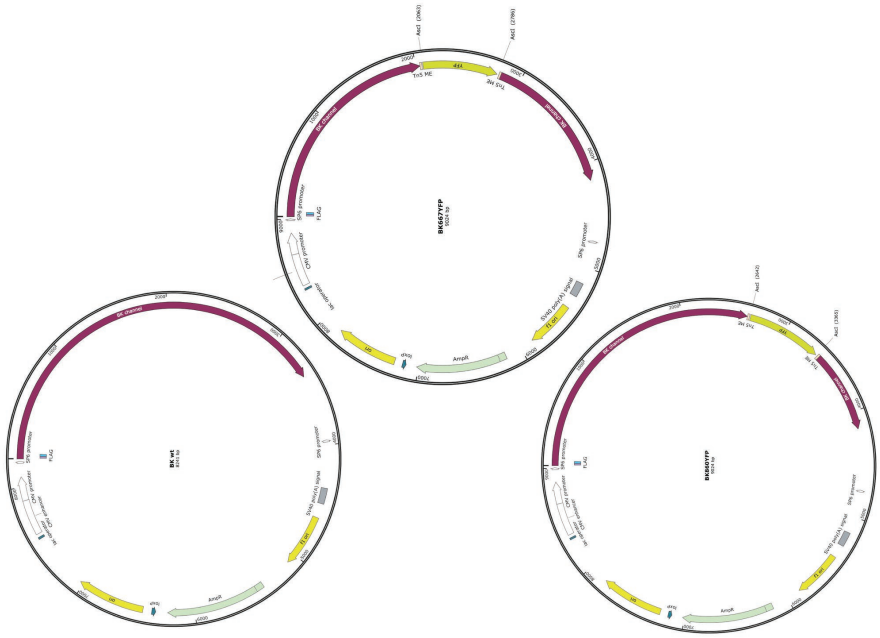

166

169

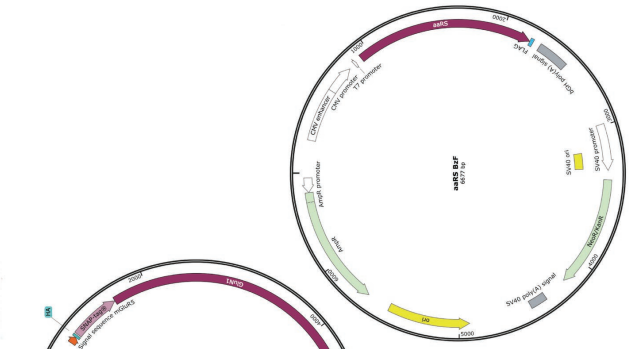

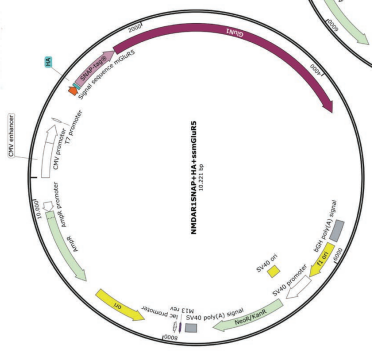

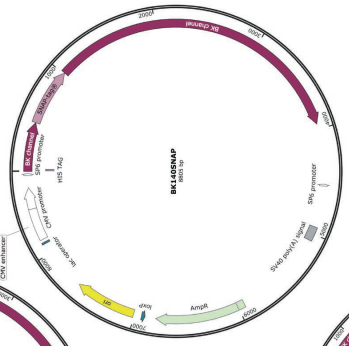

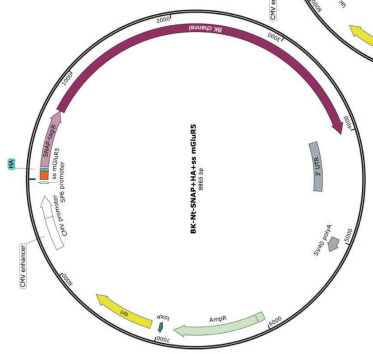

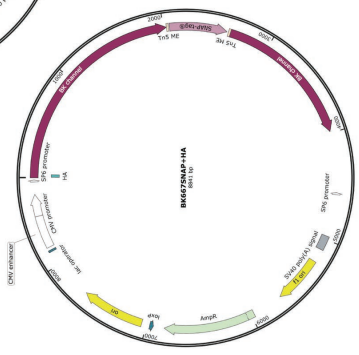

168

Annex II

Table A.II. Summary of statistical significance and tests used in each figure *(comparisons reaching statistical significance are highlighted in light yellow).*

Figure 4.3. N449A and R514A altered Ca^{2+} sensitivity in opposite ways				
PANEL	**STATISTIC**	**CONDITION**	**P VALUE**	**OUTPUT**
Fig 4.3F	Mixed effects analysis (Dunnett's multiple comparisons test)	0 μM Ca^{2+} (WT vs. N449A)	<0.0001	***
		0 μM Ca^{2+} (WT vs. R514A)	<0.0001	***
		0 μM Ca^{2+} (WT vs. S533A)	0.0654	Not significant
		0 μM Ca^{2+} (WT vs. S600A)	0.6072	Not significant
		0.5 μM Ca^{2+} (WT vs. N449A)	0.0165	*
		0.5 μM Ca^{2+} (WT vs. R514A)	0.03	*
		0.5 μM Ca^{2+} (WT vs. S533A)	0.1016	Not significant
		0.5 μM Ca^{2+} (WT vs. S600A)	0.9986	Not significant
		1 μM Ca^{2+} (WT vs. N449A)	0.0006	***
		1 μM Ca^{2+} (WT vs. R514A)	0.0002	***
		1 μM Ca^{2+} (WT vs. S533A)	0.0497	*
		1 μM Ca^{2+} (WT vs. S600A)	0.2925	Not significant
		5 μM Ca^{2+} (WT vs. N449A)	0.2180	Not significant
		5 μM Ca^{2+} (WT vs. R514A)	0.6672	Not significant
		5 μM Ca^{2+} (WT vs. S533A)	0.8400	Not significant
		5 μM Ca^{2+} (WT vs. S600A)	0.7872	Not significant
		10 μM Ca^{2+} (WT vs. N449A)	0.0568	Not significant
		10 μM Ca^{2+} (WT vs. R514A)	0.9795	Not significant
		10 μM Ca^{2+} (WT vs. S533A)	0.1264	Not significant
		10 μM Ca^{2+} (WT vs. S600A)	0.7362	Not significant
		100 μM Ca^{2+} (WT vs. N449A)	0.0370	*
		100 μM Ca^{2+} (WT vs. R514A)	0.0271	*
		100 μM Ca^{2+} (WT vs. S533A)	0.4238	Not significant
		100 μM Ca^{2+} (WT vs. S600A)	0.1439	Not significant
Fig 4.3G	Ordinary One-way ANOVA (Dunnett's multiple comparisons test)	WT vs. N449A	<0.0001	***
		WT vs. R514A	<0.0001	***
		WT vs. S533A	0.5043	Not significant
		WT vs. S600A	0.7188	Not significant
Figure 4.4. Mutation of R514A affects the RCK1 Ca2+ dependent response				
Fig 4.4C	Ordinary One-way ANOVA (Šidák's multiple comparisons test)	0.5 μM Ca^{2+} (WT vs. R514A)	>0.9999	Not significant
		1 μM Ca^{2+} (WT vs. R514A)	0.9783	Not significant
		5 μM Ca^{2+} (WT vs. R514A)	0.0082	**
		10 μM Ca^{2+} (WT vs. R514A)	<0.0001	***
		100 μM Ca^{2+} (WT vs. R514A)	<0.0001	***
Fig 4.4I	Ordinary One-way ANOVA (Dunnett's multiple comparisons test)	WT vs. R514A	<0.0001	***
		WT vs. D367A	<0.0001	***
		WT vs. D367A+R514A	<0.0001	***
		WT vs. 5D5A	0.4151	Not significant
		WT vs. R514A+5D5A	<0.0001	***

Figure 4.5. The side chains of E902, Y904 & R514 are essential for Ca^{2+} sensing in the RCK1 site.

Fig 4.5I	Ordinary One-way ANOVA (Tukey's multiple comparisons test)	WT vs. R514A	<0.0001	***
		WT vs. E902A	0.5224	Not significant
		WT vs. Y904A	0.0051	**
		WT vs. E902A+Y904A	<0.0001	***
		WT vs. R514A+E902A+Y904A	<0.0001	***

Figure 4.6. Energetic effects of the mutations

Ordinary One-way ANOVA (Dunnett's multiple comparisons test)		WT vs. N449A	<0.0001	***
		WT vs. R514A	<0.0001	***
		WT vs. D367A	<0.0001	***
		WT vs. D367A+R514A	<0.0001	***
		WT vs. 5D5A	0.005	**
		WT vs. R514A+5D5A	<0.0001	***
		WT vs. E902A	0.9961	Not significant
		WT vs. Y904A	0.1090	Not significant
		WT vs. E902A+Y904A	<0.0001	***
		WT vs. R514A+E902A+Y904A	<0.0001	***

Figure 4.7. R514K and Y904W mutants showed diminished Ca^{2+} sensitivity.

Fig 4.7E	Mixed effects analysis (Dunnett's multiple comparisons test)	5 μM Ca^{2+} (WT vs. Y904W)	<0.0001	***
		10 μM Ca^{2+} (WT vs. Y904W)	<0.0001	***
		100 μM Ca^{2+} (WT vs. Y904W)	<0.0001	***
Fig 4.7F	Ordinary One-way ANOVA (Dunnett's multiple comparisons test)	WT vs. R514A	<0.0001	***
		WT vs. R514K	<0.0001	***
		WT vs. Y904A	0.0033	**
		WT vs. Y904F	0.9873	Not significant
		WT vs. Y904W	<0.0001	***
Fig 4.7G	Ordinary One-way ANOVA (Dunnett's multiple comparisons test)	WT vs. R514K	0.0684	Not significant
		WT vs. Y904A	0.0967	Not significant
		WT vs. Y904F	0.9823	Not significant
		WT vs. Y904W	<0.0001	***

Figure 4.9. Summary of BK-BzF mutants function and UV-specific effect.

Fig 4.9C	Mixed effects analysis (Dunnett's multiple comparisons test)	100 μM Ca^{2+} (WT vs. Y163BzF)	0.0035	**
		100 μM Ca^{2+} (WT vs. F223BzF)	<0.0001	***
		100 μM Ca^{2+} (WT vs. Y336BzF)	0.9997	Not significant
		100 μM Ca^{2+} (WT vs. H379BzF)	0.6917	Not significant
Fig 4.9D	Ordinary One-way ANOVA (Dunnett's multiple comparisons test)	0 μM Ca^{2+} (WT vs. N449BzF)	0.9995	Not significant
		0 μM Ca^{2+} (WT vs. R786BzF)	0.0045	**
		0 μM Ca^{2+} (WT vs. R790BzF)	0.2558	Not significant
		100 μM Ca^{2+} (WT vs. Y332BzF)	0.9997	Not significant

	multiple comparisons test)	100 μM Ca^{2+} (WT vs. Y336BzF)	0.9991	Not significant
		100 μM Ca^{2+} (WT vs. H379BzF)	0.9993	Not significant
		100 μM Ca^{2+} (WT vs. H394BzF)	0.0601	Not significant
		100 μM Ca^{2+} (WT vs. F395BzF)	0.8727	Not significant
		100 μM Ca^{2+} (WT vs. N449BzF)	<0.0001	***
		100 μM Ca^{2+} (WT vs. Y450BzF)	0.0091	**
		100 μM Ca^{2+} (WT vs. R786BzF)	0.9195	Not significant

Figure 4.10. Functional characterization of N449BzF mutant.

Fig4.10D	Mixed effects analysis (Dunnett's multiple comparisons test)	0 μM Ca^{2+} (WT vs. N449BzF)	0.0843	Not significant
		100 μM Ca^{2+} (WT vs. N449BzF)	0.0251	*

Figure 4.18. Both GluN2A- and GluN2B-containing NMDARs can functionally couple to BK channels.

Fig. 4.18B	Kruskal-Wallis test (followed by Dunn's tests)	BK+GluN1/GluN2A vs. UNTRANSF, BK, and GluN1	<0.0001	***
		BK+GluN1/GluN2B vs. UNTRANSF, BK, and GluN1	<0.0001	***
Fig. 4.18E	Mann-Whitney U test (two-tailed)	BK+2A vs. BK (0 Ca^{2+})	<0.0001	***
		BK+2A vs. BK (1 Ca^{2+})	<0.0001	***
		BK+2A vs. BK (10 Ca^{2+})	0.6165	Not significant
		BK+2A vs. BK (100 Ca^{2+})	0.0032	**
		BK+2B vs. BK (0 Ca^{2+})	0.0003	***
		BK+2B vs. BK (1 Ca^{2+})	0.0003	***
		BK+2B vs. BK (10 Ca^{2+})	0.5743	Not significant
		BK+2B vs. BK (100 Ca^{2+})	0.0023	**
		BK+2A vs. BK+2B	0.5368	Not significant
Fig. 4.18H	Mann-Whitney U test (two-tailed)	BK+2A vs. BK (0 Ca^{2+})	0.0008	***
		BK+2B vs. BK (0 Ca^{2+})	0.0005	***

Figure 4.19. FRET-AB experiments on BK-NMDARs complexes showed a trend of GluN2B containing NMDARs to be closer to BK channel.

Fig. 4.19B	Paired t-test (two-tailed)	BK+GluN1 (Non-B vs. Bleached)	0.1186	Not significant
		BK+GluN1/2A (Non-B vs. Bleached)	0.0096	**
		BK+GluN1/2B (Non-B vs. Bleached)	<0.0001	***

Figure 4.20. Signal sequence insertion in the BK-Nt-SNAP N-terminus yielded better membrane expressed constructs.

Fig. 4.20C	Krustall-Wallis test	mGluR2-SNAP vs. BK-Nt-ss-SNAP	>0.9999	Not significant
		BK-Nt-SNAP vs. BK-Nt-ss-SNAP	0.0485	*

Annex III

Figure 4.26. BK-Nt-SNAP diffused significantly slower along the membrane in the presence of GluN2B containing NMDARs.

Fig. 4.26C	Ordinary One-way ANOVA (Holm-Šídák's multiple comparisons test)	BK-Nt-SNAP vs. BK-Nt-SNAP+GluN1-CLIP/2A	0.8917	Not significant
		BK-Nt-SNAP vs. BK-Nt-SNAP+GluN1-CLIP/2B	0.9286	Not significant
		BK-Nt-SNAP vs. BK-Nt-SNAP+GluA2	0.9286	Not significant
Fig. 4.26D	Ordinary One-way ANOVA (Tukey's multiple comparisons test)	BK-Nt-SNAP vs. BK-Nt-SNAP+GluN1-CLIP/2A	0.0813	Not significant
		BK-Nt-SNAP vs. BK-Nt-SNAP+GluN1-CLIP/2B	0.0004	***
		BK-Nt-SNAP vs. BK-Nt-SNAP+GluA2	0.4083	Not significant
		BK-Nt-SNAP+GluN1-CLIP/2A vs. BK-Nt-SNAP+GluN1-CLIP/2B	0.0372	#
		BK-Nt-SNAP+GluN1-CLIP/2B + BK-Nt-SNAP+GluA2	0.0375	#

BBA - Biomembranes 1860 (2018) 943–952

Contents lists available at ScienceDirect

BBA - Biomembranes

journal homepage: www.elsevier.com/locate/bbamem

Functional validation of Ca^{2+}-binding residues from the crystal structure of the BK ion channel☆

Aravind S. Kshatri, Alberto J. Gonzalez-Hernandez, Teresa Giraldez*

Departamento de Ciencias Médicas Basicas, Instituto de Tecnologías Biomédicas y Centro de Investigaciones Biomédicas de Canarias, Universidad de La Laguna, 38071 La Laguna, Spain

ARTICLE INFO

Keywords:
BK channels
Ca^{2+} sensitivity
Electrophysiology
Voltage dependence
Free energy difference

ABSTRACT

BK channels are dually regulated by voltage and Ca^{2+}, providing a cellular mechanism to couple electrical and chemical signalling. Intracellular Ca^{2+} concentration is sensed by a large cytoplasmic region in the channel known as "gating ring", which is formed by four tandems of regulator of conductance for K^+ (RCK1 and RCK2) domains. The recent crystal structure of the full-length BK channel from *Aplysia californica* has provided new information about the residues involved in Ca^{2+} coordination at the high-affinity binding sites located in the RCK1 and RCK2 domains, as well as their cooperativity. Some of these residues have not been previously studied in the human BK channel. In this work we have investigated, through site directed mutagenesis and electrophysiology, the effects of these residues on channel activation by voltage and Ca^{2+}. Our results demonstrate that the side chains of two non-conserved residues proposed to coordinate Ca^{2+} in the *A. californica* structure (G523 and E591) have no apparent functional role in the human BK Ca^{2+} sensing mechanism. Consistent with the crystal structure, our data indicate that in the human channel the conserved residue R514 participates in Ca^{2+} coordination in the RCK1 binding site. Additionally, this study provides functional evidence indicating that R514 also interacts with residues E902 and Y904 connected to the Ca^{2+} binding site in RCK2. Interestingly, it has been proposed that this interaction may constitute a structural correlate underlying the cooperative interactions between the two high-affinity Ca^{2+} binding sites regulating the Ca^{2+} dependent gating of the BK channel. This article is part of a Special Issue entitled: Beyond the Structure-Function Horizon of Membrane Proteins edited by Ute Hellmich, Rupak Doshi and Benjamin McIlwain.

1. Introduction

Large conductance voltage- and Ca^{2+}-gated K^+ channels (BK, Maxi K, $K_{Ca}1.1$ or Slo1) are essential regulators of membrane excitability and intracellular $[Ca^{2+}]_i$ In neurons and smooth muscle cells, when action potentials occur, Ca^{2+} influx through voltage-dependent Ca^{2+} channels (VDCCs) activates neighbouring BK channels to repolarize the membrane and eventually closing VDCC, terminating the Ca^{2+} signal. This negative feedback mechanism enables BK channels as important regulators of many physiological processes including smooth muscle contraction [1], neurotransmitter release [2] and action potential termination [3]. In comparison to other K^+ channels, BK channels exhibit an unusually large conductance ranging between 100 pS and 300 pS [4]. Functional channels are formed by four pore-forming α subunits, encoded by the *KCNMA1* gene. Each subunit is divided into three main structural domains: a voltage sensor domain that senses the changes in membrane potential, a pore gate domain, that lets K^+ ion to traverse across the membrane and a cytoplasmic domain, which senses Ca^{2+}, Mg^{2+} and other biological factors. In the intracellular region of the functional BK tetramer, four pairs of non-identical regulator of conductance of K^+ (RCK1 and RCK2) domains form the Ca^{2+} sensing apparatus known as the "gating ring" [5]. A large number of functional and structural studies have provided extensive knowledge about the structural basis of BK channels function [6]. Recently, the field has experienced great excitement with the description of the full-length BK protein structure from *Aplysia californica* (aBK), which has been unveiled in the absence and presence of Ca^{2+} and/or Mg^{2+} [7] (Fig. 1). Among other key questions related to BK function, this new structure has provided detailed structural information of all Ca^{2+}-binding sites in the gating ring, additionally presenting a possible structural basis for cooperativity between them [8].

The BK gating ring contains a key high-affinity Ca^{2+} binding site, known as the "Ca^{2+} bowl" and characterized by a stretch of aspartate residues within the RCK2 domains [9]. Structures of isolated gating rings from eukaryotic BK channels as well as the recent full-length structure from aBK revealed that this site is located at the interface between adjacent RCK dimers [10] [11,7].

In addition to the Ca^{2+} bowl, another high affinity Ca^{2+} binding site is located in the RCK1 domain. In the aBK structure, strong electron density was observed corresponding to a Ca^{2+} ion coordinated by side chains from aD356 and aD525 as well as main-chain oxygens from aR503, aG523 and aE591 [7]. This binding site was largely similar to a model proposed previously in the RCK1 domain [12]. Among these residues, aD356, aE525 and aR503 are highly conserved in BK from various species and their implication in Ca^{2+} sensing had been previously identified in extensive electrophysiological studies [13,12]. However, the functional role of residues aG523 and aE591 (corresponding to non-conserved residues hS533 and hS600) in Ca^{2+} binding has not been studied in the hBK orthologue [5] (Fig. 1).

Interestingly, the full-length *A. californica* BK structure revealed that the residue aR503 (hR514) interacts with conserved residues aE912 (hE902) and aY914 (hY904) at the Ca^{2+} bowl region. This led the authors to propose that this interaction may constitute the structural basis for cooperativity between the two Ca^{2+} binding sites [8] (Fig. 1C). Comprehensive functional studies are needed to assess the role of these residues in hBK channel function.

In this work we have explored the relevance of these novel structural findings in the aBK channel on hBK function. To this end, we have mutated the corresponding residues to alanine and studied their response to different concentrations of Ca^{2+} and voltage. Our results show that the Ca^{2+} response of hBK channels was largely unaffected by the hS533A and hS600A mutations, suggesting that the side chains of these residues are not involved in coordinating the Ca^{2+} ion at the RCK1 Ca^{2+} binding site in the human BK channel. On the other hand, the hR514A mutation affects the Ca^{2+} sensitivity of the channels, consistent with a role of this residue in Ca^{2+} ion coordination at the RCK1 Ca^{2+} binding site function. Most importantly, our data suggest that the Ca^{2+} bowl residues, hE902 and hY904 interact with the hR514 residue to stabilize the RCK1 Ca^{2+} binding site. This finding paves the way to further studies unveiling the role of this interaction in the cooperativity between the Ca^{2+} bowl and RCK1 Ca^{2+} binding sites.

2. Methods

2.1. Cloning, mutagenesis, cell culture and transfections

The human BKα subunit was isolated from uterine smooth muscle (accession no. U11058) and cloned into the pBNJ vector [14] [15,16].

☆ This article is part of a Special Issue entitled: Beyond the Structure-Function Horizon of Membrane Proteins edited by Ute Hellmich, Rupak Doshi and Benjamin McIlwain.

* Corresponding author.
E-mail address: giraldez@ull.edu.es (T. Giraldez).

http://dx.doi.org/10.1016/j.bbamem.2017.09.023
Received 26 July 2017; Received in revised form 21 September 2017; Accepted 24 September 2017
Available online 29 September 2017
0005-2736/

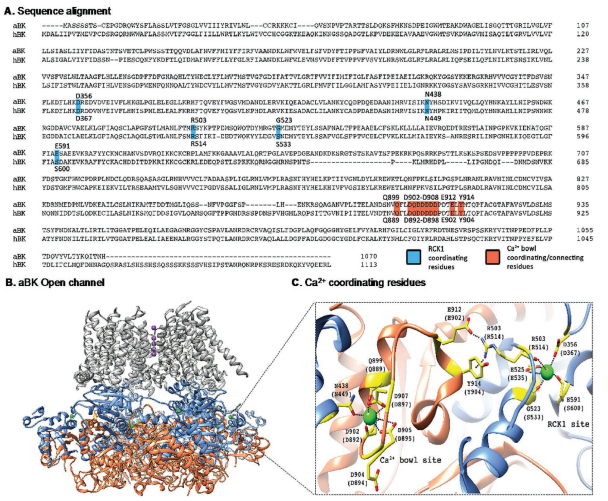

Fig. 1. Ca^{2+} modulating residues of the BK channel. A) Comparison of sequence alignments between *Aplysia californica* (aBK) and Human (hBK) BK channels. The Ca^{2+} coordinating/connecting sites in RCK1 domain are highlighted in blue whereas RCK2 domain sites are in orange. B) Open structure of the aBK channel (Ca^{2+} ions are shown as green spheres and purple spheres represent K^+ ions). The RCK1 domain is coloured in blue, RCK2 domain in orange and the rest of the channel in grey. C) Detailed structure of the boxed region in Panel B. *A. californica* residue numbers (top) and equivalent residues in the human BK channel (bottom, brackets) are indicated. At the RCK1 Ca^{2+}-binding site, the Ca^{2+} ion is coordinated by residues aD356 (hD367), aR503 (hR514), aG523 (hS533), aE525 (hE535) & aE591 (hS600). Additionally, the aR503 residue also interacts with aE912 (hY902) (hydrogen bond) and aY914 (hY904) (cation-π interaction) of the RCK2 region. At the Ca^{2+} bowl, Ca^{2+} coordinating residues are aQ899 (hQ889), aD902 (hD892), aD904 (hD894), aD905 (hD895) & aD907 (hD897). Additionally, the aN438 (hN449) residue from the neighbouring subunit RCK1 domain has been proposed to coordinate Ca^{2+} at this site.

All the mutations were performed on the human BKα background using QuikChange multi-site-directed mutagenesis kit (Agilent Genomics) and confirmed using sequencing. The neutralization of Ca^{2+} bowl was achieved by mutating the five consecutive aspartates to alanine (5D5A: 894-899). HEK293 cells were grown on 12-mm poly-lysine treated glass coverslips in DMEM enriched with 10% FBS and transfected with plasmid cDNA using jetPRIME reagent (Polyplus).

2.2. Electrophysiology

Electrophysiological recordings were carried out 24–48 h post transfection. The recordings were done using the inside-out configuration of the patch clamp technique [17] and at room temperature (22–24 °C). Patch pipettes were fabricated from thick-wall borosilicate glass (1.5 mm O.D. × 0.86 mm I.D.) using a Sutter P-92 puller and fire polished. Pipettes had a resistance of 2–5 MΩ when filled with recording solutions. Recording solutions contained (in mM): pipette- 80 $KMeSO_3$, 60 *N*-methylglucamine-$MeSO_3$, 20 HEPES, 2 KCl, 2 $MgCl_2$ (pH 7.4); bath- 80 $KMeSO_3$, 60 *N*-methylglucamine-$MeSO_3$, 20 HEPES, 2 KCl, 1 HEDTA, and $CaCl_2$ to give the desired free Ca^{2+} concentration. For Ca^{2+} solutions containing 100 μM Ca^{2+}, no Ca^{2+} chelator was added. The total amount of $CaCl_2$ need to obtain the desired Ca^{2+} concentration was calculated using the Max Chelator program and free Ca^{2+} was confirmed using a Ca^{2+}-sensitive electrode (Orion electrode; Thermo Lab Systems). Stimulus generation and data acquisition were controlled and analyzed with Clampex and Clampfit programs of pClamp10 software package (Axon Instruments). The currents were amplified using an Axopatch-200B amplifier and digitized using Digidata 1550A plus HumSilencer system. Subsequently, the data was acquired at 100 kHz and low-pass filtered at 5 kHz with a 4-pole Bessel filter.

2.3. Data analysis

Conductance-Voltage (G-V) curves were generated from tail current amplitudes normalized to the maximum obtained in 100 μM Ca^{2+}. The resultant curves were fitted with the Boltzmann equation:

$$\frac{G}{G_{max}} = \frac{1}{1 + \exp\left(\frac{\left(V_m - V_{1/2}\right)}{z}\right)}$$

where $V_{1/2}$ is the voltage of half-maximum activation, z is the slope of the curve, V_m is the test potential and G_{max} is the maximal conductance. We measured the Ca^{2+} sensitivity as the G-V shift induced by increasing the Ca^{2+} from low 0 μM to the saturating 100 μM Ca^{2+}. Thus, the shift in $V_{1/2}$ ($\Delta V_{1/2}$) is given by:

$$\Delta V_{1/2} = V_{1/2} \text{in } 0\ \mu M\ Ca^{2+} - V_{1/2} \text{in } 100\ \mu M\ Ca^{2+}$$

where $V_{1/2}$ is the half maximal activation voltage (mV).

The direct effect of Ca^{2+} on the channel can be expressed in terms of the Gibbs free energy difference (ΔG_0) between the closed and open states at 0 mV as described previously [18,19]. We obtained the slope (z) and $V_{1/2}$ values from the Boltzmann fits to the data, and calculated ΔG_0 using.

$$\Delta G_0 = 0.2389 z F V_{1/2}$$

where F is the Faraday constant. ΔG_0 has the units of energy (kJ/mol). The change in ΔG_0 produced in the presence of Ca^{2+} was calculated using.

$$\Delta\Delta G_0\,(Ca^{2+}) = \Delta G_0\,(Ca^{2+}) - \Delta G_0\,(Ca^{2+}\text{free})$$

Finally, the percent reduction of $\Delta\Delta G_0$ (Fig. 6) was calculated as.

$$\%\text{reduction} = \left(\Delta\Delta G_{0\ WT(100\mu M\ Ca^{2+})} - \Delta\Delta G_{0\text{mutant}(100\ \mu M\ Ca^{2+})}\right) / \Delta\Delta G_{0\ WT(100\ \mu M\ Ca^{2+})}$$

All data shown correspond to the mean ± SEM. The averaged $V_{1/2}$ and slope values (z) were obtained from individual experiments analyzed separately. Slight differences observed in the slope values recorded from Boltzmann fits when compared with previous publications (e.g [13,22,27].) could be due to differences in the experimental conditions. Statistical differences were assessed with one way - ANOVA followed by *post-hoc* analysis (Bonferroni correction). A p-value < 0.05 was considered statistically significant. In all figures *, **, *** indicate a p < 0.05, 0.01, 0.001 respectively.

3. Results

In general, Ca^{2+} ions are coordinated by oxygen-containing side chains, carbonyl groups of amino acids backbones as well as water molecules. Consistent with this theory, the available structures from isolated gating rings as well as the full-length aBK structure showed Ca^{2+} ions bound to oxygen atoms of amino acids at the Ca^{2+} bowl and RCK1 Ca^{2+} binding sites [10,20,7]. Among these, new residues were identified including aR503, aG523 and aE591 (hR514, hS533 and hS600) in the RCK1 site that had not been extensively studied in hBK. In the aBK structure, these residues coordinate Ca^{2+} through the main chain carbonyl oxygen atoms. We began our investigation by mutating all of these residues to alanine and tested the effects of increasing Ca^{2+} from 0 μM to 100 μM.

3.1. hR514 reduces Ca^{2+} sensitivity of hBK channels

Fig. 2 shows representative current recordings from patches containing hBKα channels (Fig. 2A) and the different mutants generated in this study (Fig. 2B–D) corresponding to voltage pulses ranging from −100 mV to +100 mV in 20 mV increments at different Ca^{2+} concentrations. The summary G-V curves are shown in Fig. 3. The $V_{1/2}$ and slope values obtained for all mutants at various Ca^{2+} concentrations are listed in Table 1. As previously shown for wild-type hBKα channels [6,9,13,14], [15,21], increasing Ca^{2+} from 0 to 100 μM led to larger outward K^+ currents due to a leftward shift in the $V_{1/2}$ (Fig. 2A). We next evaluated the role of the hS533 and hS600A mutations in coordinating Ca^{2+} at the RCK1 site. As shown in Figs. 2 and 3 (panels A, C & D), the Ca^{2+} sensitivity of the mutations hS533A and hS600A was undistinguishable from that of WT hBKα channels, indicating that the side chains of these two non-conserved residues are not involved in coordinating the Ca^{2+} ion in the human BK channel.

As shown in Fig. 2A, the WT hBKα channels began to activate at around +80 mV in 0 Ca^{2+} ($V_{1/2}$ = 207 ± 3 mV, n = 19). Interestingly, the hR514A mutation led to activation of the channels at voltages below +40 mV (Fig. 2B, $V_{1/2}$ = 158 ± 6 mV, n = 16, p < 0.001). Although this mutant is still sensitive to increasing Ca^{2+} concentrations, the apparent Ca^{2+} sensitivity in higher Ca^{2+} (5 μM–100 μM) was significantly reduced compared to the WT hBKα channels as is noticeable from its compressed G-V relationship and the mean $\Delta V_{1/2}$ summary (Fig. 3 A, B & F). Thus, R514A mutant left shifted the $V_{1/2}$ in 0 Ca^{2+} and decreased the Ca^{2+} sensitivity to higher Ca^{2+} concentrations without affecting the slope of G-V curves significantly (Table 1).

3.2. Is the hR514A mutation affecting the Ca^{2+} sensitivity of the RCK1 site directly or the RCK2 Ca^{2+} bowl site indirectly?

The magnitude of the shift in the $V_{1/2}$ induced by high Ca^{2+} concentrations (5 μM–100 μM) was significantly reduced in the hR514A mutation (Fig. 4A–C). To precisely distinguish the region that is affected by mutating the hR514 residue, we used a double mutation approach. One assumption is that, if hR514A is acting independently of

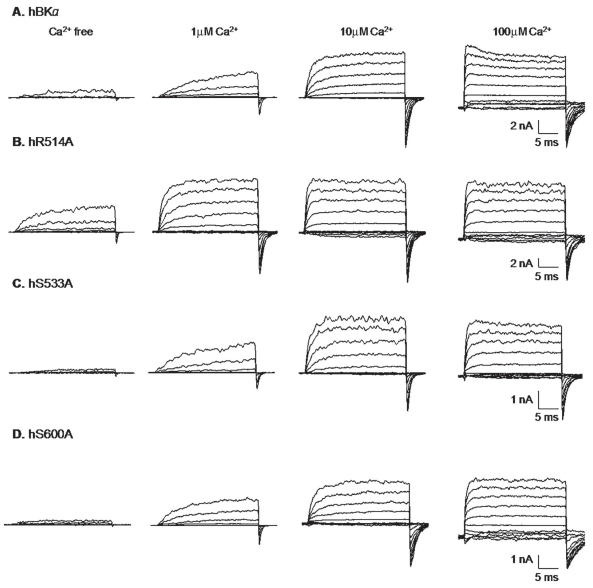

Fig. 2. Representative current recordings of wild-type hBKα and various mutations of putative Ca^{2+} coordinating sites. The current traces were recorded after depolarizating the membrane to voltages ranging from −100 mV to +100 mV in 20 mV increments at different Ca^{2+} concentrations (1 μM, 10 μM and 100 μM). The mutation of serine residues (hS533A and hS600A) did not affect the Ca^{2+} sensitivity of the channels significantly compared to the BKα channels. However, the hR514A channels activated at less positive voltages (< +40 mV) compared to BKα channels.

the RCK1 high-affinity Ca^{2+}-binding site, mutation of an additional residue in this site, such as hD367, should have additive effects; if they were both part of the same Ca^{2+}-binding site (RCK1), the effect of both mutations would not be additive. To test this hypothesis, we mutated hD367 to alanine (RCK1 Ca^{2+} binding site, [13]) in combination or not with hR514A. Consistent with previous studies [12,22], the single mutation hD367A lowered Ca^{2+} sensitivity of BKα channels by approximately 50% (Fig. 4D). Double mutant hD367A + hR514A exerted effects that are comparable to single mutant hD367A. The double mutant showed an apparent tendency towards higher sensitivity to lower [Ca^{2+}] and lower sensitivity to higher [Ca^{2+}] than the hD367A construct (Fig. 4E). However, statistical analysis of the data shows no significant differences between the apparent shifts induced by 100 μM Ca^{2+} in hD367A and hD367A + hR514A ($\Delta V_{1/2}$ = −89 ± 5 mV and $\Delta V_{1/2}$ = −78 ± 7 mV, respectively), whereas both were significantly different to the WT hBKα channels ($\Delta V_{1/2}$ = 218 ± 6 mV; Fig. 4F).

To further test our hypothesis, we next mutated the RCK2 Ca^{2+} bowl to alanine (hD894 through hD899, mutant h5D5A) in combination or not with the hR514A mutation. If hR514A affects only the RCK1 binding site, as suggested by the previous experiment, we would expect that the combination of both mutations (hR514A + h5D5A) would additively reduce the Ca^{2+} response. Fig. 4G displays the effect of increasing Ca^{2+} on the h5D5A mutation. In agreement with previous studies [22], this mutation diminished the Ca^{2+} sensitivity at lower μM ranges (0 μM–1 μM) whereas at the intermediate and higher μM Ca^{2+} ranges (5-100 μM) Ca^{2+} sensitivity was only partially affected. Interestingly, the double mutation, hR514A + h5D5A (Fig. 4H) reduced the hBKαCa^{2+} sensitivity considerably more than either of the mutations alone. In fact, this double mutant showed almost no response to Ca^{2+} between 5 μM–100 μM and also its $V_{1/2}$ appeared left-shifted similar to the other RCK1 site mutations (Fig. 5I). The $\Delta V_{1/2}$ value in 100 μM Ca^{2+} for this mutation was significantly reduced by 60% (−87 ± 5 mV, n = 9 vs. −218 ± 6 mV, n = 17 in hBKα), which was significantly higher than the 32% ($\Delta V_{1/2}$ = −148 ± 6 mV,

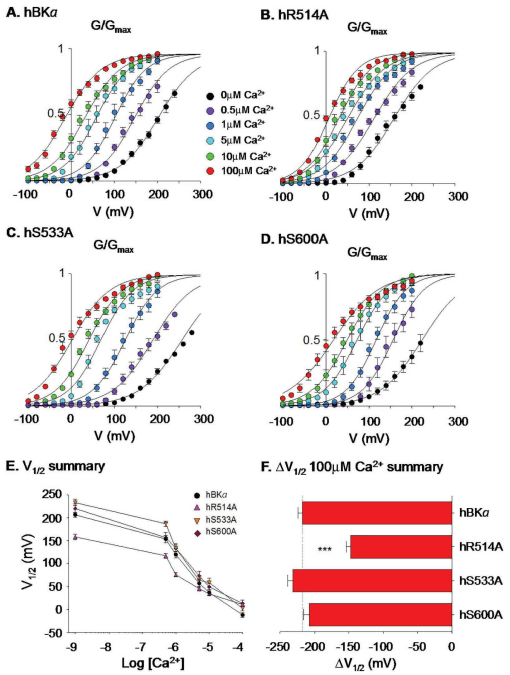

Fig. 3. hR514A mutation diminishes the Ca^{2+} sensitivity of the BK channels. (A–E) mean conductance-voltage (G-V) relationships for various alanine mutations. The shift induced by high Ca^{2+} is significantly reduced in the hR514A mutant (B) compared to the hBKα (A). E, Summary $V_{1/2}$ for WT channels and all five mutations at various $[Ca^{2+}]$. F, The mean $\Delta V_{1/2}$ produced by 100 μM Ca^{2+} in all the mutations.

n = 16) and 22% ($\Delta V_{1/2}$ = 169 ± 6 mV, n = 3) reduction in the hR514A and h5D5A mutants respectively (Fig. 4F). Taken together, these results suggest that hR514A affects BK Ca^{2+} sensitivity by directly disrupting the RCK1 binding site.

3.3. Mutation of the putative bridging residues selectively diminish the Ca^{2+} response mediated by the RCK1 site

We then examined the effects of mutating two residues hE902 and hY904, which in the full-length aBK structure are shown to interact directly with the side chain of the hR514 residue at the RCK1 site, and indirectly with the Ca^{2+} bowl site via the loop [7] (Fig. 1). The resulting summary G-V relationships are shown in Fig. 5. The mutation of hE902A failed to alter the effects of Ca^{2+} at all concentrations tested (Fig.5C, G & H). In contrast, the hY904A mutation significantly reduced the Ca^{2+} sensitivity of the channel at 100 μM Ca^{2+} (Fig. 5D & H). Moreover, this mutation also affected the voltage dependence of the channel similarly to hR514A ($V_{1/2}$ = 158 ± 6 mV, n = 16). In this case, $V_{1/2}$ at 0 Ca^{2+} is significantly left-shifted ($V_{1/2}$ = 162 ± 4 mV, n = 6) when compared to WT hBKα channels ($V_{1/2}$ = 207 ± 4 mV, n = 19). Interestingly, the reduction in the Ca^{2+} response of hY904A mutant was further enhanced with the double mutation hE902A + hY904A (Fig. 5E). Moreover, the G-V curves appear more compressed than the individual mutations (Fig. 5C & D) as well as the WT (Fig. 5A). The $\Delta V_{1/2}$ in 100 μM Ca^{2+} was reduced approximately by 50% compared to WT hBKαchannels (Fig. 5H). Remarkably, the triple mutation involving hR514A + hE902A + hY904A (Fig. 5F) induced a moderately lower reduction that was not statistically significant (p = 0.36, Student's *t*-test) to that of hE902A + hY904A channels. The $V_{1/2}$ vs. $[Ca^{2+}]$ dependence was also identical for these

Table 1
Boltzmann fit parameters for the BKα and mutant channels.

$[Ca^{2+}]_{in}$	Channel	$V_{1/2}$	z	n
0 μM Ca^{2+}	Wild type (BKα)	207 ± 5 mV	0.59 ± 0.02	19
	D367A	167 ± 2 mV	0.80 ± 0.05	10
	R514A	159 ± 2 mV	0.62 ± 0.02	16
	S533A	257 ± 3 mV	0.61 ± 0.03	13
	S600A	224 ± 5 mV	0.62 ± 0.04	12
	E902A	234 ± 4 mV	0.64 ± 0.05	6
	Y904A	166 ± 2 mV	0.57 ± 0.04	6
	5D5A	210 ± 2 mV	0.63 ± 0.05	5
	D367A + R514A	127 ± 2 mV	0.73 ± 0.03	5
	R514A + 5D5A	174 ± 2 mV	0.76 ± 0.03	9
	E902A + Y904A	152 ± 2 mV	0.7 ± 0.04	7
	R514A + E902A + Y904A	131 ± 3 mV	0.73 ± 0.06	7
0.5 μM Ca^{2+}	Wild type (BKα)	147 ± 2 mV	0.67 ± 0.02	9
	D367A	134 ± 1 mV	0.83 ± 0.06	5
	R514A	112 ± 2 mV	0.59 ± 0.03	10
	S533A	189 ± 2 mV	0.61 ± 0.06	7
	S600A	156 ± 3 mV	0.79 ± 0.04	12
	E902A	158 ± 4 mV	0.64 ± 0.05	6
	Y904A	98 ± 3 mV	0.58 ± 0.04	6
	5D5A	174 ± 2 mV	0.68 ± 0.07	4
	D367A + R514A	99 ± 3 mV	0.72 ± 0.05	5
	R514A + 5D5A	143 ± 2 mV	0.78 ± 0.03	9
	E902A + Y904A	96 ± 4 mV	0.61 ± 0.04	4
	R514A + E902A + Y904A	78 ± 2 mV	0.71 ± 0.04	7
	Wild type (BKα)	147 ± 2 mV	0.67 ± 0.02	9
	D367A	134 ± 1 mV	0.83 ± 0.06	5
	R514A	112 ± 2 mV	0.59 ± 0.03	10
	S533A	189 ± 2 mV	0.61 ± 0.06	7
	S600A	156 ± 3 mV	0.79 ± 0.04	12
	E902A	158 ± 4 mV	0.64 ± 0.05	6
	Y904A	98 ± 3 mV	0.58 ± 0.04	6
	5D5A	174 ± 2 mV	0.68 ± 0.07	4
	D367A + R514A	99 ± 3 mV	0.72 ± 0.05	5
	R514A + 5D5A	143 ± 2 mV	0.78 ± 0.03	9
	E902A + Y904A	96 ± 4 mV	0.61 ± 0.04	4
	R514A + E902A + Y904A	78 ± 2 mV	0.71 ± 0.04	7
1 μM Ca^{2+}	Wild type (BKα)	101 ± 3 mV	0.70 ± 0.05	9
	D367A	113 ± 2 mV	0.83 ± 0.06	10
	R514A	74 ± 2 mV	0.66 ± 0.03	13
	S533A	125 ± 3 mV	0.76 ± 0.05	10
	S600A	117 ± 3 mV	0.78 ± 0.06	12
	E902A	113 ± 3 mV	0.73 ± 0.07	6
	Y904A	62 ± 3 mV	0.65 ± 0.04	6
	5D5A	149 ± 2 mV	0.76 ± 0.07	4
	D367A + R514A	77 ± 2 mV	0.83 ± 0.05	5
	R514A + 5D5A	119 ± 3 mV	0.89 ± 0.04	7
	E902A + Y904A	68 ± 4 mV	0.66 ± 0.05	7
	R514A + E902A + Y904A	61 ± 2 mV	0.96 ± 0.04	5
5 μM Ca^{2+}	Wild type (BKα)	56 ± 3 mV	0.74 ± 0.02	19
	D367A	97 ± 3 mV	0.84 ± 0.04	5
	R514A	50 ± 3 mV	0.62 ± 0.04	8
	S533A	68 ± 3 mV	0.72 ± 0.05	6
	S600A	72 ± 4 mV	0.77 ± 0.05	12
	E902A	75 ± 3 mV	0.90 ± 0.07	7
	Y904A	25 ± 4 mV	0.83 ± 0.07	6
	5D5A	108 ± 3 mV	0.72 ± 0.07	4
	D367A + R514A	74 ± 2 mV	0.90 ± 0.06	5
	R514A + 5D5A	98 ± 3 mV	0.86 ± 0.04	7
	E902A + Y904A	41 ± 3 mV	0.68 ± 0.06	4
	R514A + E902A + Y904A	44 ± 3 mV	0.85 ± 0.05	7
10 μM Ca^{2+}	Wild type (BKα)	32 ± 3 mV	0.69 ± 0.02	16
	D367A	86 ± 2 mV	0.91 ± 0.04	10
	R514A	31 ± 3 mV	0.72 ± 0.04	14
	S533A	41 ± 3 mV	0.65 ± 0.03	10
	S600A	49 ± 3 mV	0.72 ± 0.03	12
	E902A	53 ± 3 mV	0.86 ± 0.06	6
	Y904A	8 ± 4 mV	0.82 ± 0.06	6
	5D5A	82 ± 2 mV	0.80 ± 0.06	5
	D367A + R514A	72 ± 2 mV	0.88 ± 0.04	5
	R514A + 5D5A	91 ± 2 mV	0.99 ± 0.03	7
	E902A + Y904A	36 ± 3 mV	0.78 ± 0.03	7
	R514A + E902A + Y904A	37 ± 3 mV	0.85 ± 0.04	7

Table 1 (*continued*)

$[Ca^{2+}]_{in}$	Channel	$V_{1/2}$	z	n
100 μM Ca^{2+}	Wild type (BKα)	13 ± 5 mV	0.72 ± 0.02	17
	D367A	78 ± 2 mV	0.83 ± 0.02	10
	R514A	7 ± 2 mV	0.80 ± 0.03	16
	S533A	2 ± 5 mV	0.66 ± 0.01	13
	S600A	18 ± 7 mV	0.73 ± 0.02	12
	E902A	12 ± 5 mV	0.85 ± 0.08	6
	Y904A	18 ± 6 mV	0.85 ± 0.05	6
	5D5A	33 ± 2 mV	0.88 ± 0.07	6
	D367A + R514A	69 ± 2 mV	0.87 ± 0.08	5
	R514A + 5D5A	88 ± 2 mV	0.92 ± 0.03	9
	E902A + Y904A	29 ± 4 mV	0.81 ± 0.05	7
	R514A + E902A + Y904A	26 ± 4 mV	0.95 ± 0.03	7

mutations (Fig. 5G), suggesting that these residues are part of the same transduction pathway involving the RCK1 site.

3.4. Effects of the mutations on free energy

Our results show that some of the mutations studied reduce the Ca^{2+} dependence of activation of the hBK channel. These effects could be due to alterations in the Ca^{2+} binding/transduction pathway or to a modification in voltage sensing. To distinguish more precisely which of these effects may be affected, we evaluated the free energies ($\Delta\Delta G_0$) from the Boltzmann fits to the data (see Methods).

The mean $\Delta\Delta G_0$ in response to 100 μM Ca^{2+} and the relative percent reduction for the putative Ca^{2+} sensitivity-reducing mutations is shown in Fig. 6. The $\Delta\Delta G_0$(100 μM Ca^{2+}) in WT hBKα was 13.11 ± 0.63 kJ/mol (n = 17). Consistent with the reduced $\Delta V_{1/2}$, the hR514A mutation also significantly reduced the free energy difference by 30%. The $\Delta\Delta G_0$ of the double mutation, hD367A + hR514A was not additive, suggesting that these sites are not influencing each other. However, the hR514A + h5D5A mutant displayed strict additivity (% reduction: hR514A - 32%, h5D5A - 27%, hR514A + h5D5A - 64%) indicating that both regions are acting independently in sensing Ca^{2+}. Interestingly, the hE902 + hY904A double mutant also showed an additive effect, ($\Delta\Delta G_0 \sim 40\%$), whereas the effect on ΔΔG0 of the triple mutation (hR514A + hE902A + hY904A) was identical to the double hE902A + hY904A mutation. Taken together, these data indicate that the reduction in Ca^{2+}-induced $V_{1/2}$ of the mutations is potentially due to an alteration in the Ca^{2+} binding/transduction pathway/s of the channel.

4. Discussion

Determination of atomic structures of biological molecules is essential to provide information about the mechanisms underlying their physiological roles in all living cells. The revolutionary Cryo-EM (electron microscopy) along with the X-ray crystallography technique has solved 3D atomic structures of numerous proteins over the recent years. However, it is extremely important to validate these structures functionally and correlate structural and functional data.

In this study, we have validated in the hBK channel the functionality of the high affinity Ca^{2+} binding sites recently identified in the aBK channel cryo-EM structure [7,8]. Although the aBK channel sequence is only ~60% similar to that of human BK, our functional data suggest that the conserved Ca^{2+} binding sites are essentially identical in both species. The full-length aBK structure shows that, at the RCK1 site, the Ca^{2+} ion is coordinated by five residues, two of which are not conserved. In the presence of Ca^{2+} ions, the side chains of conserved residues aD356, aR503 and aE525 tilt inwards towards the Ca^{2+} binding site to cradle the ion. At the Ca^{2+} bowl site, the side chain of aD907 changes its conformation significantly providing a binding site for the Ca^{2+} ion. Additionally, the side chain of the connecting residue hY914 moves closer to the RCK1 site in the presence of Ca^{2+} [8]. In the human

Fig. 4. Mutation of hR514A affects the RCK1 Ca^{2+} dependent response. (A–C). Effects of the hR514A mutation on hBKα channels. Only the shift in $V_{1/2}$ induced by 5 μM-0.9 μM Ca^{2+} is significantly reduced in this mutation. (D,E) G-V curves for the hD367A and hD367A + hR514A mutations. The non-additive effects of this mutation suggest that they both are part of the same Ca^{2+} binding site. (F) Effects of the mutations hS0S5A and hR514A + hS0S5A. The double mutation lowers the Ca^{2+} sensitivity in an additive manner. (F) $\Delta V_{1/2}$ at 100 μM Ca^{2+}. (I) average $V_{1/2}$ as a function of $[Ca^{2+}]$ for all the mutations

BK channel, the side chains of two non-conserved serine residues (hS533 and hS600) did not appear to have a functional role in Ca^{2+} sensing. This is consistent with a conserved structure of human BK channel, where the corresponding residues hS533 and hS600 participate in Ca^{2+} coordination. However, our results do not discard the possibility that additional Ca^{2+} coordination sites exist in the human BK channel, equivalent to the coordinating serine residues in the aBK channel.

Using molecular modelling Zhang et al. proposed that the side chain of the hR514 residue coordinates the Ca^{2+} ion RCK1 Ca^{2+} binding site [12]. This was confirmed by the full-length aBK structure [7]. However, Zhang et al. did not provide functional data about the gating behaviour of the R514 mutation due to the fact that only its main-chain carbonyl oxygen atom participates in Ca^{2+} coordination, so no large effects on Ca^{2+} sensitivity were expected. Bukiya et al. (2014) reported that hR514 is an important residue for ethanol sensing, since it provides a net positive charge to favour ethanol-BK interaction. Additionally, that study showed that hR514N mutation increased the NP_O of the channels, shifted the G-V curves leftwards and modestly reduced the sensitivity to 100 μM Ca^{2+} [23]. Our results with the hR514A mutant are consistent with their study since neutralizing the positive charge also shifted the G-V curves leftwards ($V_{1/2}$ = 158 ± 6 mV). In addition, the hR514A mutant displayed a significant reduction in the Ca^{2+}-dependence response, which was fitted with a concentration of 5 μM-100 μM Ca^{2+} as range. In contrast, the proposed G-V relationship reported in our study. The G-V curves of the hR514A mutant could be mainly attributed to altered Ca^{2+} binding but not voltage-sensing due to the following reasons: I) The steepness of G-V curves in the absence and presence of Ca^{2+} (Table 1) is not significantly different when compared to WT hBKα; II) The mutation decreased $\Delta\Delta G_o$ in higher Ca^{2+} by > 30% suggesting that either a reduction in Ca^{2+} binding affinity or number of Ca^{2+} binding sites has occurred. However, we cannot rule out the possibility that this mutation destabilizes the RCK1 Ca^{2+} binding site, exerting a similar role than its neighbouring residue hM513, which was proposed to maintain the structural integrity of the RCK1 site [10]. A direct biochemical approach, using a $^{45}Ca^{2+}$ gel-overlay to BKα and hR514A mutant channels would give more information about Ca^{2+} binding to this site. Remarkably, to date no study has reported any Ca^{2+} binding to the RCK1 site using this assay [22,24,25].

The effect of the hR514A mutation could be a consequence of directly altering Ca^{2+} coordination (at the RCK1 site) or indirectly modulating the Ca^{2+} bowl site (through a cooperative interaction via

Fig. 5. The side chains of E902, Y904 & R514 are essential for Ca^{2+} sensing in the RCK1 site. Mean G-V curves determined for (A) BKα (B) R514A (C) E902A (D) Y904A (E) E902A + Y904A (F) R514A + E902A + Y904A. The double mutation E902A + Y904A additively reduced the response to Ca^{2+}. The addition of R514A to this double mutation did not further decrease the Ca^{2+} response. G, Mean $V_{1/2}$ summary as a function of $[Ca^{2+}]$. H, Shift in $V_{1/2}$ induced by 100 μM Ca^{2+}.

the b902 and b904 residues Fig. 1; [7]). To discern between these two possibilities, we mutated the hR514 residue, separately and in combination with the high affinity Ca^{2+} binding sites at the RCK1 site (hD367A + hR514A) and the Ca^{2+} bowl (hR514A + hS0S5A). The argument is that if hR514 is a part of the RCK1 site, the double mutation hD367A + hR514A shall not have additive effects and conversely, simultaneous mutation of hR514A + hS0S5A will render quantitatively additive effects. Our data clearly show that hR514 forms part of the RCK1 Ca^{2+} sensitive site, since the hD367A + hR514A double mutant displayed similar features to hD367A single mutants and no additivity in Ca^{2+} sensitivity. Moreover, the hR514A + hS0S5A double mutant showed additive reduction effects. In this case, the Ca^{2+} sensitivity at both low and high Ca^{2+} concentrations was significantly reduced suggesting that these two residues are acting at independent sites. A partial response to Ca^{2+} can be seen in this mutant, which is presumably due to the persisting Ca^{2+} binding residues at the RCK1 site (hD367, hE535) or to the activation of low affinity Ca^{2+} binding sites

in the recent aBK structure, aE912 (hE902) and aY914 (hY904) residues from the Ca^{2+} bowl region were shown to interact with the side chains of the hR514 residue at the RCK1 site (Fig. 1C, [7]). Bao et al. [33] previously reported that the hE902 and hY904 residues had no functional role in the Ca^{2+} response. In that study, the effect on Ca^{2+} sensitivity of various mutations was assessed by estimating the shifts in the G-V relationships induced by 10 μM Ca^{2+}. Our data is in agreement with their results, since we did not observe any alteration in the Ca^{2+} response at that concentration for the hE902A nor the hY904A mutants (Table 1). In the present study, mutation of these residues aided us to assess their functional interaction with the hR514 residue and its effect in hBKα Ca^{2+} sensing. The shift in $V_{1/2}$ induced by 100 μM Ca^{2+} for hE902A channels appeared identical to that of WT hBKα channels, suggesting that the hydrogen bond between side chains of hE902 and hR514 is not essential for Ca^{2+} regulation. In contrast, disrupting the cation-π interaction between hY904 and hR514 by

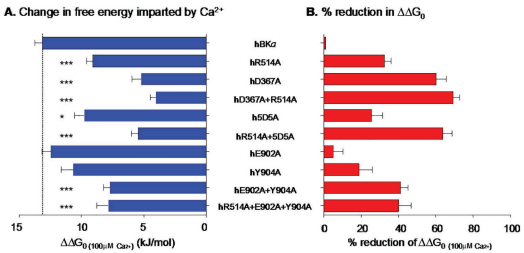

Fig. 6. Energetic effects of the mutations. (A) $\Delta\Delta G_0$ of mutations in response to 100 μM Ca^{2+}. (B) Reduction of $\Delta\Delta G_0$ (%) caused by each mutation. All mutations with the exception of hE902A and hY904A displayed significant reductions in $\Delta\Delta G_0$. Only the double mutations hR514A + h5D5A and hE902A + hY904A are quantitatively additive in reducing the $\Delta\Delta G_0$ of 100 μM Ca^{2+}.

mutating hY904 to alanine significantly reduced the response to 100 μM Ca^{2+} (as shown in Fig. 5H). Interestingly, an additive reduction in the Ca^{2+} sensitivity was observed in the hE902A + hY904A double mutant. One speculation is that, although these amino acids are located at a loop outside the Ca^{2+} bowl, the removal of side chains from hE902 and hY904 destabilizes the local structural integrity of that Ca^{2+} binding site. Alternatively, they could alter the structural integrity of the RCK1 site via the hR514 residue. Supporting the latter idea, the triple mutant, hR514A + hE902A + hY904A behaved similarly to the hE902A + hY904A double mutant. In the triple mutant, the shift in $V_{1/2}$ at all Ca^{2+} concentrations was significantly different from that of hBKα channels. Altogether, our findings provide functional evidence, in the framework of the human BK channel, of an interaction between hR514, hE902 and hY904 residues. This result gives weight to the hypothesis raised by Hite et al. [8], which was based solely on structural data from *Aplysia* BK, suggesting that this interaction constitutes a structural mechanism underlying cooperativity between the RCK1 Ca^{2+} binding site and the Ca^{2+} bowl regions. It is thus tempting to speculate that the reduced Ca^{2+} effects of the single hR514A mutation may be partially attributed to the altered cooperative effect between the two regions resulting in an impaired RCK1 Ca^{2+} sensing site.

Previous studies [27,28] proposed that cooperative interactions exist between the two high affinity Ca^{2+} binding sites (RCK1 and Ca^{2+} bowl) of the BK channel. The former study [27] used eight different combinations of the two high affinity Ca^{2+} sites to establish that BK channel exhibit positive intra-subunit cooperativity. Savalli et al. [28] used voltage clamp fluorometry and UV photolysis of intracellular caged Ca^{2+} to optically resolve the interactions between RCK1 and the Ca^{2+} bowl sites, as well as with the voltage sensor domain. Contrary to Qian et al., the study by Savalli et al. concluded that negative cooperativity exists between the two Ca^{2+} domains of the same subunit. Neither of these two studies showed the specific residues that are directly involved in maintaining these cooperative interactions. The full-length aBK structure unveiled an interaction between residues aR503, aE912 and aY914 as a possible mechanism underlying cooperativity [7]. Our results now show that in the human BK channel such interaction is conserved. Thus, we could now hypothesize that residues hE902 and hY904 from the Ca^{2+} bowl domain cooperate with the RCK1 domain to allosterically regulate channel opening in the presence of Ca^{2+}. Further studies are needed to address the nature of this cooperativity (positive or negative, inter/intra-subunit). The interaction between these residues might also be important in mediating the propagation of the Ca^{2+} bowl site conformational changes to the RCK1 Ca^{2+} site, ultimately resulting in pore opening. Further investigation using the experimental approach of the Horrigan-Aldrich (HA) model [29] is needed to quantify the effect of the disruption of such interactions on the allosteric coupling factors, C (between the Ca^{2+} sensors and the pore) and E (between the Ca^{2+} sensors and the voltage sensors).

We have relied on the $\Delta V_{1/2}$ data as a reasonable parameter to estimate the reduction in Ca^{2+} sensitivity of these mutations. However, both voltage and Ca^{2+} synergistically influence the channel to render the effects on the $V_{1/2}$ values. Therefore, it is crucial to distinguish between these two stimuli that may be affected by the mutations. It has been suggested by many studies [30–32] that the parameter, $\Delta\Delta G_0$ (change in free energy difference) depends mainly on the Ca^{2+} binding properties of the channel. According to the VD-MWC model (as outlined in [22], reduction in $\Delta\Delta G_0$ is attributed to either a change in Ca^{2+} binding affinity or the total number of Ca^{2+} binding sites of the channel. The data in Fig. 6 showing the $\Delta\Delta G_0$ values corresponding to the different mutants studied in this work further support our interpretation of their effect on hBKα Ca^{2+} sensitivity. With the exception of the hE902A and hY904A mutants (which did not induce a significant reduction), we observed reduced $\Delta\Delta G_0$ values in 100 μM Ca^{2+} for all mutations. Thus, we believe that our mutations affect the Ca^{2+}-sensing more than the voltage- sensing mechanism.

In summary, our functional data obtained with hBK are in close agreement with the proposed Ca^{2+} binding sites in the aBK channel crystal structure. Most importantly, our data provide functional evidence of an interaction between hE902, hY904 and hR514 residues in the human channel, which is consistent with the model provided by the structure suggesting a cooperativity mechanism between the RCK1 and Ca^{2+} bowl sites.

Transparency document

The Transparency document associated with this article can be found, in online version.

Acknowledgements

This work was funded by European Research Council (ERC) – under the European Union' Horizon 2020 Research and Innovation Programme (Grant 648936).

References

[1] M.T. Nelson, H. Cheng, M. Rubart, L.F. Santana, A.D. Bonev, H.J. Knot, W.J. Lederer, Relaxation of arterial smooth muscle by calcium sparks, Science 270 (1995) 633–637.
[2] G. Raffaelli, C. Saviane, M.H. Mohajerani, P. Pedarzani, E. Cherubini, BK potassium channels control transmitter release at CA3-CA3 synapses in the rat hippocampus, J. Physiol. 557 (2004) 147–157.
[3] A. Muller, M. Kukley, M. Uebachs, H. Beck, D. Dietrich, Nanodomains of single Ca2+ channels contribute to action potential repolarization in cortical neurons, J. Neurosci. 27 (2007) 483–495.
[4] R. Latorre, A. Oberhauser, P. Labarca, O. Alvarez, Varieties of calcium-activated potassium channels, Annu. Rev. Physiol. 51 (1989) 385–399.
[5] T. Giraldez, B.S. Rothberg, Understanding the conformational motions of RCK gating rings, J. Gen. Physiol. 149 (2017) 431–441.
[6] R. Latorre, K. Castillo, W. Carrasquel-Ursulaez, R.V. Sepulveda, F. Gonzalez-Nilo, C. Gonzalez, O. Alvarez, Molecular determinants of BK channel functional diversity and functioning, Physiol. Rev. 97 (2017) 39–87.
[7] X. Tao, R.K. Hite, R. MacKinnon, Cryo-EM structure of the open high-conductance Ca2+ −activated K+ channel, Nature 541 (2017) 46–51.
[8] R.K. Hite, X. Tao, R. MacKinnon, Structural basis for gating the high-conductance Ca2+ −activated K+ channel, Nature 541 (2017) 52–57.
[9] A. Wei, C. Solaro, C. Lingle, L. Salkoff, Calcium sensitivity of BK-type KCa channels determined by a separable domain, Neuron 13 (1994) 671–681.
[10] Y. Wu, Y. Yang, S. Ye, Y. Jiang, Structure of the gating ring from the human large-conductance Ca(2+)-gated K(+) channel, Nature 466 (2010) 393–397.
[11] P. Yuan, M.D. Leonetti, A.R. Pico, Y. Hslung, R. MacKinnon, Structure of the human BK channel Ca2 + −activation apparatus at 3.0 A resolution, Science 329 (2010) 182–186.
[12] G. Zhang, S.Y. Huang, J. Yang, J. Shi, X. Yang, A. Moller, X. Zou, J. Cui, Ion sensing in the RCK1 domain of BK channels, Proc. Natl. Acad. Sci. U. S. A. 107 (2010) 18700–18705.
[13] X.M. Xia, X. Zeng, C.J. Lingle, Multiple regulatory sites in large-conductance calcium-activated potassium channels, Nature 418 (2002) 880–884.
[14] T. Giraldez, T.E. Hughes, F.J. Sigworth, Generation of functional fluorescent BK channels by random insertion of GFP variants, J. Gen. Physiol. 126 (2005) 429–438.
[15] P. Miranda, J.E. Contreras, A.J. Plested, F.J. Sigworth, M. Holmgren, T. Giraldez, State-dependent FRET reports calcium- and voltage-dependent gating-ring motions in BK channels, Proc. Natl. Acad. Sci. U. S. A. 110 (2013) 5217–5222.
[16] P. Miranda, T. Giraldez, M. Holmgren, Interactions of divalent cations with calcium binding sites of BK channels reveal independent motions within the gating ring, Proc. Natl. Acad. Sci. U. S. A. 113 (2016) 14055–14060.
[17] O.P. Hamill, A. Marty, E. Neher, B. Sakmann, F.J. Sigworth, Improved patch-clamp techniques for high-resolution current recording from cells and cell-free membrane patches, Pflugers Arch. - Eur. J. Physiol. 391 (1981) 85–100.
[18] Y. Zhou, X.M. Xia, C.J. Lingle, Cysteine scanning and modification reveal major differences between BK channels and Kv channels in the inner pore region, Proc. Natl. Acad. Sci. U. S. A. 108 (2011) 12161–12166.
[19] S. Chowdhury, B. Chanda, Estimating the voltage-dependent free energy change of ion channels using the median voltage for activation, J. Gen. Physiol. 139 (2012) 3–17.
[20] P. Yuan, M.D. Leonetti, Y. Hsiung, R. MacKinnon, Open structure of the Ca2+ gating ring in the high-conductance Ca2 + − activated K + channel, Nature 481 (2011) 94–97.
[21] T.I. Webb, A.S. Kshatri, R.J. Large, A.M. Akande, S. Roy, G.P. Sergeant, N.G. McHale, K.D. Thornbury, M.A. Hollywood, Molecular mechanisms underlying the effect of the novel BK channel opener GoSlo: involvement of the S4/S5 linker and the S6 segment, Proc. Natl. Acad. Sci. U. S. A. 112 (2015) 2064–2069.
[22] L. Bao, A.M. Rapin, E.C. Holmstrand, D.H. Cox, Elimination of the BKi(Ca) channel's high-affinity Ca(2 +) sensitivity, J. Gen. Physiol. 120 (2002) 173–189.
[23] A.N. Bukiya, G. Kuntamallappanavar, J. Edwards, A.K. Singh, B. Shivakumar, A.M. Dopico, An alcohol-sensing site in the calcium- and voltage-gated, large conductance potassium (BK) channel, Proc. Natl. Acad. Sci. U. S. A. 111 (2014) 9313–9318.
[24] S. Bian, I. Favre, E. Moczydlowski, Ca2 + −binding activity of a COOH-terminal fragment of the *Drosophila* BK channel involved in Ca2 + −dependent activation, Proc. Natl. Acad. Sci. U. S. A. 98 (2001) 4776–4781.
[25] A.P. Braun, L. Sy, Contribution of potential EF hand motifs to the calcium-dependent gating of a mouse brain large conductance, calcium-sensitive K(+) channel, J. Physiol. 533 (2001) 681–695.
[26] X. Zhang, C.R. Solaro, C.J. Lingle, Allosteric regulation of BK channel gating by Ca (2+) and Mg(2 +) through a nonselective, low affinity divalent cation site, J. Gen. Physiol. 118 (2001) 607–636.
[27] X. Qian, X. Niu, K.L. Magleby, Intra- and intersubunit cooperativity in activation of BK channels by Ca2 +, J. Gen. Physiol. 128 (2006) 389–404.
[28] N. Savalli, A. Pantazis, T. Yusifov, D. Sigg, R. Olcese, The contribution of RCK domains to human BK channel allosteric activation, J. Biol. Chem. 287 (2012) 21741–21750.
[29] F.T. Horrigan, R.W. Aldrich, Coupling between voltage sensor activation, Ca2 + binding and channel opening in large conductance (BK) potassium channels, J. Gen. Physiol. 120 (2002) 267–305.
[30] D.H. Cox, J. Cui, R.W. Aldrich, Allosteric gating of a large conductance Ca-activated K+ channel, J. Gen. Physiol. 110 (1997) 257–281.
[31] J. Cui, R.W. Aldrich, Allosteric linkage between voltage and Ca(2 +)-dependent activation of BK-type mslo1 K(+) channels, Biochemistry 39 (2000) 15612–15619.
[32] D.H. Cox, R.W. Aldrich, Role of the beta1 subunit in large-conductance Ca(2 +)-activated K(+) channel gating energetics. Mechanisms of enhanced Ca(2 +) sensitivity, J. Gen. Physiol. 116 (2000) 411–432.
[33] **L. Bao, C. Kaldany, E.C. Holmstrand, D.H. Cox, Mapping the BKCa channel's 'Ca2+ bowl': side-chains essential for Ca2+ sensing., J. Gen. Physiol. 123 (2004) 475–489,** http://dx.doi.org/10.1085/jgp.200409052.

frontiers in Molecular Neuroscience

REVIEW
published: 30 July 2018
doi: 10.3389/fnmol.2018.00258

Physiological Roles and Therapeutic Potential of Ca^{2+} Activated Potassium Channels in the Nervous System

*Aravind S. Kshatri[1,2], Alberto Gonzalez-Hernandez[1,2] and Teresa Giraldez[1,2]**

[1] Department of Basic Medical Sciences, Medical School, Universidad de La Laguna, Tenerife, Spain, [2] Instituto de Tecnologías Biomédicas, Universidad de La Laguna, Tenerife, Spain

Within the potassium ion channel family, calcium activated potassium (K_{Ca}) channels are unique in their ability to couple intracellular Ca^{2+} signals to membrane potential variations. K_{Ca} channels are diversely distributed throughout the central nervous system and play fundamental roles ranging from regulating neuronal excitability to controlling neurotransmitter release. The physiological versatility of K_{Ca} channels is enhanced by alternative splicing and co-assembly with auxiliary subunits, leading to fundamental differences in distribution, subunit composition and pharmacological profiles. Thus, understanding specific K_{Ca} channels' mechanisms in neuronal function is challenging. Based on their single channel conductance, K_{Ca} channels are divided into three subtypes: small (SK, 4–14 pS), intermediate (IK, 32–39 pS) and big potassium (BK, 200–300 pS) channels. This review describes the biophysical characteristics of these K_{Ca} channels, as well as their physiological roles and pathological implications. In addition, we also discuss the current pharmacological strategies and challenges to target K_{Ca} channels for the treatment of various neurological and psychiatric disorders.

Keywords: SK channels, IK channels, BK channels, modulators, drug discovery, nervous system, neurological disease

OPEN ACCESS

Edited by:
Flavio Lasagna
Centre National de la Recherche Scientifique (CNRS), France

Reviewed by:
Ramon Latorre,
Universidad de Valparaíso, Chile
James S. Trimmer,
University of California, Davis, United States

****Correspondence:***
Teresa Giraldez
giraldez@ull.edu.es

Received: *04 May 2018*
Accepted: *06 July 2018*
Published: *30 July 2018*

Citation:
Kshatri AS, Gonzalez-Hernandez A and Giraldez T (2018) Physiological Roles and Therapeutic Potential of Ca^{2+} Activated Potassium Channels in the Nervous System. Front. Mol. Neurosci. 11:258. doi: 10.3389/fnmol.2018.00258

INTRODUCTION

Ca^{2+}-activated potassium channels (K_{Ca} channels) constitute a heterogeneous family of ion channels with variable biophysical and pharmacological properties. These channels share a common functional role by coupling the increase in intracellular Ca^{2+} concentration to hyperpolarization of the membrane potential. This intrinsic feature allows K_{Ca} channels to play key roles in controlling cellular excitability and maintaining K^+ homeostasis and cell volume in non-excitable cells. According to their single-channel conductances, K_{Ca} channels are divided into three main subfamilies: SK (small conductance; ~4–14 pS), IK (intermediate conductance; ~32–39 pS) and BK (big conductance; ~200–300 pS) channels. K_{Ca} channels are expressed in the plasma membrane as tetramers of α subunits. The gene encoding the α subunit (*slo; KCNMA1*) of BK channels (KCa1.1; slo1) was cloned in the early 1990s from *Drosophila* (Atkinson et al., 1991; Adelman et al., 1992) and mice (Butler et al., 1993). SKα subunits are products of the *KCNN1* ($K_{Ca}2.1$; SK1), *KCNN2* ($K_{Ca}2.2$; SK2) and *KCNN3* ($K_{Ca}2.3$; SK3) genes (Köhler et al., 1996), whereas IKα1 ($K_{Ca}3.1$; IK1; SK4) are encoded by the *KCNN4* gene (Ishii et al., 1997b;

Joiner et al., 1997). Phylogenetic analysis reveals that K_{Ca} channels belong to two well defined groups (Wei et al., 2005), a division that is paralleled by biophysical properties regarding voltage dependence or the Ca^{2+} sensitivity and regulatory mechanisms.

The first group comprises SK and IK channels. As shown in **Figure 1A**, α subunits of these channels consist on six transmembrane helices (S1–S6; the pore region is formed by helices S5 and S6) and cytosolic N- and C-terminal domains. One of their biophysical characteristics is that their function is independent of membrane voltage (Hirschberg et al., 1999). These channels are activated by low intracellular Ca^{2+} concentrations (≈ 0.5 μM) through a mechanism consisting on the existence of a calmodulin (CaM) binding-domain (CaMBD) within the channel's protein (Fanger et al., 1999; Adelman, 2016). The C-lobe region of CaM is associated to the CaMBD domains following a 1:1 stoichiometry, in a Ca^{2+}-independent manner (Lee and MacKinnon, 2018) (**Figure 1B**). Binding of Ca^{2+} to the N-lobes of CaM forces the CaM-CaMBD monomers to arrange structurally into a "dimer of dimers"

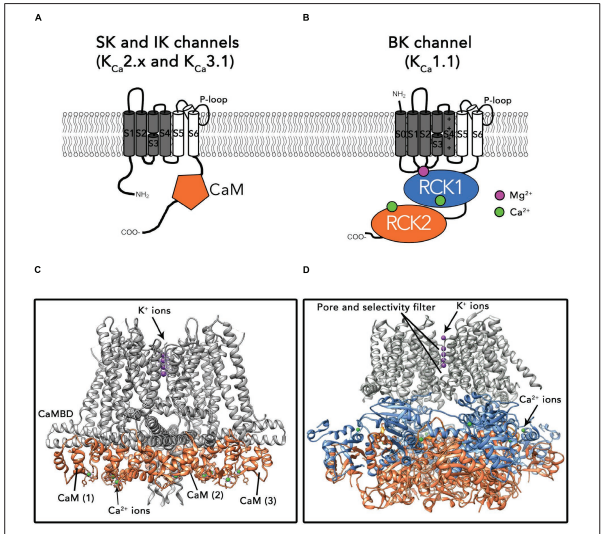

FIGURE 1 | Topology and structures of SK/IK and BK channels. **(A)** Schematic protein topology of one SKα-subunit including the CaM bound to the CaMBD (represented as an orange hexagon). **(B)** Full-length structure of the Ca^{2+}–CaM bound IK channel (PDB: 6CNN). The CaM N-lobe binds Ca^{2+} ions after association of CaM to the SK channel C-lobe. **(C)** Schematic topology of one BKα-subunit. Binding sites for divalent cations are located in the cytosolic C-terminal region of the channel. Each α subunit contains two high affinity Ca^{2+} binding sites (represented as green circles) and one low affinity Ca^{2+} and Mg^{2+} binding site, formed by residues from RCK1, S0–S1 and S2–S3 intracellular loops (purple circle). **(D)** Ca^{2+}-bound BKα homotetramer full-length structure from *Aplysia californica* (PDB: 5TJ6).

conformation, pulling the bundle-crossed helices of the pore to open the channel (Schumacher et al., 2001; Lee and MacKinnon, 2018).

BK channels belong to the second group in the K_{Ca} family (for a recent review, see Latorre et al., 2017). The topology of BK α subunits differs from the SK/IK group in the existence of an additional transmembrane helix S0 which drives the N-terminus to the extracellular side of the plasma membrane (**Figure 1C**). The large cytosolic C-terminal region of these channels is composed of two non-identical "regulator for conductance of potassium" domains (RCK1 and RCK2), each one containing a high affinity Ca^{2+} binding site (K_d = 0.8–11 μM; (Schreiber et al., 1999; Xia et al., 2002; Sweet and Cox, 2009). In the tetramer, four RCK1-RCK2 tandems form a structure known as the "gating ring" (Wu et al., 2010; Yuan et al., 2011; Hite et al., 2017; Tao et al., 2017) (**Figure 1D**). An additional regulatory site located at the interface between the gating ring and transmembrane region exhibits millimolar affinity for divalent cations such as Mg^{2+} (**Figure 1D**) (Shi et al., 2002; Xia et al., 2002; Yang et al., 2008). In contrast to SK and IK channels, BK are allosterically activated by both changes in the membrane voltage and intracellular Ca^{2+} (Horrigan and Aldrich, 2002). Similarly to other voltage-gated ion channels, the membrane voltage is sensed by charged amino acids within segments S2, S3, and S4 in the transmembrane region (Diaz et al., 1998; Ma et al., 2006; Lee and Cui, 2010; Tao et al., 2017). In contrast to SK and IK channels, Ca^{2+} directly activates BK channels by binding to the specific Ca^{2+} binding sites in the gating ring region, without involving CaM. Binding of Ca^{2+} results on structural rearrangements of the gating ring region, ultimately leading to pore opening (Yusifov et al., 2008, 2010; Lee and Cui, 2010; Javaherian et al., 2011; Yuan et al., 2011; Savalli et al., 2012; Hoshi et al., 2013). It has been proposed that the interaction of the gating ring with the voltage-sensing region of the channel plays an important role in this process (Hite et al., 2017; but see also Zhou et al., 2017) Importantly, the biophysical properties of K_{Ca} channels such as the voltage and Ca^{2+} sensitivities as well as their pharmacological characteristics are greatly influenced by the co-assembly with auxiliary subunits (e.g., β_{1-4}, γ_{1-4}; see below).

Members of the two groups comprising the K_{Ca} channels family also differ in their structural features. Available crystal structures of the SK CaMBD region bound to CaM have contributed to advance our knowledge about the regulation of these channels by various effectors (Schumacher et al., 2001, 2004; Zhang et al., 2012a,b, 2013; Zhang M. et al., 2014; Nam et al., 2017). Until very recently, structural information about BK channels was the most extensive, including X-ray crystal structures of the isolated C-terminal region known as the "gating ring" (Wu et al., 2010; Yuan et al., 2011) as well as cryo-EM structures of the full-length channel obtained in the presence and absence of Ca^{2+} (Hite et al., 2017; Tao et al., 2017; see also Giraldez and Rothberg, 2017; Zhou et al., 2017) (**Figure 1D**). Exciting new results from the MacKinnon laboratory bring now to light the cryo-electron microscopy (cryo-EM) structures of a human IK-CaM complex in closed and activated states, unveiling unprecedented insights about their gating mechanism (Lee and MacKinnon, 2018) (**Figure 1B**).

The SK, IK, and BK subfamilies show distinct tissue distribution and pharmacology. SK channels are predominantly expressed in the nervous system and are typically inhibited by the bee venom apamin (Park, 1994; Stocker and Pedarzani, 2000). IK channels are mainly distributed in blood, epithelial cells and in some peripheral neurons and are sensitive to the antifungal drug clotrimazole (Gardos, 1958; Jensen et al., 1998). BK channels are the most diverse group of K_{Ca} channels. They are ubiquitously expressed and sensitive to iberiotoxin, charybdotoxin, and paxilline (Latorre et al., 2017). The diversity of K_{Ca} physiological roles is widened by the existence of numerous splicing variants (specially for BK and SK channels) in different tissues (Navaratnam et al., 1997; Shipston, 2001; Chen et al., 2005; Scholl et al., 2014), as well as their association with auxiliary subunits. In vertebrates, BK channels co-assemble with modulatory β (β_{1-4}) and γ (γ_{1-4}) subunits to modify the channel functional properties and pharmacology (Latorre et al., 2017). In addition, K_{Ca} channels in neurons are closely associated to Ca^{2+} sources such as voltage-gated Ca^{2+} channels (VGCC) (Marrion and Tavalin, 1998; Tonini et al., 2013; Rudolph and Thanawala, 2015; Vivas et al., 2017), transient receptor potential vanilloid (TRPV) channels (Wu et al., 2013; Feetham et al., 2015) and *N*-methyl-D-aspartate receptors (NMDAR) (Isaacson and Murphy, 2001; Ngo-Anh et al., 2005) allowing the precise regulation of membrane excitability and spike firing patterns.

Mutation of genes encoding K_{Ca} channels and subsequent loss- or gain-of-function of these channels has been directly linked to a wide range of human diseases (**Table 1**). Over the last two decades, numerous studies have contributed to decipher the potential role of K_{Ca} channels in these diseases at the molecular level, paving the way for novel therapies. However, despite our current understanding about tissue specific distribution, functional diversity and clinical impact of K_{Ca} channels, they still remain underexploited as targets for drug discovery. In this review, we summarize the most recent knowledge about K_{Ca} channels, focusing on their potential as therapeutic targets in the nervous system and analyzing the factors that could contribute to the difficulties to develop novel K_{Ca} channel modulators. Some excellent reviews in the last few years relate to individual members of the K_{Ca} family, or are centered on particular aspects of K_{Ca} physiopathology (Faber, 2009; Lam et al., 2013; Gueguinou et al., 2014; Contet et al., 2016; Sugunan et al., 2016). Here we initially describe the functional roles of K_{Ca} channels in the nervous system, including their protective roles. Subsequently, the pathologies associated to malfunction of these channels are detailed. Known activators and inhibitors of K_{Ca} channels are presented in the third section of the review, as they may constitute the molecular basis of potential therapeutic strategies to treat a wide range of neurological disorders. Finally, we discuss the possible reasons why little progress has been made toward development of such strategies despite intense research efforts in academia and industry.

TABLE 1 | Mutations in K_{Ca} channels that are associated in human diseases, their location in the channel protein, functional implications and related references.

Gene/ protein	Disease phenotype	Mutation/location in the protein	Functional effects	Reference
*KCNN3/ SK3	Idiopathic non-cirrhotic portal hypertension	V450L/intracellular loop between the S4 and S5 transmembrane segments	*De novo* mutation Functional effects currently unknown.	Koot et al., 2016
*KCNN3/ SK3	Schizophrenia	hSK3Δ *(L283fs287X* mutation)/N-terminal cytoplasmic region (deletion)	Suppresses SK currents Disrupts SK-NMDAR coupling	Miller et al., 2001; Soden et al., 2013
*KCNMB1/ BKβ1	Diastolic hypertension	E65K/Extracellular loop connecting β1 two transmembrane segments.	Gain-of-function mutation rendering enhanced Ca^{2+} sensitivity	Fernandez-Fernandez et al., 2004
*KCNMA1/ BKα	Generalized epilepsy and paroxysmal dyskinesia	D434G/RCK1 domain	Gain-of-function mutation leading to enhanced Ca^{2+} sensitivity	Du et al., 2005; Yang J. et al., 2010
*KCNMA1/ BKα	Epilepsy	N999S/RCK2 domain	De *novo* mutation Shifts the voltage dependence to more negative potentials without altering Ca^{2+} sensitivity	Li et al., 2018
*KCNMB3/ BKβ3	Idiopathic generalized epilepsy	Del A750/C-terminal region (truncation of 21 amino acids)	BK inactivation	Hu et al., 2003; Lorenz et al., 2007

This table includes other mutations not linked to neurological diseases that are not discussed in detail in the main text (indicated with asterisks).

NEURONAL EXPRESSION AND FUNCTIONAL ROLES OF K_{Ca} CHANNELS

K_{Ca} channels are expressed in neurons and other cell types in the central nervous system (CNS), where they are involved in a large variety of physiological functions. Due to the vast distribution of K_{Ca} channels and their pleiotropic roles in the CNS, functional studies have been performed in different neuronal types, developmental stages or animal species. It is important to take into account the diversity of these approaches when interpreting the results described in the present review.

Activation of SK channels regulates firing in pacemaker neurons of midbrain and cerebellum, which is critical for muscle coordination and movement (Wolfart and Roeper, 2002; Womack and Khodakhah, 2003). In many neurons, action potentials are followed by a medium-duration after-hyperpolarization (mAHP) that affects their intrinsic excitability (Adelman et al., 2012). In numerous neuron types, the mAHP underlying current (I_mAHP), which can last up to hundreds of milliseconds, is Ca^{2+}-dependent but voltage-insensitive and is blocked by apamin but not by BK channel blockers, suggesting the involvement of SK channels (Sah, 1996; Stocker et al., 1999; but see Gu et al., 2005). The three SK channel α subunits, SK1, SK2 and SK3 display characteristics similar to I_mAHP in heterologous expression systems but fail to fully reproduce the pharmacological and biophysical properties observed *in vivo* (Stocker et al., 1999). This conundrum may be explained by the existence of SK heteromultimeric channels, which have been also described in heterologous expression systems (Ishii et al., 1997a). The idea that SK channels can assemble either as homo- or heteromultimeric channels *in vivo* is supported by their expression pattern in brain, which is overlapping in many regions (Stocker and Pedarzani, 2000). Interestingly, recent evidence shows that SK channels preferentially form species-specific heteromultimers when expressed in HEK cells, by interaction of their C-terminal regions (Tuteja et al., 2010; Church et al., 2015). These authors also show the physiological relevance of SK heteromultimers in CA1 pyramidal neurons (Church et al., 2015) and cardiomyocytes (Tuteja et al., 2010), highlighting the need of further studies to address the implications of heteromeric SK channels in brain and heart.

A role of SK channels in dendritic spines of pyramidal neurons in hippocampus and amygdala has been postulated, where they may regulate the amplitude of excitatory postsynaptic potentials (EPSPs) (Faber et al., 2005; Ngo-Anh et al., 2005; Bloodgood and Sabatini, 2007). During EPSPs, activation of SK channels limits Ca^{2+} influx into the spines and dendrites, thus creating a negative feedback loop controlling EPSPs amplitude. In addition, this activation of SK channels may influence NMDAR receptor activation (via voltage-dependent Mg^{2+} block), consequently affecting synaptic plasticity (Ngo-Anh et al., 2005). In agreement with this, blockade of SK channels in pyramidal neurons from hippocampus (Stackman et al., 2002) and amygdala (Faber et al., 2005; Ngo-Anh et al., 2005) enhanced long-term potentiation (LTP), suggesting that dendritic SK channels may play an important role in memory and learning processes (Stackman et al., 2002).

IK channels are widely expressed throughout the body, excluding some excitable tissues such as cardiac muscle or skeletal muscle. IK channels regulate the membrane potential and Ca^{2+} signaling and are responsible of activation and proliferation of vascular smooth cells and lymphocytes (Toyama et al., 2008; Di et al., 2010; Yu et al., 2013). Immunohistochemical staining experiments indicate that human enteric, sensory and sympathetic neurons also express IK channels (Furness et al., 2004; Bahia et al., 2005; Mongan et al., 2005). In the CNS, IK channels are mainly localized in microglia and endothelial cells (Pedarzani and Stocker, 2008). Microglial IK channels participate in controlling several functions including respiratory burst, proliferation, migration as well as lipopolysaccharide mediated nitric oxide production (Kaushal et al., 2007; Nguyen et al., 2017).

Accumulating evidence indicates that IK channels are involved in the process of astrogliosis, which occurs in most forms of CNS insults (Bouhy et al., 2011; Chen et al., 2011; Yu et al., 2014). It has been proposed that, in addition to BK (see below), IK channels also contribute to neurovascular coupling in astrocytes (Longden et al., 2011).

In many neuron types including hippocampal CA1 and CA3 pyramidal cells, repetitive firing stimulus elicits a slow, long lasting hyperpolarization, which is referred to as slow AHP (sAHP) (Adelman et al., 2012). The development of sAHP prevents the generation of new action potentials, limiting hyperexcitation of neurons in response to a long lasting or repetitive stimulus. Several studies have suggested that both SK (Lima and Marrion, 2007) and Kv7 channels (Tzingounis and Nicoll, 2008; Tzingounis et al., 2010) may contribute to sAHP. However, this assertion is contradicted by other observations showing that blockers of those channels produce only a minor reduction of the sAHP current (I_sAHP), suggesting that other channels are involved (Womble and Moises, 1993; Power and Sah, 2008). Furthermore, genetic ablation of SK1, SK2 or SK3 does not affect sAHP in CA1 pyramidal neurons (Bond et al., 2004). Although IK channels have been suggested to underlay sAHP (King et al., 2015), a recent study ruled out this hypothesis based on the pharmacological properties of I_sAHP, which were unaltered in IK knockout mice (Wang K. et al., 2016). The molecular identity of the sAHP channels remains unknown.

BK channels are localized throughout the dendrites, axon, soma and synaptic terminals of neurons in different brain regions, including cortex and hippocampus (Knaus et al., 1996; Grunnet and Kaufmann, 2004; Wang et al., 2014), where they play key roles in action potential duration, firing frequency and neurotransmitter release (for a recent review, see Contet et al., 2016). It should be noted that depending on the subcellular location where they are expressed, BK channel isoforms may exhibit different biophysical and trafficking properties, determined by the subunit composition (assembly with auxiliary subunits) and alternative splicing (Contet et al., 2016). At the synaptic terminals, it has been proposed that tight spatial coupling between BK channels and VGCCs (Marrion and Tavalin, 1998) constitutes a molecular brake for neurotransmitter release, by the BK-mediated termination of action potentials (Bielefeldt and Jackson, 1993; Hu et al., 2001; Muller et al., 2007; Contet et al., 2016). In dendrites, this association is also relevant, contributing to regulation of the magnitude and duration of dendritic Ca^{2+} spikes to influence action potential output (Engbers et al., 2013; Indriati et al., 2013). BK channels have the ability to shape the action potential waveforms and influence the frequency of firing in different ways. Pharmacological or genetic deletion of BK channels can increase or decrease the evoked or spontaneous firing frequency (Bielefeldt and Jackson, 1993; Nelson et al., 2003; Gu et al., 2007). Many studies have shown that blockade of BK channels using TEA, charybdotoxin or paxilline slows action potential repolarization and reduces the magnitude of the fast-duration AHP (Adams et al., 1982; Storm, 1987; Sah and McLachlan, 1992; Zhang and McBain, 1995; Faber and Sah, 2002). In the suprachiasmatic nucleus, BK channels contribute to spontaneous firing rate related to normal circadian behavioral rhythm (Meredith et al., 2006; Whitt et al., 2016; Whitt et al., 2018). Genetic ablation of the BKβ4 subunit in neurons from the dentate gyrus (DG) augmented the fast AHP amplitude, sharpened the action potential and increased spike frequency (Brenner et al., 2005). These findings support the idea that BK channels are not strictly excitatory or inhibitory but can be dynamically regulated to control neuronal excitability (Contet et al., 2016). Regulatory mechanisms include coupling to accessory subunits (Brenner et al., 2005; Whitt et al., 2016) and different sources of intracellular Ca^{2+} (Wang B. et al., 2016; Whitt et al., 2018).

Expression of BK has been also reported in astrocytes (Seidel et al., 2011; Seifert et al., 2018), where they have been related to astrocytic function connecting neuronal signaling to CNS vasculature (Howarth, 2014). Many studies have highlighted the role of astrocytic processes (endfeet) in modulating the vascular response by dynamically controlling intracellular Ca^{2+} (Filosa et al., 2006; Takano et al., 2006; Girouard et al., 2010). It has been proposed that activation of BK channels by elevated Ca^{2+} in astrocytic endfeet leads to vasodilation by the release of K^+ into the perivascular space (Price et al., 2002; Filosa et al., 2006). Interestingly, another study demonstrated that this mechanism can also mediate vasoconstriction, leading the authors to propose that BK channels may produce dual vascular responses depending on the Ca^{2+} levels at the astrocytic endfoot (Girouard et al., 2010).

Neuroprotective Roles of K_{Ca} Channels

Dopamine (DA) neurons in the midbrain retrorubral field (RRF), substantia nigra *pars compacta* (SNc) and ventral tegmental area (VTA) influence the neurons in target areas due to their extensive axonal projections (Matsuda et al., 2009). Thus, DA neurons are involved in regulating essential processes such as fine motor control (Bernheimer et al., 1973) learning and memory (Matsumoto and Takada, 2013), cognitive processes (Nieoullon, 2002), response to stress (Ungless et al., 2010) and noxious stimuli (Brischoux et al., 2009). SK channels control the pattern of single spike firing of DA neurons both *in vivo* and *in vitro*, as demonstrated by the reduction in firing regularity observed after treating the cells with apamin (Waroux et al., 2005; Ji and Shepard, 2006). Some studies have postulated that SK channels may exert neuroprotective effects against progressive DA neuronal death (Dolga et al., 2014), by a proposed mechanism in which activation of SK channels in SNc neurons counteracts excitotoxicity associated to NMDAR overactivation (Dolga et al., 2014; Duda et al., 2016). Additionally, SK channels could directly regulate NAPDH oxidase function, thus hampering neuronal damage by preventing production of reactive oxygen species (ROS) in mitochondria (Fay et al., 2006; Dolga et al., 2014). In mouse CA1 pyramidal neurons, a protective role of SK2 channels has been described, based on the observation that direct activation of SK channels by 1-ethyl-2- benzimidazolinone (1-EBIO) significantly reduced neuronal death in a model of cerebral ischemia induced by cardiac arrest/cardiopulmonary

resuscitation. This finding points to activation of SK channels as a potential neuroprotective target in cerebral ischemia (Allen et al., 2011).

Accumulating evidence supports multifaceted functions of IK channels (Kaushal et al., 2007; Dolga and Culmsee, 2012). Specifically, IK channels have been related to microglia activation by modulating Ca^{2+} signaling, oxidative burst, proinflammatory cytokines production and microglia-mediated neuronal cell death (Kaushal et al., 2007). According to these proposed physiological roles, a recent study demonstrated that genetic ablation or *in vivo* pharmacological blockade of IK channels in the middle cerebral artery occlusion (MCAO) mouse model reduced the infarct area as well as improved neurological deficit by reducing microglia-associated neuronal death (Chen Y.J. et al., 2016).

A protective role of BK channels in the context of acute focal cerebral ischemia has been tested *in vivo* by performing MCAO in BK knockout mouse models, which showed higher post-ischemic mortality than their WT littermates (Liao et al., 2010). In this context, it was suggested that BK plays a neuroprotective role by counteracting NMDA-induced neurotoxicity, since genetic silencing or blockade of BK channels in organotypic hippocampal slice cultures (Liao et al., 2010) or cortico-striatal brain slice cultures (Katsuki et al., 2005) showed higher levels of NMDA-induced neuronal death when they were exposed to ischemic-like conditions.

K_{Ca} channels are also expressed at inner mitochondrial membranes (mitoK_{Ca}), where they have been suggested to be involved in neuroprotection by different mechanisms, some of which are still unknown (Bednarczyk, 2009). The activation of mitoSK channels in conditions of glutamate toxicity enhanced the mitochondrial resilience and reduced cell death in mouse hippocampal cell lines (Dolga et al., 2013; Honrath et al., 2017). Additionally, mitoBK channels were found to preserve neuronal cell viability by attenuating the overall ROSs production (Kulawiak et al., 2008; Skalska et al., 2009). In addition to these reports, several others have reviewed the importance of mitoK_{Ca} channels as potential targets for neuroprotection (Szewczyk et al., 2010; Balderas et al., 2015; Krabbendam et al., 2018).

ROLE OF K_{Ca} CHANNELS IN NEUROLOGICAL AND PSYCHIATRIC DISEASES

Concomitant with their physiological roles, alterations in K_{Ca} function lead to excitability disorders that are characterized by abnormal firing of neuronal networks. The advancement of genetic linkage analysis over the past decades significantly facilitated the identification of specific loci associated to disease, many of which include genes encoding K_{Ca} channels subunits (Cooper and Jan, 1999; see **Table 1**). The role of these channels in disease has been also addressed using pharmacological tools. In this section we review the proposed contribution of BK and SK channels to neurological diseases. It is worth noting that, to our knowledge, no human diseases have been described in the literature involving K_{Ca}3.1 (IK) channel mutations. Their potential as drug targets in neurodegenerative diseases and ischemic stroke is reviewed in latter sections referring to K_{Ca} modulators.

Role of SK Channels

Malfunction of SK channels has been related to epilepsy. In pilocarpine-treated epileptic rats, the expression and function of SK channels was significantly reduced (Oliveira et al., 2010). Using thalamic slices treated with bicuculline methiodide as an experimental model of absence epilepsy, Kleiman-Weiner et al. (2009) found that blockade of SK channels modulated epileptiform oscillations by reducing intrinsic excitability of reticular neurons with no effect on relay neurons, pointing to SK channels as potential therapeutical targets for this disease. The involvement of SK in epilepsy has been further studied by using different modulators (see following section in this review).

Schizophrenia is a progressive neurodegenerative disorder that is characterized by disintegration of processes involved in thinking and emotional responsiveness (Postmes et al., 2014), that has been linked to DA imbalance (Brisch et al., 2014). A spontaneous mutation of the SK3 channel gene (*L283fs287X*) resulting in the deletion of the protein N-terminal region was identified in human schizophrenia patients (Bowen et al., 2001) and the resulting altered channels (hSK3Δ) were found to dominantly suppress SK channel currents. (Miller et al., 2001). Selective expression of this SK3 mutant in mice DA neurons additionally reduced the coupling between the SK channels and NMDAR, leading to increased burst firing as well as amplification of DA release, ultimately impacting animal behavior (Soden et al., 2013). The results by Soden et al. (2013) additionally showed that functional deficits of SK channels can alter the balance between phasic and tonic DA signals, which are normally associated to the pathogenesis of schizophrenia (Grace, 1991).

Pathogenesis of Parkinson's disease (PD), which is associated to death of DA neurons in the SNc (Surmeier et al., 2010) has been also related to K^+ channels dysfunction, including SK channels (Wang et al., 2008; Chen et al., 2018). This hypothesis is consistent with the observed roles of SK channels as regulators of dopaminergic neurotransmission in the SNc, protecting DA neurons from excitotoxic death (as reviewed in the previous section; see also Dolga et al., 2014). However, the role of SK channels in the etiology of PD remains elusive due to contradictory evidence. Some reports showed that activation of SK channels by NS309 in human DA neurons inhibited spontaneous firing, enhancing mAHP (Ji and Shepard, 2006), and reducing neurotoxicity (Dolga et al., 2014). These results suggest that increasing SK channel activity could boost or at least preserve levels of DA synthesis, which would in turn mitigate the long-term motor symptoms of PD. On the other hand, several studies have provided evidence that blockade of SK channels by apamin improved the symptoms of PD *in vitro* and *in vivo* (Doo et al., 2010; Kim et al., 2011; Alvarez-Fischer et al., 2013). This idea was further strengthened by the fact that blocking SK channels restored minimal DA activity in the striatum, alleviating the non-motor symptoms induced by partial striatal DA lesions (Chen et al., 2014). A possible interpretation of these apparently contradictory results is that SK channel positive or negative

TABLE 2 | Functional roles of clinically available/potential modulators of K_{Ca} channels.

Target	Drug	Reported effects	Comments	References
SK	1-EBIO	-Positive effects on cerebral ischemia animal models -Reduces epileptiform activity in an acute model of epilepsy	-SK activator	Allen et al., 2011; Lappin et al., 2005; Anderson et al., 2006; Oliveira et al., 2010
	NS309	Positive effects on DA neurons function related to Parkinson's disease	-SK activator	Ji and Shepard, 2006; Dolga et al., 2014
	Chlorzoxazone	Improves motor-coordination and other symptoms of episodic ataxia type-2	-SK activator -FDA-approved treatment for spasticity	Alvina and Khodakhah, 2010
	Riluzole	-Positive effects in arthritic pain model -Improves ataxia-related symptoms in human patients	-SK activator -FDA-approved treatment for ALS	Filstorl et al., 2010; Thompson et al., 2015
	DCEBIO	Reduces recall of extinction memory in rats	SK activator	Criado-Marrero et al., 2014
	Apamin	-Improves Parkinson's disease symptoms *in vitro* and *in vivo* -Positive effects on various memory deficits and spatial learning	SK inhibitor	Deschaux et al., 1997; Inan et al., 2000; Stackman et al., 2002; Mpari et al., 2005; Doo et al., 2010; Yang E.J. et al., 2010; Kim et al., 2011; Alvarez-Fischer et al., 2013; Criado-Marrero et al., 2014
IK	TRAM-34	-Positive effects in AD, ischemic stroke and multiple sclerosis mouse models - Increases formalin-induced nociceptive behavior	IK inhibitor	Reich et al., 2005; Chen Y.J. et al., 2016; Yi et al., 2016; Lu et al., 2017
	Senicapoc	-Positive effects in sickled cell anemia disease (SAD)* -Reversed tactile allodynia in rats with peripheral nerve injury	-IK inhibitor -Phase 3 clinical trials for SAD -Phase 2 clinical trials for asthma	Wulff and Castle, 2010; Stasi et al., 2017
BK	Isoprimaric acid (ISO)	-Improves cognitive defects in AD animal models	-BK activator	Wang L. et al., 2015
	GoSlo	- Inhibits spontaneous contractions in both bladder and corpus cavernosum smooth muscle tissues.	-BK activator	Large et al., 2015; Hannigan et al., 2017
	Andoblast	Positive effects on asthma treatment	-BK activator -Currently in late stage of phase 3 clinical trials for asthma	Malerba et al., 2015
	BMS204352	-Positive effects on FXS animal models -Enhances short-term habituation -Positive effects on spontaneous hypertensive rats model*	-BK and Kv7 activator -Phase 3 clinical trials for treatment of acute ischemic stroke*	Jensen, 2002; Brown and Passmore, 2009; Hebert et al., 2014; Zaman et al., 2017; Carreno-Munoz et al., 2018
	Zonisamide	-Positive effects on a wide range of epilepsies and neuropsychiatric disorders	-BK activator, Na^+ and Ca^{2+} channel modulator -Antiepileptic drug used clinically	Biton, 2007; Huang et al., 2007
	Iberiotoxin (IbTX)	Beneficial effects in rheumatoid arthritis animal models	selective BK$\alpha\beta_{1-3}$ blocker	Tanner et al., 2018

This table includes additional information, not detailed in the main text, about K_{Ca} modulators reported in the literature to treat diverse pathological conditions.

modulators could be beneficial depending on the stage (early or late) of the disease.

Role of BK Channels in Neurological Diseases

BK malfunction has been related to seizures and epilepsy, although the role of these channels in this pathological condition seems to be complex. *KCNMA1* knockout mice did not show spontaneous seizures, suggesting that CNS excitability is unaffected and discarding a prominent role of BK hypoactivity in epileptogenesis (Sausbier et al., 2004). However, growing evidence associates BKα gain-of-function or loss-of-function to neuronal pro-excitatory or pro-inhibitory effects, which may depend on the cellular context (for recent reviews, see (N'Gouemo, 2014; Contet et al., 2016). A BKα gain-of-function mutation (D434G) showing larger macroscopic currents, increased intrinsic gating and Ca^{2+} sensitivity was associated with a human syndrome of generalized epilepsy and paroxysmal dyskinesia (Du et al., 2005). Studies addressed to characterizing the mechanism underlying the strong functional impact of this mutation have greatly contributed to a better understanding of the biophysics of BK channels. Since the D434 site is located in the vicinity of the RCK1 Ca^{2+} binding site of the BK channel, its alteration was found to affect the allosteric coupling between the Ca^{2+} binding and the opening of the channel (Yang J. et al., 2010). Enhanced neuronal BK channel

activity as a result of the D434G mutation would increase the fAHP, resulting in faster recovery of sodium channels from inactivation, enabling neuronal firing at higher frequency and ultimately leading to increased neuronal excitability and seizures (Du et al., 2005; Diez-Sampedro et al., 2006; Wang et al., 2009; Yang J. et al., 2010). In a recent study, Li et al. (2018) identified a *de novo* mutation in the BKα gene (N995S) associated with epilepsy but not with paroxysmal dyskinesia. In contrast to the D434G mutant, the N995S gain-of-function variant shows alterations of the channel's sensitivity to voltage, but not to Ca^{2+} (Li et al., 2018). This notion that hyperactivity of BK channels is related to hyperexcitability and seizures is further supported by their implication in pathogenesis of alcohol withdrawal seizures (Ghezzi et al., 2014). Furthermore, blockade of BK has been shown to reduce neuronal hyperexcitability in animal models of epilepsy and seizures, but does not present anticonvulsant effects in animals with no previous seizure episodes (Jin et al., 2000; Sheehan et al., 2009). BK pro-excitatory or pro-inhibitory effects can be additionally determined and modulated by association to regulatory subunits. A recent study by Whitmire et al. (2017) showed that β_4 expression in hippocampal DG granule neurons is downregulated following pilocarpine-induced seizures, leading to gain-of-function BK and increased excitability. This result is consistent with previously observed effects in β_4 knockout mice (Wang et al., 2009; Whitmire et al., 2017). Alteration of the $BK\beta_3$ regulatory subunit as a consequence of a single base pair deletion (delA750) in the *KCNMB3* gene has also been associated to idiopathic generalized epilepsy in humans (Lorenz et al., 2007). This variant confers loss-of-function characteristics to BKα in heterologous expression systems by enhancing inactivation (Hu et al., 2003).

Two independent genome-wide association studies reported that single nucleotide polymorphisms in the *KCNMA1* gene encoding the BKα subunit (Beecham et al., 2009) and in the *KCNMAB2* gene (regulatory subunit $BK\beta_2$) (Beecham et al., 2014) are strongly linked to the pathophysiology of Alzheimer's disease (AD). Intracellular application of amyloid β peptide (*β*) in neocortical pyramidal neurons from rats and mice increased neuronal excitability by reducing function of BK channels (Yamamoto et al., 2011). In AD and depression mice models, transcranial magnetic stimulation (TMS) reduced the depression-like behavior by a proposed mechanism in which the activation of BK channels by TMS would enhance hippocampal LTP and inhibit cortical excitability (Sun et al., 2011; Wang F. et al., 2015). Interestingly, TMS was found to improve cognitive functions in human AD patients (Cotelli et al., 2006; Ahmed et al., 2012).

BK malfunction has been also related to Fragile X syndrome (FXS), a monogenic form of intellectual disability and autism, associated to transcriptional silencing of the *Fmr1* gene encoding Fragile X mental retardation protein (FMRP) (Verkerk et al., 1991). Recent evidence has shown that FMRP regulates neurotransmitter release in CA3 neurons by directly interacting with BKβ4 subunits (Deng et al., 2013). Consistent with this hypothesis, Hebert et al. (2014) restored the FXS behavioral deficits in Fmr1 knockout mice by treating the animals with selective BK channel openers (see below). These results support the idea that BK channels may be potential therapeutic targets for FXS (Brager and Johnston, 2014; Contractor et al., 2015).

Habituation is a form of learning in which the behavioral response to a stimulus decreases following repeated exposure to the stimulus (Rankin et al., 2009). Habituation to the acoustic startle response is impaired in many psychiatric disorders including schizophrenia and autism (Braff et al., 1992; Ornitz et al., 1993). BK channels have been implicated in habituation by controlling synaptic transmission (Typlt et al., 2013). Recently, it has been shown that activation of BK channels and their subsequent phosphorylation are essential for synaptic depression underlying habituation (Zaman et al., 2017).

REGULATION OF K_{Ca} CHANNELS AND IMPLICATIONS FOR THERAPEUTIC APPROACHES

As described in the previous sections, alterations in K_{Ca} channels are associated to several genetically linked and acquired diseases. In this section we review the use of various K_{Ca} modulators oriented toward disease treatment (summarized in **Table 2**), including some pharmacological considerations. The current state-of-the-art knowledge on the potential of K_{Ca} channels as therapeutic targets is summarized in **Figure 2** by representing as a weighing scale the beneficial effects resulting from either activation (left side) or blockade (right side) of each K_{Ca} subtype. Interestingly, SK and BK channels' balance is tipped toward the activation side, which seems to be more beneficial than blockade. Conversely, for IK channels blockade is more favorable than activation.

Modulators of SK Channels

Several modulators of SK function have been identified as the basis for potential treatment of neurological diseases. Chlorzoxazone (CZX) is a SK channel activator, which has been approved by the U.S. Food and Drug Administration (FDA) as a muscle relaxant to treat spasticity (Losin and McKean, 1966). In addition, it has been proposed to be a viable pharmacotherapeutic approach for episodic ataxia type-2 (EA2) treatment. Oral administration of CZX in an EA2 mouse model improved motor coordination and reduced the severity, frequency and duration of dyskinesia episodes with no side effects, by a proposed mechanism of restoring SK channels function (Alvina and Khodakhah, 2010).

Riluzole is the first FDA-approved treatment for amyotrophic lateral sclerosis (ALS) (Miller et al., 2012). Although the molecular target of riluzole remains elusive, many studies have proposed that it works by modulating SK channels (Dimitriadi et al., 2013; Lam et al., 2013). In spinal muscular atrophy animal models, treatment with riluzole ameliorated disease-related loss-of-function defects by acting on SK channels (Dimitriadi et al., 2013). A recent study demonstrated that riluzole inhibits supraspinally organized pain behavior in a rat model of arthritic pain by activating SK channels (Thompson et al., 2015). Beneficial effects of riluzole have also been reported for the treatment of spinocerebellar ataxia type 2 (SCA2), a disease involving

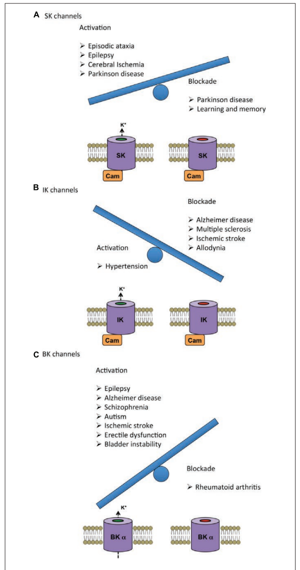

FIGURE 2 | Therapeutic benefits of either activation (left) or blockade (right) of K_{Ca} channels represented as a weighing scale. The heavier balance indicates the modulation (activation or blockade) that has been reported advantageous in a larger number of diseases. **(A,C)** In the case of SK and BK channels, activation shows more beneficial effects than inhibition. **(B)** For IK channels, pharmacological blockade has proven to be more advantageous than activation. For further information about the specific effects, see Tables and main text.

irregular firing and eventual neuronal death of Purkinje cells (PC) (Kasumu and Bezprozvanny, 2012). Administration of riluzole in patients improved ataxia-related symptoms (Ristori et al., 2010). This result was paralleled in a SCA2 transgenic mouse model, in which treatment with the SK selective activator NS13001 alleviated the symptoms of the disease (Kasumu et al., 2012). The mechanism underlying the effect of riluzole seems to reside in the activation of SK2 channels predominant in PC (Durr, 2010), which has been implicated in regulation of tonic firing (Ito, 2002; Walter et al., 2006). Consistently with this hypothesis, Walter et al. (2006) observed an improvement in motor coordination as well as restored PC firing regularity after treatment of an ataxia mouse model with SK channel modulators.

Selective activation of SK channels could be an effective therapy in some epileptic conditions. Potentiation of SK channels using ethylbenzimidazolinone (EBIO) was shown to inhibit epileptiform bursting in rat hippocampal CA3 neurons (Lappin et al., 2005). Additionally, this activator also reduced seizure incidence following maximal electroshock and increased the threshold to pentylenetetrazole-induced seizures in mice (Anderson et al., 2006).

In vivo infusion of SK activator 5,6-Dichloro-1-ethyl-1,3-dihydro-2*H*-benzimidazol-2-one (DCEBIO) in rats reduced recall of extinction memory, leading the authors to propose SK as a therapeutic target in anxiety disorders (Criado-Marrero et al., 2014). However, this result also suggests that the effect of SK activators on learning and memory should be taken into account in potential therapies.

The use of SK channel blockers has been also explored for disease treatment. Initial studies showed that SK blockers are not neuroprotective and might detrimentally accelerate neurodegeneration (Mourre et al., 1997). However, administration of apamin in rats and mice accelerated spatial learning (Deschaux et al., 1997; Stackman et al., 2002), promoted object recognition memory (Mpari et al., 2005) and facilitated the recall of extinction memory (Criado-Marrero et al., 2014). Additionally, apamin also mitigated the memory deficits associated to scopolamine- or electroconvulsive shock-induced amnesia (Inan et al., 2000). In summary, SK activators and blockers seem to be involved in distinct beneficial effects that would need to be balanced in order to design specific therapies.

Modulators of IK Channels

Consistent with the physiological roles of IK channels described in previous sections of this review, the selective inhibitor TRAM-34 (1-[(2- chlorophenyl)diphenylmethyl]-1*H*-pyrazole) decreased astrogliosis and microglial activation and attenuated memory loss in an AD mouse model (Yi et al., 2016). Furthermore, reduced microglia activation after blocking IK channels in an ischemic stroke mouse model has also been documented, which resulted in reduced infarction size and improved neurological deficit (Chen Y.J. et al., 2016). Additionally, application of TRAM-34 alleviated the symptoms of experimental autoimmune encephalomyelitis, a murine model of multiple sclerosis (Reich et al., 2005). Together, these data suggest that pharmacological blockade or genetic deletion of IK channels may represent a therapeutic target for various neurodegenerative disorders and ischemic stroke. Nonetheless, it is important to point out that although pharmacological blockade of IK channels appeared to be safe and well tolerated in animal models and humans, the genetic deletion induced an increase in blood pressure (Si et al., 2006). On the other hand, no study has yet reported increased blood pressure with IK channel

blockers including treatment of mice with TRAM-34 (Toyama et al., 2008) or human volunteers taking Senicapoc (Ataga et al., 2008). Finally, recent evidence suggests that IK inhibitors should be used with caution since they may also increase tonic pain in certain clinical conditions. A recent study demonstrated that pharmacological inhibition of IK channels using TRAM-34 in mice increased formalin-induced nociceptive behavior (Liu et al., 2017). Conversely, another study showed that blocking IK channels with Senicapoc reversed tactile allodynia in rats with peripheral nerve injury (Staal et al., 2017).

Modulators of BK Channels

Zonisamide is an antiepileptic drug used clinically as adjunctive therapy in refractory partial-onset seizures that has also shown beneficial effects in a wide range of epilepsies and neuropsychiatric disorders (Biton, 2007). In addition to inhibiting neuronal Na^+ and Ca^{2+} ion channels, Huang et al. showed that zonisamide activated BK channels in a hippocampal neuron-derived cell line, suggesting that the effects of zonisamide may be mediated, at least partly, by modulation of these channels (Huang et al., 2007).

A recent study suggests that BK channel activators could have therapeutic potential for cognitive defects in AD patients. Chronic application of the BK channel activator isoprimaric acid (ISO) enhanced non-spatial memory in AD mice, restoring the basic synaptic transmission and LTP at the hippocampal CA1 synapses, which were elevated and suppressed respectively in the disease model (Wang L. et al., 2015). Interestingly, ISO treatment not only enhanced BK channel activity but also reduced the Aβ fraction suggesting that a two-way relationship exists between BK channels and the Aβ plaque (Wang L. et al., 2015).

Treatment of *FMR1* knockout mice, an animal model of FXS, with the selective BK channel opener BMS-204352 reversed the abnormal dendritic spine phenotype *in vitro*. Additionally, direct injection of the activator restored hippocampal glutamate homeostasis and corrected disturbances in social recognition and interaction, non-social anxiety and spatial memory (Hebert et al., 2014). In another study, BMS-204352 efficiently reversed the cortical hyperexcitability and increased acoustic startle seen in *FMR1* knockout mice (Carreno-Munoz et al., 2018), suggesting that this treatment could alleviate sensory hypersensitivity symptoms in FXS patients.

Finally, BK channel openers have been tested to restore impaired habituation associated to some psychiatric disorders. Systemic administration of BMS-204352 greatly attenuated synaptic depression in the sensorimotor neurons of the caudal pontine reticular nucleus in the brain stem, which was associated with enhanced short-term habituation (Zaman et al., 2017).

MOLECULAR STRATEGIES AND CURRENT CHALLENGES TO TARGET K_{Ca} CHANNELS IN DRUG DISCOVERY

Ion channels are expressed at distinct physiological niches in the human body where they mediate diverse functions. Although numerous drugs are available to modulate K^+ channels, currently no K_{Ca} modulators are clinically used. One potential reason for this comparative failure in the drug discovery process relates to the fact that the study of channel complexes in physiological conditions is challenging, due to their intricate functional mechanisms. For instance, the diversity of physiological roles fulfilled by BKα channels in neurons is greatly enhanced by coexpression with tissue specific auxiliary β subunits, which confer tissue- and subcellular-specific characteristics to the BK currents determining the action potential shape, firing rate and pharmacology (Jaffe et al., 2011; Wang et al., 2014; Whitt et al., 2016). This otherwise beautiful example of evolutionary complexity imposes an arduous task on the drug designing process, which must specifically target the various subunit compositions. Although some encouraging results may have been obtained in heterologous expression systems, quite often the potential compounds modulating K_{Ca} channels are less potent *in vivo*, leading to undesirable side effects. This section reviews some considerations about the existing technical approaches to test the efficiency and efficacy of potential modulators, as well as the use of other structural and genetic approaches to improve targeting of specific K_{Ca} channel subunits to particular tissues.

Electrophysiological testing of ion channel function on heterologous expression systems still remains the backbone for functional validation of potential modulators. However, the major downside of both conventional and automated electrophysiology is that throughput efficiency is limited and operational costs are high, so there is a significant need for the development of novel robust, affordable and effective high-throughput screening methods (Picones et al., 2016). Membrane potential-based drug assays constitute a robust method for assessing the K^+ channel response to numerous drug candidates, although they seem to be subject to a large number of false positives (Solly et al., 2008). Ion flux assays are useful tools for screening compounds in drug discovery processes (Gill et al., 2003) including BK channel modulators (Jorgensen et al., 2008, 2013). This approach utilizes thallium or rubidium radioisotopes as K^+ ion substitutes providing sensitive, precise and reproducible results, yet with some limitations related to the radioactivity and toxicity of these ions. A novel and imaginative cell free assay is the liposome flux assay (LFA), where purified K^+ channels are reconstituted into lipid vesicles from which K^+ flux is recorded and optically monitored with a high signal-to-noise ratio. Su et al. (2016) demonstrated the robustness of this technique by screening a library of 300,000 compounds targetting K^+ ion channels, including BK.

Structural data is an essential tool supporting and complementing the discovery of ion channel-modulating drugs by providing information about drug–protein binding interactions. This knowledge is in turn necessary to improve the potency, efficacy and selectivity of the candidate drug compounds. Until very recently, available SK crystal structures were restricted to the Ca^{2+}-gating domains (CaM and CaMBD) (Schumacher et al., 2001, 2004; Li et al., 2009; Zhang et al., 2012a,b, 2013; Zhang M. et al., 2014; Nam et al., 2017), lacking information about the transmembrane domains, therefore making the structure-based drug discovery a complicated task. Based on available structural information, some positive

modulators of SK channels including PHU, 1-EBIO and NS309 were proposed to bind to the CaM/CaMBD interface (Strobaek et al., 2004; Zhang et al., 2012b, 2013; Morales et al., 2013; Brown et al., 2017; Nam et al., 2017). However, these conclusions are now challenged by the cryo-EM full-length IK-CaM structures only recently unveiled by the MacKinnon laboratory, which redefine the native interface between the CaM N-lobe and the C-terminal end of S6, showing a predominant role of the S4-S5 linker in Ca-CaM mediated channel gating (Lee and MacKinnon, 2018). Previous considerations should be revisited in light of these novel findings, which undoubtedly set an unprecedented ground for SK channels drug discovery. These new IK structures appear barely 1 year after the cryo-EM structures of the full-length BK channel in the open and closed states was obtained (Hite et al., 2017; Tao et al., 2017), revealing new and interesting insights in the channel structure–function relationships (Giraldez and Rothberg, 2017; Zhou et al., 2017; Kshatri et al., 2018). In this context, other techniques such as patch-clamp fluorometry (Zheng and Zagotta, 2003; Wulf and Pless, 2018) have proven to be useful tools to study conformational changes between subunits at the level of the gating ring during activation of functional BK channels (Giraldez et al., 2005; Miranda et al., 2013, 2016), and could also be extended to study other members of the K_{Ca} subfamily. Altogether, these approaches are revolutionizing our knowledge about how these ion channels can be selectively drug-targeted.

Developing specific rodent disease models based on characterized mutations has become a standard procedure to understanding their physiological relevance. In most cases, these models recapitulate the disease phenotypes and are useful as probing tools to characterize the channel's cellular and neuronal functions. Furthermore, they might constitute preclinical tools to attain a better understanding of the disease-causing mechanisms, consequently helping to build therapeutic strategies targeting the disease. The development of the CRISPR genome editing technique has facilitated generation of disease models by introducing loss- or gain-of-function mutations, allowing to study the effects of underlying genetic aberrations (Chen S. et al., 2016).

In addition, taking advantage of novel molecular techniques, new strategies have been developed to target the mutated genes *in vivo*. One example consists on the administration of antisense oligonucleotides to reduce the levels of mutant proteins that could be responsible for the neurodegenerative diseases. In an animal model of ALS caused by a mutation in the SOD1 protein, direct delivery of antisense oligonucleotides significantly slowed disease progression (Smith et al., 2006). In this context, the CRISPR technique undoubtedly constitutes a promising molecular approach to reverse the alterations in proteins and restore their physiological activity. Cheng et al. (2013) demonstrated that injection of CRISPR components into mouse zygotes efficiently activated several endogenous genes. The application of these techniques to target K_{Ca} channels and associated pathologies needs further exploration.

A strategy that has progressed toward clinical trials is gene-based therapy. The first and only phase I trial using this approach was performed on human patients with erectile dysfunction (ED). Plasmids encoding BK channels were injected directly into the penis corpus cavernosum of patients with ED, rendering positive encouraging results, suggesting that gene therapy represents a valuable treatment for ED (Melman et al., 2006, 2007) and could be considered for other K_{Ca}-related pathologies.

Finally, combination therapies that integrate tissue delivery of genes and drugs has been shown to be a viable approach enhancing drug specificity (Chen J. et al., 2016). This is especially relevant in the case of BK channels, which are expressed ubiquitously throughout the body, so systemic drug administration often results in off-target effects (Lappin et al., 2005).

CONCLUSION AND FUTURE PERSPECTIVES

K_{Ca} channels are relevant determinants of neuronal excitability and their dysfunction is implicated in many inherited and acquired neurological and psychiatric diseases, thus constituting appealing targets for pharmacological intervention. Over the last few years, the drug discovery field has significantly advanced to identify lead compounds for K_{Ca} channel modulators. Available therapeutic strategies to target these channels are challenging due to their diverse physiological roles and tissue distribution, so the design of modulators that recognize tissue-specific subunit combinations is of special relevance. Structural biology has dramatically advanced over the last decade to reveal many ion channel structures with atomic resolution, including the long-awaited structure of the full-length BK channel and of the human IK-CaM complex. Knowledge of genetic- and drug-induced regulation of K_{Ca} channels coupled to investigation of their structure–function relationships will facilitate the development of disease-specific treatment strategies.

AUTHOR CONTRIBUTIONS

AK, AG-H, and TG designed and wrote the manuscript.

FUNDING

The authors' work is supported by grants from the Spanish Ministry of Economy and Competitiveness (BFU2015-66490 and RYC-2012-11349 to TG; FPU15/02528 to AG-H) and the European Research Council (ERC) under the European Union's Horizon 2020 Research and Innovation Program (Grant Agreement 648936 to TG).

ACKNOWLEDGMENTS

We thank Ricardo Gomez-Garcia, David Bartolome-Martin, Diego Alvarez de la Rosa, and Tomas Gonzalez-Hernandez for useful comments on the manuscript.

REFERENCES

Adams, P. R., Constanti, A., Brown, D. A., and Clark, R. B. (1982). Intracellular Ca^{2+} activates a fast voltage-sensitive K^+ current in vertebrate sympathetic neurones. *Nature* 296, 746–749. doi: 10.1038/296746a0

Adelman, J. P. (2016). SK channels and calmodulin. *Channels (Austin)* 10, 1–6. doi: 10.1080/19336950.2015.1029868

Adelman, J. P., Maylie, J., and Sah, P. (2012). Small-conductance Ca2+-activated K^+ channels: form and function. *Annu. Rev. Physiol.* 74, 245–269. doi: 10.1146/annurev-physiol-020911-153336

Adelman, J. P., Shen, K. Z., Kavanaugh, M. P., Warren, R. A., Wu, Y. N., Lagrutta, A., et al. (1992). Calcium-activated potassium channels expressed from cloned complementary DNAs. *Neuron* 9, 209–216. doi: 10.1016/0896-6273(92)90160-F

Ahmed, M. A., Darwish, E. S., Khedr, E. M., El Serogy, Y. M., and Ali, A. M. (2012). Effects of low versus high frequencies of repetitive transcranial magnetic stimulation on cognitive function and cortical excitability in Alzheimer's dementia. *J. Neurol.* 259, 83–92. doi: 10.1007/s00415-011-6128-4

Allen, D., Nakayama, S., Kuroiwa, M., Nakano, T., Palmateer, J., Kosaka, Y., et al. (2011). SK2 channels are neuroprotective for ischemia-induced neuronal cell death. *J. Cereb. Blood Flow Metab.* 31, 2302–2312. doi: 10.1038/jcbfm.2011.90

Alvarez-Fischer, D., Noelker, C., Vulinovic, F., Grunewald, A., Chevarin, C., Klein, C., et al. (2013). Bee venom and its component apamin as neuroprotective agents in a Parkinson disease mouse model. *PLoS One* 8:e61700. doi: 10.1371/journal.pone.0061700

Alvina, K., and Khodakhah, K. (2010). KCa channels as therapeutic targets in episodic ataxia type-2. *J. Neurosci.* 30, 7249–7257. doi: 10.1523/JNEUROSCI.6341-09.2010

Anderson, N. J., Slough, S., and Watson, W. P. (2006). In vivo characterisation of the small-conductance KCa (SK) channel activator 1-ethyl-2-benzimidazolinone (1-EBIO) as a potential anticonvulsant. *Eur. J. Pharmacol.* 546, 48–53. doi: 10.1016/j.ejphar.2006.07.007

Ataga, K. I., Smith, W. R., De Castro, L. M., Swerdlow, P., Saunthararajah, Y., Castro, O., et al. (2008). Efficacy and safety of the gardos channel blocker, senicapoc (ICA-17043), in patients with sickle cell anemia. *Blood* 111, 3991–3997. doi: 10.1182/blood-2007-08-110098

Atkinson, N. S., Robertson, G. A., and Ganetzky, B. (1991). A component of calcium-activated potassium channels encoded by the *Drosophila* slo locus. *Science* 253, 551–555. doi: 10.1126/science.1857984

Bahia, P. K., Suzuki, R., Benton, D. C., Jowett, A. J., Chen, M. X., Trezise, D. J., et al. (2005). A functional role for small-conductance calcium-activated potassium channels in sensory pathways including nociceptive processes. *J. Neurosci.* 25, 3489–3498. doi: 10.1523/JNEUROSCI.0597-05.2005

Balderas, E., Zhang, J., Stefani, E., and Toro, L. (2015). Mitochondrial BKCa channel. *Front. Physiol.* 6:104. doi: 10.3389/fphys.2015.00104

Bednarczyk, P. (2009). Potassium channels in brain mitochondria. *Acta Biochim. Pol.* 56, 385–392.

Beecham, G. W., Hamilton, K., Naj, A. C., Martin, E. R., Huentelman, M., Myers, A. J., et al. (2014). Genome-wide association meta-analysis of neuropathologic features of Alzheimer's disease and related dementias. *PLoS Genet.* 10:e1004606. doi: 10.1371/journal.pgen.1004606

Beecham, G. W., Martin, E. R., Li, Y. J., Slifer, M. A., Gilbert, J. R., Haines, J. L., et al. (2009). Genome-wide association study implicates a chromosome 12 risk locus for late-onset Alzheimer disease. *Am. J. Hum. Genet.* 84, 35–43. doi: 10.1016/j.ajhg.2008.12.008

Bernheimer, H., Birkmayer, W., Hornykiewicz, O., Jellinger, K., and Seitelberger, F. (1973). Brain dopamine and the syndromes of Parkinson and Huntington. Clinical, morphological and neurochemical correlations. *J. Neurol. Sci.* 20, 415–455. doi: 10.1016/0022-510X(73)90175-5

Bielefeldt, K., and Jackson, M. B. (1993). A calcium-activated potassium channel causes frequency-dependent action-potential failures in a mammalian nerve terminal. *J. Neurophysiol.* 70, 284–298. doi: 10.1152/jn.1993.70.1.284

Biton, V. (2007). Clinical pharmacology and mechanism of action of zonisamide. *Clin. Neuropharmacol.* 30, 230–240.

Bloodgood, B. L., and Sabatini, B. L. (2007). Nonlinear regulation of unitary synaptic signals by CaV(2.3) voltage-sensitive calcium channels located in dendritic spines. *Neuron* 53, 249–260. doi: 10.1016/j.neuron.2006.12.017

Bond, C. T., Herson, P. S., Strassmaier, T., Hammond, R., Stackman, R., Maylie, J., et al. (2004). Small conductance Ca2+-activated K+ channel knock-out mice reveal the identity of calcium-dependent afterhyperpolarization currents. *J. Neurosci.* 24, 5301–5306. doi: 10.1523/JNEUROSCI.0182-04.2004

Bouhy, D., Ghasemlou, N., Lively, S., Redensek, A., Rathore, K. I., Schlichter, L. C., et al. (2011). Inhibition of the Ca(2)(+)-dependent K(+) channel, KCNN4/KCa3.1, improves tissue protection and locomotor recovery after spinal cord injury. *J. Neurosci.* 31, 16298–16308. doi: 10.1523/JNEUROSCI.0047-11.2011

Bowen, T., Williams, N., Norton, N., Spurlock, G., Wittekindt, O. H., Morris-Rosendahl, D. J., et al. (2001). Mutation screening of the KCNN3 gene reveals a rare frameshift mutation. *Mol. Psychiatry* 6, 259–260. doi: 10.1038/sj.mp.4000128

Braff, D. L., Grillon, C., and Geyer, M. A. (1992). Gating and habituation of the startle reflex in schizophrenic patients. *Arch. Gen. Psychiatry* 49, 206–215. doi: 10.1001/archpsyc.1992.01820030038005

Brager, D. H., and Johnston, D. (2014). Channelopathies and dendritic dysfunction in fragile X syndrome. *Brain Res. Bull.* 103, 11–17. doi: 10.1016/j.brainresbull.2014.01.002

Brenner, R., Chen, Q. H., Vilaythong, A., Toney, G. M., Noebels, J. L., and Aldrich, R. W. (2005). BK channel beta4 subunit reduces dentate gyrus excitability and protects against temporal lobe seizures. *Nat. Neurosci.* 8, 1752–1759. doi: 10.1038/nn1573

Brisch, R., Saniotis, A., Wolf, R., Bielau, H., Bernstein, H. G., Steiner, J., et al. (2014). The role of dopamine in schizophrenia from a neurobiological and evolutionary perspective: old fashioned, but still in vogue. *Front. Psychiatry* 5:47. doi: 10.3389/fpsyt.2014.00047

Brischoux, F., Chakraborty, S., Brierley, D. I., and Ungless, M. A. (2009). Phasic excitation of dopamine neurons in ventral VTA by noxious stimuli. *Proc. Natl. Acad. Sci. U.S.A.* 106, 4894–4899. doi: 10.1073/pnas.0811507106

Brown, B. M., Shim, H., Zhang, M., Yarov-Yarovoy, V., and Wulff, H. (2017). Structural Determinants for the Selectivity of the Positive KCa3.1 Gating Modulator 5-Methylnaphtho[2,1-d]oxazol-2-amine (SKA-121). *Mol. Pharmacol.* 92, 469–480. doi: 10.1124/mol.117.109421

Brown, D. A., and Passmore, G. M. (2009). Neural KCNQ (Kv7) channels. *Br. J. Pharmacol.* 156, 1185–1195. doi: 10.1111/j.1476-5381.2009.00111.x

Butler, A., Tsunoda, S., Mccobb, D. P., Wei, A., and Salkoff, L. (1993). mSlo, a complex mouse gene encoding "maxi" calcium-activated potassium channels. *Science* 261, 221–224. doi: 10.1126/science.7687074

Carreno-Munoz, M. I., Martins, F., Medrano, M. C., Aloisi, E., Pietropaolo, S., Dechaud, C., et al. (2018). Potential involvement of impaired BKCa channel function in sensory defensiveness and some behavioral disturbances induced by unfamiliar environment in a mouse model of Fragile × Syndrome. *Neuropsychopharmacology* 43, 492–502. doi: 10.1038/npp.2017.149

Chen, J., Guo, Z., Tian, H., and Chen, X. (2016). Production and clinical development of nanoparticles for gene delivery. *Mol. Ther. Methods Clin. Dev.* 3, 16023. doi: 10.1038/mtm.2016.23

Chen, L., Delthiel, T., Turle-Lorenzo, N., Liberge, M., Rosier, C., Watabe, I., et al. (2014). SK channel blockade reverses cognitive and motor deficits induced by nigrostriatal dopamine lesions in rats. *Int. J. Neuropsychopharmacol.* 17, 1295–1306. doi: 10.1017/S1461145714000236

Chen, L., Tian, L., Macdonald, S. H., Mcclafferty, H., Hammond, M. S., Huibant, J. M., et al. (2005). Functionally diverse complement of large conductance calcium- and voltage-activated potassium channel (BK) alpha-subunits generated from a single site of splicing. *J. Biol. Chem.* 280, 33599–33609. doi: 10.1074/jbc.M503383200

Chen, S., Sun, H., Miao, K., and Deng, C. X. (2016). CRISPR-Cas9: from genome editing to cancer research. *Int. J. Biol. Sci.* 12, 1427–1436. doi: 10.7150/ijbs.17421

Chen, X., Xue, B., Wang, J., Liu, H., Shi, L., and Xie, J. (2018). Potassium Channels: a potential therapeutic target for parkinson's disease. *Neurosci. Bull.* 34, 341–348. doi: 10.1007/s12264-017-0177-3

Chen, Y. J., Nguyen, H. M., Maezawa, I., Grossinger, E. M., Garing, A. L., Kohler, R., et al. (2016). The potassium channel KCa3.1 constitutes a pharmacological target for neuroinflammation associated with ischemia/reperfusion stroke. *J. Cereb. Blood Flow Metab.* 36, 2146–2161. doi: 10.1177/0271678X15611434

Chen, Y. J., Raman, G., Bodendiek, S., O'donnell, M. E., and Wulff, H. (2011). The KCa3.1 blocker TRAM-34 reduces infarction and neurological deficit in a rat model of ischemia/reperfusion stroke. *J. Cereb. Blood Flow Metab.* 31, 2363–2374. doi: 10.1038/jcbfm.2011.101

Cheng, A. W., Wang, H., Yang, H., Shi, L., Katz, Y., Theunissen, T. W., et al. (2013). Multiplexed activation of endogenous genes by CRISPR-on, an RNA-guided transcriptional activator system. *Cell Res.* 23, 1163–1171. doi: 10.1038/cr.2013.122

Church, T. W., Weatherall, K. L., Correa, S. A., Peole, D. L., Brown, J. T., and Marrion, N. V. (2015). Preferential assembly of heteromeric small conductance calcium-activated potassium channels. *Eur. J. Neurosci.* 41, 305–315. doi: 10.1111/ejn.12789

Contet, C., Goulding, S. P., Kuljis, D. A., and Barth, A. L. (2016). BK channels in the central nervous system. *Int. Rev. Neurobiol.* 128, 281–342. doi: 10.1016/bs.irn.2016.04.001

Contractor, A., Klyachko, V. A., and Portera-Cailliau, C. (2015). Altered neuronal and circuit excitability in Fragile × Syndrome. *Neuron* 87, 699–715. doi: 10.1016/j.neuron.2015.06.017

Cooper, E. C., and Jan, L. Y. (1999). Ion channel genes and human neurological disease: recent progress, prospects, and challenges. *Proc. Natl. Acad. Sci. U.S.A.* 96, 4759–4766. doi: 10.1073/pnas.96.9.4759

Cotelli, M., Manenti, R., Cappa, S. F., Geroldi, C., Zanetti, O., Rossini, P. M., et al. (2006). Effect of transcranial magnetic stimulation on action naming in patients with Alzheimer disease. *Arch. Neurol.* 63, 1602–1604. doi: 10.1001/archneur.63.11.1602

Criado-Marrero, M., Santini, E., and Porter, J. T. (2014). Modulating fear extinction memory by manipulating SK potassium channels in the infralimbic cortex. *Front. Behav. Neurosci.* 8:96. doi: 10.3389/fnbeh.2014.00096

Deng, P. Y., Rotman, Z., Blundon, J. A., Cho, Y., Cui, J., Cavalli, V., et al. (2013). FMRP regulates neurotransmitter release and synaptic information transmission by modulating action potential duration via BK channels. *Neuron* 77, 696–711. doi: 10.1016/j.neuron.2012.12.018

Deschaux, O., Bizot, J. C., and Goyffon, M. (1997). Apamin improves learning in an object recognition task in rats. *Neurosci. Lett.* 222, 159–162. doi: 10.1016/S0304-3940(97)13367-5

Di, L., Srivastava, S., Zhdanova, O., Ding, Y., Li, Z., Wulff, H., et al. (2010). Inhibition of the K^+ channel KCa3.1 ameliorates T cell-mediated colitis. *Proc. Natl. Acad. Sci. U.S.A.* 107, 1541–1546. doi: 10.1073/pnas.0910133107

Diaz, L., Meera, P., Amigo, J., Stefani, E., Alvarez, O., Toro, L., et al. (1998). Role of the S4 segment in a voltage-dependent calcium-sensitive potassium (hSlo) channel. *J. Biol. Chem.* 273, 32430–32436. doi: 10.1074/jbc.273.49.32430

Diez-Sampedro, A., Silverman, W. R., Bautista, J. F., and Richerson, G. B. (2006). Mechanism of increased open probability by a mutation of the BK channel. *J. Neurophysiol.* 96, 1507–1516. doi: 10.1152/jn.00461.2006

Dimitriadi, M., Kye, M. J., Kalloo, G., Yersak, J. M., Sahin, M., and Hart, A. C. (2013). The neuroprotective drug riluzole acts via small conductance Ca2+-activated K+ channels to ameliorate defects in spinal muscular atrophy models. *J. Neurosci.* 33, 6557–6562. doi: 10.1523/JNEUROSCI.1536-12.2013

Dolga, A. M., and Culmsee, C. (2012). Protective roles for potassium SK/K(Ca)2 channels in microglia and Neurons. *Front. Pharmacol.* 3:196. doi: 10.3389/fphar.2012.00196

Dolga, A. M., De Andrade, A., Meissner, L., Knaus, H. G., Hollerhage, M., Christophersen, P., et al. (2014). Subcellular expression and neuroprotective effects of SK channels in human dopaminergic neurons. *Cell Death Dis.* 5:e999. doi: 10.1038/cddis.2013.530

Dolga, A. M., Netter, M. F., Perocchi, F., Doti, N., Meissner, L., Tobaben, S., et al. (2013). Mitochondrial small conductance SK2 channels prevent glutamate-induced oxytosis and mitochondrial dysfunction. *J. Biol. Chem.* 288, 10792–10804. doi: 10.1074/jbc.M113.453522

Doo, A. R., Kim, S. T., Kim, S. N., Moon, W., Yin, C. S., Chae, Y., et al. (2010). Neuroprotective effects of bee venom pharmaceutical acupuncture in acute 1-methyl-4-phenyl-1,2,3,6-tetrahydropyridine-induced mouse model of Parkinson's disease. *Neurol. Res.* 32 (Suppl 1), 88–91. doi: 10.1179/016164109X125370627942 82

Du, W., Bautista, J. F., Yang, H., Diez-Sampedro, A., You, S. A., Wang, L., et al. (2005). Calcium-sensitive potassium channelopathy in human epilepsy and paroxysmal movement disorder. *Nat. Genet.* 37, 733–738. doi: 10.1038/ng1585

Duda, J., Potschke, C., and Liss, B. (2016). Converging roles of ion channels, calcium, metabolic stress, and activity pattern of Substantia nigra dopaminergic neurons in health and Parkinson's disease. *J. Neurochem.* 139 (Suppl 1), 156–178. doi: 10.1111/jnc.13572

Durr, A. (2010). Autosomal dominant cerebellar ataxias: polyglutamine expansions and beyond. *Lancet Neurol.* 9, 885–894. doi: 10.1016/S1474-4422(10)70183-6

Engbers, J. D., Anderson, D., Zamponi, G. W., and Turner, R. W. (2013). Signal processing by T-type calcium channel interactions in the cerebellum. *Front. Cell Neurosci.* 7:230. doi: 10.3389/fncel.2013.00230

Faber, E. S. (2009). Functions and modulation of neuronal SK channels. *Cell Biochem. Biophys.* 55, 127–139. doi: 10.1007/s12013-009-9062-7

Faber, E. S., and Sah, P. (2002). Physiological role of calcium-activated potassium currents in the rat lateral amygdala. *J. Neurosci.* 22, 1618–1628. doi: 10.1523/JNEUROSCI.22-05-01618.2002

Faber, E. S., Delaney, A. J., and Sah, P. (2005). SK channels regulate excitatory synaptic transmission and plasticity in the lateral amygdala. *Nat. Neurosci.* 8, 635–641. doi: 10.1038/nn1450

Fanger, C. M., Ghanshani, S., Logsdon, N. J., Rauer, H., Kalman, K., Zhou, J., et al. (1999). Calmodulin mediates calcium-dependent activation of the intermediate conductance KCa Channel, IKCa1. *J. Biol. Chem.* 274, 5746–5754. doi: 10.1074/jbc.274.9.5746

Fay, A. J., Qian, X., Jan, Y. N., and Jan, L. Y. (2006). SK channels mediate NADPH oxidase-independent reactive oxygen species production and apoptosis in granulocytes. *Proc. Natl. Acad. Sci. U.S.A.* 103, 17548–17553. doi: 10.1073/pnas.0607914103

Feetham, C. H., Nunn, N., Lewis, R., Dart, C., and Barrett-Jolley, R. (2015). TRPV4 and K(Ca) ion channels functionally couple as osmosensors in the paraventricular nucleus. *Br. J. Pharmacol.* 172, 1753–1768. doi: 10.1111/bph.13023

Fernandez-Fernandez, J. M., Tomas, M., Vazquez, E., Orio, P., Latorre, R., Senti, M., et al. (2004). Gain-of-function mutation in the KCNMB1 potassium channel subunit is associated with low prevalence of diastolic hypertension. *J. Clin. Invest.* 113, 1032–1039. doi: 10.1172/JCI200420347

Filosa, J. A., Bonev, A. D., Straub, S. V., Meredith, A. L., Wilkerson, M. K., Aldrich, R. W., et al. (2006). Local potassium signaling couples neuronal activity to vasodilation in the brain. *Nat. Neurosci.* 9, 1397–1403. doi: 10.1038/nn1779

Furness, J. B., Kearney, K., Robbins, H. L., Hunne, B., Selmer, I. S., Neylon, C. B., et al. (2004). Intermediate conductance potassium (IK) channels occur in human enteric neurons. *Auton. Neurosci.* 112, 93–97. doi: 10.1016/j.autneu.2004.02.003

Gardos, G. (1958). The function of calcium in the potassium permeability of human erythrocytes. *Biochim. Biophys. Acta* 30, 653–654. doi: 10.1016/0006-3002(58)90124-0

Ghezzi, A., Krishnan, H. R., and Atkinson, N. S. (2014). Susceptibility to ethanol withdrawal seizures is produced by BK channel gene expression. *Addict. Biol.* 19, 332–337. doi: 10.1111/j.1369-1600.2012.00465.x

Gill, S., Gill, R., Lee, S. S., Hesketh, J. C., Fedida, D., Rezazadeh, S., et al. (2003). Flux assays in high throughput screening of ion channels in drug discovery. *Assay Drug Dev. Technol.* 1, 709–717. doi: 10.1089/154065803771661066

Giraldez, T., and Rothberg, B. S. (2017). Understanding the conformational motions of RCK gating rings. *J. Gen. Physiol.* 149, 431–441. doi: 10.1085/jgp.201611726

Giraldez, T., Hughes, T. E., and Sigworth, F. J. (2005). Generation of functional fluorescent BK channels by random insertion of GFP variants. *J. Gen. Physiol.* 126, 429–438. doi: 10.1085/jgp.200509368

Girouard, H., Bonev, A. D., Hannah, R. M., Meredith, A., Aldrich, R. W., and Nelson, M. T. (2010). Astrocytic endfoot Ca2+ and BK channels determine both arteriolar dilation and constriction. *Proc. Natl. Acad. Sci. U.S.A.* 107, 3811–3816. doi: 10.1073/pnas.0914722107

Grace, A. A. (1991). Phasic versus tonic dopamine release and the modulation of dopamine system responsivity: a hypothesis for the etiology of schizophrenia. *Neuroscience* 41, 1–24. doi: 10.1016/0306-4522(91)90196-U

Grunnet, M., and Kaufmann, W. A. (2004). Coassembly of big conductance Ca2+ activated K+ channels and L-type voltage-gated Ca2+ channels in rat brain. *J. Biol. Chem.* 279, 36445–36453. doi: 10.1074/jbc.M404254200

Gu, N., Vervaeke, K., and Storm, J. F. (2007). BK potassium channels facilitate high-frequency firing and cause early spike frequency adaptation in rat CA1 hippocampal pyramidal cells. *J. Physiol.* 580, 859–882. doi: 10.1113/jphysiol.2006.126367

Krabbendam, I. E., Honrath, B., Culmsee, C., and Dolga, A. M. (2018). Mitochondrial Ca(2+)-activated K(+) channels and their role in cell life and death pathways. *Cell Calcium* 69, 101–111. doi: 10.1016/j.ceca.2017.07.005

Kshatri, A. S., Gonzalez-Hernandez, A. J., and Giraldez, T. (2018). Functional validation of Ca(2+)-binding residues from the crystal structure of the BK ion channel. *Biochim. Biophys. Acta* 1860, 943–952. doi: 10.1016/j.bbamem.2017.09.023

Kulawiak, B., Kudin, A. P., Szewczyk, A., and Kunz, W. S. (2008). BK channel openers inhibit ROS production of isolated rat brain mitochondria. *Exp. Neurol.* 212, 543–547. doi: 10.1016/j.expneurol.2008.05.004

Lam, J., Coleman, N., Garing, A. L., and Wulff, H. (2013). The therapeutic potential of small-conductance KCa2 channels in neurodegenerative and psychiatric diseases. *Expert Opin. Ther. Targets* 17, 1203–1220. doi: 10.1517/14728222.2013.823161

Lappin, S. C., Dale, T. J., Brown, J. T., Trezise, D. J., and Davies, C. H. (2005). Activation of SK channels inhibits epileptiform bursting in hippocampal CA3 neurons. *Brain Res.* 1065, 37–46. doi: 10.1016/j.brainres.2005.10.024

Large, R. J., Kshatri, A., Webb, T. I., Roy, S., Akande, A., Bradley, E., et al. (2015). Effects of the novel BK (KCa 1.1) channel opener GoSlo-SR-5-130 are dependent on the presence of BKbeta subunits. *Br. J. Pharmacol.* 172, 2544–2556. doi: 10.1111/bph.13085

Latorre, R., Castillo, K., Carrasquel-Ursulaez, W., Sepulveda, R. V., Gonzalez-Nilo, F., Gonzalez, C., et al. (2017). Molecular determinants of BK channel functional diversity and functioning. *Physiol. Rev.* 97, 39–87. doi: 10.1152/physrev.00001.2016

Lee, C., and MacKinnon, R. (2018). Activation mechanism of a human SK-calmodulin channel complex elucidated by cryo-EM structures. *Science* 360, 508–513. doi: 10.1126/science.aas9466

Lee, U. S., and Cui, J. (2010). BK channel activation: structural and functional insights. *Trends Neurosci.* 33, 415–423. doi: 10.1016/j.tins.2010.06.004

Li, W., Halling, D. B., Hall, A. W., and Aldrich, R. W. (2009). EF hands at the N-lobe of calmodulin are required for both SK channel gating and stable SK-calmodulin interaction. *J. Gen. Physiol.* 134, 281–293. doi: 10.1085/jgp.200910295

Li, X., Poschmann, S., Chen, Q., Fazeli, W., Oundjian, N. J., Snoeijen-Schouwenaars, F. M., et al. (2018). De novo BK channel variant causes epilepsy by affecting voltage gating but not Ca(2+) sensitivity. *Eur. J. Hum. Genet.* 26, 220–229. doi: 10.1038/s41431-017-0073-3

Liao, Y., Kristiansen, A. M., Oksvold, C. P., Tuynes, F. A., Gu, N., Runden-Pran, E., et al. (2010). Neuronal Ca2+-activated K+ channels limit brain infarction and promote survival. *PLoS One* 5:e15601. doi: 10.1371/journal.pone.0015601

Lima, P. A., and Marrion, N. V. (2007). Mechanisms underlying activation of the slow AHP in rat hippocampal neurons. *Brain Res.* 1150, 74–82. doi: 10.1016/j.brainres.2007.02.067

Longden, T. A., Dunn, K. M., Draheim, H. J., Nelson, M. T., Weston, A. H., and Edwards, G. (2011). Intermediate-conductance calcium-activated potassium channels participate in neurovascular coupling. *Br. J. Pharmacol.* 164, 922–933. doi: 10.1111/j.1476-5381.2011.1014 47.x

Lorenz, S., Heils, A., Kasper, J. M., and Sander, T. (2007). Allelic association of a truncation mutation of the KCNMB3 gene with idiopathic generalized epilepsy. *Am. J. Med. Genet. B Neuropsychiatr. Genet.* 144B, 10–13. doi: 10.1002/ajmg.b.30369

Losin, S., and McKean, C. M. (1966). Chlorzoxazone (paraflex) in the treatment of severe spasticity. *Dev. Med. Child Neurol.* 8, 768–769. doi: 10.1111/j.1469-8749.1966.tb01839.x

Lu, R., Flauaus, C., Kennel, L., Petersen, J., Drees, O., Kallenborn-Gerhardt, W., et al. (2017). KCa3.1 channels modulate the processing of noxious chemical stimuli in mice. *Neuropharmacology* 125, 386–395. doi: 10.1016/j.neuropharm.2017.08.021

Ma, Z., Lou, X. J., and Horrigan, F. T. (2006). Role of charged residues in the S1–S4 voltage sensor of BK channels. *J. Gen. Physiol.* 127, 309–328. doi: 10.1085/jgp.200509421

Malerba, M., Amato, D. M., Radaeli, A., Giacovelli, G., Rovati, L., Arshad, S. H., et al. (2015). Efficacy of andolast in mild to moderate asthma: a randomized, controlled, double-blind multicenter study (the andast trial). *Curr. Pharm. Des.* 21, 3835–3843. doi: 10.2174/1381612821666150407101614

Marrion, N. V., and Tavalin, S. J. (1998). Selective activation of Ca^{2+}-activated K^+ channels by co-localized Ca^{2+} channels in hippocampal neurons. *Nature* 395, 900–905. doi: 10.1038/27674

Matsuda, W., Furuta, T., Nakamura, K. C., Hioki, H., Fujiyama, F., Arai, R., et al. (2009). Single nigrostriatal dopaminergic neurons form widely spread and highly dense axonal arborizations in the neostriatum. *J. Neurosci.* 29, 444–453. doi: 10.1523/JNEUROSCI.4029-08.2009

Matsumoto, M., and Takada, M. (2013). Distinct representations of cognitive and motivational signals in midbrain dopamine neurons. *Neuron* 79, 1011–1024. doi: 10.1016/j.neuron.2013.07.002

Melman, A., Bar-Chama, N., Mccullough, A., Davies, K., and Christ, G. (2006). hMaxi-K gene transfer in males with erectile dysfunction: results of the first human trial. *Hum. Gene Ther.* 17, 1165–1176. doi: 10.1089/hum.2006.17.1165

Melman, A., Bar-Chama, N., Mccullough, A., Davies, K., and Christ, G. (2007). Plasmid-based gene transfer for treatment of erectile dysfunction and overactive bladder: results of a phase I trial. *ISR Med. Assoc. J.* 9, 143–146.

Meredith, A. L., Wiler, S. W., Miller, B. H., Takahashi, J. S., Fodor, A. A., Ruby, N. F., et al. (2006). BK calcium-activated potassium channels regulate circadian behavioral rhythms and pacemaker output. *Nat. Neurosci.* 9, 1041–1049. doi: 10.1038/nn1740

Miller, M. J., Rauer, H., Tomita, H., Rauer, H., Gargus, J. J., Gutman, G. A., et al. (2001). Nuclear localization and dominant-negative suppression by a mutant SKCa3 N-terminal channel fragment identified in a patient with schizophrenia. *J. Biol. Chem.* 276, 27753–27756. doi: 10.1074/jbc.C100221200

Miller, R. G., Mitchell, J. D., and Moore, D. H. (2012). Riluzole for amyotrophic lateral sclerosis (ALS)/motor neuron disease (MND). *Cochrane Database Syst. Rev.* 2:CD001447. doi: 10.1002/14651858.CD001447.pub3

Miranda, P., Contreras, J. E., Plested, A. J., Sigworth, F. J., Holmgren, M., and Giraldez, T. (2013). State-dependent FRET reports calcium- and voltage-dependent gating-ring motions in BK channels. *Proc. Natl. Acad. Sci. U.S.A.* 110, 5217–5222. doi: 10.1073/pnas.1219611110

Miranda, P., Giraldez, T., and Holmgren, M. (2016). Interactions of divalent cations with calcium binding sites of BK channels reveal independent motions within the gating ring. *Proc. Natl. Acad. Sci. U.S.A.* 113, 14055–14060. doi: 10.1073/pnas.1611415113

Mongan, L. C., Hill, M. J., Chen, M. X., Tate, S. N., Collins, S. D., Buckley, L., et al. (2005). The distribution of small and intermediate conductance calcium-activated potassium channels in the rat sensory nervous system. *Neuroscience* 131, 161–175. doi: 10.1016/j.neuroscience.2004.09.062

Morales, P., Garneau, L., Klein, H., Lavoie, M. F., Parent, L., and Sauve, R. (2013). Contribution of the KCa3.1 channel-calmodulin interactions to the regulation of the KCa3.1 gating process. *J. Gen. Physiol.* 142, 37–60. doi: 10.1085/jgp.201210933

Mourre, C., Fournier, C., and Soumireu-Mourat, B. (1997). Apamin, a blocker of the calcium-activated potassium channel, induces neurodegeneration of Purkinje cells exclusively. *Brain Res.* 778, 405–408. doi: 10.1016/S0006-8993(97)01165-7

Mpari, B., Regaya, I., Escoffier, G., and Mourre, C. (2005). Differential effects of two blockers of small conductance Ca2+-activated K+ channels, apamin and lei-Dab7, on learning and memory in rats. *J. Integr. Neurosci.* 4, 381–396. doi: 10.1142/S0219635205000884

Muller, A., Kukley, M., Uebachs, M., Beck, H., and Dietrich, D. (2007). Nanodomains of single Ca2+ channels contribute to action potential repolarization in cortical neurons. *J. Neurosci.* 27, 483–495. doi: 10.1523/JNEUROSCI.3816-06.2007

Nam, Y. W., Orfali, R., Liu, T., Yu, K., Cui, M., Wulff, H., et al. (2017). Structural insights into the potency of SK channel positive modulators. *Sci. Rep.* 7:7178. doi: 10.1038/s41598-017-16607-8

Navaratnam, D. S., Bell, T. J., Tu, T. D., Cohen, E. L., and Oberholtzer, J. C. (1997). Differential distribution of Ca2+ activated K+ channel splice variants among hair cells along the tonotopic axis of the chick cochlea. *Neuron* 19, 1077–1085. doi: 10.1016/S0896-6273(00)80398-0

Nelson, A. B., Krispel, C. M., Sekirnjak, C., and Du Lac, S. (2003). Long-lasting increases in intrinsic excitability triggered by inhibition. *Neuron* 40, 609–620. doi: 10.1016/S0896-6273(03)00641-X

Ngo-Anh, T. J., Bloodgood, B. L., Lin, M., Sabatini, B. L., Maylie, J., and Adelman, J. P. (2005). SK channels and NMDA receptors form a Ca2+-mediated feedback loop in dendritic spines. *Nat. Neurosci.* 8, 642–649. doi: 10.1038/nn1449

Gu, N., Vervaeke, K., Hu, H., and Storm, J. F. (2005). Kv7/KCNQ/M and HCN/h, but not KCa2/SK channels, contribute to the somatic medium after-hyperpolarization and excitability control in CA1 hippocampal pyramidal cells. *J. Physiol.* 566, 689–715. doi: 10.1113/jphysiol.2005.086835

Gueguinou, M., Chantome, A., Fromont, G., Bougnoux, P., Vandier, C., and Potier-Cartereau, M. (2014). KCa and Ca(2+) channels: the complex thought. *Biochim. Biophys. Acta* 1843, 2322–2333. doi: 10.1016/j.bbamcr.2014.02.019

Hannigan, K. I., Griffin, C. S., Large, R. J., Sergeant, G. P., Hollywood, M. A., Mchale, N. G., et al. (2017). The role of Ca(2+)-activated Cl(-) current in tone generation in the rabbit corpus cavernosum. *Am. J. Physiol. Cell Physiol.* 313, C475-C486. doi: 10.1152/ajpcell.00025.2017

Hebert, B., Pietropaolo, S., Meme, S., Laudier, B., Laugeray, A., Doisne, N., et al. (2014). Rescue of fragile X syndrome phenotypes in Fmr1 KO mice by a BKCa channel opener molecule. *Orphanet. J. Rare Dis.* 9, 124. doi: 10.1186/s13023-014-0124-6

Hirschberg, B., Maylie, J., Adelman, J. P., and Marrion, N. V. (1999). Gating Properties of single SK channels in hippocampal CA1 pyramidal neurons. *Biophys. J.* 77, 1905–1913. doi: 10.1016/S0006-3495(99)77032-3

Hite, R. K., Tao, X., and Mackinnon, R. (2017). Structural basis for gating the high-conductance Ca^{2+}-activated K^+ channel. *Nature* 541, 52–57. doi: 10.1038/nature20775

Honrath, B., Matschke, L., Meyer, T., Magerhans, L., Perocchi, F., Ganjam, G. K., et al. (2017). SK2 channels regulate mitochondrial respiration and mitochondrial Ca(2+) uptake. *Cell Death Differ.* 24, 761–773. doi: 10.1038/cdd.2017.2

Horrigan, F. T., and Aldrich, R. W. (2002). Coupling between voltage sensor activation, Ca^{2+} Binding and channel opening in large conductance (BK) potassium channels. *J. Gen. Physiol.* 120, 267–305. doi: 10.1085/jgp.20028605

Hoshi, T., Pantazis, A., and Olcese, R. (2013). Transduction of voltage and Ca^{2+} signals by Slo1 BK channels. *Physiology (Bethesda)* 28, 172–189. doi: 10.1152/physiol.00055.2012

Howarth, C. (2014). The contribution of astrocytes to the regulation of cerebral blood flow. *Front. Neurosci.* 8:103. doi: 10.3389/fnins.2014.00103

Hu, H., Shao, L. R., Chavoshy, S., Gu, N., Trieb, M., Behrens, R., et al. (2001). Presynaptic Ca^{2+}-activated K^+ channels in glutamatergic hippocampal terminals and their role in spike repolarization and regulation of transmitter release. *J. Neurosci.* 21, 9585–9597. doi: 10.1523/JNEUROSCI.21-24-09585.2001

Hu, S., Labuda, M. Z., Pandolfo, M., Goss, G. G., Mcdermid, H. E., and Ali, D. W. (2003). Variants of the KCNMB3 regulatory subunit of maxi BK channels affect channel inactivation. *Physiol. Genom.* 15, 191–198. doi: 10.1152/physiolgenomics.00110.2003

Huang, C. W., Huang, C. C., and Wu, S. N. (2007). Activation by zonisamide, a newer antiepileptic drug, of large-conductance calcium-activated potassium channel in differentiated hippocampal neuron-derived H19-7 cells. *J. Pharmacol. Exp. Ther.* 321, 98–106. doi: 10.1124/jpet.106.116954

Inan, S. Y., Aksu, F., and Baysal, F. (2000). The effects of some K(+) channel blockers on scopolamine- or electroconvulsive shock-induced amnesia in mice. *Eur. J. Pharmacol.* 407, 159–164. doi: 10.1016/S0014-2999(00)00736-6

Indriati, D. W., Kamasawa, N., Matsui, K., Meredith, A. L., Watanabe, M., and Shigemoto, R. (2013). Quantitative localization of Cav2.1 (P/Q-type) voltage-dependent calcium channels in Purkinje cells: somatodendritic gradient and distinct somatic coclustering with calcium-activated potassium channels. *J. Neurosci.* 33, 3668–3678. doi: 10.1523/JNEUROSCI.2921-12.2013

Isaacson, J. S., and Murphy, G. J. (2001). Glutamate-mediated extrasynaptic inhibition: direct coupling of NMDA receptors to $Ca(2^+)$-activated K^+ channels. *Neuron* 31, 1027–1034. doi: 10.1016/S0896-6273(01)00428-7

Ishii, T. M., Maylie, J., and Adelman, J. P. (1997a). Determinants of apamin and d-tubocurarine block in SK potassium channels. *J. Biol. Chem.* 272, 23195–23200. doi: 10.1074/jbc.272.37.23195

Ishii, T. M., Silvia, C., Hirschberg, B., Bond, C. T., Adelman, J. P., and Maylie, J. (1997b). A human intermediate conductance calcium-activated potassium channel. *Proc. Natl. Acad. Sci. U.S.A.* 94, 11651–11656. doi: 10.1073/pnas.94.21.11651

Ito, M. (2002). Historical review of the significance of the cerebellum and the role of Purkinje cells in motor learning. *Ann. N. Y. Acad. Sci.* 978, 273–288. doi: 10.1111/j.1749-6632.2002.tb07574.x

Jaffe, D. B., Wang, B., and Brenner, R. (2011). Shaping of action potentials by type I and type II large-conductance Ca(2)+-activated K+ channels. *Neuroscience* 192, 205–218. doi: 10.1016/j.neuroscience.2011.06.028

Javaherian, A. D., Yusifov, T., Pantazis, A., Franklin, S., Gandhi, C. S., and Olcese, R. (2011). Metal-driven operation of the human large-conductance voltage- and Ca2+-dependent potassium channel (BK) gating ring apparatus. *J. Biol. Chem.* 286, 20701–20709. doi: 10.1074/jbc.M111.235234

Jensen, B. S. (2002). BMS-204352: a potassium channel opener developed for the treatment of stroke. *CNS Drug Rev.* 8, 353–360. doi: 10.1111/j.1527-3458.2002.tb00233.x

Jensen, B. S., Strobaek, D., Christophersen, P., Jorgensen, T. D., Hansen, C., Silahtaroglu, A., et al. (1998). Characterization of the cloned human intermediate-conductance Ca2+-activated K+ channel. *Am. J. Physiol.* 275, C848–C856. doi: 10.1152/ajpcell.1998.275.3.C848

Ji, H., and Shepard, P. D. (2006). SK Ca2+-activated K+ channel ligands alter the firing pattern of dopamine-containing neurons in vivo. *Neuroscience* 140, 623–633. doi: 10.1016/j.neuroscience.2006.02.020

Jin, W., Sugaya, A., Tsuda, T., Ohguchi, H., and Sugaya, E. (2000). Relationship between large conductance calcium-activated potassium channel and bursting activity. *Brain Res.* 860, 21–28. doi: 10.1016/S0006-8993(00)01943-0

Joiner, W. J., Wang, L. Y., Tang, M. D., and Kaczmarek, L. K. (1997). hSK4, a member of a novel subfamily of calcium-activated potassium channels. *Proc. Natl. Acad. Sci. U.S.A.* 94, 11013–11018. doi: 10.1073/pnas.94.20.11013

Jorgensen, S., Dyhring, T., Brown, D. T., Strobaek, D., Christophersen, P., and Demnitz, J. (2013). A high-throughput screening campaign for detection of $\alpha(2+)$-activated k(+) channel activators and inhibitors using a fluorometric imaging plate reader-based tl(+)-influx assay. *Assay Drug Dev. Technol.* 11, 163–172. doi: 10.1089/adt.2012.479

Jorgensen, S., Johansen, T. H., and Dyhring, T. (2008). Fluorescence-based Tl(+)-influx assays as a novel approach for characterization of small-conductance $Ca(2+)$-activated K (+) channel modulators. *Methods Mol. Biol.* 491, 257–266. doi: 10.1007/978-1-59745-526-8_20

Kasumu, A. W., Hougaard, C., Rode, F., Jacobsen, T. A., Sabatier, J. M., Eriksen, B. L., et al. (2012). Selective positive modulator of calcium-activated potassium channels exerts beneficial effects in a mouse model of spinocerebellar ataxia type 2. *Chem. Biol.* 19, 1340–1353. doi: 10.1016/j.chembiol.2012.07.013

Kasumu, A., and Bezprozvanny, I. (2012). Deranged calcium signaling in Purkinje cells and pathogenesis in spinocerebellar ataxia 2 (SCA2) and other ataxias. *Cerebellum* 11, 630–639. doi: 10.1007/s12311-010-0182-9

Katsuki, H., Shinohara, A., Fujimoto, S., Kume, T., and Akaike, A. (2005). Tetraethylammonium exacerbates ischemic neuronal injury in rat cerebrocortical slice cultures. *Eur. J. Pharmacol.* 508, 85–91. doi: 10.1016/j.ejphar.2004.11.058

Kaushal, V., Koeberle, P. D., Wang, Y., and Schlichter, L. C. (2007). The Ca^{2+}-activated K^+ channel KCNN4/KCa3.1 contributes to microglia activation and nitric oxide-dependent neurodegeneration. *J. Neurosci.* 27, 234–244. doi: 10.1523/JNEUROSCI.3593-06.2007

Kim, J. I., Yang, E. J., Lee, M. S., Kim, Y. S., Huh, Y., Cho, I. H., et al. (2011). Bee venom reduces neuroinflammation in the MPTP-induced model of Parkinson's disease. *Int. J. Neurosci.* 121, 209–217. doi: 10.3109/00207454.2010.548613

King, B., Rizwan, A. P., Asmara, H., Heath, N. C., Engbers, J. D., Dykstra, S., et al. (2015). IKCa channels are a critical determinant of the slow AHP in CA1 pyramidal neurons. *Cell Rep.* 11, 175–182. doi: 10.1016/j.celrep.2015.03.026

Kleiman-Weiner, M., Beenhakker, M. P., Segal, W. A., and Huguenard, J. R. (2009). Synergistic roles of GABAA receptors and SK channels in regulating thalamocortical oscillations. *J. Neurophysiol.* 102, 203–213. doi: 10.1152/jn.91158.2008

Knaus, H. G., Schwarzer, C., Koch, R. O., Eberhart, A., Kaczorowski, G. J., Glossmann, H., et al. (1996). Distribution of high-conductance Ca(2+)-activated K+ channels in rat brain: targeting to axons and nerve terminals. *J. Neurosci.* 16, 955–963. doi: 10.1523/JNEUROSCI.16-03-00955.1996

Köhler, M., Hirschberg, B., Bond, C. T., Kinzie, J. M., Marrion, N. V., Maylie, J., et al. (1996). Small-conductance, calcium-activated potassium channels from mammalian brain. *Science* 273, 1709–1714. doi: 10.1126/science.273.5282.1709

Koot, B. G., Alders, M., Verheij, J., Beuers, U., and Cobben, J. M. (2016). A de novo mutation in KCNN3 associated with autosomal dominant idiopathic non-cirrhotic portal hypertension. *J. Hepatol.* 64, 974–977. doi: 10.1016/j.jhep.2015.11.027

N'Gouemo, P. (2014). BKCa channel dysfunction in neurological diseases. *Front. Physiol.* 5:373. doi: 10.3389/fphys.2014.00373
Nguyen, H. M., Grossinger, E. M., Horiuchi, M., Davis, K. W., Jin, L. W., Maezawa, I., et al. (2017). Differential Kv1.3, KCa3.1, and Kir2.1 expression in "classically" and "alternatively" activated microglia. Glia 65, 106–121. doi: 10.1002/glia.23078
Nieoullon, A. (2002). Dopamine and the regulation of cognition and attention. *Prog. Neurobiol.* 67, 53–83. doi: 10.1016/S0301-0082(02)00011-4
Oliveira, M. S., Skinner, F., Arshadmansab, M. F., Garcia, I., Mello, C. F., Knaus, H. G., et al. (2010). Altered expression and function of small-conductance (SK) Ca(2+)-activated K+ channels in pilocarpine-treated epileptic rats. *Brain Res.* 1348, 187–199. doi: 10.1016/j.brainres.2010.05.095
Ornitz, E. M., Lane, S. J., Sugiyama, T., and De Traversay, J. (1993). Startle modulation studies in autism. *J. Autism. Dev. Disord.* 23, 619–637. doi: 10.1007/BF01046105
Park, Y. B. (1994). Ion selectivity and gating of small conductance Ca(2+)-activated K+ channels in cultured rat adrenal chromaffin cells. *J. Physiol.* 481 (Pt 3), 555–570. doi: 10.1113/jphysiol.1994.sp020463
Pedarzani, P., and Stocker, M. (2008). Molecular and cellular basis of small–and intermediate-conductance, calcium-activated potassium channel function in the brain. *Cell Mol. Life Sci.* 65, 3196–3217. doi: 10.1007/s00018-008-8216-x
Picones, A., Loza-Huerta, A., Segura-Chama, P., and Lara-Figueroa, C. O. (2016). Contribution of automated technologies to ion channel drug discovery. *Adv. Protein Chem. Struct. Biol.* 104, 357–378. doi: 10.1016/bs.apcsb.2016.01.002
Postmes, L., Sno, H. N., Goedhart, S., Van Der Stel, J., Heering, H. D., and De Haan, L. (2014). Schizophrenia as a self-disorder due to perceptual incoherence. *Schizophr. Res.* 152, 41–50. doi: 10.1016/j.schres.2013.07.027
Power, J. M., and Sah, P. (2008). Competition between calcium-activated K+ channels determines cholinergic action on firing properties of basolateral amygdala projection neurons. *J. Neurosci.* 28, 3209–3220. doi: 10.1523/JNEUROSCI.4310-07.2008
Price, D. L., Ludwig, J. W., Mi, H., Schwarz, T. L., and Ellisman, M. H. (2002). Distribution of rSlo Ca2+-activated K+ channels in rat astrocyte perivascular endfeet. *Brain Res.* 956, 183–193. doi: 10.1016/S0006-8993(02)03266-3
Rankin, C. H., Abrams, T., Barry, R. J., Bhatnagar, S., Clayton, D. F., Colombo, J., et al. (2009). Habituation revisited: an updated and revised description of the behavioral characteristics of habituation. *Neurobiol. Learn. Mem.* 92, 135–138. doi: 10.1016/j.nlm.2008.09.012
Reich, E. P., Cui, L., Yang, L., Pugliese-Sivo, C., Golovko, A., Petro, M., et al. (2005). Blocking ion channel KCNN4 alleviates the symptoms of experimental autoimmune encephalomyelitis in mice. *Eur. J. Immunol.* 35, 1027–1036. doi: 10.1002/eji.200425954
Ristori, G., Romano, S., Visconti, A., Cannoni, S., Spadaro, M., Frontali, M., et al. (2010). Riluzole in cerebellar ataxia: a randomized, double-blind, placebo-controlled pilot trial. *Neurology* 74, 839–845. doi: 10.1212/WNL.0b013e3181d31e23
Rudolph, S., and Thiagiwala, M. S. (2015). Location matters: somatic and dendritic SK channels answer to distinct calcium signals. *J. Neurophysiol.* 114, 1–5. doi: 10.1152/jn.00181.2014
Sah, P. (1996). Ca(2+)-activated K+ currents in neurones: types, physiological roles and modulation. *Trends Neurosci.* 19, 150–154. doi: 10.1016/S0166-2236(96)80026-9
Sah, P., and McLachlan, E. M. (1992). Potassium currents contributing to action potential repolarization and the afterhyperpolarization in rat vagal motoneurons. *J. Neurophysiol.* 68, 1834–1841. doi: 10.1152/jn.1992.68.5.1834
Sausbier, M., Hu, H., Arntz, C., Feil, S., Kamm, S., Adelsberger, H., et al. (2004). Cerebellar ataxia and Purkinje cell dysfunction caused by Ca2+-activated K+ channel deficiency. *Proc. Natl. Acad. Sci. U.S.A.* 101, 9474–9478. doi: 10.1073/pnas.0401702101
Savalli, N., Pantazis, A., Yusifov, T., Sigg, D., and Olcese, R. (2012). The contribution of RCK domains to human BK channel allosteric activation. *J. Biol. Chem.* 287, 21741–21750. doi: 10.1074/jbc.M112.346171
Scholl, E. S., Pirone, A., Cox, D. H., Duncan, R. K., and Jacob, M. H. (2014). Alternative splice isoforms of small conductance calcium-activated SK2 channels differ in molecular interactions and surface levels. *Channels (Austin)* 8, 62–75. doi: 10.4161/chan.27470
Schreiber, M., Yuan, A., and Salkoff, L. (1999). Transplantable sites confer calcium sensitivity to BK channels. *Nat. Neurosci.* 2, 416–421. doi: 10.1038/8077
Schumacher, M. A., Crum, M., and Miller, M. C. (2004). Crystal structures of apocalmodulin and an apocalmodulin/SK potassium channel gating domain complex. *Structure* 12, 849–860. doi: 10.1016/j.str.2004.03.017
Schumacher, M. A., Rivard, A. F., Bächinger, H. P., and Adelman, J. P. (2001). Structure of the gating domain of a Ca^{2+}-activated K^+ channel complexed with Ca2+/calmodulin. *Nature* 410, 1120–1124. doi: 10.1038/35074145
Seidel, K. N., Derst, C., Salzmann, M., Holtje, M., Priller, J., Markgraf, R., et al. (2011). Expression of the voltage- and Ca2+-dependent BK potassium channel subunits BKbeta1 and BKbeta4 in rodent astrocytes. *Glia* 59, 893–902. doi: 10.1002/glia.21160
Seifert, G., Henneberger, C., and Steinhauser, C. (2018). Diversity of astrocyte potassium channels: an update. *Brain Res. Bull.* 136, 26–36. doi: 10.1016/j.brainresbull.2016.12.002
Sheehan, J. J., Benedetti, B. L., and Barth, A. L. (2009). Anticonvulsant effects of the BK-channel antagonist paxilline. *Epilepsia* 50, 711–720. doi: 10.1111/j.1528-1167.2008.01888.x
Shi, J., Krishnamoorthy, G., Yang, Y., Hu, L., Chaturvedi, N., Harilal, D., et al. (2002). Mechanism of magnesium activation of calcium-activated potassium channels. *Nature* 418, 876–880. doi: 10.1038/nature00941
Shipston, M. J. (2001). Alternative splicing of potassium channels: a dynamic switch of cellular excitability. *Trends Cell Biol.* 11, 353–358. doi: 10.1016/S0962-8924(01)02068-2
Si, H., Heyken, W. T., Wolfle, S. E., Tysiac, M., Schubert, R., Grgic, I., et al. (2006). Impaired endothelium-derived hyperpolarizing factor-mediated dilations and increased blood pressure in mice deficient of the intermediate-conductance Ca2+-activated K+ channel. *Circ. Res.* 99, 537–544. doi: 10.1161/01.RES.0000238377.08219.0c
Skalska, J., Bednarczyk, P., Piwonska, M., Kulawiak, B., Wilczynski, G., Dolowy, K., et al. (2009). Calcium ions regulate K(+) uptake into brain mitochondria: the evidence for a novel potassium channel. *Int. J. Mol. Sci.* 10, 1104–1120. doi: 10.3390/ijms10031104
Smith, R. A., Miller, T. M., Yamanaka, K., Monia, B. P., Condon, T. P., Hung, G., et al. (2006). Antisense oligonucleotide therapy for neurodegenerative disease. *J. Clin. Invest.* 116, 2290–2296. doi: 10.1172/JCI25424
Soden, M. E., Jones, G. L., Sanford, C. A., Chung, A. S., Guler, A. D., Chavkin, C., et al. (2013). Disruption of dopamine neuron activity pattern regulation through selective expression of a human KCNN3 mutation. *Neuron* 80, 997–1009. doi: 10.1016/j.neuron.2013.07.044
Solly, K., Cassaday, J., Felix, J. P., Garcia, M. L., Ferrer, M., Strulovici, B., et al. (2008). Miniaturization and HTS of a FRET-based membrane potential assay for K(ir) channel inhibitors. *Assay Drug Dev. Technol.* 6, 225–234. doi: 10.1089/adt.2008.123
Staal, R. G. W., Khayrullina, T., Zhang, H., Davis, S., Fallon, S. M., Cajina, M., et al. (2017). Inhibition of the potassium channel KCa3.1 by sensicapoc reverses tactile allodynia in rats with peripheral nerve injury. *Eur. J. Pharmacol.* 795, 1–7. doi: 10.1016/j.ejphar.2016.11.031
Stackman, R. W., Hammond, R. S., Linardatos, E., Gerlach, A., Maylie, J., Adelman, J. P., et al. (2002). Small conductance Ca2+–activated K+ channels modulate synaptic plasticity and memory encoding. *J. Neurosci.* 22, 10163–10171. doi: 10.1523/JNEUROSCI.22-23-10163.2002
Stocker, M., and Pedarzani, P. (2000). Differential distribution of three Ca(2+)-activated K(+) channel subunits, SK1, SK2, and SK3, in the adult rat central nervous system. *Mol. Cell. Neurosci.* 15, 476–493. doi: 10.1006/mcne.2000.0842
Stocker, M., Krause, M., and Pedarzani, P. (1999). An apamin-sensitive Ca^{2+}-activated K+ current in hippocampal pyramidal neurons. *Proc. Natl. Acad. Sci. U.S.A.* 96, 4662–4667. doi: 10.1073/pnas.96.8.4662
Storm, J. F. (1987). Action potential repolarization and a fast after-hyperpolarization in rat hippocampal pyramidal cells. *J. Physiol.* 385, 733–759. doi: 10.1113/jphysiol.1987.sp016517
Strobaek, D., Teuber, L., Jorgensen, T. D., Ahring, P. K., Kjaer, K., Hansen, R. S., et al. (2004). Activation of human IK and SK Ca2+ -activated K+ channels by NS309 (6,7 -dichloro-1H-indole-2,3-dione 3-oxime). *Biochim. Biophys. Acta* 1665, 1–5. doi: 10.1016/j.bbamem.2004.07.006
Su, Z., Brown, E. C., Wang, W., and Mackinnon, R. (2016). Novel cell-free high-throughput screening method for pharmacological tools targeting K+ channels. *Proc. Natl. Acad. Sci. U.S.A.* 113, 5748–5753. doi: 10.1073/pnas.1602815113

Sugunan, S., Nampoothiri, S. S., Garg, T., and Krishnamurthy, R. G. (2016). Role of KCa3.1 Channels in CNS diseases: a concise review. *CNS Neurol. Disord. Drug Targets* 15, 1299–1305. doi: 10.2174/1871527315666160822111913
Sun, P., Wang, F., Wang, L., Zhang, Y., Yamamoto, R., Sugai, T., et al. (2011). Increase in cortical pyramidal cell excitability accompanies depression-like behavior in mice: a transcranial magnetic stimulation study. *J. Neurosci.* 31, 16464–16472. doi: 10.1523/JNEUROSCI.1542-11.2011
Surmeier, D. J., Guzman, J. N., Sanchez-Padilla, J., and Goldberg, J. A. (2010). What causes the death of dopaminergic neurons in Parkinson's disease? *Prog. Brain Res.* 183, 59–77. doi: 10.1016/S0079-6123(10)83004-3
Sweet, T. B., and Cox, D. H. (2009). Measuring the influence of the BKCa [beta]1 subunit on Ca2+ binding to the BKCa channel. *J. Gen. Physiol.* 133, 139–150. doi: 10.1085/jgp.200810129
Szewczyk, A., Kajma, A., Malinska, D., Wrzosek, A., Bednarczyk, P., Zablocka, B., et al. (2010). Pharmacology of mitochondrial potassium channels: dark side of the field. *FEBS Lett.* 584, 2063–2069. doi: 10.1016/j.febslet.2010.02.048
Takano, T., Tian, G. F., Peng, W., Lou, N., Libionka, W., Han, X., et al. (2006). Astrocyte-mediated control of cerebral blood flow. *Nat. Neurosci.* 9, 260–267. doi: 10.1038/nn1623
Tanner, M. R., Pennington, M. W., Chamberlain, B. H., Huq, R., Gehrmann, E. J., Laragione, T., et al. (2018). Targeting KCa1.1 channels with a scorpion venom peptide for the therapy of rat models of rheumatoid arthritis. *J. Pharmacol. Exp. Ther.* 365, 227–236. doi: 10.1124/jpet.117.245118
Tao, X., Hite, R. K., and Mackinnon, R. (2017). Cryo-EM structure of the open high-conductance Ca^{2+}-activated K^+ channel. *Nature* 541, 46–51. doi: 10.1038/nature20608
Thompson, J. M., Ji, G., and Neugebauer, V. (2015). Small-conductance calcium-activated potassium (SK) channels in the amygdala mediate pain-inhibiting effects of clinically available riluzole in a rat model of arthritis pain. *Mol. Pain* 11, 51. doi: 10.1186/s12990-015-0055-9
Tonini, R., Ferraro, T., Sampedro-Castaneda, M., Cavaccini, A., Stocker, M., Richards, C. D., et al. (2013). Small-conductance Ca2+-activated K+ channels modulate action potential-induced Ca2+ transients in hippocampal neurons. *J. Neurophysiol.* 109, 1514–1524. doi: 10.1152/jn.00346.2012
Toyama, K., Wulff, H., Chandy, K. G., Azam, P., Raman, G., Saito, T., et al. (2008). The intermediate-conductance calcium-activated potassium channel KCa3.1 contributes to atherogenesis in mice and humans. *J. Clin. Invest.* 118, 3025–3037. doi: 10.1172/JCI30836
Tuteja, D., Rafizadeh, S., Timofeyev, V., Wang, S., Zhang, Z., Li, N., et al. (2010). Cardiac small conductance Ca2+-activated K+ channel subunits form heteromultimers via the coiled-coil domains in the C termini of the channels. *Circ. Res.* 107, 851–859. doi: 10.1161/CIRCRESAHA.109.215269
Typlt, M., Mirkowski, M., Azzopardi, E., Ruth, P., Pilz, P. K., and Schmid, S. (2013). Habituation of reflexive and motivated behavior in mice with deficient BK channel function. *Front. Integr. Neurosci.* 7:79. doi: 10.3389/fnint.2013.00079
Tzingounis, A. V., and Nicoll, R. A. (2008). Contribution of KCNQ2 and KCNQ3 to the medium and slow afterhyperpolarization currents. *Proc. Natl. Acad. Sci. U.S.A.* 105, 19974–19979. doi: 10.1073/pnas.0810535105
Tzingounis, A. V., Heidenreich, M., Kharkovets, T., Spitzmaul, G., Jensen, H. S., Nicoll, R. A., et al. (2010). The KCNQ5 potassium channel mediates a component of the afterhyperpolarization current in mouse hippocampus. *Proc. Natl. Acad. Sci. U.S.A.* 107, 10232–10237. doi: 10.1073/pnas.1004644107
Ungless, M. A., Argilli, E., and Bonci, A. (2010). Effects of stress and aversion on dopamine neurons: implications for addiction. *Neurosci. Biobehav. Rev.* 35, 151–156. doi: 10.1016/j.neubiorev.2010.04.006
Verkerk, A. J., Pieretti, M., Sutcliffe, J. S., Fu, Y. H., Kuhl, D. P., Pizzuti, A., et al. (1991). Identification of a gene (FMR-1) containing a CGG repeat coincident with a breakpoint cluster region exhibiting length variation in fragile X syndrome. *Cell* 65, 905–914. doi: 10.1016/0092-8674(91)90397-H
Vivas, O., Moreno, C. M., Santana, L. F., and Hille, B. (2017). Proximal clustering between BK and CaV1.3 channels promotes functional coupling and BK channel activation at low voltage. *Elife* 6:e28029. doi: 10.7554/eLife.28029
Walter, J. T., Alvina, K., Womack, M. D., Chevez, C., and Khodakhah, K. (2006). Decreases in the precision of Purkinje cell pacemaking cause cerebellar dysfunction and ataxia. *Nat. Neurosci.* 9, 389–397. doi: 10.1038/nn1648
Wang, B., Bugay, V., Ling, L., Chuang, H. H., Jaffe, D. B., and Brenner, R. (2016). Knockout of the BK beta4-subunit promotes a functional coupling of BK channels and ryanodine receptors that mediate a fAHP-induced increase in excitability. *J. Neurophysiol.* 116, 456–465. doi: 10.1152/jn.00857.2015
Wang, B., Jaffe, D. B., and Brenner, R. (2014). Current understanding of iberiotoxin-resistant BK channels in the nervous system. *Front. Physiol.* 5:382. doi: 10.3389/fphys.2014.00382
Wang, B., Rothberg, B. S., and Brenner, R. (2009). Mechanism of increased BK channel activation from a channel mutation that causes epilepsy. *J. Gen. Physiol.* 133, 283–294. doi: 10.1085/jgp.200810141
Wang, F., Zhang, Y., Wang, L., Sun, P., Luo, X., Ishigaki, Y., et al. (2015). Improvement of spatial learning by facilitating large-conductance calcium-activated potassium channel with transcranial magnetic stimulation in Alzheimer's disease model mice. *Neuropharmacology* 97, 210–219. doi: 10.1016/j.neuropharm.2015.05.027
Wang, K., Mateos-Aparicio, P., Honigsperger, C., Raghuram, V., Wu, W. W., Ridder, M. C., et al. (2016). IK1 channels do not contribute to the slow afterhyperpolarization in pyramidal neurons. *Elife* 5:e11206. doi: 10.7554/eLife.11206
Wang, L., Kang, H., Li, Y., Shui, Y., Yamamoto, R., Sugai, T., et al. (2015). Cognitive recovery by chronic activation of the large-conductance calcium-activated potassium channel in a mouse model of Alzheimer's disease. *Neuropharmacology* 92, 8–15. doi: 10.1016/j.neuropharm.2014.12.033
Wang, Y., Yang, P. L., Tang, J. F., Lin, J. F., Cai, X. H., Wang, X. T., et al. (2008). Potassium channels: possible new therapeutic targets in Parkinson's disease. *Med. Hypotheses* 71, 546–550. doi: 10.1016/j.mehy.2008.05.021
Waroux, O., Massotte, L., Alleva, L., Graulich, A., Thomas, E., Liegeois, J. F., et al. (2005). SK channels control the firing pattern of midbrain dopaminergic neurons in vivo. *Eur. J. Neurosci.* 22, 3111–3121. doi: 10.1111/j.1460-9568.2005.04484.x
Wei, A. D., Gutman, G. A., Aldrich, R., Chandy, K. G., Grissmer, S., and Wulff, H. (2005). International Union of Pharmacology. LII. Nomenclature and molecular relationships of calcium-activated potassium channels. *Pharmacol. Rev.* 57, 463–472. doi: 10.1124/pr.57.4.9
Whitmire, L. E., Ling, L., Bugay, V., Carver, C. M., Timilsina, S., Chuang, H. H., et al. (2017). Downregulation of KCNMB4 expression and changes in BK channel subtype in hippocampal granule neurons following seizure activity. *PLoS One* 12:e0180064. doi: 10.1371/journal.pone.0180064
Whitt, J. P., Mcnally, B. A., and Meredith, A. L. (2018). Differential contribution of Ca(2+) sources to day and night BK current activation in the circadian clock. *J. Gen. Physiol.* 150, 259–275. doi: 10.1085/jgp.201711945
Whitt, J. P., Montgomery, J. R., and Meredith, A. L. (2016). BK channel inactivation gates daytime excitability in the circadian clock. *Nat. Commun.* 7:10837. doi: 10.1038/ncomms10837
Wolfart, J., and Roeper, J. (2002). Selective coupling of T-type calcium channels to SK potassium channels prevents intrinsic bursting in dopaminergic midbrain neurons. *J. Neurosci.* 22, 3404–3413. doi: 10.1523/JNEUROSCI.22-09-03404.2002
Womack, M. D., and Khodakhah, K. (2003). Somatic and dendritic small-conductance calcium-activated potassium channels regulate the output of cerebellar Purkinje neurons. *J. Neurosci.* 23, 2600–2607. doi: 10.1523/JNEUROSCI.23-07-02600.2003
Womble, M. D., and Moises, H. C. (1993). Muscarinic modulation of conductances underlying the afterhyperpolarization in neurons of the rat basolateral amygdala. *Brain Res.* 621, 87–96. doi: 10.1016/0006-8993(93)90301-3
Wu, Y., Liu, Y., Hou, P., Yan, Z., Kong, W., Liu, B., et al. (2013). TRPV1 channels are functionally coupled with BK(mSlo1) channels in rat dorsal root ganglion (DRG) neurons. *PLoS One* 8:e78203. doi: 10.1371/journal.pone.0078203
Wu, Y., Yang, Y., Ye, S., and Jiang, Y. (2010). Structure of the gating ring from the human large-conductance Ca(2+)-gated K(+) channel. *Nature* 466, 393–397. doi: 10.1038/nature09252
Wulff, M., and Pless, S. A. (2018). High-sensitivity fluorometry to resolve ion channel conformational dynamics. *Cell Rep.* 22, 1615–1626. doi: 10.1016/j.celrep.2018.01.029
Wulff, H., and Castle, N. A. (2010). Therapeutic potential of KCa3.1 blockers: recent advances and promising trends. *Exp. Rev. Clin. Pharmacol.* 3, 385–396. doi: 10.1586/ecp.10.11
Xia, X. M., Zeng, X., and Lingle, C. J. (2002). Multiple regulatory sites in large-conductance calcium-activated potassium channels. *Nature* 418, 880–884. doi: 10.1038/nature00956

Yamamoto, K., Ueta, Y., Wang, L., Yamamoto, R., Inoue, N., Inokuchi, K., et al. (2011). Suppression of a neocortical potassium channel activity by intracellular amyloid-beta and its rescue with Homer1a. *J. Neurosci.* 31, 11100–11109. doi: 10.1523/JNEUROSCI.6752-10.2011

Yang, E. J., Jiang, J. H., Lee, S. M., Yang, S. C., Hwang, H. S., Lee, M. S., et al. (2010). Bee venom attenuates neuroinflammatory events and extends survival in amyotrophic lateral sclerosis models. *J. Neuroinflammat.* 7:69. doi: 10.1186/1742-2094-7-69

Yang, H., Shi, J., Zhang, G., Yang, J., Delaloye, K., and Cui, J. (2008). Activation of Slo1 BK channels by Mg2+ coordinated between the voltage sensor and RCK1 domains. *Nat. Struct. Mol. Biol.* 15, 1152–1159. doi: 10.1038/nsmb.1507

Yang, J., Krishnamoorthy, G., Saxena, A., Zhang, G., Shi, J., Yang, H., et al. (2010). An epilepsy/dyskinesia-associated mutation enhances BK channel activation by potentiating Ca2+ sensing. *Neuron* 66, 871–883. doi: 10.1016/j.neuron.2010.05.009

Yi, M., Yu, P., Lu, Q., Geller, H. M., Yu, Z., and Chen, H. (2016). KCa3.1 constitutes a pharmacological target for astrogliosis associated with Alzheimer's disease. *Mol. Cell. Neurosci.* 76, 21–32. doi: 10.1016/j.mcn.2016.08.008

Yu, Z. H., Wang, Y. X., Song, Y., Lu, H. Z., Hou, L. N., Cui, Y. Y., et al. (2013). Up-regulation of KCa3.1 promotes human airway smooth muscle cell phenotypic modulation. *Pharmacol. Res.* 77, 30–38. doi: 10.1016/j.phrs.2013.09.002

Yu, Z., Yu, P., Chen, H., and Geller, H. M. (2014). Targeted inhibition of KCa3.1 attenuates TGF-beta-induced reactive astrogliosis through the Smad2/3 signaling pathway. *J. Neurochem.* 130, 41–49. doi: 10.1111/jnc.12710

Yuan, P., Leonetti, M. D., Hsiung, Y., and Mackinnon, R. (2011). Open structure of the Ca2+ gating ring in the high-conductance Ca2+-activated K+ channel. *Nature* 481, 94–97. doi: 10.1038/nature10670

Yusifov, T., Javaherian, A. D., Pantazis, A., Gandhi, C. S., and Olcese, R. (2010). The RCK1 domain of the human BKCa channel transduces Ca2+ binding into structural rearrangements. *J. Gen. Physiol.* 136, 189–202. doi: 10.1085/jgp.200910374

Yusifov, T., Savalli, N., Gandhi, C. S., Ottolia, M., and Olcese, R. (2008). The RCK2 domain of the human BKCa channel is a calcium sensor. *Proc. Natl. Acad. Sci. U.S.A.* 105, 376–381. doi: 10.1073/pnas.0705261105

Zaman, T., De Oliveira, C., Smoka, M., Narla, C., Poulter, M. O., and Schmid, S. (2017). BK channels mediate synaptic plasticity underlying habituation in rats. *J. Neurosci.* 37, 4540–4551. doi: 10.1523/JNEUROSCI.3699-16.2017

Zhang, L., and McBain, C. J. (1995). Potassium conductances underlying repolarization and after-hyperpolarization in rat CA1 hippocampal interneurones. *J. Physiol.* 488(Pt 3), 661–672. doi: 10.1113/jphysiol.1995.sp020998

Zhang, M., Abrams, C., Wang, L., Gizzi, A., He, L., Lin, R., et al. (2012a). Structural basis for calmodulin as a dynamic calcium sensor. *Structure* 20, 911–923. doi: 10.1016/j.str.2012.03.019

Zhang, M., Pascal, J. M., Schumann, M., Armen, R. S., and Zhang, J. F. (2012b). Identification of the functional binding pocket for compounds targeting small-conductance Ca(2)(+)-activated potassium channels. *Nat. Commun.* 3:1021. doi: 10.1038/ncomms2017

Zhang, M., Meng, X. Y., Cui, M., Pascal, J. M., Logothetis, D. E., and Zhang, J. F. (2014). Selective phosphorylation modulates the PIP2 sensitivity of the CaM-SK channel complex. *Nat. Chem. Biol.* 10, 753–759. doi: 10.1038/nchembio.1592

Zhang, M., Pascal, J. M., and Zhang, J. (2013). Unstructured to structured transition of an intrinsically disordered protein peptide in coupling Ca2+-sensing and SK channel activation. *Proc. Natl. Acad. Sci. U.S.A.* 110, 4828–4833. doi: 10.1073/pnas.1220253110

Zheng, J., and Zagotta, W. N. (2003). Patch-clamp fluorometry recording of conformational rearrangements of ion channels. *Sci. STKE* 2003:PL7. doi: 10.1126/stke.2003.176.pl7

Zhou, Y., Yang, H., Cui, J., and Lingle, C. J. (2017). Threading the biophysics of mammalian Slo1 channels onto structures of an invertebrate Slo1 channel. *J. Gen. Physiol.* 149, 985–1007. doi: 10.1085/jgp.201711845

Conflict of Interest Statement: The authors declare that the research was conducted in the absence of any commercial or financial relationships that could be construed as a potential conflict of interest.

Journal Club

Editor's Note: These short reviews of recent *JNeurosci* articles, written exclusively by students or postdoctoral fellows, summarize the important findings of the paper and provide additional insight and commentary. If We of the highlighted article have written a response to the Journal Club, the response can be found by viewing the Journal Club at www.jneurosci.org. For more information on the format, review process, and purpose of Journal Club articles, please see http://jneurosci.org/content/preparing-manuscript#journalclub.

Cereblon Regulates BK Channel Expression at Presynaptic and Postsynaptic Sites in Excitatory Synapses

Alberto J. Gonzalez-Hernandez,[1,2] Laura E. Maglio,[1,2] and Ricardo Gómez[1,2]

[1]Departamento de Ciencias Médicas Básicas (Área de Fisiología), Facultad de Medicina, and [2]Instituto de Tecnologías Biomédicas (ITB), Universidad de La Laguna, 38071 Tenerife, Spain

Review of Choi et al.

Cereblon is a substrate receptor protein for the CRL4A E3 ubiquitin ligase complex. As such, cereblon binds to different proteins to promote their ubiquitination and degradation (Zheng and Shabek, 2017). Cereblon is highly expressed in brain tissues, including the hippocampus, cortex, cerebellum, and striatum (Higgins et al., 2010; Aizawa et al., 2011). Missense mutations of this protein and deletion or microduplication of the chromosomal segment harboring the *Cereblon* gene have been linked to human intellectual disability (Higgins et al., 2004; Dijkhuizen et al., 2006; Papuc et al., 2015).

To elucidate how cereblon mutations might lead to intellectual disability, Choi et al. (2018) studied behavior and synaptic function in mice lacking or expressing mutated forms of cereblon. Macroscopic brain architecture and dendritic spine morphology were similar in wild-type and cereblon-null animals. Furthermore, no apparent differences were found in spontaneous synaptic transmission or long-term synaptic plasticity after cereblon deletion. Similar results were found in *Drosophila*. In contrast, lack of cereblon led to a reduction in the amplitude of evoked excitatory synaptic transmission (eEPSC). Furthermore, mice lacking cereblon performed abnormally in passive avoidance and novel object recognition tests. These results suggest that loss of cereblon impairs cognitive function by reducing presynaptic glutamate release probability.

The probability of glutamate release from presynaptic terminals was assessed by computing the paired-pulse ratio: the relative amplitude of postsynaptic responses elicited by two presynaptic spikes (second response/first response). This ratio was increased, suggesting release probability was reduced after cereblon knock-out in both species. This presynaptic impairment was also present in animals expressing mutant forms of cereblon that mimic mutations related to mild intellectual disability in humans, namely, the R419X cereblon mutant in mice and the G552X mutant in *Drosophila*. A similar decrease in glutamate release was suggested by experiments involving a short-term synaptic plasticity protocol consisting of 20-pulse train stimulation: the amplitude of successive eEPSCs increased in cereblon-null mice, suggesting a presynaptic origin of the impairment.

As part of the CRL4A E3 ubiquitin ligase complex, cereblon regulates the trafficking and plasma membrane expression of the large-conductance Ca^{2+}-activated K^+ channel (BK) α subunit (Jo et al., 2005; Liu et al., 2014). BK channels are thought to be key regulators of neurotransmitter release in many synapses (for review, see Griguoli et al., 2016). Therefore, Choi et al. (2018) studied whether the reduction in neurotransmitter release in cereblon-null animals resulted from modifications in BK function and/or channel expression levels. Total expression levels of BK channels in hippocampal CA1 pyramidal neurons were unaffected by cereblon knock-out, but surface expression and the amplitude of BK-mediated currents were increased. Furthermore, blocking BK currents restored glutamate release probability to wild-type levels and rescued abnormal cognitive behaviors in cereblon-null animals.

Choi et al. (2018) present clear evidence that loss of cereblon impairs cognitive function by increasing surface expression of BK channels and reducing presynaptic glutamate release probability in excitatory synapses. However, how these effects are linked remains unclear. Because BK channels are expressed at both presynaptic and postsynaptic synaptic terminals, as well as in the soma of multiple cellular types in the central nervous system (Latorre et

Received May 30, 2018; revised Aug. 3, 2018; accepted Aug. 8, 2018.

A.J.G.-H. was supported by Spanish Ministerio de Educación, Cultura y Deporte Predoctoral Fellowship FPU15/02528. L.E.M. and R.G. were supported by European Research Council Postdoctoral Contracts, under Horizon 2020 Research and Innovation Programme Grant 648936. We thank Dr. Teresa Giráldez for providing feedback during the preparation of the manuscript.

The authors declare no competing financial interests.

Correspondence should be addressed to Dr. Ricardo Gómez, Departamento de Ciencias Médicas Básicas (Área de Fisiología), Facultad de Medicina, Universidad de La Laguna, Campus de Ofra s/n, 38071 La Laguna, Tenerife, Spain. E-mail: rgomezgo@ull.edu.es.

DOI:10.1523/JNEUROSCI.1402-18.2018

 0270-6474/18/387932-03$15.00/0

al., 2017), mutations disrupting surface expression of BK channels at any of these locations might impair synaptic transmission.

At presynaptic active zones, BK channels coassemble with voltage-gated Ca^{2+} channels (VGCCs) (Grunnet and Kaufmann, 2004; Berkefeld et al., 2006). Opening of VGCCs produces the Ca^{2+} influx necessary for BK activation, which in turn repolarizes the presynaptic terminal, curtailing the opening of VGCCs and thus terminating Ca^{2+} influx and neurotransmitter release. Therefore, the increase in BK function occurring after cereblon deletion would be expected to reduce Ca^{2+} influx at the presynaptic terminal, thus reducing release probability. BK blockers would abolish this "brake" in VGCC-dependent Ca^{2+} influx, increasing glutamate release. However, this model is difficult to reconcile with previous results demonstrating that BK channels do not modulate transmitter release under basal conditions or during high-frequency stimulation in hippocampal CA3-CA1 synapses (Hu et al., 2001). The model is also inconsistent with results demonstrating that mutations disrupting the BK channel orthologue encoded by the *slowpoke* gene have little effect on glutamate release in *Drosophila* neuromuscular junction (Lee et al., 2008). An alternative model to explain the effects of cereblon deletion on glutamate release is that cereblon modulates BK channels at the soma of the presynaptic cell.

Somatic BK channels play a pivotal role in modulating action potential shape and frequency (Sailer et al., 2006), with inhibition of BK channels leading to either an increase or a decrease in action potential firing (Latorre et al., 2017). In hippocampal CA3 pyramidal neurons (the presynaptic cells in the mouse experiments by Choi et al., 2018), a decrease in BK channel activity is associated with a broadening of action potential duration and an increase in glutamate release, a situation that was reversed using a BK channel blocker (Deng et al., 2013). Conversely, the increase in BK channel function described by Choi et al. (2018) would be expected to shorten the action potential duration in CA3 pyramidal neurons, causing a decrease in glutamate release; the subsequent application of a BK channel blocker would then abolish this decrease, as described in the article.

Finally, some results in the work by Choi et al. (2018) cannot be explained without taking into account possible roles of postsynaptic BK channels. Indeed, the authors measured BK current amplitude only in CA1 pyramidal neurons, the postsynaptic cells in their experiments. In postsynaptic cells, BK channels are often located in close proximity with postsynaptic proteins, such as PSD95 and NMDA receptors (NMDARs). Indeed, a functional coupling between NMDAR and BK channels has been described in olfactory bulb granule cells (Isaacson and Murphy, 2001). In this context, an increase in BK channel expression/function would reduce the influx through NMDAR at the postsynaptic terminals in a similar way to what has been described for VGCC-BK association: Ca^{2+} influx through NMDAR would be enough to produce BK activation, thus repolarizing the postsynaptic terminal and terminating NMDAR-dependent Na^{+} and Ca^{2+} influx. Consistent with this mechanism, a decrease in the amplitude of the eEPSCs (due to both AMPA and NMDA receptors) was observed (Choi et al., 2018, their Fig. 2*A*), without any modification of the spontaneous EPSC (mainly due to AMPA receptors) (Choi et al., 2018, their Fig. 2*B*). This could also explain why eEPSCs were reduced in mice, whereas *Drosophila* excitatory junction currents were unaffected in cereblon-deficient animals, given that glutamatergic postsynaptic receptors at the *Drosophila* neuromuscular junction (DGluRIIA and DGluRIIB) are homologous to vertebrate AMPA and kainate receptors (Petersen et al., 1997; Davis et al., 1998). An inhibitory effect of BK on NMDAR could also be presumed from the current traces of EPSCs recorded from cereblon knock-out mice because the decay kinetics are slightly accelerated compared with wild-type (e.g., Choi et al., 2018, their Fig. 2*C*), as they would be if NMDAR-driven currents were inhibited.

In conclusion, the work by Choi et al. (2018) highlights the importance of BK channels on synaptic excitability, specifically related to their location. Undoubtedly, these results open a new and exciting avenue for research. In particular, future work should address the extent to which presynaptic and postsynaptic BK channels contribute to altered synaptic transmission and cognitive defects. More broadly, BK channels might be a promising pharmacological target in the search for new ways of treating intellectual disabilities.

References

Aizawa M, Abe Y, Ito T, Handa H, Nawa H (2011) mRNA distribution of the thalidomide binding protein cereblon in adult mouse brain. Neurosci Res 69:343–347. CrossRef Medline

Berkefeld H, Sailer CA, Bildl W, Rohde V, Thumfart JO, Eble S, Klugbauer N, Reisinger E, Bischofberger J, Oliver D, Knaus HG, Schulte U, Fakler B (2006) BKCa-Cav channel complexes mediate rapid and localized Ca^{2+}-activated K^{+} signaling. Science 314:615–620. CrossRef Medline

Choi TY, Lee SH, Kim YJ, Bae JR, Lee KM, Jo Y, Kim SJ, Lee AR, Choi S, Choi LM, Bang S, Song MR, Chung J, Lee KJ, Kim SH, Park CS, Choi SY (2018) Cereblon maintains synaptic and cognitive function by regulating BK channel. J Neurosci 38:3571–3583. CrossRef Medline

Davis GW, DiAntonio A, Petersen SA, Goodman CS (1998) Postsynaptic PKA controls quantal size and reveals a retrograde signal that regulates presynaptic transmitter release in *Drosophila*. Neuron 20:305–315. CrossRef Medline

Deng PY, Rotman Z, Blundon JA, Cho Y, Cui J, Cavalli V, Zakharenko SS, Klyachko VA (2013) FMRP regulates neurotransmitter release and synaptic information transmission by modulating action potential duration via BK channels. Neuron 77:696–711. CrossRef Medline

Dijkhuizen T, van Essen T, van der Vlies P, Verheij JB, Sikkema-Raddatz B, van der Veen AY, Gerssen-Schoorl KB, Buys CH, Kok K (2006) FISH and array-CGH analysis of a complex chromosome 3 aberration suggests that loss of CNTN4 and CRBN contributes to mental retardation in 3pter deletions. Am J Med Genet A 140:2482–2487. CrossRef Medline

Griguoli M, Sgritta M, Cherubini E (2016) Presynaptic BK channels control transmitter release: Physiological relevance and potential therapeutic implications. J Physiol 594:3489–3500. CrossRef Medline

Grunnet M, Kaufmann WA (2004) Coassembly of big conductance Ca^{2+}-activated K^{+} channels and L-type voltage-gated Ca^{2+} channels in rat brain. J Biol Chem 279:36445–36453. CrossRef Medline

Higgins JJ, Pucilowska J, Lombardi RQ, Rooney JP (2004) A mutation in a novel ATP-dependent Lon protease gene in a kindred with mild mental retardation. Neurology 63:1927–1931. CrossRef Medline

Higgins JJ, Tal AL, Sun X, Hauck SC, Hao J, Kosofosky BE, Rajadhyaksha AM (2010) Temporal and spatial mouse brain expression of cereblon, an ionic channel regulator involved in human intelligence. J Neurogenet 24:18–26. CrossRef Medline

Hu H, Shao LR, Chavoshy S, Gu N, Trieb M, Behrens R, Laake P, Pongs O, Knaus HG, Ottersen OP, Storm JF (2001) Presynaptic Ca^{2+}-activated K^{+} channels in glutamatergic hippocampal terminals and their role in spike repolarization and regulation of transmitter release. J Neurosci 21:9585–9597. CrossRef Medline

Isaacson JS, Murphy GJ (2001) Glutamate-mediated extrasynaptic inhibition: Direct coupling of NMDA receptors to Ca^{2+}-activated K^{+} channels. Neuron 31:1027–1034. CrossRef Medline

Jo S, Lee KH, Song S, Jung YK, Park CS (2005) Identification and functional characterization of cereblon as a binding protein for large-conductance calcium-activated potassium channel in rat brain. J Neurochem 94:1212–1224. CrossRef Medline

Latorre R, Castillo K, Carrasquel-Ursulaez W, Sepulveda RV, Gonzalez-Nilo F, Gonzalez C, Alvarez O (2017) Molecular determinants of BK channel functional diversity and functioning. Physiol Rev 97:39–87. CrossRef Medline

Lee J, Ueda A, Wu CF (2008) Pre- and post-synaptic mechanisms of synaptic strength homeostasis revealed by slowpoke and shaker K^{+} channel mutations in *Drosophila*. Neuroscience 154:1283–1296. CrossRef Medline

Liu J, Ye J, Zou X, Xu Z, Feng Y, Zou X, Chen Z, Li Y, Cang Y (2014) CRL4A(CRBN) E3 ubiquitin ligase restricts BK channel activity and prevents epileptogenesis. Nat Commun 5:3924. CrossRef Medline

Papuc SM, Hackmann K, Andrieux J, Vincent-Delorme C, Budisteanu M, Arghir A, Schrock E, Tutulan-Cunita AC, Di Donato N (2015) Microduplications of 3p26.3p26.2 containing CRBN gene in patients with intellectual disability and behavior abnormalities. Eur J Med Genet 58:319–323. CrossRef Medline

Petersen SA, Fetter RD, Noordermeer JN, Goodman CS, DiAntonio A (1997) Genetic analysis of glutamate receptors in *Drosophila* reveals a retrograde signal regulating presynaptic transmitter release. Neuron 19:1237–1248. CrossRef Medline

Sailer CA, Kaufmann WA, Kogler M, Chen L, Sausbier U, Ottersen OP, Ruth P, Shipston MJ, Knaus HG (2006) Immunolocalization of BK channels in hippocampal pyramidal neurons. Eur J Neurosci 24:442–454. CrossRef Medline

Zheng N, Shabek N (2017) Ubiquitin ligases: Structure, function, and regulation. Annu Rev Biochem 86:129–157. CrossRef Medline

PNAS
www.pnas.org

NMDA receptor–BK channel coupling regulates synaptic plasticity in the barrel cortex

Ricardo Gómez[1,2*], Laura E. Maglio[1,2], Alberto J. Gonzalez-Hernandez[1,2], Belinda Rivero-Pérez[1,2], David Bartolomé-Martín[1,2], and Teresa Giraldez[1,2*]

[1] Departamento de Ciencias Médicas Básicas-Fisiologia, Facultad de Medicina, Universidad de La Laguna, Campus de Ciencias de la Salud s/n 38200, Tenerife, Spain.

[2] Instituto de Tecnologías Biomédicas (ITB), Universidad de La Laguna, Campus de Ciencias de la Salud s/n 38200, Tenerife, Spain.

* Ricardo Gómez, Teresa Giraldez

Email: rgomezga@ull.edu.es, giraldez@ull.edu.es

Author Contributions: Conceptualization: RG, LEM, TG; Methodology: RG and LEM; Formal analysis: RG, LEM, AJGH, BRP, DBM; Investigation: RG, LEM, AJGH, BRP, DBM; Writing – original draft: RG, TG; Writing – review & editing: RG, TG; Visualization: RG, TG; Supervision: TG, RG; Project administration: TG; Funding acquisition: TG

Competing Interest Statement: The authors declare no competing interests.

Classification: Biological Sciences, Physiology.

Keywords: Large-conductance Ca^{2+}- and voltage-activated K^+ channels (BK), functional coupling, ion channel macromolecular complexes, synaptic plasticity

This PDF file includes:

Main Text
Figures 1 to 8

Abstract

Postsynaptic N-methyl-D-aspartate receptors (NMDARs) are crucial mediators of synaptic plasticity due to their ability to act as coincidence detectors of presynaptic and postsynaptic neuronal activity. However, NMDARs exist within the molecular context of a variety of postsynaptic signaling proteins, which can fine-tune their function. Here we describe a novel form of NMDAR suppression by large-conductance Ca^{2+}- and voltage-gated K^+ (BK) channels in the basal dendrites of a subset of barrel cortex layer 5 pyramidal neurons. We show that NMDAR activation increases intracellular Ca^{2+} in the vicinity of BK channels, thus activating K^+ efflux and strong negative feedback inhibition. We further show that neurons exhibiting such NMDAR–BK coupling serve as high-pass filters for incoming synaptic inputs, precluding the induction of spike-timing-dependent plasticity. Together, these data suggest that NMDAR-localized BK channels regulate synaptic integration and provide input-specific synaptic diversity to a thalamocortical circuit.

Significance Statement

NMDA receptors are critical triggers for plasticity. We show that BK channels serve as feedback regulators of NMDA receptor-mediated calcium influx to shape NMDA receptor-mediated synaptic potentials, and consequently elevate the threshold for triggering plasticity at a subset of synapses.

Introduction

Glutamate is the primary excitatory chemical transmitter in the mammalian central nervous system (CNS), where it is essential for neuronal viability, network function, and behavioural responses (1). Glutamate activates a variety of pre- and postsynaptic receptors, including ionotropic receptors (iGluRs) that form ligand-gated cation-permeable ion channels. The iGluR superfamily includes α-amino-3-hydroxy-5-methyl-4-isoxazolepropionic acid receptors (AMPARs), kainate receptors, and N-methyl-D-aspartate receptors (NMDARs), all of which form tetrameric assemblies that are expressed throughout the CNS (2).

NMDARs exhibit high sensitivity to glutamate (apparent EC_{50} in the micromolar range) and voltage-dependent block by Mg^{2+} (3, 4), slow gating kinetics (5), and high permeability to Ca^{2+} (6, 7) (for a review, see (8)). Together, these characteristics confer postsynaptic NMDARs with the ability to detect and decode coincidental activity of pre- and postsynaptic neurons: presynaptic glutamate release bringing about occupation of the agonist-binding site and AMPAR-driven postsynaptic depolarization removing voltage-dependent Mg^{2+} block. The coincidence of these two events leads to NMDAR activation and Ca^{2+} influx through the channel (8, 9), which initiates several forms of synaptic plasticity (10, 11).

Large-conductance Ca^{2+}- and voltage-gated K^+ (BK) channels are opened by a combination of membrane depolarization and relatively high levels of intracellular Ca^{2+} (12, 13). In CNS neurons, such micromolar Ca^{2+} increases are usually restricted to the immediate vicinity of Ca^{2+} sources, including voltage-gated Ca^{2+} channels (VGCCs) (14-16) and ryanodine receptors (RyRs) (17, 18). In addition, Ca^{2+} influx through non-selective cation-permeable channels, including NMDARs, has also been shown to activate BK channels in granule cells from the olfactory bulb and dentate gyrus (19-21). In these neurons, Ca^{2+} entry through NMDARs opens BK channels in somatic and perisomatic regions, causing repolarization of the surrounding plasma membrane and subsequent closure of NMDARs. Because BK channel activation blunts NMDAR-mediated excitatory responses, it provides a negative feedback mechanism that modulates the excitability of these neurons (19, 20). Thus, the same characteristics that make NMDARs key components in excitatory synaptic transmission and plasticity can paradoxically give rise to an inhibitory response when NMDARs are located in the proximity of BK channels. However, it is unclear whether functional NMDAR–BK coupling is relevant at dendrites and dendritic spines.

The barrel field area in the primary somatosensory cortex, also known as the barrel cortex (BC), processes information from peripheral sensory receptors for onward transmission to cortical and subcortical brain regions (22, 23). Sensory information is received in the barrel cortex from different nuclei of the thalamus. Among these nuclei, ventral posterior medial nucleus, ventrobasal nucleus, and posterior medial nucleus are known to directly innervate layer 5 pyramidal neurons (BC-L5PNs) (24-27). In basal dendrites of BC-L5PN, coactivation of neighboring dendritic inputs can initiate NMDAR-mediated dendritically-restricted spikes characterized by large Ca^{2+} transients and long-lasting depolarizations (28-30), providing the appropriate environment for BK activation.

To determine whether functional NMDAR–BK coupling plays a role in synaptic transmission, and potentially synaptic plasticity, we investigated the thalamocortical synapses at basal dendrites of BC-L5PNs. We found that suppression of NMDAR activity by BK channels occurs in the basal dendrites of about 40% of BC-L5PNs, where NMDAR activation triggers strong negative feedback inhibition by delivering Ca^{2+} to nearby BK channels. This inhibition regulates the amplitude of postsynaptic responses and increases the threshold for induction of synaptic plasticity. Our findings thus unveil a calibration mechanism that can decode the amount and frequency of afferent synaptic inputs by selectively attenuating synaptic plasticity and providing input-specific synaptic diversity to a thalamocortical circuit.

Main Text

Results

NMDAR activation opens BK channels in BC-L5PN basal dendrites

To investigate whether NMDA receptors are functionally coupled to other channel types in the basal dendrites of BC-L5PNs, we obtained whole-cell voltage-clamp recordings from pyramidal neurons located beneath layer 4 barrels in acute mouse brain slices (n = 108) (Figure 1A). Localization and large pyramidal-shaped somata suggest that we predominantly recorded from layer 5a neurons. In the presence of Mg^{2+}-free ACSF supplemented with tetrodotoxin (TTX; 1 µM) and glycine (10 µM), puff application of 200 µM NMDA to the basal dendrites of BC-L5PNs evoked a NMDAR-resembling inward current in all neurons (Figure 1B). Remarkably, about 40% of the BC-L5PNs developed a slower outward current at holding potentials more positive than -40 mV (Figure 1B), which showed a clear dependence on membrane voltage (Figure 1C). These two populations of BC-L5PNs were assigned as A-type neurons (lacking the outward current; n = 65, 60.2%) and B-type neurons (showing the outward current; n = 43, 39.8%). Inward current amplitude was directly proportional to the holding potential in both populations (Figure 1D, left), indicating that a similar molecular species carries the inward current in both neuronal types. Interestingly, activation of the outward current in B-type neurons significantly reduced net inward current flow, decreasing the inward charge transfer (Figure 1D, right). When NMDA was applied at the same distance from the soma as previously but towards layer 4, only inward current was observed (Figure S1). These results suggest that NMDA can evoke an outward current in the basal dendrites of B-type BC-L5PNs, but not in the soma, oblique/truncated dendrites, or initial segment of the apical dendrite. Our findings are in contrast to what has been found in other neurons such as hippocampal CA1 pyramidal cells, where NMDA-dependent outward currents were observed at the soma (21) but not at dendrites (Figure S2).

We performed the pharmacological characterization of inward and outward currents in B-type neurons at a holding potential of -20 mV (Figure 1E). The complete abrogation of inward current by the selective NMDAR antagonist D-AP5 (100 µM) confirmed that it was due to cation flow through NMDARs. Moreover, because outward current was also abolished in the presence of AP5, we surmised that NMDAR activation is mandatory for outward current generation (Figure 1E and 1F). Selective inhibition of GluN2A- or GluN2B-containing NMDARs using 100 nM $ZnCl_2$ or 5 µM ifenprodil, respectively, partially suppressed the outward current (Figures 1E and 1F). This suggests that inward current flow through both GluN2A- and GluN2B-containing NMDARs leads to activation of the outward current in B-type neurons.

The voltage dependence and direction of net ionic flow (Figure 1C) suggests that NMDAR-dependent outward current is driven by a voltage-dependent K^+ channel. Because this current is reminiscent of that carried by BK channels in granule cells from the olfactory bulb and dentate gyrus (19, 20), we applied NMDA to basal dendrites of BC-L5PNs in the presence of the specific BK channel pore blocker paxilline (1 µM) (31). Paxilline completely abolished the NMDAR-dependent outward current without eliminating the inward component, suggesting that NMDAR activation in the basal dendrites of B-type neurons causes BK channels to open, and therefore that NMDARs and BK channels are functionally coupled.

NMDARs and BK channels are within functional proximity in B-type BC-L5PNs

Our results suggested that activation of NMDARs in the basal dendrites of B-type BC-L5PNs provides the Ca^{2+} needed to activate BK channels. To confirm this hypothesis, we recorded NMDA-evoked current in the presence of the intracellular Ca^{2+} chelators BAPTA and EGTA, which we delivered through the recording pipette. BAPTA and EGTA are useful biochemical tools to estimate the linear distance that Ca^{2+} diffuses from its source (32). This approach has been previously used to calculate the distance between channels in BK-VGCC macrocomplexes (e.g., (33, 34); see also (14) and references within). Both chelators present similar affinities for Ca^{2+} but BAPTA has a faster association rate than EGTA. Therefore, outward current through BK channels would be recorded in the presence of EGTA, but not BAPTA, if both channels are located in close proximity. If the distance between both channels is larger, Ca^{2+} entering through NMDARs would be captured by both chelators before reaching BK, and no outward current would be observed. Taking into account the dendritic complexity of pyramidal neurons, we used higher concentrations of chelators than those described in previous studies assessing NMDAR-BK somatic associations in hippocampal neurons (20).

We failed to observe NMDA-induced outward currents in any BC-L5PNs in the presence of 15 mM BAPTA (Figure 2A and 2D), confirming that Ca^{2+} entry through NMDARs is responsible for activation of BK channels. However, when the slower chelator EGTA was used at the same concentration, two populations of BC-L5PNs could be distinguished (Figure 2B). As in control conditions, the outward current in B-type neurons activated at holding potentials positive to -40 mV and exhibited a clear dependence on membrane voltage, but its amplitude was significantly reduced due to substantial Ca^{2+} chelation (compare Figure 2E with Figure 1C). When BAPTA concentration was reduced to 1 mM, outward current could again be recorded (Figure 2C) and was quantitatively identical to that obtained in control conditions (compare Figure 2F with Figure 1C). Using described Ca^{2+} linear diffusion data in the presence of BAPTA and EGTA (32), we estimated that NMDAR and BK channels are located within 15-60 nm of each other in the basal dendrites of B-type BC-L5PNs (Figure 2G); in close enough proximity to explain the specific functional coupling that we observed.

Both GluN2A- and GluN2B-containing NMDARs can functionally couple to BK channels

Because GluN2 subunits determine the deactivation kinetics and ion conductance of NMDARs (35), we reasoned that the molecular composition of NMDARs might affect NMDAR-BK coupling efficiency. We first tested whether BK preferentially associates with specific NMDAR subunit combinations using a proximity ligation assay (PLA). In agreement with our pharmacological data (Figure 1F), positive PLA signals were observed for HEK293T cells co-expressing BK and either GluN1/GluN2A or GluN1/GluN2B NMDARs (Figure 3A), without any preference between GluN2A and GluN2B subunits (Figure 3B).

Having confirmed that NMDARs and BK channels are located in close proximity in the plasma membrane when co-expressed in HEK293T cells, we characterized functional coupling between specific channel/subunit combinations. By using the inside-out configuration of the patch-clamp technique, we were able to monitor channel function while controlling 'intracellular' Ca^{2+} concentration in the bath solution (36). NMDARs were activated by including 200 µM NMDA and 10 µM glycine in the 'extracellular' pipette solution. Under these conditions, desensitization of NMDAR is significantly reduced (37). The relative conductance (G) of BK channels exposed to different intracellular Ca^{2+} concentrations (from 0 to 100 µM) in patches from cells expressing BK channels but no NMDARs (Figure 3C) corresponded to typical Ca^{2+}-dependent activation curves for these channels (38, 39). We reasoned that addition of Ca^{2+} to the intracellular side of the patch through a Ca^{2+} source such as NMDARs would result in a leftward shift of the BK activation curve in zero Ca^{2+} bath solution. This would be favoured if the channels were closely located, allowing Ca^{2+} to activate BK before being diluted in the large Ca^{2+}-free bath solution (following an analogous reasoning than the experiments using chelators above). Indeed, co-expression of BK channels with either GluN1/GluN2A or GluN1/GluN2B NMDARs produced a significant leftward shift of the BK activation curve (Figure 3D). Interestingly, the shift resulted in an activation curve comparable to that recorded with 10 µM intracellular Ca^{2+} in patches expressing BK alone (Figure 3E and Table S1). Of note, the reduction of the driving force for Ca^{2+} at very positive voltages was not paralleled by diminished values in the G-V curves, as is commonly observed in VGCC-BK coupling experiments (15), probably due to increased permeation of K^+ through NMDAR (40). These results suggest that NMDAR activation increases Ca^{2+} concentration in the close vicinity of BK channels, favouring their activation.

NMDARs are non-selective cation channels that are permeable to Na^+, K^+, and Ca^{2+} (2, 8). Under physiological conditions, the proportion of NMDAR current carried by Ca^{2+} corresponds to 10-15% of the total current (41-43). However, because the above-mentioned inside-out patch experiments were performed in the absence of Na^+, inward current through NMDARs could only be due to Ca^{2+} ions, whose permeability is increased as extracellular Na concentration is reduced (7). We may therefore be overestimating the effects of NMDAR-

dependent Ca^{2+} activation on BK channels in our zero Na^+ experimental conditions.
Nevertheless, activation of GluN1/GluN2A or GluN1/GluN2B NMDARs in excised inside-out patches using physiological concentrations of Na^+ still produced a leftward shift in the BK activation curve (Figures 3F–3H). Interestingly, GluN1/GluN2B produced larger shifts than GluN1/GluN2A.

Taken together, these results demonstrate that both GluN2A- and GluN2B-containing NMDARs can provide sufficient Ca^{2+} for BK activation, consistent with our data from BC-L5PN basal dendrites (Figure 1F).

A subpopulation of regular-spiking BC-L5PNs exhibit NMDAR–BK functional coupling
BC neurons can be classified into fast-spiking nonpyramidal GABAergic interneurons and regular-spiking or intrinsically-bursting pyramidal neurons according to their electrophysiological properties (24, 44, 45). Regular-spiking neurons from layers 5 and 6, where regularly-timed trains of action potentials are observed in response to somatic current injection, can be further characterized by the presence or absence of a depolarizing afterpotential known as a Ca^{2+} spike (24, 46). To determine whether NMDAR–BK functional coupling is restricted to a specific neuronal subtype, we performed whole-cell current-clamp recordings in regular-spiking BC-L5PNs in mouse brain slices (n = 197) in the presence of physiological concentrations of Mg^{2+} and Ca^{2+}. By inducing single action potentials in BC-L5PNs, we confirmed the presence of two populations of neurons that either exhibited a Ca^{2+} spike (n = 130, 66.0%) or not (n = 67, 34.0%) (Figure 4A and 4B), similar to those previously described (24, 46, 47).

We next investigated whether these two populations of BC-L5PNs could be correlated with NMDAR–BK functional coupling by subsequently perfusing the brain slices with a Mg^{2+}-free solution supplemented with TTX (1 μM) and glycine (10 μM). Voltage clamp recordings were carried out in the same neurons upon puff application of NMDA to their basal dendrites (Figure 4C). None of the BC-L5PNs exhibiting a Ca^{2+} spike presented an outward current in response to NMDAR activation. Conversely, all BC-L5PNs lacking a Ca^{2+} spike showed a robust BK outward current after NMDA application (Figures 4B and 4C). No further intrinsic or evoked differences were observed between A-type and B-type neurons (Figures 4D–4I), except for those that were directly related to the presence of the Ca^{2+} spike (Figures 4J and 4K). We therefore conclude that the presence of NMDAR–BK coupling in basal dendrites is restricted to a population of regular-spiking BC-L5PNs that are characterized by the absence of Ca^{2+} spikes.

BK-dependent inhibition of NMDARs reduces amplitude and slows down kinetics of the postsynaptic response
Having demonstrated that BK channels in the basal dendrites of BC-L5PNs are activated after Ca^{2+} entry through proximal NMDARs, we predicted that this coupling would give rise to a negative feedback loop similar to that described for the coupling of VGCCs and BK channels in presynaptic terminals (48) or NMDARs and small-conductance Ca^{2+}-activated K^+ channels (SK) in postsynaptic terminals (49). In such a scheme, NMDAR activation and subsequent entry of Ca^{2+} would open BK channels, which would repolarize the membrane due to outward flux of K^+ and therefore reinstate voltage-dependent Mg^{2+} block of NMDARs, in turn truncating Ca^{2+} entry. If that were the case, the presence of postsynaptic NMDAR–BK coupling in B-type neurons should have a significant impact on synaptic transmission. Indeed, our finding that BK activation reduced NMDAR-mediated inward current in B-type neurons (Figure 1D) suggested the presence of such a negative feedback loop.

To investigate the effect of NMDAR–BK coupling on synaptic transmission, we electrically stimulated the afferent inputs to BC-L5PN basal dendrites and recorded evoked postsynaptic potentials (PSPs) in physiological conditions (with Mg^{2+} in the external solution). Presynaptic stimulation of basal afferent inputs was performed at the limit between layers 5 and 6 to activate ascending thalamocortical fibers (50, 51), many of which are known to make direct contacts with BC-L5PNs (24-27). The presence or absence of a Ca^{2+} spike in evoked action potentials allowed us to classify BC-L5PNs as either A-type or B-type. Stimulation intensity was then adjusted to obtain 3-5 mV PSPs in all recorded neurons (Figure 5A). These values correspond to depolarizations of >30 mV occurring at basal dendrites, taking into account the signal attenuation from dendrites to the soma (28, 29). BK channel block using bath perfusion of 1 μM paxilline increased PSP amplitude and slowed PSP kinetics (Figure 5B) (but only in B-type neurons), suggesting an increase of postsynaptic NMDAR availability in B-type neurons. Although a selective inhibition of BK channels at presynaptic sites that target B-type neurons cannot be excluded, the lack of any effect of paxilline on PSPs in A-type neurons, characterized by the absence of NMDAR-BK functional complexes, supports the absence of effects of presynaptic BK channels in the synapses we studied. Further addition of AP5 (100 μM) to the perfusate accelerated PSP kinetics and completely abolished the PSP amplitude increase below control levels (Figure 5B), revealing that the AMPAR component is not increased in our experimental conditions. In summary, this data suggests that NMDAR-dependent activation of postsynaptic BK channels reduces the contribution of NMDARs to PSPs, thereby regulating synaptic transmission.

Coactivation of clustered neighboring basal inputs to BC-L5PNs initiates local dendritic NMDAR-dependent spikes that are characterized by large Ca^{2+} transients (28, 30). We induced NMDA-dependent Ca^{2+} spikes by increasing the stimulation intensity applied to the afferent inputs to BC-L5PN basal dendrites while blocking action potentials by including the Na^+ channel blocker QX-314 (2 mM) in the recording pipette. As expected, larger PSPs were observed in these experimental conditions (Figure 5C). Paxilline (1 μM) induced a further increase in PSP amplitude in B-type neurons but had no effect on A-type neurons (Figures 5C and 5D). Further addition of AP5 (100 μM) reversed the PSP amplitude increase in B-type neurons to below control values and to a similar amplitude in both neuronal types (Figures 5C and 5D). It must be noted that in our experimental conditions we may be underestimating this effect, taking into account that QX-314 may partially inhibit BK channels, similarly to other quaternary ammonium compounds. These results demonstrate that BK channels in the basal dendrites of B-type neurons are able to abrogate NMDAR current, including under conditions where NMDAR spikes are taking place.

NMDAR–BK coupling increases the threshold for induction of synaptic plasticity
The inhibitory effect of NMDAR–BK coupling on synaptic transmission in BC-L5PNs led us to wonder whether it may play a role in other physiological mechanisms, including forms of long-term synaptic plasticity involving NMDAR activation (10, 11). Spike-timing-dependent plasticity (STDP) is one such mechanism and relies on the precise coincidence of presynaptic and postsynaptic activity (11, 52). The timing and order of presynaptic and postsynaptic action potentials determine the direction of the change in synaptic strength: a presynaptic action potential followed by a postsynaptic action potential within a window of tens of ms results in long-term potentiation (LTP), whereas the reverse order within a similar timeframe results in long-term depression (LTD) (11, 52, 53). Both mechanisms are dependent on NMDAR activation (54) but only spike-timing-dependent LTP (t-LTP) depends on postsynaptic NMDAR activation and the consequential rise in dendritic spine Ca^{2+} concentration (54) (Figure S3). Therefore, this experimental approach allowed us to restrict our study to the postsynaptic mechanisms related to NMDAR-BK functional coupling. Because NMDAR activity is blunted by BK activation in the basal dendrites of B-type BC-L5PNs, we hypothesized that t-LTP would be less prominent in these neurons compared to A-type BC-L5PNs, or possibly absent. We therefore studied the effects of pairing pre- and postsynaptic action potentials in A-type and B-type BC-L5PNs.

We measured PSPs evoked by electrical stimulation of basal afferent inputs to BC-L5PNs before and after pre–post pairings at 0.20 Hz (Figure 6A). A low number of pre–post associations (30 pairings) induced t-LTP in A-type but not B-type neurons (Figure 6B, left). This is consistent with a reduction in the amount of Ca^{2+} entering the basal dendrites of B-type neurons due to NMDAR-dependent activation of BK channels. The difference between the two populations was abolished when 500 nM paxilline was included in the recording pipette (Figure 6B, right), suggesting that the release of NMDARs from BK-induced negative feedback favours t-LTP by reducing the threshold for its induction. This action of paxilline applied to the postsynaptic cell is enough to abolish the BK channel effect on plasticity. Although paxilline crosses cell membranes and could therefore conceivably affect BK channels beyond the patched cell, both dilution by the larger extracellular volume fraction and bath perfusion, and reduced efficiency of inhibition from the external side of the membrane (31) would all serve to reduce any paxilline reaching neighbouring cells to negligible levels. The degree of t-LTP in both neuronal types in the presence of paxilline was significantly greater than that elicited in A-type neurons in control conditions (Figure 6B, right versus left).

consistent with the key role of BK channels in the regulation of neuronal excitability (12). Interestingly, these data imply that BK channels are functionally expressed in both A-type and B-type BC-L5PNs, which we confirmed by recording BK currents in both types of BC-L5PN (Figure S4).

As our data indicated that NMDAR–BK coupling is restricted to the basal dendrites of BC-L5PNs, we asked whether the difference in synaptic plasticity threshold between A-type and B-type neurons was limited to basal dendrites, or could also occur in apical dendrites. We electrically stimulated the afferent inputs to the apical dendrites of BC-L5PNs (Figure 6C) and carried out 30 pre–post pairings at 0.20 Hz. This failed to induce synaptic plasticity in any of the neurons tested (Figure 6D, left), but when the number of pre–post pairings was increased to 90, t-LTP was induced in both types of neurons (Figure 6D, right). The potentiation was of a similar amplitude in both A- and B-type neurons, but significantly lower than that induced in basal dendrites by 30 pairings (compare Figure 6D, right with Figure 6B, left). These results confirm that functional NMDAR–BK coupling occurs exclusively in the basal dendrites of B-type BC-L5PNs, where it increases the threshold for synaptic plasticity and therefore modulates neuronal circuits involving these dendrites.

A high number and frequency of pre–post pairings relieves BK-dependent NMDAR inhibition

Our results indicated that BK reduces, but does not completely abolish, the influx of ions through NMDARs, and therefore increases the threshold for the induction of synaptic plasticity (Figure 6B). We reasoned that by tuning the experimental conditions to induce greater NMDAR activation, the concentration of Ca^{2+} in postsynaptic terminals would eventually reach sufficient levels to induce plasticity in B-type BC-L5PNs. In A-type neurons, increasing the number of pre–post pairings to 50 or 90 increased the extent of t-LTP, as previously described in other brain areas including the hippocampus (55-57). Importantly, we were also able to induce t-LTP in B-type neurons by increasing the number of pre–post associations (Figure 7A), confirming that sufficient NMDAR activation can overcome the higher threshold for plasticity in these neurons. However, the extent of PSP potentiation in B-type neurons was significantly less than in A-type neurons for a given number of pairings (Figure 7B). These results therefore demonstrate that NMDAR–BK coupling regulates the threshold to induce synaptic plasticity in the basal dendrites of B-type BC-L5PNs.

The magnitude of t-LTP can be also regulated by changing the frequency or modifying the time window of pairings (9, 54), although the latter results in considerable STDP variability depending on the synapse studied (9). We hypothesized that by increasing the frequency of pairings, a condition would be reached where the inhibitory effect of BK on NMDARs completely disappears. For this purpose, we applied 30, 50, and 90 pairings at a frequency of 0.33 Hz (pre–post pairings delivered every 3 s) and found that the degree of t-LTP in each condition was greater than that at 0.20 Hz for both types of neurons (compare Figure 7C with Figure 7A). Furthermore, there was no difference in the extent of PSP potentiation between A-type and B-type neurons following the delivery of 90 pairings (Figure 7D). Thus, the inhibitory effect of BK on NMDARs can be abolished with high rates of pre- and postsynaptic coincident activity. Moreover, although t-LTP appeared to saturate following 50 pairings in A-type neurons subjected to 0.33 Hz stimulation, B-type BC-L5PNs remained able to discriminate between the number of pairings in the protocol.

Discussion

We have described the functional association of NMDARs and BK channels, and the role of this coupling in synaptic function, in the basal dendrites of a population of regular-spiking BC-L5PNs. NMDAR activation and subsequent Ca^{2+} entry promotes BK opening, which repolarizes the cell membrane and halts NMDAR activity. Both GluN2A- and GluN2B-containing NMDARs can activate BK channels, although our data suggest that GluN2B-containing NMDARs are more efficient. Functional coupling of NMDARs and BK channels in the basal dendrites of this specific BC-L5PN population modulates synaptic transmission and produces an increase in the threshold for induction of synaptic plasticity, indicating that NMDAR–BK association critically influences how specific neuronal types integrate afferent synaptic inputs. In fact, NMDAR–BK functional coupling bestows B-type BC-L5PNs with the ability to work as high-pass filters of incoming inputs, depending on the number and frequency of afferent stimuli.

In the CNS, BK channels can couple to different Ca^{2+}-conducting channels, including VGCCs (14-16) and RyRs (17, 18). Such Ca^{2+} sources provide the Ca^{2+} needed for BK activation, but membrane depolarization is generally provided by a coincident action potential (48). Interestingly, NMDAR activation can provide both the membrane depolarization and the Ca^{2+} entry required for BK activation (8), particularly in restricted compartments such as the dendritic spine, where Ca^{2+} concentrations reach micromolar levels after NMDAR activation (58, 59). In contrast to previous studies using Mg^{2+}-containing ACSF (19, 20), we initially observed functional association of NMDARs and BK channels in the absence of Mg^{2+}. These data revealed that NMDAR-dependent BK activation occurs at potentials positive to -40 mV, within a range of potentials at which the NMDAR-dependent current is maximal (3, 4). This was subsequently corroborated in synaptic transmission experiments performed in the presence of Mg^{2+}, in which inhibition of NMDARs by BK channels became evident.

Consistent with previous studies (19, 20), our results showed that NMDAR-mediated increases in Ca^{2+} concentration are required in the immediate vicinity of BK channels in order to influence their activation. Thus, the coupling mechanism relies on the close proximity of NMDARs and BK channels in the plasma membrane. Our experiments using Ca^{2+} chelators allowed us to estimate that the two proteins must be situated within 15-60 nm of each other for functional coupling to occur. However, this estimate must be taken with caution, as the exact concentration of chelators that reach dendrites is not known. In fact, our experiments using PLAs suggest that the maximum distance between the two channels may be even shorter (below 40 nm). Close association of these channels in the soma has been also shown by co-immunoprecipitation and biochemical approaches (20). Our results demonstrate strong functional coupling between NMDARs and BK channels in basal dendrites of BC-L5PNs, regardless of whether the channels physically interact with each other. Further work is needed to determine what fraction of this functional association is due to looser coupling and/or the summation from multiple NMDARs.

Our work provides the first evidence for a functional role of NMDAR–BK coupling in neuronal dendrites. This result differs from previous studies in which functional coupling between NMDARs and BK channels has been observed in the soma of granule cells from the olfactory bulb (19) and dentate gyrus (20). Some evidence also points to NMDAR–BK interactions in hippocampal CA1 pyramidal neuron somata (21) but not dendrites(49) (Figure S2). At the soma, NMDAR-dependent activation of BK channels would likely constitute a mechanism that regulates action potential shape, and controls neuronal excitability, independently of dendritic input.

In dendrites, NMDAR–BK coupling would generate a negative feedback mechanism that could have dramatic effects on synaptic transmission and forms of synaptic plasticity that involve NMDARs and Ca^{2+} entry. Here we have demonstrated that B-type BC-L5PNs exhibiting NMDAR–BK functional coupling show reduced synaptic transmission and have a higher threshold for the induction of long-term synaptic plasticity. This phenomenon of selective plasticity attenuation is restricted to the basal dendrites of these neurons, as the effect was not observed when afferent inputs to apical dendrites were stimulated. Similar basal versus apical polarity differences that affect synaptic input integration have been described in other brain areas, including the hippocampus (60).

A concern from this study might be the potential confounding factor of presynaptic BK channels, which may impact on the amount of glutamate released. Although our experiments do not specifically address the presence of BK channels at presynaptic sites in thalamic neurons projecting onto BC-L5PN, the lack of paxilline effects on A-type PSPs supports the absence of effects of presynaptic BK channels in the synapses we studied. Two additional lines of evidence suggest a dominant role for postsynaptic NMDA-BK complexes: the modification in PSP kinetics after paxilline application exclusively in B-type neurons (Figure 5) and the selective effect of intracellular paxilline on post-synaptic plasticity in B-type neurons (Figure 6).

The interpretation of our results must take into account the possible influence of other coupling mechanisms involving BK and additional ion channels at dendrites. For instance, our experiments do not rule out the possibility that dendritic VGCC (61) or NMDAR-uncoupled BK channels may partially contribute to modulate the observed effects. Interestingly, a recent study suggests that SK-mediated inhibition of NMDARs is a general mechanism that regulates synaptic plasticity associated with BC-L5PN to BC-L5PN communication (62). This backward regulatory mechanism affects intralayer communication between regular-spiking BC-L5PNs and depends on back-propagating action potentials rather than NMDA activation. Although we cannot exclude a contribution from this process, there are three lines of evidence to suggest that the majority of effects we describe are due to NMDAR–BK coupling: (i) NMDAR activation resulted only in BK channel-mediated current; (ii) BK-specific inhibition completely abolished the I-LTP differences between A-type and B-type BC-L5PNs; and (iii) BK-mediated inhibition of NMDARs remained when basal afferent inputs were electrically stimulated and was independent of back-propagating action potentials. Therefore, although two different mechanisms for inhibition of NMDARs may be present in the basal dendrites of BC-L5PNs, our data strongly suggest that NMDAR–BK modulation of synaptic transmission and long-term synaptic plasticity is a forward regulatory mechanism involving thalamocortical projections to a restricted population of BC-L5PNs in conditions where prior activation of postsynaptic NMDARs is mandatory and action potentials are not required.

We used a low frequency STDP protocol to induce LTP in our study. Under these experimental conditions, it has been proposed that GluN1/GluN2B NMDARs make a larger contribution to the total charge transfer than GluN1/GluN2A NMDARs (63), as expected from the slower deactivation rates of GluN2B-containing NMDARs (35). Taking this into account, GluN2B-containing NMDARs should conduct more Ca^{2+} than GluN1/GluN2A channels in our experimental conditions, activating BK more efficiently. That being the case, Ca^{2+} entry through GluN2B-containing NMDARs would be the main contributor to BK activation and thus the inhibitory mechanism underlying modulation of synaptic transmission and LTP. This notion corresponds with our heterologous expression experiments using physiological concentrations of extracellular Na^+, in which GluN1/GluN2B NMDARs produced a larger leftward shift in the BK activation curve than GluN1/GluN2A. It also correlates with our observations in basal dendrites of BC-L5PNs, where specific blockade of GluN2B-containing NMDARs produced a larger reduction in the NMDA-evoked outward current. In summary, we have demonstrated that GluN2A- and GluN2B-containing NMDARs are able to activate BK channels in both heterologous expression systems and the basal dendrites of BC-L5PNs. Whether B-type neurons express a combination of GluN1/GluN2A and GluN1/GluN2B heteromers, or GluN1/GluN2A/GluN2B triheteromers (8), requires further investigation.

An interesting question arises from the observation that functional NMDAR–BK association is exclusive to the basal dendrites of a subpopulation of regular-spiking BC-L5PNs: is it associated with the specific expression of particular GluN2 subunits? Although the role of GluN2C and GluN2D subunits was not investigated, a differential distribution of these, and other, subunits between A-type and B-type neurons would be reflected in the macroscopic NMDAR conductance, which is similar in both A-type and B-type BC-L5PNs. Therefore, we believe that both populations of BC-L5PNs exhibit a similar distribution of GluN2 subunits. Why, then, do NMDAR–BK associations occur only in the basal dendrites of B-type neurons? As both cell types express BK channels and NMDARs, a plausible explanation is that B-type neurons exhibit a distinct mechanism to target specific channels to dendritic compartments. This could be achieved by engaging scaffolding proteins, such as the receptor for activated C kinase 1 (RACK1) and caveolin-1, which are known to bind both the GluN2B NMDAR subunit (64, 65) and BK channels (66, 67). In addition, we observed a larger BK current in B-type than in A-type neurons, suggesting a higher abundance of BK channels in their membrane. Therefore, it is tempting to speculate that the formation of complexes and their targeting to the basal dendrites of B-type neurons depends on the overall abundance of BK channels and thus their availability to couple to NMDARs.

In this study, we uncover two populations of regular-spiking BC-L5PNs that are distinguished by the absence (A-type, ~64%) or presence (B-type, ~36%) of NMDAR–BK functional coupling in basal dendrites. Interestingly, this distribution resembles the electrophysiological characteristics and neuronal ratio of two previously described populations of mouse and rat BC-L5PNs, which were classified according to the presence or absence of a Ca^{2+} spike (24, 46, 47). Functional NMDAR–BK coupling is exclusive to the basal dendrites of B-type neurons (Figure 8), which exhibit a higher threshold for the induction of LTP due to BK-dependent inhibition of NMDARs. A-type neurons lack this molecular brake, and therefore reach saturation at a lower stimulation frequency, independent of the number of synaptic inputs. This leads us to propose that BK-dependent inhibition of NMDARs endows B-type neurons with a calibration mechanism that allows them to decode the number and frequency of afferent synaptic inputs using selective synaptic plasticity attenuation. As a result of this discrimination capability, we hypothesize that the basal dendrites of B-type BC-L5PN function as high-pass filters of thalamic afferent inputs, displaying the same output as A-type neurons when a strong stimulus or series of stimuli reach the dendrites (such as during high levels of pre- and postsynaptic coincident activity), but attenuating signals below a specific stimulation threshold. This cutoff would be mainly determined by the number of BK channels that are available to functionally couple to NMDARs in the basal dendrites of B-type neurons: the larger the number of available BK channels, the higher the threshold for induction of synaptic plasticity. This mechanism would provide B-type BC-L5PNs with a dynamic range of output responses for the same afferent input stimuli, thus increasing the computational power of the somatosensory cortex.

In summary, we have demonstrated that functional coupling of NMDARs and BK channels in the basal dendrites of a specific set of BC-L5PNs modulates synaptic transmission and synaptic plasticity in thalamocortical circuits. This finding unmasks the critical influence that functional association of ion channels can have on the integration of afferent synaptic inputs by neurons.

Methods

Animal procedures and brain slices preparation

All experimental procedures were approved by and carried out in accordance with University de La Laguna (ULL) Ethics Committee (CEIBA), Spanish (RD 53/2013) and European Commission (2010/63/EU) animal care guidelines. C57BL/6J mice (The Jackson Laboratory #000664) were housed in standard laboratory cages with *ad libitum* access to water and food in temperature- and humidity-controlled rooms under a 12:12 h light-dark cycle at the ULL animal facilities (registry number ES380230024514). C57BL/6J adult male mice (postnatal 28-36) were slightly anesthetized with isoflurane, decapitated, and the brain quickly removed and immersed in an ice-cold high-sucrose solution (in mM: 189 sucrose, 10 glucose, 26 $NaHCO_3$, 3 KCl, 5 $MgSO_4$, 0.1 $CaCl_2$, and 1.25 NaH_2PO_4), continuously bubbled with carbogen (95% oxygen/5% carbon dioxide). Coronal brain slices (350 µm) were obtained using a Microm HM650V vibratome (Thermo Scientific). Slices were maintained for 1-1.5 h in artificial cerebrospinal fluid (ACSF; in mM: 124 NaCl, 2.69 KCl, 1.25 KH_2PO_4, 2 $MgSO_4$, 26 $NaHCO_3$, 10 glucose, 2 $CaCl_2$, and 0.4 ascorbic acid; pH 7.35) bubbled with carbogen at room temperature (22-24°C).

Electrophysiology in brain slices

Electrophysiological recordings in brain slices were performed using the whole-cell configuration of the patch-clamp technique (68) in a recording chamber mounted onto an upright Olympus BX51WI microscope (Olympus), where they were continuously perfused with carbogen-bubbled ACSF. Patch pipettes were made from 1.50 OD/0.86 ID borosilicate glass capillaries (GC150F-10; Harvard Apparatus) using a P-97 micropipette puller (Sutter Instruments) and had resistances of 5-8 MΩ when filled with the internal solution (in mM: 135 $KMeSO_4$, 10 KCl, 10 HEPES, 5 NaCl; 2.5 ATP-Mg, and 0.3 GTP-Na; pH 7.3). Series resistance was compensated (≈70%) and recordings were discarded when the access resistance varied >20% during the experiment. Data were acquired at 10 kHz and lowpass-filtered at 4 kHz with a MultiClamp 700A amplifier (Molecular Devices) through an Axon Digidata 1550B interface board (Molecular Devices), controlled by pClamp software (Molecular Devices). All experiments were performed at room temperature (22-24°C). Pyramidal neurons from layer 5 of the somatosensory 1 barrel field area (S1BF) were visualized by infrared microscopy and differential interference contrast (IR-DIC) using an ORCA-Flash4 0LT digital camera (Hamamatsu). Barrel cortex layer 5 pyramidal neurons (BC-L5PN) were identified by their location (just below layer 4), shape (characteristic somatic morphology), and electrophysiological properties (only regular-spiking neurons were used in the study; intrinsically-bursting and fast-spiking neurons were discarded), suggesting that we predominantly recorded from slender-tufted neurons located in layer 5a, as described previously (50, 51).

Currents evoked by NMDA application at different holding potentials (from -60 to 0 mV) were recorded from BC-L5PN using the voltage-clamp mode in the whole-cell configuration of the patch-clamp technique in Mg^{2+}-free ACSF (by replacing Mg^{2+} with Ca^{2+}), supplemented with tetrodotoxin (TTX; 1 µM) and NMDAR coagonist glycine (10 µM). NMDA (200 µM) was locally delivered (puff-application) at different dendritic locations of BC-L5PN through a glass pipette (GC150F-10 borosilicate glass capillaries) using a PMI-100 Pressure Microinjector (Dagan Corporation) at 1 bar during 50-200 ms. The duration of the NMDA puff-application was adjusted to obtain inward currents of 200-250 pA peak amplitude at -60 mV. NMDA-evoked inward currents (I_{Inward}) were measured as the maximum peak amplitude. NMDA-evoked inward and outward total ionic charges (Q_{Inward}, $Q_{Outward}$) were calculated as the area under the trace. In the experiments where BAPTA (15 or 1 mM) and EGTA (15 mM) Ca^{2+} chelators were added to the recording pipette, $KMeSO_4$ was equimolarly replaced by BAPTA-K or EGTA-K to maintain the total internal K^+ concentration.

BC-L5PN action potentials were recorded using the current-clamp mode in the whole-cell configuration of the patch-clamp technique in normal ACSF (including 2 mM $MgSO_4$ and 2 mM $CaCl_2$) as indicated in Figure legends. Resting membrane potential, action potential firing, and cell input resistance were calculated from these recordings. Individual action potentials were evoked either by presynaptic electrical stimulation of basal afferent inputs or by a brief current injection through the recording pipette (5 ms, 200-400 pA). No differences between both methods were observed (Fig. S5A). Action potential characteristics were calculated from these recordings (Figure S5).

Postsynaptic potentials (PSP) were obtained by presynaptic electrical stimulation of basal afferent inputs in the limit between layers 5 and 6 (50, 51). Stimulation pipettes were made from 1.50 OD/1.02 ID thick septum theta borosilicate glass capillaries (TST150-6; World Precision Instruments) using a P-97 micropipette puller and filled with ACSF. Single pulses (100 µs) were delivered at 0.20 Hz by a Master-8 pulse Stimulator (A.M.P.I.) through an ISU-165 isolation unit (Cibertec). Stimulus intensity was adjusted to obtain 3-5 mV PSP responses and was unchanged for the entire experiment. In those experiments in which the stimulus intensity was adjusted to evoke NMDAR-dependent Ca^{2+} spikes, voltage-gated Na^+ channel blocker QX-314 (2 mM) was included in the recording pipette (30, 51). In all experiments, basal PSP were recorded for 10-15 min before any drug application.

Induction of spike-timing-dependent plasticity (STDP) long-term potentiation (t-LTP) was achieved by pairing pre- and postsynaptic action potentials (Δt = 10 ms). Presynaptic action potentials were evoked by electrical stimulation of basal afferent inputs as described above. Postsynaptic action potentials were elicited by brief current injection through the recording pipette (5 ms, 200-400 pA). The extent of PSP potentiation was evaluated by quantifying the PSP amplitude during 5 min before and 50 min after t-LTP induction protocols (30, 50, and 90 pairings). In Figure 6B, paxilline (500 nM) was applied intracellularly through the recording pipette. In some experiments, presynaptic electrical stimulation was performed within the limit between layers 1 and 2 to stimulate the afferent inputs to BC-L5PNs apical dendrites.

Electrophysiology in HEK293T cells

Human embryonic kidney cells (HEK293T; ATCC #CRL-3216) were grown on 12-mm poly-lysine treated glass coverslips in Dulbecco's Modified Eagle Medium supplemented with 10% fetal bovine serum and 1% penicillin-streptomycin and maintained in an incubator at 37°C and 5% carbon dioxide atmosphere. Transient transfection was performed using jetPRIME (Polyplus Transfection) and different combinations of cDNA plasmids encoding for BK alpha subunit (pBNJ-hSloTAG (36)), GluN1 (pEYFP-NR1a; Addgene plasmid #17928), GluN2A (pEGFP-NR2A; Addgene plasmid #17924), and GluN2B (pEGFP-NR2B; Addgene plasmid #17925). All fluorescently tagged NMDAR plasmids were a gift from Stefano Vicini (69).

Electrophysiological recordings were performed 36–48 h post-transfection using the inside-out configuration of the patch-clamp technique on an inverted Nikon Eclipse Ti-U microscope (Nikon) coupled to an Axopatch-200B amplifier and a Digidata 1550A interface (Molecular Devices) (38, 68). All experiments were performed at room temperature (22-24°C). Patch pipettes were fabricated from GC150F-10 borosilicate glass capillaries and fire-polished with a MF-200 microforge (World Precision Instruments) to obtain a tip resistance of 2–5 MΩ when filled with the 'extracellular' solution (in mM: 80 $KMeSO_3$, 60 N-methylglucamine-$MeSO_3$, 20 HEPES, 2 KCl, and 2 $CaCl_2$; pH 7.4), supplemented with NMDA (200 µM) and glycine (10 µM) to ensure activation and significantly reduced desensitization of NMDAR during the experiment, as previously described (70, 71). Bath ('intracellular') solution contained (in mM): 80 $KMeSO_3$, 60 N-methylglucamine-$MeSO_3$, 20 HEPES, 2 KCl, and 1 HEDTA (pH 7.4). In recordings from patches expressing BK channels alone, $CaCl_2$ was added to the bath solution to obtain the desired free Ca^{2+} concentration calculated using the MaxChelator program (MAXC; (72)). Free Ca^{2+} was confirmed using a Ca^{2+}-sensitive electrode (ThermoLab Systems). Solutions containing 100 µM Ca^{2+} did not include HEDTA chelator. Data were acquired at 100 kHz and lowpass-filtered at 5 kHz. BK currents were elicited from a holding potential of -60 mV, stepping from -100 to 200 mV for 25 ms in 20 mV increments and then repolarizing to -80 mV for 100 ms. Conductance-voltage (G-V) curves were generated from tail current amplitudes normalized to the maximum amplitude obtained in 100 µM Ca^{2+}. A Boltzmann equation was fitted to the data according to the equation:

$$G / G_{max} = 1 / (1 + \exp((V_m - V_{half}) / z))$$

where V_{half} is the voltage of half-maximum activation, z is the slope of the curve, V_m is the test potential, and G_{max} is the maximal conductance.

In some experiments (Figures 3F-H), inside-out recordings were performed using slightly modified brain slices solutions to achieve physiological Na^+ concentrations. Briefly, the pipette 'extracellular' solution contained normal ACSF supplemented with NMDA (200 µM) and glycine (10 µM) to ensure NMDAR activation. The bath 'intracellular' solution contained (in mM): 135 $KMeSO_4$, 10 KCl, 10 HEPES, 5 NaCl, 2.5 ATP-Mg, and 0.3 GTP-Na (pH 7.3), and was supplemented with EGTA (10 mM) to obtain a Ca^{2+}-free solution. BK currents were

elicited from a holding potential of -60 mV, applying a family of pulses from -100 to +200 mV in 20 mV steps, for 100 ms. In this case, G-V curves were generated from the I-V relationships ($G = I / (V_m - E_{rev})$); where I is the current amplitude at the end of the depolarizing pulse for each test potential (V_m) and E_{rev} is the reversal potential for K^+.

Proximity Ligation Assay

Proximity ligation assay (PLA) was performed using the DuoLink kit (Sigma-Aldrich). HEK293T cells expressing different combinations of NMDAR and BK channels were fixed with 4% paraformaldehyde for 20 min, permeabilized, and then blocked for 1 h at 37ºC to avoid non-specific binding of antibodies. BK channel was detected using a rabbit polyclonal anti-Maxi K^+ channel alpha subunit primary antibody (1:200, #ab219072; Abcam). GluN1, GluN2A, and GluN2B subunits of NMDAR were detected using goat polyclonal primary antibodies anti-NMDAR1 (1:200, #NB100-41105; Novus Biologicals), mouse monoclonal anti-NMDAc1 (1:200, #sc-515148; Santa Cruz Biotechnology) and anti-NMDAc2 (1:200, #sc-365597; Santa Cruz Biotechnology), respectively. Secondary antibodies conjugated with oligonucleotides were supplied with the PLA DuoLink kit. Controls consisted of untransfected HEK293T cells or cells expressing individually the BK alpha subunit or single NMDAR subunits. Image acquisition and analysis was performed using the Duolink Image Tool (Sigma-Aldrich) and Fiji (73) software on a Leica SP8 inverted confocal microscope (Leica Biosystems). The PLA technique allows the detection of protein-protein interactions (less than 40 nm) as quantifiable fluorescent dots (74). Results are expressed as the number of fluorescent signals per cell area (PLA signals/μm^2).

Drugs and Reagents

D-AP5 (D-2-amino-5-phosphonovalerate, AP5), glycine, ifenprodil (IFEN), N-methyl-D-aspartate (NMDA), paxilline (PAX), QX-314, and tetrodotoxin (TTX) were purchased from Tocris. EGTA and HEDTA were purchased from Sigma-Aldrich. BAPTA and $ZnCl_2$ were purchased from Abcam and Merck, respectively. Drugs were dissolved in the adequate solvent (DMSO or water) and prepared as 1000-10000x stock solutions. Subsequent dilution in ACSF (bath application) or pipette recording solution was performed to obtain the final concentration used in the experiments.

Statistical analysis

Data were analyzed with pClamp (Molecular Devices) and GraphPad Prism8 (GraphPad). Data are shown as mean ± SEM or as individual values (symbols) plus median and 25^{th}-75^{th} percentile (boxes) values. Two-tailed *t*-tests were used to analyze data from the same neuron measured before and after treatments (e.g., pharmacological characterization in Figure 1E or t-LTP in Figures 6 and 7). Two-tailed unpaired *t*-tests (Gaussian distribution) or Mann-Whitney U tests (non-Gaussian distribution) were used to analyze A-type vs. B-type BC-L5PN electrophysiological data. Kruskal-Wallis test (followed by Dunn's tests) was used to analyze PLA data. Statistical significance is stated as *p<0.05, **p<0.01, or ***p<0.001. Statistical details related to main and supplementary figures are specified in Table S1.

Acknowledgements

Authors thank Drs. A. J. Plested, W. Bufo, J. S. Diamond and A. Pérez-Álvarez for their critical reading of the manuscript. Funding: European Research Council, under Horizon 2020 Research and Innovation Programme Grant (ERC-CoG-2014 648936) (TG); Spanish Ministerio de Ciencia, Innovación y Universidades grant RTI2018-098788-B-I00 (TG); Spanish Ministerio de Educación, Cultura y Deporte grant FPU15/02528 (AGH).

REFERENCES

1. A. Reiner, J. Levitz, Glutamatergic Signaling in the Central Nervous System: Ionotropic and Metabotropic Receptors in Concert. *Neuron* **98**, 1080-1098 (2018).
2. S. F. Traynelis *et al.*, Glutamate receptor ion channels: structure, regulation, and function. *Pharmacol Rev* **62**, 405-496 (2010).
3. M. L. Mayer, G. L. Westbrook, P. B. Guthrie, Voltage-dependent block by Mg2+ of NMDA responses in spinal cord neurones. *Nature* **309**, 261-263 (1984).
4. L. Nowak, P. Bregestovski, P. Ascher, A. Herbet, A. Prochiantz, Magnesium gates glutamate-activated channels in mouse central neurones. *Nature* **307**, 462-465 (1984).
5. R. A. Lester, J. D. Clements, G. L. Westbrook, C. E. Jahr, Channel kinetics determine the time course of NMDA receptor-mediated synaptic currents. *Nature* **346**, 565-567 (1990).
6. A. B. MacDermott, M. L. Mayer, G. L. Westbrook, S. J. Smith, J. L. Barker, NMDA-receptor activation increases cytoplasmic calcium concentration in cultured spinal cord neurones. *Nature* **321**, 519-522 (1986).
7. M. L. Mayer, G. L. Westbrook, Permeation and block of N-methyl-D-aspartic acid receptor channels by divalent cations in mouse cultured central neurones. *The Journal of physiology* **394**, 501-527 (1987).
8. P. Paoletti, C. Bellone, Q. Zhou, NMDA receptor subunit diversity: impact on receptor properties, synaptic plasticity and disease. *Nature reviews. Neuroscience* **14**, 383-400 (2013).
9. N. Caporale, Y. Dan, Spike timing-dependent plasticity: a Hebbian learning rule. *Annu Rev Neurosci* **31**, 25-46 (2008).
10. R. C. Malenka, R. A. Nicoll, NMDA-receptor-dependent synaptic plasticity: multiple forms and mechanisms. *Trends in neurosciences* **16**, 521-527 (1993).
11. H. Markram, J. Lübke, M. Frotscher, B. Sakmann, Regulation of synaptic efficacy by coincidence of postsynaptic APs and EPSPs. *Science* **275**, 213-215 (1997).
12. R. Latorre *et al.*, Molecular Determinants of BK Channel Functional Diversity and Functioning. *Physiological reviews* **97**, 39-87 (2017).
13. A. S. Kshatri, A. Gonzalez-Hernandez, T. Giraldez, Physiological Roles and Therapeutic Potential of Ca(2+) Activated Potassium Channels in the Nervous System. *Front Mol Neurosci* **11**, 258 (2018).
14. B. Fakler, J. P. Adelman, Control of K(Ca) channels by calcium nano/microdomains. *Neuron* **59**, 873-881 (2008).
15. H. Berkefeld *et al.*, BKCa-Cav channel complexes mediate rapid and localized Ca2+-activated K+ signaling. *Science* **314**, 615-620 (2006).
16. O. Vivas, C. M. Moreno, L. F. Santana, B. Hille, Proximal clustering between BK and CaV1.3 channels promotes functional coupling and BK channel activation at low voltage. *Elife* **6** (2017).
17. P. Chavis, F. Ango, J. M. Michel, J. Bockaert, L. Fagni, Modulation of big K+ channel activity by ryanodine receptors and L-type Ca2+ channels in neurons. *Eur J Neurosci* **10**, 2322-2327 (1998).
18. J. P. Whitt, B. A. McNally, A. L. Meredith, Differential contribution of Ca(2+) sources to day and night BK current activation in the circadian clock. *The Journal of general physiology* **150**, 259-275 (2018).
19. J. S. Isaacson, G. J. Murphy, Glutamate-mediated extrasynaptic inhibition: direct coupling of NMDA receptors to Ca(2+)-activated K+ channels. *Neuron* **31**, 1027-1034 (2001).
20. J. Zhang *et al.*, Glutamate-activated BK channel complexes formed with NMDA receptors. *Proceedings of the National Academy of Sciences of the United States of America* **115**, E9006-E9014 (2018).
21. C. F. Zorumski, L. L. Thio, G. D. Clark, D. B. Clifford, Calcium influx through N-methyl-D-aspartate channels activates a potassium current in postnatal rat hippocampal neurons. *Neurosci Lett* **99**, 293-299 (1989).
22. C. C. H. Petersen, Sensorimotor processing in the rodent barrel cortex. *Nature reviews. Neuroscience* **20**, 533-546 (2019).

23. R. S. Erzurumlu, P. Gaspar. How the Barrel Cortex Became a Working Model for Developmental Plasticity: A Historical Perspective. *The Journal of neuroscience : the official journal of the Society for Neuroscience* **40**, 6460-6473 (2020).
24. A. Agmon, B. W. Connors. Correlation between intrinsic firing patterns and thalamocortical synaptic responses of neurons in mouse barrel cortex. *The Journal of neuroscience : the official journal of the Society for Neuroscience* **12**, 319-329 (1992).
25. C. M. Constantinople, R. M. Bruno. Deep cortical layers are activated directly by thalamus. *Science* **340**, 1591-1594 (2013).
26. S. El-Boustani *et al.*, Anatomically and functionally distinct thalamocortical inputs to primary and secondary mouse whisker somatosensory cortices. *Nature communications* **11**, 3342 (2020).
27. J. Rodríguez-Moreno *et al.*, Area-Specific Synapse Structure in Branched Posterior Nucleus Axons Reveals a New Level of Complexity in Thalamocortical Networks. *The Journal of neuroscience : the official journal of the Society for Neuroscience* **40**, 2663-2679 (2020).
28. J. Schiller, G. Major, H. J. Koester, Y. Schiller, NMDA spikes in basal dendrites of cortical pyramidal neurons. *Nature* **404**, 285-289 (2000).
29. T. Nevian, M. E. Larkum, A. Polsky, J. Schiller, Properties of basal dendrites of layer 5 pyramidal neurons: a direct patch-clamp recording study. *Nature neuroscience* **10**, 206-214 (2007).
30. A. Polsky, B. Mel, J. Schiller, Encoding and decoding bursts by NMDA spikes in basal dendrites of layer 5 pyramidal neurons. *The Journal of neuroscience : the official journal of the Society for Neuroscience* **29**, 11891-11903 (2009).
31. H. G. Knaus *et al.*, Tremorgenic indole alkaloids potently inhibit smooth muscle high-conductance calcium-activated potassium channels. *Biochemistry* **33**, 5819-5828 (1994).
32. M. Naraghi, E. Neher, Linearized buffered Ca2+ diffusion in microdomains and its implications for calculation of [Ca2+] at the mouth of a calcium channel. *The Journal of neuroscience : the official journal of the Society for Neuroscience* **17**, 6961-6973 (1997).
33. M. Prakriya, C. J. Lingle, Activation of BK channels in rat chromaffin cells requires summation of Ca(2+) influx from multiple Ca(2+) channels. *J Neurophysiol* **84**, 1123-1135 (2000).
34. A. Araque, W. Buno, Fast, persistent, Ca(2+)-dependent K+ current controls graded electrical activity in crayfish muscle. *Pflugers Archiv : European journal of physiology* **430**, 541-551 (1995).
35. S. Vicini *et al.*, Functional and pharmacological differences between recombinant N-methyl-D-aspartate receptors. *J Neurophysiol* **79**, 555-566 (1998).
36. T. Giraldez, T. E. Hughes, F. J. Sigworth, Generation of functional fluorescent BK channels by random insertion of GFP variants. *The Journal of general physiology* **126**, 429-438 (2005).
37. J. Lema, Spemine regulates N-methyl-D-aspartate receptor desensitization. *Neuron* **8**, 343-352 (1992).
38. A. S. Kshatri, A. J. Gonzalez-Hernandez, T. Giraldez, Functional validation of Ca(2+)-binding residues from the crystal structure of the BK ion channel. *Biochim Biophys Acta Biomembr* **1860**, 943-952 (2018).
39. F. T. Horrigan, R. W. Aldrich, Coupling between voltage sensor activation, Ca2+ binding and channel opening in large conductance (BK) potassium channels. *The Journal of general physiology* **120**, 267-305 (2002).
40. T. Ichinose, S. Yu, X. Q. Wang, S. P. Yu, Ca2+-independent, but voltage- and activity-dependent regulation of the NMDA receptor outward K+ current in mouse cortical neurons. *The Journal of physiology* **551**, 403-417 (2003).
41. O. Garaschuk, R. Schneggenburger, C. Schirra, F. Tempia, A. Konnerth, Fractional Ca2+ currents through somatic and dendritic glutamate receptor channels of rat hippocampal CA1 pyramidal neurones. *The Journal of physiology* **491 (Pt 3)**, 757-772 (1996).
42. T. Plant, C. Schirra, O. Garaschuk, J. Rossier, A. Konnerth, Molecular determinants of NMDA receptor function in GABAergic neurones of rat forebrain. *The Journal of physiology* **499 (Pt 1)**, 47-63 (1997).
43. N. Burnashev, Z. Zhou, E. Neher, B. Sakmann, Fractional calcium currents through recombinant GluR channels of the NMDA, AMPA and kainate receptor subtypes. *The Journal of physiology* **485 (Pt 2)**, 403-418 (1995).
44. D. A. McCormick, B. W. Connors, J. W. Lighthall, D. A. Prince, Comparative electrophysiology of pyramidal and sparsely spiny stellate neurons of the neocortex. *J Neurophysiol* **54**, 782-806 (1985).
45. A. Agmon, B. W. Connors, Repetitive burst-firing neurons in the deep layers of mouse somatosensory cortex. *Neurosci Lett* **99**, 137-141 (1989).
46. Y. Chagnac-Amitai, B. W. Connors, Synchronized excitation and inhibition driven by intrinsically bursting neurons in neocortex. *J Neurophysiol* **62**, 1149-1162 (1989).
47. L. E. Maglio, J. A. Noriega-Prieto, M. J. Maraver, D. Fernandez de Sevilla, Endocannabinoid-Dependent Long-Term Potentiation of Synaptic Transmission at Rat Barrel Cortex. *Cereb Cortex* **28**, 1568-1581 (2018).
48. M. Griguoli, M. Sgritta, E. Cherubini, Presynaptic BK channels control transmitter release: physiological relevance and potential therapeutic implications. *The Journal of physiology* **594**, 3489-3500 (2016).
49. T. J. Ngo-Anh *et al.*, SK channels and NMDA receptors form a Ca2+-mediated feedback loop in dendritic spines. *Nature neuroscience* **8**, 642-649 (2005).
50. I. D. Manns, B. Sakmann, M. Brecht, Sub- and suprathreshold receptive field properties of pyramidal neurones in layers 5A and 5B of rat somatosensory barrel cortex. *The Journal of physiology* **556**, 601-622 (2004).
51. A. Nunez, S. Dominguez, W. Buno, D. Fernandez de Sevilla, Cholinergic-mediated response enhancement in barrel cortex layer V pyramidal neurons. *J Neurophysiol* **108**, 1656-1668 (2012).
52. G. Q. Bi, M. M. Poo, Synaptic modifications in cultured hippocampal neurons: dependence on spike timing, synaptic strength, and postsynaptic cell type. *The Journal of neuroscience : the official journal of the Society for Neuroscience* **18**, 10464-10472 (1998).
53. D. E. Feldman, Timing-based LTP and LTD at vertical inputs to layer II/III pyramidal cells in rat barrel cortex. *Neuron* **27**, 45-56 (2000).
54. T. Nevian, B. Sakmann, Spine Ca2+ signaling in spike-timing-dependent plasticity. *The Journal of neuroscience : the official journal of the Society for Neuroscience* **26**, 11001-11013 (2006).
55. G. M. Wittenberg, S. S. Wang, Malleability of spike-timing-dependent plasticity at the CA3-CA1 synapse. *The Journal of neuroscience : the official journal of the Society for Neuroscience* **26**, 6610-6617 (2006).
56. J. C. Zhang, P. M. Lau, G. Q. Bi, Gain in sensitivity and loss in temporal contrast of STDP by dopaminergic modulation at hippocampal synapses. *Proceedings of the National Academy of Sciences of the United States of America* **106**, 13028-13033 (2009).
57. D. Fernandez de Sevilla, W. Buno, The muscarinic long-term enhancement of NMDA and AMPA receptor-mediated transmission at Schaffer collateral synapses develop through different intracellular mechanisms. *The Journal of neuroscience : the official journal of the Society for Neuroscience* **30**, 11032-11042 (2010).
58. B. L. Sabatini, T. G. Oertner, K. Svoboda, The life cycle of Ca(2+) ions in dendritic spines. *Neuron* **33**, 439-452 (2002).
59. M. J. Higley, B. L. Sabatini, Calcium signaling in dendritic spines. *Cold Spring Harb Perspect Biol* **4**, a005686 (2012).
60. J. H. Comfort *et al.*, Dendritic NMDA receptors in parvalbumin neurons enable strong and stable neuronal assemblies. *Elife* **8** (2019).
61. T. Blackmer, S. P. Kuo, K. J. Bender, P. F. Apostolides, L. O. Trussell, Dendritic calcium channels and their activation by synaptic signals in auditory coincidence detector neurons. *J Neurophysiol* **102**, 1218-1226 (2009).
62. S. L. Jones, M. S. Yo, G. J. Stuart, Dendritic small conductance calcium-activated potassium channels activated by action potentials suppress EPSPs and gate spike-timing dependent synaptic plasticity. *Elife* **6** (2017).
63. K. Erreger, S. M. Dravid, T. G. Banke, D. J. Wyllie, S. F. Traynelis, Subunit-specific gating controls rat NR1/NR2A and NR1/NR2B NMDA channel kinetics and synaptic signalling profiles. *The Journal of physiology* **563**, 345-358 (2005).

64. R. Yaka *et al.*, NMDA receptor function is regulated by the inhibitory scaffolding protein, RACK1. *Proceedings of the National Academy of Sciences of the United States of America* **99**, 5710-5715 (2002).
65. J. X. Yang *et al.*, Caveolin-1 in the anterior cingulate cortex modulates chronic neuropathic pain via regulation of NMDA receptor 2B subunit. *The Journal of neuroscience : the official journal of the Society for Neuroscience* **35**, 36-52 (2015).
66. C. K. Isacson, Q. Lu, R. H. Karas, D. H. Cox, RACK1 is a BKCa channel binding protein. *American journal of physiology. Cell physiology* **292**, C1459-1466 (2007).
67. X. L. Wang *et al.*, Caveolae targeting and regulation of large conductance Ca(2+)-activated K+ channels in vascular endothelial cells. *The Journal of biological chemistry* **280**, 11656-11664 (2005).
68. O. P. Hamill, A. Marty, E. Neher, B. Sakmann, F. J. Sigworth, Improved patch-clamp techniques for high-resolution current recording from cells and cell-free membrane patches. *Pflugers Archiv : European journal of physiology* **391**, 85-100 (1981).
69. J. H. Luo *et al.*, Functional expression of distinct NMDA channel subunits tagged with green fluorescent protein in hippocampal neurons in culture. *Neuropharmacology* **42**, 306-318 (2002).
70. Z. G. Xiong *et al.*, Regulation of N-methyl-D-aspartate receptor function by constitutively active protein kinase C. *Mol Pharmacol* **54**, 1055-1063 (1998).
71. W. F. Borschel, S. E. Murthy, E. M. Kasperek, G. K. Popescu, NMDA receptor activation requires remodelling of intersubunit contacts within ligand-binding heterodimers. *Nature communications* **2**, 498 (2011).
72. D. M. Bers, C. W. Patton, R. Nuccitelli, A practical guide to the preparation of Ca(2+) buffers. *Methods Cell Biol* **99**, 1-26 (2010).
73. J. Schindelin *et al.*, Fiji: an open-source platform for biological-image analysis. *Nat Methods* **9**, 676-682 (2012).
74. M. S. Alam, Proximity Ligation Assay (PLA). *Curr Protoc Immunol* **123**, e58 (2018).

Figure Legends

Figure 1. NMDAR activation opens BK channels in BC-L5PN basal dendrites. (A) Left, schematic representation of a mouse brain slice with the barrel cortex area highlighted in yellow. Right, schematic representation of the barrel cortex, depicting the BC-L5PNs under investigation. **(B)** Representative current traces obtained at the indicated holding potentials after application of NMDA to the basal dendrites. Scale bar represents 10 s and 200 pA. **(C)** Average charge-voltage (Q-V) relationships for A-type (red) and B-type (blue) neurons. **(D)** Normalized current-voltage (I-V, left) and Q-V (right) relationships for NMDAR inward currents from A-type and B-type neurons. Data points in **(C)** and **(D)** represent mean ± SEM. A-type: n = 15, B-type: n = 8; *p<0.05 and **p<0.01 (B-type vs. A-type). **(E)** Pharmacological characterization of NMDA-activated current in BC-L5PN basal dendrites. Normalized charge for the outward ($Q_{outward}$, top) and inward (Q_{inward}, bottom) component after the addition of different drugs. Data correspond to mean ± SEM. **p<0.01 and ***p<0.001 (treatment vs. ACSF); #p<0.05, ##p<0.01, and ###p<0.01 (drug+AP5 vs. drug alone). **(F)** Representative current traces obtained at -20 mV after NMDA application to the basal dendrites of B-type neurons in control conditions (ACSF, black traces) and after the application of different drugs. Traces are color-coded corresponding to the different treatments shown in **(E)**. Scale bars represent 5 s and 50 pA. In **(E)** and **(F)**, AP5, D-AP5 (100 µM; n = 6); IFEN, Ifenprodil (5 µM; n = 5); PAX, paxilline (1 µM; n = 5); Zn^{2+}, $ZnCl_2$ (100 nM; n = 5).

Figure 2. NMDARs and BK channels are within functional proximity in B-type BC-L5PNs. (A–C) Representative current traces obtained at the indicated holding potentials after application of NMDA to the basal dendrites of BC-L5PNs in the presence of **(A)** 15 mM BAPTA, **(B)** 15 mM EGTA, and **(C)** 1 mM BAPTA in the recording pipette. Scale bars represent 10 s and 200 pA. **(D–F)** Average Q-V relationships corresponding to experiments described in (A–C); Data points represent mean ± SEM; **(D)** n = 18, **(E)** A-type: n = 8, B-type: n = 5, **(F)** A-type: n = 9, B-type: n = 5; Blue dashed line in F represents data taken from Figure 1C (B-type neurons), for comparison; *p<0.05 and **p<0.01 (B-type vs. A-type); **(G)** Schematic representation of the relative location of NMDARs and BK channels in the plasma membrane. Distances are estimated from the experimental data.

Figure 3. Both GluN2A- and GluN2B-containing NMDARs can functionally couple to BK channels. (A) Representative confocal microscopy images of PLA experiments in HEK293 cells expressing the protein combinations indicated at the top of the images. Each row corresponds to an imaging channel (top, DAPI, blue; middle, NMDAR, green; bottom, PLA, red). **(B)** Average PLA signals/µm^2 for all conditions shown in **(A)**. Data points represent individual measurements. Four independent experiments were performed for each condition. Black lines represent mean ± SEM. ***p<0.001 vs. untransfected cells (UNTRANSF), BK alone (BK), and GluN1 alone (GluN1); **(C)** Normalized conductance-voltage (G-V) relationships obtained from excised inside-out patches expressing BK channels alone (n = 12) in the presence of different intracellular Ca^{2+} concentrations in symmetrical K^+ solutions. Data points represent mean ± SEM. Lines represent the best fit of a Boltzmann equation to the data. Ca^{2+} concentrations are color-coded as indicated in the legend. **(D)** Normalized G-V relationships from excised inside-out patches co-expressing BK channels with GluN1/GluN2A (left; n = 6) or GluN1/GluN2B (right; n = 5) in the absence of intracellular Ca^{2+}, with 200 µM NMDA/10 µM Glycine in the pipette. Data points represent mean ± SEM. Lines represent the best fit of a Boltzmann equation to the data. **(E)** V_{half} values obtained from experiments depicted in **(C)** and **(D)**. Data points represent individual measurements and lines represent mean ± SEM. **(F)** Representative current traces recorded in physiological Na^+ solutions from excised inside-out patches containing BK alone (left), BK+GluN1/GluN2A (middle), and BK+GluN1/GluN2B (right). Scale bars represent 30 ms and 2000 pA. Currents recorded at +140 mV are highlighted in red. **(G)** Normalized G-V relationships from excised inside-out patches containing BK and GluN1/GluN2A (left, red; n = 6) or GluN1/GluN2B (right, blue; n = 5) in solutions containing physiological concentrations of Na^+ (see methods). Black traces in both graphs correspond to G-V curves for BK channels expressed alone (n = 11). Data points represent mean ± SEM. Lines represent the best fit of a Boltzmann equation to the data. **(H)** Summary of V_{half} values from experiments in **(G)**. Data points represent individual measurements and lines represent mean ± SEM. ***p<0.001 vs. BK alone.

Figure 4. A subpopulation of regular-spiking BC-L5PNs exhibit NMDAR–BK functional coupling. (A) Representative current-clamp traces elicited with 500-ms depolarizing steps from -100 to 320 pA in A-type (red) and B-type (blue) BC-L5PNs. Scale bars represent 200 ms and 50 mV. **(B)** Single action potentials recorded from the same neurons shown in **(A)**. The arrow points to the Ca^{2+} spike apparent in A-type BC-L5PNs. Scale bars represent 100 ms and 20 mV. **(C)** NMDA-evoked currents recorded from the same neurons depicted in **(A)** and **(B)** at holding potentials of -20 and -60 mV with a Mg^{2+}-free external solution containing 1 µM TTX and 10 µM glycine. Scale bars represent 5 s and 150 pA. **(D–K)** Values for resting membrane potential **(D)**, input resistance **(E)**, cell capacitance **(F)**, action potential frequency **(G)**, action potential threshold **(H)**, action potential amplitude **(I)**, action potential duration **(J)**, and afterhyperpolarization amplitude **(K)**. Data correspond to individual measurements (symbols) and median and 25^{th}–75^{th} percentiles (boxes) from A-type (red; n = 130) and B-type (blue, n = 67) BC-L5PNs, except for **(G)**, where data points represent mean ± SEM. In **(J)** and **(K)**, **p<0.001 (B-type vs. A-type).

Figure 5. BK-dependent inhibition of NMDARs reduces postsynaptic response amplitude. (A) Representative synaptically-evoked postsynaptic potential (PSP) traces recorded from A-type (top, red) and B-type (bottom, blue) neurons in control conditions (ACSF, left), after the application of 1 µM paxilline (PAX, middle), and with 1 µM PAX plus 100 µM AP5 (PAX+AP5, right). Scale bars represent 50 ms and 3 mV. **(B)** Values for the normalized PSP amplitude (top left), area (top right), rise time (bottom left), and decay time (bottom right) in the experimental conditions in **(A)**. Data points represent individual measurements (n = 7 in both types of neuron) and boxes represent median and 25^{th}–75^{th} percentile values. **(C)** Representative synaptically-evoked PSP traces recorded from A-type (top, red) and B-type (bottom, blue) neurons after increasing the electrical stimulation intensity applied to the afferent inputs. Conditions were the same as in **(A)** (ACSF, PAX, PAX+AP5). The pipette solution included 2 mM QX-314 to avoid action potential firing. Scale bars represent 50 ms and 3 mV. **(D)** Values for PSP amplitude (top left), area (top right), rise time (bottom left), and decay time (bottom right) for the experimental conditions shown in **(C)**. Data points represent individual measurements and boxes represent median and 25^{th}-75^{th} percentile values. A-type: n = 5; B-type: n = 6. In **(B)** and **(D)**, *p<0.05, **p<0.01, and ***p<0.001.

Figure 6. NMDAR–BK coupling increases the threshold for induction of synaptic plasticity. (A) Schematic representation of the experimental design used to induce t-LTP via stimulation of basal afferent inputs to BC-L5PNs. **(B)** Development of t-LTP over time in A-type (red) and B-type (blue) neurons in control conditions (ACSF, left) and in the presence of 500 nM intracellular paxilline (PAX, right). Data points represent mean ± SEM. A-type (ACSF): n = 6; B-type (ACSF): n = 4; A-type (PAX): n = 6; B-type (PAX): n = 4. ***p<0.001 (t-LTP vs. basal conditions). **(C)** Schematic representation of the experimental design used to induce t-LTP via stimulation of apical afferent inputs to BC-L5PNs. **(D)** Development of t-LTP over time in A-type (red) and B-type (blue) neurons in control conditions (ACSF) using 30 (left) or 90 (right) STDP pairings. Data points represent mean ± SEM. A-type (30 pairings): n = 3; A-type (90 pairings): n = 6; B-type (90 pairings): n = 3.

Figure 7. A high number and frequency of pre–post pairings relieves BK-dependent NMDAR inhibition. (A) Time course of t-LTP development over time in A-type (red) and B-type (blue) neurons using 30 (left), 50 (middle), or 90 (right) pairing STDP protocols at frequency of 0.20 Hz using the experimental design represented in Figure 6A. Data points represent mean ± SEM. A-type (30 pairings): n = 6; B-type (30 pairings): n = 4; A-type (50 pairings): n = 6; B-type (50 pairings): n = 4; A-type (90 pairings): n = 6; B-type (90 pairings): n = 5. Data in the left panel (30 pairings) are the same as in Figure 6B. **(B)** Summary of t-LTP extent for A-type (red) and B-type (blue) neurons under the experimental conditions depicted in **(A)**. **(C)** Time course of t-LTP development over time in A-type (red) and B-type (blue) neurons using 30 (left), 50 (middle), or 90 (right) pairing STDP protocols at a frequency of 0.33 Hz. Data points represent mean ± SEM. A-type (30 pairings): n = 6, B-type (30 pairings): n = 4; A-type (50 pairings): n = 7; B-type (50 pairings): n = 5; A-type (90 pairings): n = 5; B-type (90 pairings): n = 6. **(D)** Summary of t-LTP extent for A-type (red) and B-type (blue) neurons under the experimental conditions depicted in **(A)** and **(C)**. ***p<0.001 (t-LTP vs. basal conditions). In **(B)** and **(D)**, ####p<0.001 (B-type vs. A-type). See also Table S1.

Figure 8. NMDAR–BK coupling controls dendrite-specific synaptic plasticity. Two populations of regular-spiking BC-L5PNs can be distinguished by the absence (A-type, left, red) or presence (B-type, right, blue) of NMDAR-BK functional association in basal dendrites. In B-type neurons (~36%), NMDAR–BK coupling provides a negative feedback mechanism whereby the entry of Ca^{2+} associated with NMDAR activation **(1)** opens neighbouring BK channels **(2)** that allow outward flow of K^+. The resultant membrane hyperpolarization **(-Vm)** reinstates voltage-dependent Mg^{2+} block of NMDARs **(3)**, truncating Ca^{2+} entry and increasing the threshold for long-term synaptic plasticity **(↓LTP)**. We show in this study that B-type BC-L5PNs exhibit a higher threshold for induction of t-LTP. On the other hand, A-type neurons (~64%) lacking the NMDAR–BK molecular break undergo long-term potentiation **(3)** associated with Ca^{2+} entry **(2)** via NMDARs **(1)**. Our data reveal that A-type neurons reach saturation at a lower stimulation frequency than B-type, independent of the number of synaptic inputs.

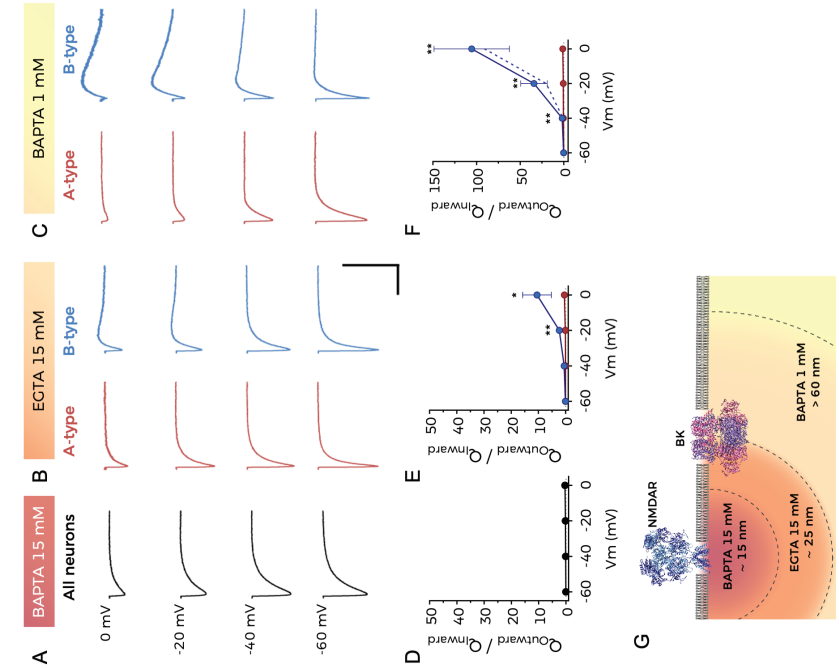

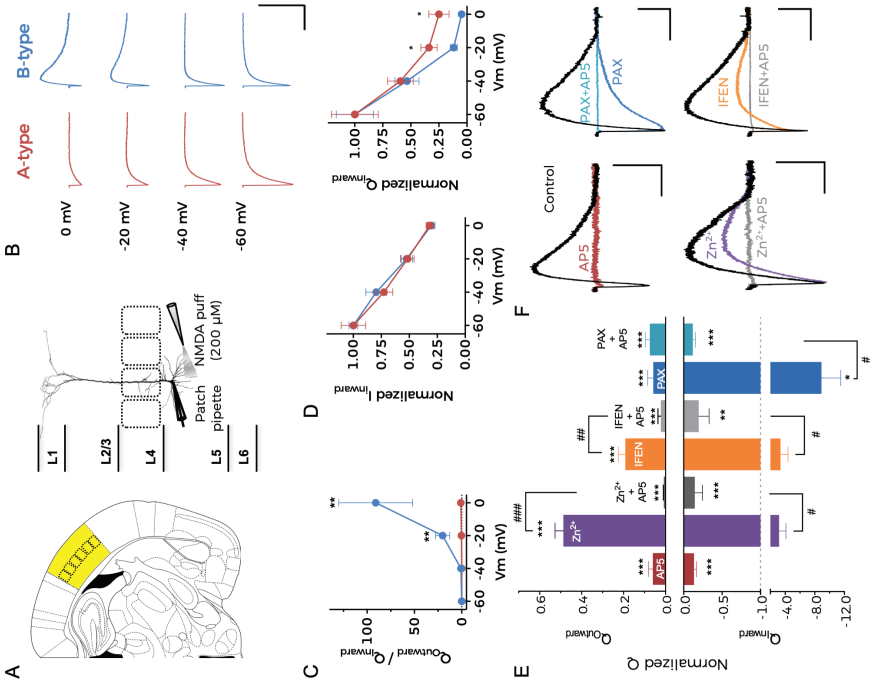

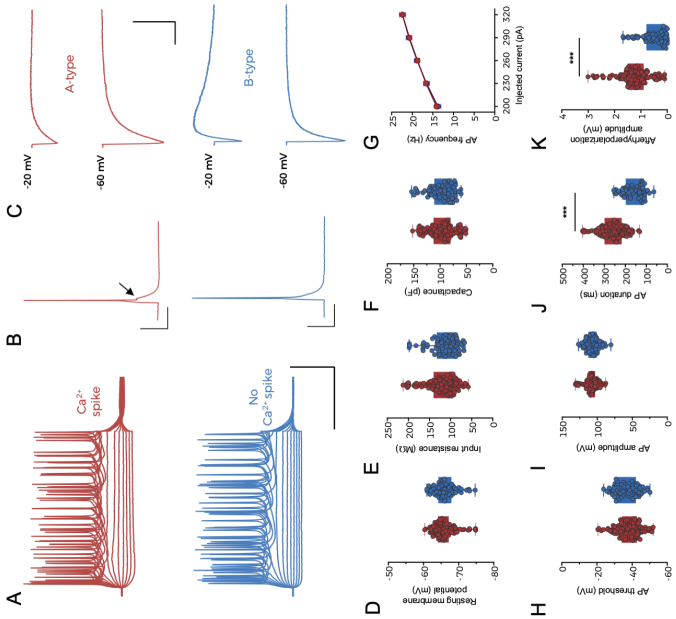

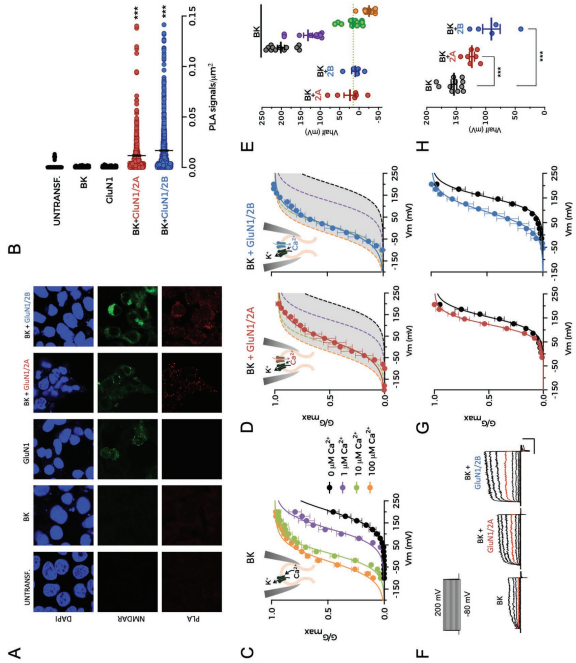

237

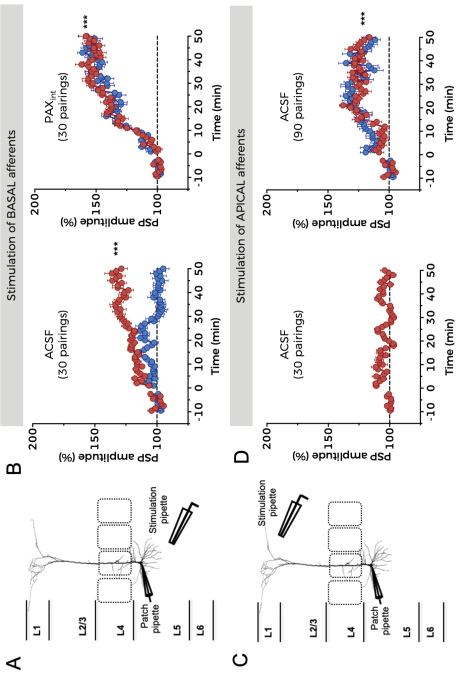

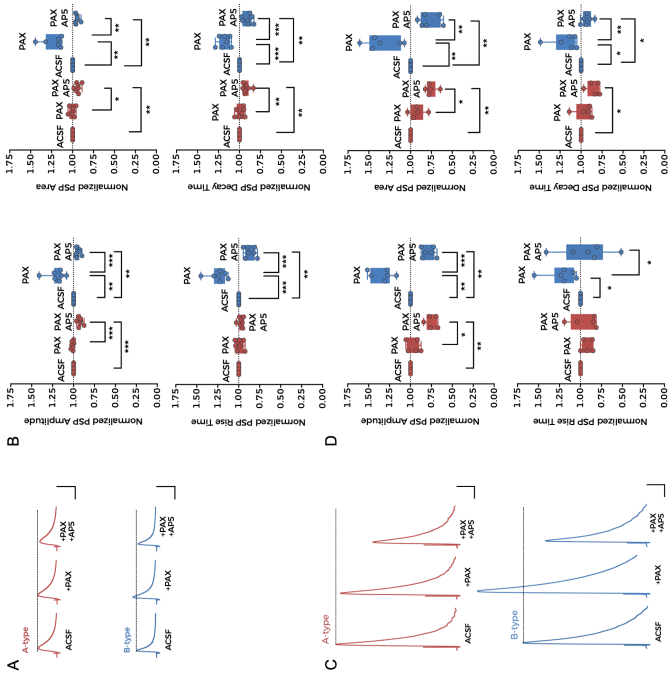

236

239

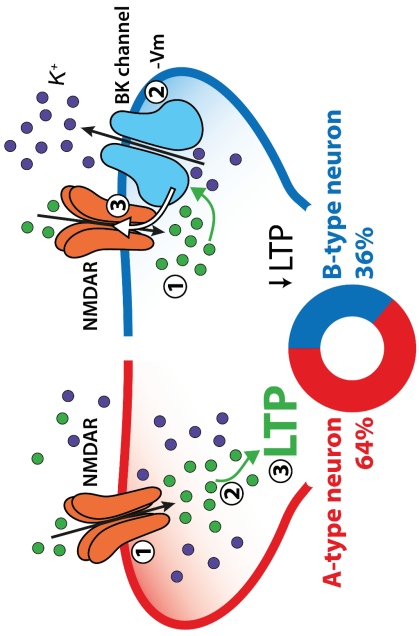

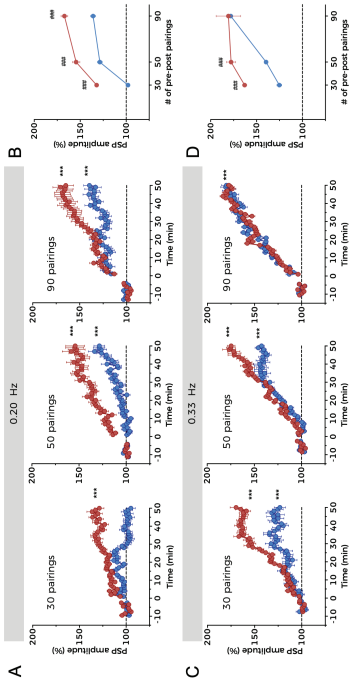

238

PNAS
www.pnas.org

Supplementary Information for

NMDA receptor–BK channel coupling regulates synaptic plasticity in the barrel cortex

Ricardo Gómez, Laura E. Maglio, Alberto J. Gonzalez-Hernandez, Belinda Rivero- Pérez, David Bartolomé-Martín, and Teresa Giraldez

* Ricardo Gómez, *Teresa Giraldez

Email: *rgomezga@ull.edu.es *giraldez@ull.edu.es

This PDF file includes:
Figures S1 to S5
Table S1
Table S2
SI References

Fig. S1. NMDAR-dependent outward currents are absent in oblique dendrites and the initial segment of the apical dendrite. (**A**) Left, general representation view of a mouse brain slice with the barrel cortex area highlighted in yellow. Right, schematic representation of the experimental design. (**B**) Representative current traces obtained at the indicated holding potentials after NMDA application. Scale bars represent 10 s and 200 pA. (**C**) Average G-V relationships. Data points represent mean ± SEM; n=12. Dashed lines represent data from Figure 1C for a better comparison.

Fig. S2. NMDA-evoked currents in dendrites from hippocampal CA1 pyramidal neurons. Representative current traces obtained at the indicated holding potentials after NMDA application at different dendrite locations of hippocampal CA1 pyramidal neurons. No outward currents were observed in any case. Scale bars represent 10 s and 200 pA.

Fig. S3. NMDAR activation is mandatory for t-LTP induction. (A) Time course of t-LTP development over time in A-type (red) and B-type neurons (blue) in control conditions (ACSF), following the experimental design depicted in Figure 6A. **(B)** Same experiments as in panel **A** were performed in the presence of 100 µM AP5. Data points represent mean ± SEM. A-type (ACSF): n=5; B-type (ACSF): n=6; A-type (AP5): n=5; B-type (AP5) n=4. Data in panel **A** are the same as Figure 7C (right panel) and are shown here for a better comparison. In **A**, ***p<0.001 (t-LTP vs. basal conditions).

Fig. S4. BK channels are present in the plasma membrane of both types of BC-L5PN. (A) ***BK current recordings***. Representative BK current traces obtained from an A-type (red) and a B-type neuron (blue) using the voltage protocol shown at the top and obtained as the paxilline-sensitive currents. BK currents from BC-L5PN were recorded as paxilline-sensitive currents using the voltage-clamp mode in the whole-cell configuration of the patch-clamp technique in normal ACSF (including 2 mM $MgSO_4$ and 2 mM $CaCl_2$) supplemented with TTX (1 µM). Patch pipettes were filled with a modified recording solution (in mM: 123 $KMeSO_3$, 9 NaCl, 9 HEPES, 0.9 EGTA, 14 Tris-phosphocreatine, 2 ATP-Mg, 2 ATP-Na, and 0.3 GTP-Tris; pH 7.3), as previously described (1). I-V relationships were elicited from a holding potential of -70 mV, stepping from -110 to +90 mV for 150 ms in 20 mV increments. BK currents were isolated by current subtraction after bath application of the BK blocker paxilline (1 µM) and normalized to BC-L5PN capacitance (1). **(B)** BK current density for A-type (red; n=8) and B-type (blue; n=4) neurons as a function of different membrane potentials. Data points represent mean ± SEM. In **B**, **p<0.01 and ***p<0.001 (B-type vs. A-type).

Table S1. Summary of statistical significance and tests used in each figure (comparisons reaching statistical significance are highlighted in light yellow)

Figure 1. NMDAR activation opens BK channels in BC-L5PN basal dendrites					
PANEL	**STATISTIC**	**CONDITION**	**P VALUE**	**OUTPUT**
Fig. 1C Qoutward/ Qinward	Unpaired t-test (two-tailed)	-60 mV (B vs. A)	0.1851	Not significant
		-40 mV (B vs. A)	0.0990	Not significant
		-20 mV (B vs. A)	0.0014	**
		0 mV (B vs. A)	0.0041	**
Fig. 1D NMDAR Current	Unpaired t-test (two-tailed)	-60 mV (B vs. A)	0.9994	Not significant
		-40 mV (B vs. A)	0.6021	Not significant
		-20 mV (B vs. A)	0.9175	Not significant
		0 mV (B vs. A)	0.7962	Not significant
Fig. 1D NMDAR Charge	Unpaired t-test (two-tailed)	-60 mV (B vs. A)	0.9997	Not significant
		-40 mV (B vs. A)	0.7394	Not significant
		-20 mV (B vs. A)	0.0449	*
		0 mV (B vs. A)	0.0435	*
Fig. 1E (top) Outward component	Paired t-test (two-tailed)	ACSF vs. AP5	<0.0001	***
		ACSF vs. Zn^{2+}	0.0002	***
		ACSF vs. Zn^{2+}+AP5	<0.0001	***
		Zn^{2+} vs. Zn^{2+}+AP5	0.0003	###
		ACSF vs. IFEN	<0.0001	***
		ACSF vs. IFEN+AP5	<0.0001	***
		IFEN vs. IFEN+AP5	0.0057	##
		ACSF vs. PAX	<0.0001	***
		ACSF vs. PAX+AP5	<0.0001	***
		PAX vs. PAX+AP5	0.5845	Not significant
Fig. 1E (bottom) Inward component	Paired t-test (two-tailed)	ACSF vs. AP5	<0.0001	***
		ACSF vs. Zn^{2+}	0.0781	Not significant
		ACSF vs. Zn^{2+}+AP5	0.0010	***
		Zn^{2+} vs. Zn^{2+}+AP5	0.0274	#
		ACSF vs. IFEN	0.0785	Not significant
		ACSF vs. IFEN+AP5	0.0040	**
		IFEN vs. IFEN+AP5	0.0413	#
		ACSF vs. PAX	0.0381	*
		ACSF vs. PAX+AP5	<0.0001	***
		PAX vs. PAX+AP5	0.0283	#

Fig. S5. Single action potential characteristics and measurements. (A) Representative single action potentials recorded from the same A-type BC-L5PN, evoked through pipette depolarization (left) or after electrical stimulation of basal afferent synaptic inputs (right). **(B)** Schematic description of the single action potential parameters determination summarized in Figure 4: threshold, amplitude, and total duration. **(C)** Determination of single action potential parameters summarized in Figure 4.

Figure 2. NMDARs and BK channels are within functional proximity in B-type BC-L5PNs

PANEL	STATISTIC	CONDITION	P VALUE	OUTPUT
Fig. 2E	Unpaired t-test (two-tailed, multiple t-test)	-60 mV (B vs. A)	0.5963	Not significant
		-40 m V (B vs. A)	0.0541	Not significant
EGTA 15 mM		-20 m V (B vs. A)	0.0040	**
		0 m V (B vs. A)	0.0310	*
Fig. 2F	Unpaired t-test (two-tailed, multiple t-test)	-60 mV (B vs. A)	0.6245	Not significant
		-40 m V (B vs. A)	0.0020	**
BAPTA 1 mM		-20 m V (B vs. A)	0.0095	**
		0 m V (B vs. A)	0.0058	**

Figure 3. Both GluN2A- and GluN2B-containing NMDARs can functionally couple to BK channels

PANEL	STATISTIC	CONDITION	P VALUE	OUTPUT
Fig. 3B	Kruskal-Wallis test (followed by Dunn's tests)	BK+GluN1/GluN2A vs. UNTRANSF. BK, and GluN1	<0.0001	***
PLA		BK+GluN1/GluN2B vs. UNTRANSF. BK, and GluN1	<0.0001	***
Fig. 3E	Mann-Whitney U test (two-tailed)	BK+2A vs. BK (0 Ca^{2+})	<0.0001	***
		BK+2A vs. BK (1 Ca^{2+})	<0.0001	***
V_{half}		BK+2A vs. BK (10 Ca^{2+})	0.6165	Not significant
		BK+2A vs. BK (100 Ca^{2+})	0.0032	**
Symm. K^+		BK+2B vs. BK (0 Ca^{2+})	0.0003	***
		BK+2B vs. BK (1 Ca^{2+})	0.0003	***
		BK+2B vs. BK (10 Ca^{2+})	0.5743	Not significant
		BK+2B vs. BK (100 Ca^{2+})	0.0023	**
Fig. 3H	Mann-Whitney U test (two-tailed)	BK+2A vs. BK+2B	0.5368	Not significant
V_{half}		BK+2A vs. BK (0 Ca^{2+})	0.0008	***
Slices sol.		BK+2B vs. BK (0 Ca^{2+})	0.0005	***

Figure 4. A subpopulation of regular-spiking BC-L5PNs exhibit NMDAR–BK functional coupling

PANEL	STATISTIC	CONDITION	P VALUE	OUTPUT
Fig. 4D	Mann-Whitney U test (two-tailed) B-type vs. A-type	Resting membrane potential	0.4595	Not significant
Fig. 4E		Input resistance	0.2386	Not significant
Fig. 4F		Capacitance	0.8766	Not significant
Fig. 4G		Action potential freq. (200 pA)	0.4088	Not significant
		Action potential freq. (230 pA)	0.6359	Not significant
		Action potential freq. (260 pA)	0.8089	Not significant
		Action potential freq. (290 pA)	0.8481	Not significant
		Action potential freq. (320 pA)	0.8815	Not significant
Fig. 4H		Action potential threshold	0.2285	Not significant
Fig. 4I		Action potential amplitude	0.6334	Not significant
Fig. 4J		Action potential duration	<0.0001	***
Fig. 4K		I_{AHP} amplitude	<0.0001	***

Figure 5. BK-dependent inhibition of NMDARs reduces postsynaptic response amplitude

PANEL	STATISTIC	CONDITION	P VALUE	OUTPUT
Fig. 5B	Paired t-test (two-tailed)	A-type: ACSF vs. PAX	0.0631	Not significant
		A-type: ACSF vs. PAX+AP5	0.0004	***
PSP Amplitude		A-type: PAX vs. PAX+AP5	0.0003	***
		B-type: ACSF vs. PAX	0.0021	**
		B-type: ACSF vs. PAX+AP5	0.0027	**
		B-type: PAX vs. PAX+AP5	0.0004	***
Fig. 5B	Paired t-test (two-tailed)	A-type: ACSF vs. PAX	0.8007	Not significant
		A-type: ACSF vs. PAX+AP5	0.0018	**
PSP Area		A-type: PAX vs. PAX+AP5	0.0179	*
		B-type: ACSF vs. PAX	0.0029	**
		B-type: ACSF vs. PAX+AP5	0.0010	**
		B-type: PAX vs. PAX+AP5	0.0021	**
Fig. 5B	Paired t-test (two-tailed)	A-type: ACSF vs. PAX	0.7043	Not significant
		A-type: ACSF vs. PAX+AP5	0.0785	Not significant
Rise Time		A-type: PAX vs. PAX+AP5	0.3442	Not significant
		B-type: ACSF vs. PAX	0.0008	***
		B-type: ACSF vs. PAX+AP5	0.0014	**
		B-type: PAX vs. PAX+AP5	<0.0001	***
Fig. 5B	Paired t-test (two-tailed)	A-type: ACSF vs. PAX	0.4604	Not significant
		A-type: ACSF vs. PAX+AP5	0.0028	**
Decay Time		A-type: PAX vs. PAX+AP5	0.0076	**
		B-type: ACSF vs. PAX	0.0004	***
		B-type: ACSF vs. PAX+AP5	0.0030	**
		B-type: PAX vs. PAX+AP5	<0.0001	***
Fig. 5D	Paired t-test (two-tailed)	A-type: ACSF vs. PAX	0.3446	Not significant
		A-type: ACSF vs. PAX+AP5	0.0011	**
PSP Amplitude		A-type: PAX vs. PAX+AP5	0.0102	*
		B-type: ACSF vs. PAX	0.0015	**
		B-type: ACSF vs. PAX+AP5	0.0011	**
		B-type: PAX vs. PAX+AP5	0.0003	***
Fig. 5D	Paired t-test (two-tailed)	A-type: ACSF vs. PAX	0.1448	Not significant
		A-type: ACSF vs. PAX+AP5	0.0013	**
PSP Area		A-type: PAX vs. PAX+AP5	0.0158	*
		B-type: ACSF vs. PAX	0.0092	**
		B-type: ACSF vs. PAX+AP5	0.0073	**
		B-type: PAX vs. PAX+AP5	0.0040	**
Fig. 5D	Paired t-test (two-tailed)	A-type: ACSF vs. PAX	0.0518	Not significant
		A-type: ACSF vs. PAX+AP5	0.4969	Not significant
Rise Time		A-type: PAX vs. PAX+AP5	0.8170	Not significant
		B-type: ACSF vs. PAX	0.0303	*
		B-type: ACSF vs. PAX+AP5	0.5845	Not significant
		B-type: PAX vs. PAX+AP5	0.0237	*
Fig. 5D	Paired t-test (two-tailed)	A-type: ACSF vs. PAX	0.4425	Not significant
		A-type: ACSF vs. PAX+AP5	0.0124	*
Decay Time		A-type: PAX vs. PAX+AP5	0.0648	Not significant
		B-type: ACSF vs. PAX	0.0394	*
		B-type: ACSF vs. PAX+AP5	0.0339	*
		B-type: PAX vs. PAX+AP5	0.0047	**

Figure 6. NMDAR–BK coupling increases the threshold for induction of synaptic plasticity

PANEL	STATISTIC	CONDITION	P VALUE	OUTPUT
Fig. 6B Basal afferents (ACSF)	Paired t-test (two-tailed)	A-type (30 p) Basal vs. t-LTP	<0.0001	***
		B-type (30 p) Basal vs. t-LTP	0.4115	Not significant
	Unpaired t-test (two-tailed)	B-type vs. A-type (30 p) t-LTP	<0.0001	###
Fig. 6B Basal afferents (PAX_{MM})	Paired t-test (two-tailed)	A-type (30 p) Basal vs. t-LTP	<0.0001	***
		B-type (30 p) Basal vs. t-LTP	<0.0001	***
	Unpaired t-test (two-tailed)	B-type vs. A-type (30 p) t-LTP	0.9336	Not significant
Fig. 6D Apical afferents (ACSF)	Paired t-test (two-tailed)	A-type (30 p) Basal vs. t-LTP	0.3306	Not significant
		A-type (90 p) Basal vs. t-LTP	<0.0001	***
		B-type (90 p) Basal vs. t-LTP	<0.0001	***
	Unpaired t-test (two-tailed)	B-type vs. A-type (90 p) t-LTP	0.7896	Not significant

Figure 7. A high number and frequency of pre-post pairings relieves BK-dependent NMDAR inhibition

PANEL	STATISTIC	CONDITION	P VALUE	OUTPUT
Fig. 7A t-LTP 0.20 Hz	Paired t-test (two-tailed)	A-type (30 p) Basal vs. t-LTP	<0.0001	***
		B-type (30 p) Basal vs. t-LTP	0.4115	Not significant
		A-type (50 p) Basal vs. t-LTP	<0.0001	***
		B-type (50 p) Basal vs. t-LTP	<0.0001	***
		A-type (90 p) Basal vs. t-LTP	<0.0001	***
		B-type (90 p) Basal vs. t-LTP	<0.0001	***
Fig. 7B Summary 0.20 Hz	Unpaired t-test (two-tailed)	B-type vs. A-type (30 p) t-LTP	<0.0001	###
		B-type vs. A-type (50 p) t-LTP	<0.0001	###
		B-type vs. A-type (90 p) t-LTP	<0.0001	###
Fig. 7C t-LTP 0.33 Hz	Paired t-test (two-tailed)	A-type (30 p) Basal vs. t-LTP	<0.0001	***
		B-type (30 p) Basal vs. t-LTP	<0.0001	***
		A-type (50 p) Basal vs. t-LTP	<0.0001	***
		B-type (50 p) Basal vs. t-LTP	<0.0001	***
		A-type (90 p) Basal vs. t-LTP	<0.0001	***
		B-type (90 p) Basal vs. t-LTP	<0.0001	***

Figure 7 (continuation).
A high number and frequency of pre-post pairings relieves BK-dependent NMDAR inhibition

PANEL	STATISTIC	CONDITION	P VALUE	OUTPUT
Fig. 7D Summary 0.33 Hz	Unpaired t-test (two-tailed)	B-type vs. A-type (30 p) t-LTP	<0.0001	###
		B-type vs. A-type (50 p) t-LTP	<0.0001	###
		B-type vs. A-type (90 p) t-LTP	0.4680	Not significant

Supplementary Figure 3 (related to Figure 6).
NMDAR activation is mandatory for t-LTP induction

PANEL	STATISTIC	CONDITION	P VALUE	OUTPUT
Fig. S2A t-LTP 0.33 Hz (ACSF)	Paired t-test (two-tailed)	A-type (90 p) Basal vs. t-LTP	<0.0001	***
		B-type (90 p) Basal vs. t-LTP	<0.0001	***
	Unpaired t-test (two-tailed)	B-type vs. A-type (90 p) t-LTP	0.4680	Not significant
Fig. S2B t-LTP 0.33 Hz (AP5)	Paired t-test (two-tailed)	A-type (90 p) Basal vs. t-LTP	0.1026	Not significant
		B-type (90 p) Basal vs. t-LTP	0.0821	Not significant
	Unpaired t-test (two-tailed)	B-type vs. A-type (90 p) t-LTP	0.4210	Not significant

Supplementary Figure 4 (related to Figure 6).
BK channels are present in the plasma membrane of both types of BC-L5PN

PANEL	STATISTIC	CONDITION	P VALUE	OUTPUT
Fig. S3B BK current	Unpaired t-test (two-tailed)	-10 mV (B vs. A)	0.8611	Not significant
		+10 mV (B vs. A)	0.1025	Not significant
		+30 mV (B vs. A)	0.0073	**
		+50 mV (B vs. A)	0.0012	**
		+70 mV (B vs. A)	0.0002	***
		+90 mV (B vs. A)	<0.0001	***

Supplementary Table 2.

KEY RESOURCES TABLE

REAGENT or RESOURCE	SOURCE	IDENTIFIER
Antibodies		
Rabbit polyclonal anti-Maxi potassium channel α (BK α subunit)	Abcam	Cat#ab219072
Goat polyclonal anti-NMDAR1 (GluN1 subunit)	Novus Biologicals	Cat#NB100-41105
Mouse monoclonal anti-NMDA:1 (GluN2A subunit)	Santa Cruz Biotechnology	Cat#sc-515148
Mouse monoclonal anti-NMDA:2 (GluN2B subunit)	Santa Cruz Biotechnology	Cat#sc-365597
Chemicals, Peptides, and Recombinant Proteins		
D-AP5 (D-2-amino-5-phosphonovalerate, AP5)	Tocris	Cat#0106
BAPTA (1,2-bis(o-aminophenoxy)ethane-N,N,N′,N′-tetraacetic acid)	Abcam	Cat#ab144924
EGTA (Ethylene glycol-bis(β-aminoethyl ether)-N,N,N′,N′-tetraacetic acid)	Sigma-Aldrich	Cat#E4378
Glycine	Tocris	Cat#0219
HEDTA (N-(2-Hydroxyethyl)ethylenediamine-N,N′,N′-triacetic acid)	Sigma-Aldrich	Cat#H8126
Ifenprodil	Tocris	Cat#0545
NMDA (N-methyl-D-aspartate)	Tocris	Cat#0114
Paxilline	Tocris	Cat#2006
QX-314 (N-(2,6-Dimethylphenylcarbamoylmethyl)-triethylammonium bromide)	Tocris	Cat#1014
TTX (Tetrodotoxin)	Tocris	Cat#1078
ZnCl2 (Zinc chloride)	Merck	Cat#1.08816.1000
Critical Commercial Assays		
PLA: DuoLink In Situ Detection Reagents Red	Sigma-Aldrich	Cat#DUO92008
PLA: DuoLink In Situ PLA Probe Anti-Rabbit PLUS Antibody	Sigma-Aldrich	Cat#DUO92002; RRID:AB_10950581
PLA: DuoLink In Situ PLA Probe Anti-Mouse MINUS Antibody	Sigma-Aldrich	Cat#DUO92004; RRID:AB_2713942
PLA: DuoLink In Situ PLA Probe Anti-Goat MINUS Antibody	Sigma-Aldrich	Cat#DUO92006; RRID:AB_10953178
Cell transfection: jetPRIME reagent	Polyplus transfection	Cat#114-75
Experimental Models: Cell Lines		
Human: HEK293T cells	ATCC	Cat#CRL-3216
Experimental Models: Organisms/Strains		
Mouse: C57BL/6J	The Jackson Laboratory	Cat#000664; RRID:IMSR_JAX:000664
Recombinant DNA		
Plasmid: pBNJ-hsloTAG	(2)	N/A
Plasmid: pEYFP-NR1a	(3)	RRID: Addgene_17928
Plasmid: pEGFP-NR2A	(3)	RRID: Addgene_17924
Plasmid: pEGFP-NR2B	(3)	RRID: Addgene_17925
Software and Algorithms		
pClamp software package (Clampex, Clampfit)	Molecular Devices	https://www.moleculardevices.com/products/axon-patch-clamp-system/acquisition-and-analysis-software/pclamp-software-suite RRID:SCR_011323
MaxChelator	(4)	https://somapp.ucdmc.ucdavis.edu/pharmacology/bers/maxchelator/index.html
Prism8	GraphPad Inc.	https://www.graphpad.com/scientific-software/prism/ RRID:SCR_002798
Fiji	(5)	http://fiji.sc RRID:SCR_002285

SI References

1. J. P. Whitt, B. A. McNally, A. L. Meredith, Differential contribution of Ca(2+) sources to day and night BK current activation in the circadian clock. *The Journal of general physiology* **150**, 259-275 (2018).
2. T. Giraldez, T. E. Hughes, F. J. Sigworth, Generation of functional fluorescent BK channels by random insertion of GFP variants. *The Journal of general physiology* **126**, 429-438 (2005).
3. J. H. Luo *et al.*, Functional expression of distinct NMDA channel subunits tagged with green fluorescent protein in hippocampal neurons in culture. *Neuropharmacology* **42**, 306-318 (2002).
4. D. M. Bers, C. W. Patton, R. Nuccitelli, A practical guide to the preparation of Ca(2+) buffers. *Methods Cell Biol* **99**, 1-26 (2010).
5. J. Schindelin *et al.*, Fiji: an open-source platform for biological-image analysis. *Nat Methods* **9**, 676-682 (2012).

Calcium-activated Potassium channels

Alberto J. Gonzalez-Hernandez[1,2], A. Kshatri[1,2] and Teresa Giraldez[1,2]
[1]Dept. Basic Medical Sciences, Medical School and [2]Instituto de Tecnologias Biomedicas, Universidad de La Laguna, 38071-Tenerife, Spain.

1.Introduction

Calcium activated potassium (K_{Ca}) channels are unique members of the potassium ion channel family able to couple intracellular Ca^{2+} signals to membrane potential variations. K_{Ca} channels play fundamental roles ranging from regulating neuronal excitability to controlling muscle contraction. The K_{Ca} family of ion channels comprises three main subfamilies that are classified according to their single channel conductance: SK (small conductance; ~4-14 pS), IK (intermediate conductance; ~32-39 pS) and BK (large conductance; ~200-300 pS). Although they present distinct biophysical and pharmacological characteristics, all members of the K_{Ca} family are expressed at the plasma membrane as tetramers of α subunits encoded by different genes. Phylogenetically, the genes encoding α subunits of SK/IK and those of BK belong to two separated groups (Wei et al., 2005). This classification is paralleled by differences in their biophysical properties, Ca^{2+} sensitivity and regulatory mechanisms.

The following sections describe the function and physiological roles of K_{Ca} channel family members, as well as the underlying structural features. Additionally, different mechanisms regulating their function are discussed, as well as the pathologies that have been related to their malfunction.

2.BK channels

BK function and physiological roles

Large conductance voltage- and Ca^{2+}-activated K^+ channels (BK, MaxiK channels, Slo1 or KCa1.1 channels) were first described in the early 1980s as calcium and voltage-activated potassium currents (Marty, 1981; Pallotta et al., 1981). A distinctive feature was their sensitivity to the scorpion toxins charybdotoxin (Miller et al., 1985) and iberiotoxin (Galvez et al., 1990). In

Book Chapter for 'Calcium Signals: From single molecules to physiology'
e-book (IOP - Biophysical Society series; *in press*).

comparison to other K^+ channels, BK channels exhibit an unusually large conductance ranging between 100 pS - 300 pS (Latorre et al., 2017). The BKα subunit is encoded by the gene KCNMA1 (also known as *Slowpoke*), which was cloned from Drosophila (Adelman et al., 1992; Atkinson et al., 1991), mice (Butler et al., 1993) and human (Dworetzky et al., 1994; McCobb et al., 1995). BK channels are synergistically activated by intracellular Ca^{2+} and membrane depolarization. The channel's conductance (G) increases with voltage, analogously to other voltage-gated potassium channels; in addition, this G-V relationship is shifted towards negative voltages as Ca^{2+} concentration increases (**Fig.1**). This complex kinetic behavior was elegantly described by the work of the Magleby (Magleby, 2003; McManus and Magleby, 1988; Rothberg and Magleby, 1999) and Aldrich (Cox et al., 1997; Horrigan and Aldrich, 1999; Horrigan et al., 1999) laboratories, leading to the widely accepted allosteric model of Horrigan and Aldrich (Horrigan and Aldrich, 2002). The physiological relevance of this activation mechanism is significant because of its wide dynamic range, covering voltage values from -200 mV to +300 mV and Ca^{2+} concentrations up to 10 mM (Magleby, 2003). Not surprisingly, BK channels constitute an essential link between membrane excitability and intracellular [Ca^{2+}] signalling (Rothberg, 2012).

Unlike other members of the K_{Ca} family, BK channels are widely expressed in a variety of excitable and non-excitable cells (Latorre et al., 2017). In many cell types, BK activation relies on the local influx of Ca^{2+} to achieve micromolar levels (Fakler and Adelman, 2008). In neurons and smooth muscle cells, membrane depolarization provided by an action potential triggers Ca^{2+} influx through voltage-dependent Ca^{2+} channels (VDCCs) (Griguoli et al., 2016), coincidentally activating neighboring BK channels to repolarize the membrane and eventually closing VDCCs, terminating the Ca^{2+}signal (Marrion and Tavalin, 1998). This negative feedback mechanism enables BK channels as important regulators of many physiological processes including smooth muscle contraction (Meredith et al., 2004; Nelson et al., 1995; Semenov et al., 2011), insuline secretion (Houamed et al., 2010), neurotransmitter release (Lingle et al., 1996; Raffaelli et al., 2004; Robitaille et al., 1993), circadian rhythm (Meredith et al., 2006; Whitt et al., 2016), action potential termination (Montgomery and Meredith, 2012; Muller et al., 2007; Storm, 1987) and heart regulation (Lai et al., 2014).

Numerous studies have identified the VDCC subtypes mediating this coupling mechanism (Fakler and Adelman, 2008). These include Cav2.1 (Berkefeld and Fakler, 2008; Berkefeld et al., 2006; Edgerton and Reinhart, 2003; Womack et al., 2004), Cav2.2 (Berkefeld et al., 2006; Loane et al., 2007; Prakriya and Lingle, 1999), Cav1.2 (Berkefeld and Fakler, 2008; Berkefeld et al., 2006;

Grunnet and Kaufmann, 2004; Prakriya and Lingle, 1999), Cav1.3 (Prakriya and Lingle, 1999; Vivas et al., 2017) and Cav3.2 (Gackiere et al., 2013; Rehak et al., 2013). Interestingly, although it was originally suggested that BK channels do not interact with Cav2.3 (Berkefeld et al., 2006; Cerrada et al., 2018), recent evidence suggests that functional association with these channels may occur in CA1 pyramidal neurons (Gutzmann et al., 2019). Additionally, accessory subunits of Cav channels have been proposed to interact independently with BK channels. Zou et al. (2008) demonstrated that interaction with Cavβ**1** reduces Ca^{2+} sensitivity and slows down gating of the BK channel without affecting its relative membrane expression, although this finding remains to be shown in native tissues (Zou et al., 2008). Another recent finding suggests that high affinity interactions of the Cavα**2**δ**1** subunit with the BK channel N-terminus result in reduced membrane expression of Cav2 channels. This mechanism has been proposed to be of physiological relevance, since the administration of a BK N-terminus peptide leads to decreased inflammatory and neuropathic pain in mice (Zhang et al., 2018a).

The functional association of BK to Ca^{2+} sources is quite versatile, not restricted to VDCC but including other Ca^{2+} sources, such as ryanodine (RyR) (Chavis et al., 1998; Irie and Trussell, 2017; Wang et al., 2016; Whitt et al., 2018; Yamamura et al., 2012) and inositol 1,4,5-triphosphate (InsP3R) receptors (Zhao et al., 2010 (Zhao et al., 2010). Additionally, Ca^{2+} influx through other non-selective cation-permeable channels, such as N-methyl-D-aspartate receptors (NMDAR) or transient receptor potential (TRP) channels have been shown to activate BK channels. NMDARs associate with BK channels in the neuronal postsynaptic membrane where they modulate excitability (Isaacson and Murphy, 2001; Zhang et al., 2018b) and synaptic plasticity (Gómez et al., 2019). In the case of TRP channels, multiple subtypes of this large family of ion channels have been shown to form tight complexes with BK channels in a wide range of tissues. TRPV1 interacts with BK in dorsal root ganglion cells, where BK-mediated negative feedback has been proposed to modulate pain perception (Wu et al., 2013). In cerebral artery smooth muscle cells, TRPV4 has been proposed to activate BK channels via RyR-mediated Ca^{2+} release to induce artery relaxation (Earley et al., 2005; Liu et al., 2020; Szarka et al., 2018). In kidney podocytes, TRPC3 and TRPC6 physically interact with BK channels. These complexes have been proposed to be mechanically activated by glomeruli swelling, regulating glomerular filtration (Kim et al., 2009). Lastly, Ca^{2+} influx through menthol activated TRPM8 channels has been also shown to activate BK channel currents in glioblastoma cells, linking these Ca^{2+} signaling complexes to tumor invasion (Wondergem and Bartley, 2009).

The full functional picture of BK and its association to different calcium sources must take into account the regulation by auxiliary subunits and the characteristics of specific BK splice variants (see below). Although the dynamics of these complexes has not been fully explored in all physiological settings, it is tempting to hypothesize that the fine-tuning of this combinatorial complexity constitutes the basis for a large diversity of physiological outputs. An example of such complexity has been shown in the brain suprachiasmatic nucleus (SCN), where BK coupling to different calcium sources and auxiliary subunits during day and night leads to distinct excitability patterns (Whitt et al., 2018).

BK regulation by auxiliary subunits

In contrast to voltage-gated potassium channels, where functional diversity arises from evolution of different genes, the variety of distinctive BK channel phenotypes in different cells and tissues is derived from modifications of the single KCNMA1 gene encoding the BKα subunit (Dworetzky et al., 1996; McManus et al., 1995). Such mechanisms include alternative splicing (Shipston, 2001), post-translational modifications (Kyle and Braun, 2014) and association with auxiliary subunits (Latorre et al., 2017). Native BK channels are known to co-express with one of the two classes of structurally and functionally distinct modulatory subunits, β (1-4) and γ (1-4) (Brenner et al., 2000; Knaus et al., 1994; Wallner et al., 1999; Yan and Aldrich, 2012; Yan and Aldrich, 2010). The association of these subunits modifies almost all aspects of BK channel gating such as its kinetics, voltage dependence, Ca^{2+} sensitivity as well as the pharmacological properties of BK channels [reviewed in (Gonzalez-Perez and Lingle, 2019)].

The β subunits of the BK channel, coded by the genes KCNMB1-4, have a molecular size of ~20 KDa and share a common topology of two transmembrane homologous segments, TM1 and TM2, with a large extracellular loop and intracellular N and C-terminal regions (**Fig. 2**; reviewed in (Latorre et al., 2017)). In the recently solved human BK- β4 cryogenic electron microscopy (cryo-EM) structure, the two TM helices of β subunits are sandwiched between the voltage sensor domains of the four BK subunits and their large extracellular loop forms a crown over the central pore (Tao and MacKinnon, 2019); see following section). Each of the four β subunits have different functional signatures that match their defined physiological roles. Despite sharing a common gating mechanism to modify the BK channel functions, the biophysical properties conferred to BK

by each of these subunits are entirely unique (Yang and Cui, 2015). The β1, β2, and β4 subunits modify the Ca^{2+} sensitivity of BK channel activation. β1 and β2 increase the apparent Ca^{2+} sensitivity and slow down channel gating kinetics (Latorre et al., 2017). Although β4 exerts a more complex regulation in the presence of symmetrical K+, it increases Ca^{2+} sensitivity under physiological conditions (Jaffe et al., 2011; Latorre et al., 2017). β1 and β4 subunits do not display either inactivation or instantaneous current rectification, which differentiates them from β2 and some splice variants of the β3 subunits (Latorre et al., 2017). With the exception of the β3 subunits, the β1, β2 and β4 subunits regulate BK channel gating by stabilizing the voltage sensor domain (VSD) in its active conformation (Contreras et al., 2012). The association of BKα subunits with β subunits also confers sensitivity or resistance to various compounds of either pharmacological or physiological relevance (Latorre et al., 2017). For instance, the regulation of BK by 17 β-estradiol requires the presence of the β1 or β4 subunits, which also modulate the sensitivity of BK channels to alcohol (Feinberg-Zadek et al., 2008). The β4 subunit also confers BK channel resistance to iberiotoxin and charybdotoxin (Meera et al., 2000).

All γ subunits (~35 KDa) belong to the superfamily of Leucine-rich repeat containing (LRRC) proteins and are encoded by genes LRRC26 (γ1), LRRC52 (γ2), LRRC55 (γ3), and LRRC38 (γ4). They share a similar structure, consisting of an N-terminal cleavable signal peptide, a single transmembrane segment (TM), a large extracellular leucine rich repeat domain (LRRD) and an intracellular C-terminus (**Fig. 2**; (Gonzalez-Perez and Lingle, 2019; Yan and Aldrich, 2012; Yan and Aldrich, 2010). Unlike the complex effects of β subunits on the gating of BK channels, all γ subunits produce a hyperpolarizing shift in the voltage dependence of BK activation, to differing extents (γ1 > γ2 > γ3 > γ4). γ1 subunits produce the largest gating shifts (approximately −140 mV), resulting in BK opening at physiological voltages, even at resting intracellular Ca^{2+} concentrations (Yan and Aldrich, 2010). Growing evidence points to γ1-containing BK channels as being relevant players in the physiology of epithelial cells (Gonzalez-Perez and Lingle, 2019; Gonzalez-Perez et al., 2021). Additionally, γ1 makes BK channels resistant to activators such as Mallotoxin and GoSlo (Almassy and Begenisich, 2012; Giraldez, 2017; Kshatri et al., 2017). Another notable feature of these subunits is the "all or none" gating mechanism, where their functional effects are independent of the number of subunits present in the BK channels (Gonzalez-Perez et al., 2014). In other words, only one γ1 subunit is enough to produce the full gating effect on BK channels, whereas the functional effect of β subunits is incremental based on the number of β subunits associated with the BKα channels. It is also interesting to note that both γ1 and β2 subunits could

assemble simultaneously with BK subunits resulting in an additive gating shift (Gonzalez-Perez et al., 2015).

Structural basis of BK channel function

BK channels have unique features that distinguish them from other members of the calcium-gated and voltage-gated potassium channels families. BKα subunits show a modular structure (**Fig. 2**) consisting of a N-terminal domain embedded in the plasma membrane (MD) and a large C-terminal cytosolic domain that encompasses about one-third of the channel protein (Yang and Cui, 2015). The MD core is reminiscent of voltage-gated potassium channels, consisting of six transmembrane (TM) segments S1-S6 which include a conserved region (S1-S4) known as the voltage sensor domain (VSD), and a pore domain (PD) region formed by segments S5-S6, which constitutes the ion conducting pathway (**Fig. 2**). One striking feature of BK channels is their large conductance, which stands out within the potassium channels superfamily. Rather than differences in the sequence of the selectivity filter, which is highly conserved (Neyton and Miller, 1988), this characteristic is partly due to the presence of rings of negatively charged amino acids acting as an electrostatic bait to concentrate K^+ ions at the intracellular and extracellular cavities of the channel (Brelidze et al., 2003; Carvacho et al., 2008; Nimigean et al., 2003). Another relevant feature is the apparently large size of the inner cavity of around 8-10 Å, which results in inhibition by relatively large molecules (Tang et al., 2009; Wilkens and Aldrich, 2006) from the intracellular side (Li and Aldrich, 2004) and provides accessibility to MTS reagents (Zhou et al., 2011). In addition, BK has an extra TM segment S0, leading the NH_2 terminus of the protein to the extracellular side. The function of this segment has been related to VSD function, as well as to interactions with the auxiliary subunits (Castillo et al., 2016; Koval et al., 2007; Wallner et al., 1996).

Full BK tetramers are embedded in the membrane with central PD regions forming a pore, surrounded by four VSDs and S0 segments at the periphery (**Fig. 2**). Similar to other members of the K_{Ca} family (see below) and bacterial Ca^{2+}-gated channels (MthK; (Posson et al., 2013), it has been proposed that the gate of the BK channel that controls ion permeation is located near the selectivity filter and not at the cytosolic end of S6, although this issue remains controversial and is not fully answered by available structural data [for thorough analyses of this topic, see ((Latorre et al., 2017) and (Zhou et al., 2017)]. Both movement of the VSD and Ca^{2+} binding to the C-terminal domain (see below) regulate the function of this gate.

Unlike other voltage-gated K^+ channels, the gating charges in BK's VSD are not confined to the S4 TM segment, but are distributed between the S2, S3 and S4 segments (Yang and Cui, 2015). In fact, the voltage dependence of BK is relatively weak compared with Kv channels, (Horrigan and Aldrich, 1999; Rothberg and Magleby, 2000). It has been suggested that rather than undergoing a substantial movement of S4 as described in voltage-gated potassium channels, voltage-dependent gating in BK may involve small movements of S2, S3, and S4 (Ma et al., 2006; Pantazis et al., 2010). Additionally, interactions of the VSD with S0 (Koval et al., 2007) and the C-terminal domain (see below) modulate the unique VSD movements associated with channel activation (Ma et al., 2006; Pantazis et al., 2010). Unexpectedly, the cryo-EM structures of BK showed that, contrary to voltage-gated K^+ channels, the VSD is not domain-swapped, i.e. is located next to the PD of the same subunit (Tao et al., 2017).

The large cytosolic C-terminal domain of these channels contains two highly conserved domains known as Regulator of Conduction of K^+ (RCK1 and RCK2). Interestingly, RCK domains are also found in prokaryotic channels and other members of the Slo gene potassium channel family, playing a key role in gating and transporter activity (Giraldez and Rothberg, 2017). In the BK tetramer, four RCK tandems form a characteristic structure known as the "gating ring" (Hite et al., 2017; Tao et al., 2017; Wu et al., 2010; Yuan et al., 2011). This Ca^{2+}-sensing structural module contains distinct ion binding sites at the RCK1 and RCK2 domains (twelve in total in the full BK tetramer), which were identified in a large body of structure-function studies and account for the whole range of physiological Ca^{2+} concentrations activating the channel (Schreiber and Salkoff, 1997; Shi et al., 2002; Sweet and Cox, 2008; Xia et al., 2002; Zhang et al., 2010). The high calcium sensitivity of BK channels has been attributed to a binding site containing a cluster of acidic residues within RCK2, known as the calcium bowl (Schreiber and Salkoff, 1997; Schreiber et al., 1999; Wei et al., 1994). Two additional independent sites have been proposed to bind Ca^{2+} within the RCK1 domain, a high affinity site within the more N-terminal part of RCK1 and a low affinity site at the C-terminal lobe of RCK1 (Xia et al., 2002; Zhang et al., 2010). The latter has been proposed to be normally occupied by Mg^{2+} under physiological conditions (Latorre et al., 2017). Altogether, these three sites within the gating ring account for all of the Ca^{2+} sensitivity of the channel. In fact, substitution of the C-terminal domain by that of the pH-gated channel Slo3 (Xia et al., 2004), or removal of the whole gating ring (Budelli et al., 2013) abolishes all of the Ca^{2+}

and Mg^{2+} sensitivity of the channel, ruling out the possibility that other Ca^{2+} binding sites exist outside of the C-terminal domain. An intriguing question in the field relates to the cooperativity between Ca^{2+} binding sites. Several studies addressing this question arrived at different conclusions, although in all cases the level of cooperativity found was low (Qian et al., 2006; Sweet and Cox, 2008). Intriguingly, the cryo-EM structures suggest that interactions between sites may occur, paving the way for new functional studies (Hite et al., 2017; Zhou et al., 2017). In addition to Ca^{2+} and Mg^{2+}, other divalent cations can also activate BK channels including Sr^{2+}, Cd^{2+}, Mn^{2+}, Co^{2+}, and Ni^{2+} (Zeng et al., 2005). In addition, Ba^{2+} has been shown to activate the BK channel by binding to the calcium bowl (Zhou et al., 2012). BK channels can also be activated by protons binding to the RCK1 site (Hou et al., 2008).

Understanding how the binding of calcium to the gating ring is mechanically transduced into pore opening constitutes an important question regarding BK channel function. Based on the structure of the gating ring from a bacterial Ca^{2+}-activated channel (Jiang et al., 2002), it was proposed that expansion of this region upon Ca^{2+} binding would be transmitted to the PD via a stretch of amino acids linking the RCK1 domain to the end of the S6 TM (known as the C-linker; (Niu et al., 2004)). Structural data showing no significant conformational changes in the C-linker upon calcium binding together with further functional studies seem to draw a more complex picture (Zhou et al., 2017). Thus, conformational changes of the gating ring could be partly transmitted to the PD partly via the C-linker, in addition to noncovalent interactions between the C-terminal domain and the MD (Lee and Cui, 2010). In fact, cryo-EM structures of full BK channels unveiled close associations of the gating ring with the MD (Hite et al., 2017; Tao et al., 2017; Tao and MacKinnon, 2019), which is consistent with previous findings showing alterations in the voltage dependence of gating charge movements upon Ca^{2+} binding (Horrigan and Aldrich, 2002; Savalli et al., 2012). Recent functional studies further support the idea that the interaction between the calcium sensing domain and VSDs constitutes an important mechanism modulating voltage-dependent gating and pore opening in BK channels (Geng et al., 2020; Lorenzo-Ceballos et al., 2019; Miranda et al., 2018). Interestingly, some studies suggest that the two high affinity sites (RCK1 and Ca^{2+} bowl) may use distinct pathways leading to channel activation (Yang and Cui, 2015; Zhou et al., 2017). Evidence supporting this idea includes the identification of a number of residues that seem to participate in BK activation by Ca^{2+} binding to the RCK1 site but not the Ca^{2+} bowl (Bao et al., 2002; Yang et al., 2010). In addition, fluorescence studies have shown that RCK1 and RCK2 domains move independently when their specific binding sites are occupied (Miranda et al., 2016).

Finally, both sites have shown different voltage sensitivities (Miranda et al., 2013; Savalli et al., 2012; Sweet and Cox, 2008).

3. SK and IK channels

SK and IK function and physiological roles

The existence of calcium-activated and voltage-independent potassium channels was first proposed by Gárdos in erythrocytes, where he described a Ca^{2+}-mediated increase in potassium permeability induced by glycolysis inhibition (Gardos, 1958; Maher and Kuchel, 2003). Later work confirmed the role of intracellular Ca^{2+} ions in mediating rapid K^+-driven hyperpolarization of the neuronal membrane in invertebrates (Meech, 1972; Meech, 1974; Meech and Standen, 1974; Thomas and Gorman, 1977), amphibians (Barrett and Barret, 1976) and mammals (Krnjevic et al., 1975). SKα subunits are products of the KCNN1 (KCa2.1; SK1), KCNN2 (KCa2.2; SK2) and KCNN3 (KCa2.3; SK3) genes (Köhler et al., 1996), whereas IKα (KCa3.1; IK1; SK4) are encoded by the KCNN4 gene (Ishii et al., 1997b; Joiner et al., 1997). In contrast to BK channels, the function of SK and IK is independent of membrane voltage (Hirschberg et al., 1999). Consequently, their gating mechanisms can be attributed to a simpler model than BK, which was first proposed by the Marrion group twenty years ago (Hirschberg et al., 1998). These channels are activated through a mechanism mediated by their intrinsic association with cytosolic calcium-binding protein calmodulin (CaM) (Adelman, 2016). This tight association with CaM makes SK and IK channels highly sensitive to intracellular Ca^{2+} (~200 – 500 nM) (Köhler et al., 1996; Xia et al., 1998).

The SK and IK subfamilies have distinct tissue distribution and pharmacology. SK channels are mainly expressed in the nervous system (Stocker and Pedarzani, 2000) and are selectively blocked by the bee venom peptide apamin at different concentrations depending on the particular isoform (Blatz and Magleby, 1986; Grunnet et al., 2001; Ishii et al., 1997a). IK channels are predominantly distributed in blood cells, epithelial cells and in some peripheral neurons and are sensitive to charybdotoxin or iberiotoxin (de-Allie et al., 1996) as well as by imidazoles such as clotrimazole (Brugnara et al., 1993; Gardos, 1958; Jensen et al., 1998).

The physiological roles of SK and IK channels are very diverse, in tune with their well differentiated expression patterns. In non-excitable tissues, IK channels contribute to regulation of the membrane potential and Ca^{2+} signaling (Di et al., 2010; Toyama et al., 2008; Yu et al., 2013). Expression of IK channels has also been shown by immunohistochemical staining in human enteric, sensory and sympathetic neurons (Bahia et al., 2005; Furness et al., 2004; Mongan et al., 2005). Additionally, IK channels are localized to microglia and endothelial cells in the CNS (Pedarzani and Stocker, 2008). Microglial IK channels have been shown to have diverse functional roles including in respiratory burst, cell proliferation, cell migration and lipopolysaccharide-mediated nitric oxide production (Kaushal et al., 2007; Nguyen et al., 2017). Finally, growing evidence points to a role of IK channels in astrogliosis, which is associated with most forms of CNS insult (Bouhy et al., 2011 (Bouhy et al., 2011; Chen et al., 2011; Yu et al., 2014). In the CNS, SK channels play a major physiological role in the control of neuronal excitability, contributing to the action potential afterhyperpolarization (Sah and McLachlan, 1991; Zhang and McBain, 1995) and modulating spike firing frequency (Stackman et al., 2002). Additionally, they have been proposed to modulate synaptic plasticity (Faber et al., 2005; Jones et al., 2017; Ngo-Anh et al., 2005) [reviewed in (Faber, 2009)]. In contrast to BK channels, close proximity to Ca^{2+} sources is not mandatory for SK and IK channels in most physiological contexts, due to their higher Ca^{2+} sensitivity. Therefore, SK channels show a wider spatial distribution from their Ca^{2+} sources (Fakler and Adelman, 2008). In many (but not all) physiological contexts, SK channels provide negative feedback mechanisms on the associated Ca^{2+} sources similar to those discussed above for BK channels. For instance, SK channels have been shown to associate to L-type VGCCs in hippocampal neurons (Bowden et al., 2001; Marrion and Tavalin, 1998) and cardiac myocytes (Lu et al., 2007). Additionally, they functionally associate to NMDAR and VGCC Cav2.3 in the postsynaptic terminals of hippocampal and cortical neurons, where they regulate neuronal plasticity by blunting NMDAR-driven Ca^{2+} influx (Jones et al., 2017; Ngo-Anh et al., 2005). In the postsynaptic density of Purkinje cells, SK channels have been shown to form unusually close associations with mGlu1α and Cav2.1 (< 20 nm) in dendritic spines and shafts (Lujan et al., 2018). Interestingly, these channels have also been proposed to interact with TRPV4 in paraventricular nuclei neurons (PVN), participating in the control of renal and cardiovascular function. In this context, Ca^{2+} entering through mechano-activated TRPV4 activates SK channels, which in turn lead to cell depolarization, decreasing the PVN firing and neurohormone secretion from these nuclei (Feetham et al., 2015). Additionally, in auditory hair cells SK channels mediate inhibitory responses by coupling to Ca^{2+}-permeable nicotinic acetylcholine receptors (Oliver et al., 2000).

264

10

Structural determinants of SK/IK channel function and regulation by CaM

The cloning of SK/IK-**α** channels revealed that they have a conserved topology reminiscent of the voltage-gated potassium channel family, containing six transmembrane domains with intracellular N- and C-termini (Köhler et al., 1996 (Ishii et al., 1997b; Joiner et al., 1997; Köhler et al., 1996). However, consistent with their voltage-independence, these channels lack VSDs in their structures (Hirschberg et al., 1998; Hirschberg et al., 1999; Köhler et al., 1996). SK1-3 and IK channels share common features in their topology. All of them are constitutively associated with CaM, even in the absence of Ca^{2+}. Two conserved regions have been proposed to associate to CaM and mediate channel gating. The first consists of two **α**-helices in the intracellular S4-S5 linker, named S45A and S45B (**Fig. 2**). The second is made up of two long cytoplasmic helices in the C-terminal domain of the channel (HA and HB, known as the CaM binding-domain, CaMBD) (**Fig 2**). CaM is a small acidic protein consisting of a central domain linking two globular regions (the lobes N and C); each lobe contains two EF hand motifs that bind Ca^{2+} (Chattopadhyaya et al., 1992). The main SK/IK-CaM interaction interface is formed by the CaMBD and the N- and C-terminal lobes of CaM. Upon Ca^{2+} binding, the S45A and S45B helices of one channel subunit interact with its bound CaM molecule and with the HA helix of the adjacent subunit in a domain-swapped conformation, allowing synergistic channel activation (see below; (Lee and MacKinnon, 2018)).

Sequence identity between SK1, SK2 and SK3 is above 60%, whereas they show less than 40% homology with IK (Joiner et al., 1997). However, the main residues underlying the gating machinery and interactions with CaM are notably conserved (Fanger et al., 1999; Joiner et al., 1997). This fact, taken together with similar functional profiles of all members of this subfamily, led to the proposal that they all share common mechanisms of Ca^{2+} gating. A combination of functional and structural studies have provided useful insights into these mechanisms. Partial crystal structures are available for SK2 CaMBD-Ca^{2+}-CaM (Schumacher et al., 2001) and the apocalmodulin-SK complex (Schumacher et al., 2004), whereas the full-length structures of the IK-apoCaM and IK-Ca^{2+}-CaM have been recently solved (Lee and MacKinnon, 2018). Structural data confirmed, as had been largely demonstrated in functional studies (Adelman, 2016) that SK and IK channels are pre-associated with CaM through the CaMBD, in a Ca^{2+}-independent manner, displaying 1:1 stoichiometry (Lee and MacKinnon, 2018; Schumacher et al., 2004; Schumacher et al., 2001)(**Fig. 2**). Such CaM-SK conformational assembly prevents binding of Ca^{2+} at the CaM C-lobe. Therefore, the Ca^{2+}-free C-lobe holds SK-CaMBD while the N-lobe is

11

265

able to move freely as an intrinsically disordered domain (Keen et al., 1999; Lee and MacKinnon, 2018; Schumacher et al., 2004; Schumacher et al., 2001). In the presence of Ca^{2+}, Ca^{2+}-bound SK-CaM monomers are rearranged in pairs, forming a "dimer of dimers". The Ca^{2+}-CaM N-lobe interacts with the S45A helix, pulling S45B and displacing S5 and S6 from the central cavity of the pore, resulting in channel opening (**Fig. 2**) (Lee and MacKinnon, 2018).

Complementary structural studies have unveiled new insights into the mechanisms underlying the effect of endogenous and exogenous modulators of these channels. Phosphatidylinositol 4,5-bisphosphate (PIP_2), an endogenous positive modulator of SK function, binds to the CaM-SK interface and stabilizes their interaction (Zhang et al., 2014). Similarly, binding of phenylurea (PHU) and its derivatives at the CaM-CaMBD interface enhances channel activation (Nam et al., 2017; Zhang et al., 2012). A proposed mechanism for this potentiation is the transition of an intrinsically disordered portion of the S6-CaMBD linker to a more stable ordered conformation, facilitating mechanical activation of the channel (Zhang et al., 2013). Furthermore, a recent structural study demonstrates that hydrophobic interactions among the HA, S45A and S45B helices in SK2 and IK channels are crucial for their Ca^{2+} sensitivity and efficient coupling (Nam et al., 2021a), which is consistent with previous IK functional data (Morales et al., 2013). Structural data has led to the development of novel modulators of channel activity (Nam et al., 2017; Zhang et al., 2015a).

Understanding the characteristics of the PD and gate of SK and IK channels constitutes a relevant question related to the function of these channels. Using methanethiosulfonate compounds and substituted cysteine accesibility mutagenesis (SCAM), the groups of Maylie (SK channels; (Bruening-Wright et al., 2007; Bruening-Wright et al., 2002)) and Sauvé (IK channels; (Simoes et al., 2002); Klein et al., 2007) suggested that, similarly to what has been proposed for BK channels (see above), the channel gate is close to the pore cavity, probably at the selectivity filter. The authors noted a narrow constriction in the permeation pathway generated by a valine in position 282 (V282). However, it did not block the entry of small molecules and, therefore, of K^+ ions. This constriction was also observed in the full-length structure of the Ca^{2+}-unbound IK channel (Lee and MacKinnon, 2018).

A source of functional diversity of both SK and IK channels is their physiological regulation by phosphorylation/dephosphorylation. All of them include target residues for specific kinases in their sequences (Köhler et al 1996). In fact, in addition to their intrinsic association with CaM, SK channels have been shown to form constitutive complexes with the serine-threonine kinase CK2

and protein phosphatase 2A (PP2A) (Bildl et al., 2004). Interestingly, the effects of CK2 and PP2A are state-dependent (Allen et al., 2007). Thus, Ca^{2+} sensitivity is modulated by the relation between phosphorylation of closed channels by CK2 and dephosphorylation of open channels by PP2A (Adelman, 2016; Allen et al., 2007; Bildl et al., 2004). Intriguingly, the target of phosphorylation by CK2 is located within the linker domain of CaM and not in the SK channel. Phosphorylation reduces the affinity of CaM for the CaMBD, resulting in a diminished Ca^{2+} sensitivity of SK and IK channels (Bildl et al., 2004; Nam et al., 2021b)).

Reversible post-translational modifications and interaction with cofactors ultimately depend on the integration of the channel with upstream signalling pathways that may cooperate or antagonize each other to open or close the channels. For instance, activation of G-coupled protein receptors (GPCR) such as the receptor for the neurotransmitter norepinephrine mediate intracellular pathways activating CK2, resulting in sensitization of sensory neurons (Maingret et al., 2008). Interestingly, CaM phosphorylation also inhibits PIP_2 modulation of SK channels, potentially increasing channel inhibition by G protein-mediated PIP2 hydrolysis (Zhang et al., 2014). Other kinases that have been shown to actively modulate SK and IK channels in different physiological contexts include protein kinase A (PKA) and CaM kinase II (CaMKII). Phosphorylation by PKA of the CaMBD in IK channels leads to decreased CaM affinity for CaMBD, therefore reducing channel activity (Wong and Schlichter, 2014). Finally, although CaMKII has been shown to interact with SK and IK channels, many aspects of this regulatory mechanism remain unclear (Ferreira et al., 2015; Mizukami et al., 2015; Shrestha et al., 2019; Tenma et al., 2018).

KCa channelopathies

Although the members of the K_{Ca} channels family (BK, IK and SK) display differences in their biophysical characteristics, molecular structures and pharmacological signatures, they all play an essential physiological role by coupling intracellular Ca^{2+} to changes in cell membrane potential. Consistent with the relevance of this process, inherited defects in the function of K_{Ca} channels lead to a wide array of human diseases. A list of mutations encoding K_{Ca} genes are presented in **Table 1**. This section describes a selection of these mutations and their associated pathologies.

A frame shift mutation in exon 1 of SK3 channels has been reported in human schizophrenia patients (Bowen et al., 2001). It was later demonstrated that this dominant-negative mutation suppresses SK-mediated currents by generating truncated channels (Miller et al., 2001). Subsequently, the functional implication of this mutation in the pathogenesis of schizophrenia was

established by Soden and collaborators (Soden et al., 2013). In mice, expression of this mutation in dopamine neurons reduced the coupling between SK channels and NMDAR receptors leading to enhanced excitability and elevated dopamine release, eventually leading to impaired sensorimotor gating associated with psychotic behaviour in schizophrenia (Soden et al., 2013). Koot and collaborators (Koot et al., 2016) identified a de novo mutation (V450L) in SK3 channels associated with autosomal dominant idiopathic non-cirrhotic portal hypertension. This amino acid substitution makes SK3 channels constitutively active even under basal conditions, generating a sustained K^+ conductance deleterious to liver cells, leading to portal hypertension (Koot et al., 2016). A recent study reported a series of missense mutations (K269E, G350D, S436C) in SK3 channels causing Zimmermann-Laband syndrome (ZLS) (Bauer et al., 2019). These gain-of-function (GOF) mutations were shown to enhance the Ca^{2+} sensitivity of SK3 channels and their activation rate. Although the exact pathophysiological mechanism of these mutations remains unclear, one plausible hypothesis is that the excessive K^+ conductance from SK3 channels results in arterial vasodilation, increasing capillary hydrostatic pressure. The ZLS phenotype could arise from vascular rupture or tissue damage during organogenesis (Bauer et al., 2019).

IK channels are the major source for K^+ permeability in red blood cells (RBCs), where they are involved in maintaining water and solute homeostasis (Begenisich et al., 2004). Many studies have identified de novo missense mutations in IK channels (R352H, V282M, V282E) that are linked to dehydrated hereditary stomatocytosis (DHSt) disorder (Andolfo et al., 2015; Glogowska et al., 2015; Rapetti-Mauss et al., 2015). Importantly, the R352H mutation located in the CaMB domain was found to stabilize the activated state and increase the Ca^{2+} sensitivity of IK channels, leading to augmented K^+ efflux from RBCs and dehydration, followed by haemolytic anaemia (Rapetti-Mauss et al., 2015). While it has not been tested functionally, V282M and V282E mutations would alter the ion conduction pathway due to their location in the S6 hydrophobic constriction (see previous section). In fact, V282G mutation produced constitutively open and 'leaky' channels (Garneau et al., 2009).

Human BK channel channelopathies are primarily associated with neurological conditions such as seizures, movement disorders, developmental delay, and intellectual disability [reviewed in (Bailey et al., 2019)]. GOF mutations in BK channels have been implicated in the development of neuronal excitability disorders. A single GOF mutation -D434G- increases the Ca^{2+} sensitivity of BK channels and causes autosomal-dominant epilepsy with paroxysmal dyskinesias (Du et al., 2005). Similarly, another GOF mutation -N995S- was found to enhance the voltage dependence

of BK channel activation and cause epilepsy (Li et al., 2018). Both of these mutations would enhance neuronal BK channel activity and therefore increase the fast afterhyperpolarization of the action potential, ultimately leading to increased neuronal excitability. In addition to the BKα subunits, mutations in its accessory subunits have also been reported to cause idiopathic generalized epilepsy (IGE) (Lorenz et al., 2007). For instance, a deletion of base A450 in exon 4 of the β3 gene, results in a frame shift that alters three amino acids and truncates the protein by 18 amino acids (Hu et al., 2003). Functionally, this alteration causes a rapid inactivation of BK channels and also shifts the activation curve rightwards, which has been associated with reduced synaptic inhibition, and therefore increased neuronal excitability and seizure susceptibility (Hu et al., 2003). A recent study by (Du et al., 2020) identified a loss-of-function mutation in the selectivity filter of the BK channels (G354S) associated with progressive cerebellar degeneration, ataxia, and cognitive impairment. This mutation dramatically reduced BK single channel conductance and ion selectivity, leading to depolarization and mitochondrial dysfunction. Subsequently, this was associated with a reduction in cellular viability and cerebellar ataxia (Du et al., 2020).

Concluding remarks

In recent years, our understanding of the physiological roles, structural basis of function and pathophysiology of K_{Ca} channels has significantly evolved since they were first discovered almost forty years ago. In addition to a large body of functional and electrophysiological studies, we now have access to full-length structures of the BK channel with and without the β4 auxiliary subunit, as well as the human IK-CaM complex structures, allowing us to disentangle the mechanisms underlying gating and function with unprecedented precision. Significant advances have been made in our knowledge about the structure–function relations of the diverse structural architectures characterizing the members of the K_{Ca} family. A growing number of pathologies associated with K_{Ca} channel dysfunction has emerged in recent years, highlighting the importance of the physiological roles played by these channels, mainly related to the coupling of Ca^{2+} with membrane voltage signalling. Regardless of their different structural, biophysical and pharmacological features, members of the K_{Ca} family are commonly associated with other channels or regulatory proteins to form functional supercomplexes. Further studies of K_{Ca} channels within such functional complexes in their native environment will lead to a new level of fundamental discoveries. In the long run, this will pave the way to drug design studies or genetic

Figures and Figure legends

Figure 1. Macroscopic currents of BK channels. (A) Macroscopic currents of BK channels in response to a family of voltage pulses (schematized below the current traces) in the absence of Ca^{2+}. (B) Macroscopic currents of BK channels in response to increasing Ca^{2+} concentrations (color coded in the legend). (C) Increasing intracellular Ca2+ concentrations shift the voltage-dependent activation curves (G–V relations) towards more negative voltages. Ca^{2+} concentrations are color-coded as in B.

strategies that recognize tissue-specific subunit combinations or K_{Ca}-protein supercomplexes and help enable more efficient treatments of K_{Ca} channelopathies.

Figure 2. Topology and structures of BK and SK/IK channels. (A) *Top*, schematic topology of BKα (center) and auxiliary subunits **β** (right) and **γ** (left). In the BKα subunit, binding sites for divalent cations are located in the cytosolic C-terminal region of the channel. Each α subunit contains two high affinity Ca^{2+} binding sites (shown as green circles) and one low affinity Ca^{2+} and Mg^{2+} binding site, formed by residues from RCK1, S0-S1 and S2-S3 intracellular loops (not shown). *Bottom*, Ca^{2+}-bound BKα homotetramer full-length structure from human (PDB: 6V38). (B) *Top*, schematic protein topology of one SKα-subunit including CaM (in blue) bound to the CaMBD. Relevant regions involved in SK gating are indicated: helices S45A, S45B, and the CaMB formed by helices HA and HB. *Bottom*, full-length structure of the Ca^{2+}-CaM bound IK channel (PDB: 6CNN).

Table 1

Gene/protein	Disease Phenotype	Mutation/ location in the protein	Functional effects	Reference
KCNMA1// BKα	A, CI, tremor and hypertelorism	S351Y/Pore	No current	(Liang et al., 2019)
KCNMA1// BKα	A, CA, CI, E + PD, ID	G354S/Pore	Reduced current and slower activation kinetics	(Du et al., 2020)
KCNMA1// BKα	A, CA, DD, H	G356R/Pore	No current	(Liang et al., 2019)
KCNMA1// BKα	CA, CM, DD, E, ID, H,	G375R/S6	No current	(Liang et al., 2019)
KCNMA1// BKα	A, CA, CM, DD, ID, H and strabismus	C413Y+N449Is/S6-RCK1 linker	Reduced current (G-V shift to depolarized potentials) (C413Y) + No current (N449Is)	(Liang et al., 2019)
KCNMA1// BKα	E + PD	D434G/RCK1 domain	Gain-of-function mutation leading to enhanced Ca2+ sensitivity	(Du et al., 2005; Yang et al., 2010)
KCNMA1// BKα	Non-described	H444Q/RCK1	Loss-of-function mutation (G-V shift to depolarized potentials, slower activation and faster deactivation)	(Moldenhauer et al., 2020b)
KCNMA1// BKα	A, CA, PD	K457E/RCK1	No specified (putative loss-of-function mutation)	(Buckley et al., 2020)
KCNMA1// BKα	A, CA, E + PD, DD, ID	R458Ter/RCK1	Truncation	(Yesil et al., 2018)
KCNMA1// BKα	E, PD	I512V/RCK1	No difference	(Tian et al., 2018)
KCNMA1// BKα	E (not directly linked to this mutation)	K518N/RCK1	No difference	(Li et al., 2018)
KCNMA1// BKα	CA, PD, ID	N536H/RCK1	Gain-of-function mutation	(Zhang et al., 2020)
KCNMA1// BKα	E (not directly linked to this mutation)	E656A/RCK1-RCK2 linker	No difference	(Li et al., 2018)
KCNMA1// BKα	A, DD, ID, H and strabismus	I663V/RCK1-RCK2 linker	No current	(Liang et al., 2019)

KCNMA1/ BKα	E, DD, ID	Y676Lfs*7/RCK1-RCK2 linker	Truncation	(Tabarki et al., 2016)
KCNMA1/ BKα	CA, CI, DD, ID,	P805L/RCK2	Reduced current (G-V shift to depolarized potentials) and reduced expression	(Liang et al., 2019)
KCNMA1/ BKα	DD, ID, PD	E884K/RCK2	Not available	(Zhang et al., 2015b)
KCNMA1/ BKα	Non-described	D965V/RCK2	Loss-of-function mutation (G-V shift to depolarized potentials, slower activation).	(Moldenhauer et al., 2020b)
KCNMA1/ BKα	CI, E, ID	D984N/RCK2	Not available	(Liang et al., 2019)
KCNMA1/ BKα	E	N995S or N999S or N1053S and N999S+R1128W double mutant/RCK2 domain	De novo mutation Shifts the voltage dependence to more negative potentials without altering Ca2+ sensitivity	(Li et al., 2018; Plante et al., 2019)
KCNMA1/ BKα	Non-described	R1097H/RCK2 domain	Loss-of-function mutation (G-V shift to depolarized potential only at low [Ca^{2+}])	(Moldenhauer et al., 2020a)
KCNMA1/ BKα	E (not directly linked to this mutation)	N1159S/C-terminal	No difference	(Li et al., 2018)
KCNMB1/ BKβ1	Diastolic hypertension	E65K/Extracellular loop connecting β1 two transmembrane segments.	Gain-of-function mutation rendering enhanced Ca2+ sensitivity	(Fernandez-Fernandez et al., 2004)
KCNMB3/ BKβ3	Idiopathic generalized epilepsy	Del A750/C-terminal region (truncation of 21 amino acids)	BK inactivation	(Hu et al., 2003; Lorenz et al., 2007)
KCNN3/ SK3	Idiopathic non-cirrhotic portal hypertension	V450L/Cytoplasmic loop between the S4 and S5 transmembrane segments	Increased Ca^{2+} sensitivity and faster activation kinetics	(Bauer et al., 2019; Koot et al., 2016)
KCNN3/ SK3	Schizophrenia	hSK3Δ (L283fs287X mutation)/N-terminal cytoplasmic region (deletion)	Suppresses SK currents / Disrupts SK-NMDAR coupling	(Miller et al., 2001; Soden et al., 2013)
KCNN3/ SK3	Zimmermann-Laband syndrome	K269E/Cytoplasmic N-terminus	Increased Ca^{2+} sensitivity and faster activation kinetics	(Bauer et al., 2019)
KCNN3/ SK3	Zimmermann-Laband syndrome	G350D/Cytoplasmic linker S2-S3	Increased Ca^{2+} sensitivity and faster activation kinetics	(Bauer et al., 2019)
KCNN3/ SK3	Zimmermann-Laband syndrome	S436C/Cytoplasmic loop between the S4 and S5 transmembrane segments	Increased Ca^{2+} sensitivity and faster activation kinetics	(Bauer et al., 2019)
KCNN4/ IK	Dehydrated hereditary stomatocytosis	R352H/ Cytosolic CaMBD	Increased currents and Ca^{2+} sensitivity	(Andolfo et al., 2015; Rapetti-Mauss et al., 2015)
KCNN4/ IK	Dehydrated hereditary stomatocytosis	V282M/S6 cytosolic part	-	(Andolfo et al., 2015; Glogowska et al., 2015)
KCNN4/ IK	Dehydrated hereditary stomatocytosis	V282E/S6 cytosolic part	-	(Glogowska et al., 2015)

A: ataxia; CA: cerebral/cerebellar atrophy; CI: cognitive impairment; CM: congenital malformations; DD: developmental delay; E: epilepsy; H: hypotonia; ID: intelectual disability; PD: paroxysmal dyskinesia.

TABLE 1: K_{Ca} channelopathies. This table summarizes mutations, pathophysiological phenotype, location within the protein, functional effects, and related references. Note that only mutations that have been functionally characterised are included. For extended information regarding human KCNMA1 mutations, see (Miller et al., 2021) and https://www.kciaf.org.

References

Adelman, J. P., 2016. SK channels and calmodulin. Channels (Austin). 10, 1-6.

Adelman, J. P., et al., 1992. Calcium-activated potassium channels expressed from cloned complementary DNAs. Neuron. 9, 209-16.

Allen, D., et al., 2007. Organization and regulation of small conductance Ca2+-activated K+ channel multiprotein complexes. J Neurosci. 27, 2369-76.

Almassy, J., Begenisich, T., 2012. The LRRC26 protein selectively alters the efficacy of BK channel activators. Mol Pharmacol. 81, 21-30.

Andolfo, I., et al., 2015. Novel Gardos channel mutations linked to dehydrated hereditary stomatocytosis (xerocytosis). Am J Hematol. 90, 921-6.

Atkinson, N. S., et al., 1991. A component of calcium-activated potassium channels encoded by the Drosophila slo locus. Science. 253, 551-5.

Bahia, P. K., et al., 2005. A functional role for small-conductance calcium-activated potassium channels in sensory pathways including nociceptive processes. J Neurosci. 25, 3489-98.

Bailey, C. S., et al., 2019. KCNMA1-linked channelopathy. J Gen Physiol. 151, 1173-1189.

Bao, L., et al., 2002. Elimination of the BK(Ca) channel's high-affinity Ca(2+) sensitivity. J Gen Physiol. 120, 173-89.

Barrett, E. F., Barret, J. N., 1976. Separation of two voltage-sensitive potassium currents, and demonstration of a tetrodotoxin-resistant calcium current in frog motoneurones. J Physiol. 255, 737-74.

Bauer, C. K., et al., 2019. Gain-of-Function Mutations in KCNN3 Encoding the Small-Conductance Ca(2+)-Activated K(+) Channel SK3 Cause Zimmermann-Laband Syndrome. Am J Hum Genet. 104, 1139-1157.

Begenisich, T., et al., 2004. Physiological roles of the intermediate conductance, Ca2+-activated potassium channel Kcnn4. J Biol Chem. 279, 47681-7.

Berkefeld, H., Fakler, B., 2008. Repolarizing responses of BKCa-Cav complexes are distinctly shaped by their Cav subunits. J Neurosci. 28, 8238-45.

Berkefeld, H., et al., 2006. BKCa-Cav channel complexes mediate rapid and localized Ca2+-activated K+ signaling. Science. 314, 615-20.
Bildl, W., et al., 2004. Protein kinase CK2 is coassembled with small conductance Ca(2+)-activated K+ channels and regulates channel gating. Neuron. 43, 847-58.
Blatz, A. L., Magleby, K. L., 1986. Single apamin-blocked Ca-activated K+ channels of small conductance in cultured rat skeletal muscle. Nature. 323, 718-20.
Bouhy, D., et al., 2011. Inhibition of the Ca(2)(+)-dependent K(+) channel, KCNN4/KCa3.1, improves tissue protection and locomotor recovery after spinal cord injury. J Neurosci. 31, 16298-308.
Bowden, S. E., et al., 2001. Somatic colocalization of rat SK1 and D class (Ca(v)1.2) L-type calcium channels in rat CA1 hippocampal pyramidal neurons. J Neurosci. 21, RC175.
Bowen, T., et al., 2001. Mutation screening of the KCNN3 gene reveals a rare frameshift mutation. Mol Psychiatry. 6, 259-60.
Brelidze, T. I., et al., 2003. A ring of eight conserved negatively charged amino acids doubles the conductance of BK channels and prevents inward rectification. Proc Natl Acad Sci U S A. 100, 9017-22.
Brenner, R., et al., 2000. Cloning and functional characterization of novel large conductance calcium-activated potassium channel beta subunits, hKCNMB3 and hKCNMB4. J Biol Chem. 275, 6453-61.
Bruening-Wright, A., et al., 2007. Evidence for a deep pore activation gate in small conductance Ca2+-activated K+ channels. J Gen Physiol. 130, 601-10.
Bruening-Wright, A., et al., 2002. Localization of the Activation Gate for Small Conductance Ca2+-Activated K+ Channels. J Neurosci. 22, 6499-6506.
Brugnara, C., et al., 1993. Inhibition of Ca(2+)-dependent K+ transport and cell dehydration in sickle erythrocytes by clotrimazole and other imidazole derivatives. J Clin Invest. 92, 520-6.
Buckley, C., et al., 2020. Status Dystonicus, Oculogyric Crisis and Paroxysmal Dyskinesia in a 25 Year-Old Woman with a Novel KCNMA1 Variant, K457E. Tremor Other Hyperkinet Mov (N Y). 10, 49.
Budelli, G., et al., 2013. Properties of Slo1 K+ channels with and without the gating ring. Proc Natl Acad Sci U S A. 110, 16657-62.
Butler, A., et al., 1993. mSlo, a complex mouse gene encoding "maxi" calcium-activated potassium channels. Science. 261, 221-4.
Carvacho, I., et al., 2008. Intrinsic electrostatic potential in the BK channel pore: role in determining single channel conductance and block. J Gen Physiol. 131, 147-61.
Castillo, J. P., et al., 2016. beta1-subunit-induced structural rearrangements of the Ca2+- and voltage-activated K+ (BK) channel. Proc Natl Acad Sci U S A. 113, E3231-9.
Cerrada, A., et al., 2018. Quantitative Analysis of Subcellular Nanodomains Formed by BK and Voltage-Gated Calcium Channels. Biophysical Journal. 114, 479a-480a.
Chattopadhyaya, R., et al., 1992. Calmodulin structure refined at 1.7 A resolution. J Mol Biol. 228, 1177-92.
Chavis, P., et al., 1998. Modulation of big K+ channel activity by ryanodine receptors and L-type Ca2+ channels in neurons. Eur J Neurosci. 10, 2322-7.
Chen, Y. J., et al., 2011. The KCa3.1 blocker TRAM-34 reduces infarction and neurological deficit in a rat model of ischemia/reperfusion stroke. J Cereb Blood Flow Metab. 31, 2363-74.
Contreras, G. F., et al., 2012. Modulation of BK channel voltage gating by different auxiliary beta subunits. Proc Natl Acad Sci U S A. 109, 18991-6.
Cox, D. H., et al., 1997. Allosteric gating of a large conductance Ca-activated K+ channel. J Gen Physiol. 110, 257-81.

de-Allie, F. A., et al., 1996. Characterization of Ca(2+)-activated 86Rb+ fluxes in rat C6 glioma cells: a system for identifying novel IKCa-channel toxins. Br J Pharmacol. 117, 479-487.
Di, L., et al., 2010. Inhibition of the K+ channel KCa3.1 ameliorates T cell-mediated colitis. Proc Natl Acad Sci U S A. 107, 1541-6.
Du, W., et al., 2005. Calcium-sensitive potassium channelopathy in human epilepsy and paroxysmal movement disorder. Nat Genet. 37, 733-8.
Du, X., et al., 2020. Loss-of-function BK channel mutation causes impaired mitochondria and progressive cerebellar ataxia. Proc Natl Acad Sci U S A. 117, 6023-6034.
Dworetzky, S. I., et al., 1996. Phenotypic alteration of a human BK (hSlo) channel by hSlobeta subunit coexpression: changes in blocker sensitivity, activation/relaxation and inactivation kinetics, and protein kinase A modulation. J Neurosci. 16, 4543-50.
Dworetzky, S. I., et al., 1994. Cloning and expression of a human large-conductance calcium-activated potassium channel. Brain Res Mol Brain Res. 27, 189-93.
Earley, S., et al., 2005. TRPV4 forms a novel Ca2+ signaling complex with ryanodine receptors and BKCa channels. Circ Res. 97, 1270-9.
Edgerton, J. R., Reinhart, P. H., 2003. Distinct contributions of small and large conductance Ca2+-activated K+ channels to rat Purkinje neuron function. J Physiol. 548, 53-69.
Faber, E. S., 2009. Functions and modulation of neuronal SK channels. Cell Biochem Biophys. 55, 127-39.
Faber, E. S., et al., 2005. SK channels regulate excitatory synaptic transmission and plasticity in the lateral amygdala. Nat Neurosci. 8, 635-41.
Fakler, B., Adelman, J. P., 2008. Control of K(Ca) channels by calcium nano/microdomains. Neuron. 59, 873-81.
Fanger, C. M., et al., 1999. Calmodulin Mediates Calcium-dependent Activation of the Intermediate Conductance KCa Channel, IKCa1. J Biol Chem. 274, 5746-5754.
Feetham, C. H., et al., 2015. TRPV4 and K(Ca) ion channels functionally couple as osmosensors in the paraventricular nucleus. Br J Pharmacol. 172, 1753-68.
Feinberg-Zadek, P. L., et al., 2008. BK channel subunit composition modulates molecular tolerance to ethanol. Alcohol Clin Exp Res. 32, 1207-16.
Fernandez-Fernandez, J. M., et al., 2004. Gain-of-function mutation in the KCNMB1 potassium channel subunit is associated with low prevalence of diastolic hypertension. J Clin Invest. 113, 1032-9.
Ferreira, R., et al., 2015. KCa3.1/IK1 Channel Regulation by cGMP-Dependent Protein Kinase (PKG) via Reactive Oxygen Species and CaMKII in Microglia: An Immune Modulating Feedback System? Front Immunol. 6, 153.
Furness, J. B., et al., 2004. Intermediate conductance potassium (IK) channels occur in human enteric neurons. Auton Neurosci. 112, 93-7.
Gackiere, F., et al., 2013. Functional coupling between large-conductance potassium channels and Cav3.2 voltage-dependent calcium channels participates in prostate cancer cell growth. Biol Open. 2, 941-51.
Galvez, A., et al., 1990. Purification and characterization of a unique, potent, peptidyl probe for the high conductance calcium-activated potassium channel from venom of the scorpion Buthus tamulus. J Biol Chem. 265, 11083-90.
Gardos, G., 1958. The function of calcium in the potassium permeability of human erythrocytes. Biochim Biophys Acta. 30, 653-4.
Garneau, L., et al., 2009. Hydrophobic interactions as key determinants to the KCa3.1 channel closed configuration. An analysis of KCa3.1 mutants constitutively active in zero Ca2+. J Biol Chem. 284, 389-403.
Geng, Y., et al., 2020. Coupling of Ca(2+) and voltage activation in BK channels through the alphaB helix/voltage sensor interface. Proc Natl Acad Sci U S A. 117, 14512-14521.

Giraldez, T., 2017. The GoSlo family of BK channel activators: A no-go for gamma subunits? Channels (Austin). 11, 89-90.
Giraldez, T., Rothberg, B. S., 2017. Understanding the conformational motions of RCK gating rings. J Gen Physiol. 149, 431-441.
Glogowska, E., et al., 2015. Mutations in the Gardos channel (KCNN4) are associated with hereditary xerocytosis. Blood. 126, 1281-4.
Gómez, R., et al., 2019. Role of NMDAR-BK Complexes in the Integration of Synaptic Inputs of Barrel Cortex Pyramidal Neurons. Biophys J. 116, 36A.
Gonzalez-Perez, V., Lingle, C. J., 2019. Regulation of BK Channels by Beta and Gamma Subunits. Annu Rev Physiol. 81, 113-137.
Gonzalez-Perez, V., et al., 2021. Goblet cell LRRC26 regulates BK channel activation and protects against colitis in mice. Proc Natl Acad Sci U S A. 118.
Gonzalez-Perez, V., et al., 2014. Functional regulation of BK potassium channels by gamma1 auxiliary subunits. Proc Natl Acad Sci U S A. 111, 4868-73.
Gonzalez-Perez, V., et al., 2015. Two classes of regulatory subunits coassemble in the same BK channel and independently regulate gating. Nat Commun. 6, 8341.
Griguoli, M., et al., 2016. Presynaptic BK channels control transmitter release: physiological relevance and potential therapeutic implications. J Physiol. 594, 3489-500.
Grunnet, M., et al., 2001. Apamin interacts with all subtypes of cloned small-conductance Ca2+-activated K+ channels. Pflugers Arch. 441, 544-50.
Grunnet, M., Kaufmann, W. A., 2004. Coassembly of big conductance Ca2+-activated K+ channels and L-type voltage-gated Ca2+ channels in rat brain. J Biol Chem. 279, 36445-53.
Gutzmann, J. J., et al., 2019. Functional Coupling of Cav2.3 and BK Potassium Channels Regulates Action Potential Repolarization and Short-Term Plasticity in the Mouse Hippocampus. Front Cell Neurosci. 13, 27.
Hirschberg, B., et al., 1998. Gating of Recombinant Small-Conductance Ca-activated K+Channels by Calcium. The Journal of General Physiology. 111, 565-581.
Hirschberg, B., et al., 1999. Gating Properties of Single SK Channels in Hippocampal CA1 Pyramidal Neurons. Biophysical Journal. 77, 1905-1913.
Hite, R. K., et al., 2017. Structural basis for gating the high-conductance Ca2+-activated K+ channel. Nature. 541, 52-57.
Horrigan, F. T., Aldrich, R. W., 1999. Allosteric voltage gating of potassium channels II. Mslo channel gating charge movement in the absence of Ca(2+). J Gen Physiol. 114, 305-36.
Horrigan, F. T., Aldrich, R. W., 2002. Coupling between voltage sensor activation, Ca2+ binding and channel opening in large conductance (BK) potassium channels. J Gen Physiol. 120, 267-305.
Horrigan, F. T., et al., 1999. Allosteric voltage gating of potassium channels I. Mslo ionic currents in the absence of Ca(2+). J Gen Physiol. 114, 277-304.
Hou, S., et al., 2008. Reciprocal regulation of the Ca2+ and H+ sensitivity in the SLO1 BK channel conferred by the RCK1 domain. Nat Struct Mol Biol. 15, 403-10.
Houamed, K. M., et al., 2010. BK channels mediate a novel ionic mechanism that regulates glucose-dependent electrical activity and insulin secretion in mouse pancreatic beta-cells. J Physiol. 588, 3511-23.
Hu, S., et al., 2003. Variants of the KCNMB3 regulatory subunit of maxi BK channels affect channel inactivation. Physiol Genomics. 15, 191-8.
Irie, T., Trussell, L. O., 2017. Double-Nanodomain Coupling of Calcium Channels, Ryanodine Receptors, and BK Channels Controls the Generation of Burst Firing. Neuron. 96, 856-870 e4.
Isaacson, J. S., Murphy, G. J., 2001. Glutamate-mediated extrasynaptic inhibition: direct coupling of NMDA receptors to Ca(2+)-activated K+ channels. Neuron. 31, 1027-34.

Ishii, T. M., et al., 1997a. Determinants of apamin and d-tubocurarine block in SK potassium channels. J Biol Chem. 272, 23195-200.
Ishii, T. M., et al., 1997b. A human intermediate conductance calcium-activated potassium channel. Proc Natl Acad Sci U S A. 94, 11651-6.
Jaffe, D. B., et al., 2011. Shaping of action potentials by type I and type II large-conductance Ca(2)+-activated K+ channels. Neuroscience. 192, 205-18.
Jensen, B. S., et al., 1998. Characterization of the cloned human intermediate-conductance Ca2+-activated K+ channel. Am J Physiol. 275, C848-56.
Jiang, Y., et al., 2002. Crystal structure and mechanism of a calcium-gated potassium channel. Nature. 417, 515-22.
Joiner, W. J., et al., 1997. hSK4, a member of a novel subfamily of calcium-activated potassium channels. Proc Natl Acad Sci U S A. 94, 11013-8.
Jones, S. L., et al., 2017. Dendritic small conductance calcium-activated potassium channels activated by action potentials suppress EPSPs and gate spike-timing dependent synaptic plasticity. Elife. 6.
Kaushal, V., et al., 2007. The Ca2+-activated K+ channel KCNN4/KCa3.1 contributes to microglia activation and nitric oxide-dependent neurodegeneration. J Neurosci. 27, 234-44.
Keen, J. E., et al., 1999. Domains responsible for constitutive and Ca(2+)-dependent interactions between calmodulin and small conductance Ca(2+)-activated potassium channels. J Neurosci. 19, 8830-8.
Kim, E. Y., et al., 2009. Canonical transient receptor potential channel (TRPC)3 and TRPC6 associate with large-conductance Ca2+-activated K+ (BKCa) channels: role in BKCa trafficking to the surface of cultured podocytes. Mol Pharmacol. 75, 466-77.
Knaus, H. G., et al., 1994. Pharmacology and structure of high conductance calcium-activated potassium channels. Cell Signal. 6, 861-70.
Köhler, M., et al., 1996. Small-Conductance, Calcium-Activated Potassium Channels from Mammalian Brain. Science. 273, 1709-1714.
Koot, B. G., et al., 2016. A de novo mutation in KCNN3 associated with autosomal dominant idiopathic non-cirrhotic portal hypertension. J Hepatol. 64, 974-7.
Koval, O. M., et al., 2007. A role for the S0 transmembrane segment in voltage-dependent gating of BK channels. J Gen Physiol. 129, 209-20.
Krnjević, K., et al., 1975. Evidence for Ca2+-activated K+ conductance in cat spinal motoneurons from intracellular EGTA injections. Can J Physiol Pharmacol. 53, 1214-8.
Kshatri, A. S., et al., 2017. Differential efficacy of GoSlo-SR compounds on BKalpha and BKalphagamma1-4 channels. Channels (Austin). 11, 66-78.
Kyle, B. D., Braun, A. P., 2014. The regulation of BK channel activity by pre- and post-translational modifications. Front Physiol. 5, 316.
Lai, M. H., et al., 2014. BK channels regulate sinoatrial node firing rate and cardiac pacing in vivo. Am J Physiol Heart Circ Physiol. 307, H1327-38.
Latorre, R., et al., 2017. Molecular Determinants of BK Channel Functional Diversity and Functioning. Physiol Rev. 97, 39-87.
Lee, C. H., MacKinnon, R., 2018. Activation mechanism of a human SK-calmodulin channel complex elucidated by cryo-EM structures. Science. 360, 508-513.
Lee, U. S., Cui, J., 2010. BK channel activation: structural and functional insights. Trends Neurosci. 33, 415-23.
Li, W., Aldrich, R. W., 2004. Unique inner pore properties of BK channels revealed by quaternary ammonium block. J Gen Physiol. 124, 43-57.
Li, X., et al., 2018. De novo BK channel variant causes epilepsy by affecting voltage gating but not Ca(2+) sensitivity. Eur J Hum Genet. 26, 220-229.

Liang, L., et al., 2019. De novo loss-of-function KCNMA1 variants are associated with a new multiple malformation syndrome and a broad spectrum of developmental and neurological phenotypes. Hum Mol Genet. 28, 2937-2951.
Lingle, C. J., et al., 1996. Calcium-activated potassium channels in adrenal chromaffin cells. Ion Channels. 4, 261-301.
Liu, N., et al., 2020. Channels that Cooperate with TRPV4 in the Brain. J Mol Neurosci. 70, 1812-1820.
Loane, D. J., et al., 2007. Co-assembly of N-type Ca2+ and BK channels underlies functional coupling in rat brain. J Cell Sci. 120, 985-95.
Lorenz, S., et al., 2007. Allelic association of a truncation mutation of the KCNMB3 gene with idiopathic generalized epilepsy. Am J Med Genet B Neuropsychiatr Genet. 144B, 10-3.
Lorenzo-Ceballos, Y., et al., 2019. Calcium-driven regulation of voltage-sensing domains in BK channels. Elife. 8.
Lu, L., et al., 2007. Molecular coupling of a Ca2+-activated K+ channel to L-type Ca2+ channels via alpha-actinin2. Circ Res. 100, 112-20.
Lujan, R., et al., 2018. SK2 Channels Associate With mGlu1alpha Receptors and CaV2.1 Channels in Purkinje Cells. Front Cell Neurosci. 12, 311.
Ma, Z., et al., 2006. Role of charged residues in the S1-S4 voltage sensor of BK channels. J Gen Physiol. 127, 309-28.
Magleby, K. L., 2003. Gating mechanism of BK (Slo1) channels: so near, yet so far. J Gen Physiol. 121, 81-96.
Maher, A. D., Kuchel, P. W., 2003. The Gardos channel: a review of the Ca2+-activated K+ channel in human erythrocytes. Int J Biochem Cell Biol. 35, 1182-97.
Maingret, F., et al., 2008. Neurotransmitter modulation of small-conductance Ca2+-activated K+ channels by regulation of Ca2+ gating. Neuron. 59, 439-49.
Marrion, N. V., Tavalin, S. J., 1998. Selective activation of Ca2+-activated K+ channels by co-localized Ca2+ channels in hippocampal neurons. Nature. 395, 900-5.
Marty, A., 1981. Ca-dependent K channels with large unitary conductance in chromaffin cell membranes. Nature. 291, 497-500.
McCobb, D. P., et al., 1995. A human calcium-activated potassium channel gene expressed in vascular smooth muscle. Am J Physiol. 269, H767-77.
McManus, O. B., et al., 1995. Functional role of the beta subunit of high conductance calcium-activated potassium channels. Neuron. 14, 645-50.
McManus, O. B., Magleby, K. L., 1988. Kinetic states and modes of single large-conductance calcium-activated potassium channels in cultured rat skeletal muscle. J Physiol. 402, 79-120.
Meech, R. W., 1972. Intracellular calcium injection causes increased potassium conductance in Aplysia nerve cells. Comp Biochem Physiol A Comp Physiol. 42, 493-9.
Meech, R. W., 1974. The sensitivity of Helix aspersa neurones to injected calcium ions. J Physiol. 237, 259-77.
Meech, R. W., Standen, N. B., 1974. Calcium-mediated potassium activation in Helix neurones. J Physiol. 237, 43P-44P.
Meera, P., et al., 2000. A neuronal beta subunit (KCNMB4) makes the large conductance, voltage- and Ca2+-activated K+ channel resistant to charybdotoxin and iberiotoxin. Proc Natl Acad Sci U S A. 97, 5562-7.
Meredith, A. L., et al., 2004. Overactive bladder and incontinence in the absence of the BK large conductance Ca2+-activated K+ channel. J Biol Chem. 279, 36746-52.
Meredith, A. L., et al., 2006. BK calcium-activated potassium channels regulate circadian behavioral rhythms and pacemaker output. Nat Neurosci. 9, 1041-9.
Miller, C., et al., 1985. Charybdotoxin, a protein inhibitor of single Ca2+-activated K+ channels from mammalian skeletal muscle. Nature. 313, 316-8.

Miller, J. P., et al., 2021. An emerging spectrum of variants and clinical features in KCNMA1-linked channelopathy. Channels (Austin). 15, 447-464.
Miller, M. J., et al., 2001. Nuclear localization and dominant-negative suppression by a mutant SKCa3 N-terminal channel fragment identified in a patient with schizophrenia. J Biol Chem. 276, 27753-6.
Miranda, P., et al., 2013. State-dependent FRET reports calcium- and voltage-dependent gating-ring motions in BK channels. Proceedings of the National Academy of Sciences of the United States of America. 110, 5217-5222.
Miranda, P., et al., 2016. Interactions of divalent cations with calcium binding sites of BK channels reveal independent motions within the gating ring. Proc Natl Acad Sci U S A. 113, 14055-14060.
Miranda, P., et al., 2018. Voltage-dependent dynamics of the BK channel cytosolic gating ring are coupled to the membrane-embedded voltage sensor. Elife. 7.
Mizukami, K., et al., 2015. Small-conductance Ca2+-activated K+ current is upregulated via the phosphorylation of CaMKII in cardiac hypertrophy from spontaneously hypertensive rats. Am J Physiol Heart Circ Physiol. 309, H1066-74.
Moldenhauer, H. J., et al., 2020a. Comparative gain-of-function effects of the KCNMA1-N999S mutation on human BK channel properties. J Neurophysiol. 123, 560-570.
Moldenhauer, H. J., et al., 2020b. Characterization of New Human KCNMA1 Loss-of-function Mutations. Biophys J. 118, 114A.
Mongan, L. C., et al., 2005. The distribution of small and intermediate conductance calcium-activated potassium channels in the rat sensory nervous system. Neuroscience. 131, 161-75.
Montgomery, J. R., Meredith, A. L., 2012. Genetic activation of BK currents in vivo generates bidirectional effects on neuronal excitability. Proc Natl Acad Sci U S A. 109, 18997-9002.
Morales, P., et al., 2013. Contribution of the KCa3.1 channel-calmodulin interactions to the regulation of the KCa3.1 gating process. J Gen Physiol. 142, 37-60.
Muller, A., et al., 2007. Nanodomains of single Ca2+ channels contribute to action potential repolarization in cortical neurons. J Neurosci. 27, 483-95.
Nam, Y. W., et al., 2021a. Hydrophobic interactions between the HA helix and S4-S5 linker modulate apparent Ca((2+)) sensitivity of SK2 channels. Acta Physiol (Oxf). 231, e13552.
Nam, Y. W., et al., 2021b. Differential modulation of SK channel subtypes by phosphorylation. Cell Calcium. 94, 102346.
Nam, Y. W., et al., 2017. Structural insights into the potency of SK channel positive modulators. Sci Rep. 7, 17178.
Nelson, M. T., et al., 1995. Relaxation of arterial smooth muscle by calcium sparks. Science. 270, 633-7.
Neyton, J., Miller, C., 1988. Discrete Ba2+ block as a probe of ion occupancy and pore structure in the high-conductance Ca2+ -activated K+ channel. J Gen Physiol. 92, 569-86.
Ngo-Anh, T. J., et al., 2005. SK channels and NMDA receptors form a Ca2+-mediated feedback loop in dendritic spines. Nat Neurosci. 8, 642-9.
Nguyen, H. M., et al., 2017. Differential Kv1.3, KCa3.1, and Kir2.1 expression in "classically" and "alternatively" activated microglia. Glia. 65, 106-121.
Nimigean, C. M., et al., 2003. Electrostatic tuning of ion conductance in potassium channels. Biochemistry. 42, 9263-8.
Niu, X., et al., 2004. Linker-gating ring complex as passive spring and Ca(2+)-dependent machine for a voltage- and Ca(2+)-activated potassium channel. Neuron. 42, 745-56.
Oliver, D., et al., 2000. Gating of Ca2+-activated K+ channels controls fast inhibitory synaptic transmission at auditory outer hair cells. Neuron. 26, 595-601.
Pallotta, B. S., et al., 1981. Single channel recordings of Ca2+-activated K+ currents in rat muscle cell culture. Nature. 293, 471-4.

Pantazis, A., et al., 2010. Operation of the voltage sensor of a human voltage- and Ca2+-activated K+ channel. Proc Natl Acad Sci U S A. 107, 4459-64.
Plante, A. E., et al., 2019. Effects of Single Nucleotide Polymorphisms in Human KCNMA1 on BK Current Properties. Front Mol Neurosci. 12, 285.
Posson, D. J., et al., 2013. The voltage-dependent gate in MthK potassium channels is located at the selectivity filter. Nat Struct Mol Biol. 20, 159-66.
Prakriya, M., Lingle, C. J., 1999. BK channel activation by brief depolarizations requires Ca2+ influx through L- and Q-type Ca2+ channels in rat chromaffin cells. J Neurophysiol. 81, 2267-78.
Qian, X., et al., 2006. Intra- and intersubunit cooperativity in activation of BK channels by Ca2+. J Gen Physiol. 128, 389-404.
Raffaelli, G., et al., 2004. BK potassium channels control transmitter release at CA3-CA3 synapses in the rat hippocampus. J Physiol. 557, 147-57.
Rapetti-Mauss, R., et al., 2015. A mutation in the Gardos channel is associated with hereditary xerocytosis. Blood. 126, 1273-80.
Rehak, R., et al., 2013. Low voltage activation of KCa1.1 current by Cav3-KCa1.1 complexes. PLoS One. 8, e61844.
Robitaille, R., et al., 1993. Functional colocalization of calcium and calcium-gated potassium channels in control of transmitter release. Neuron. 11, 645-55.
Rothberg, B. S., 2012. The BK channel: a vital link between cellular calcium and electrical signaling. Protein Cell. 3, 883-92.
Rothberg, B. S., Magleby, K. L., 1999. Gating kinetics of single large-conductance Ca2+-activated K+ channels in high Ca2+ suggest a two-tiered allosteric gating mechanism. J Gen Physiol. 114, 93-124.
Rothberg, B. S., Magleby, K. L., 2000. Voltage and Ca2+ activation of single large-conductance Ca2+-activated K+ channels described by a two-tiered allosteric gating mechanism. J Gen Physiol. 116, 75-99.
Sah, P., McLachlan, E. M., 1991. Ca(2+)-activated K+ currents underlying the afterhyperpolarization in guinea pig vagal neurons: a role for Ca(2+)-activated Ca2+ release. Neuron. 7, 257-64.
Savalli, N., et al., 2012. The contribution of RCK domains to human BK channel allosteric activation. J Biol Chem. 287, 21741-50.
Schreiber, M., Salkoff, L., 1997. A novel calcium-sensing domain in the BK channel. Biophys J. 73, 1355-63.
Schreiber, M., et al., 1999. Transplantable sites confer calcium sensitivity to BK channels. Nat Neurosci. 2, 416-21.
Schumacher, M. A., et al., 2004. Crystal structures of apocalmodulin and an apocalmodulin/SK potassium channel gating domain complex. Structure. 12, 849-60.
Schumacher, M. A., et al., 2001. Structure of the gating domain of a Ca2+-activated K+ channel complexed with Ca2+/calmodulin. Nature. 410, 1120-4.
Semenov, I., et al., 2011. BK channel beta1 subunits regulate airway contraction secondary to M2 muscarinic acetylcholine receptor mediated depolarization. J Physiol. 589, 1803-17.
Shi, J., et al., 2002. Mechanism of magnesium activation of calcium-activated potassium channels. Nature. 418, 876-80.
Shipston, M. J., 2001. Alternative splicing of potassium channels: a dynamic switch of cellular excitability. Trends Cell Biol. 11, 353-8.
Shrestha, A., et al., 2019. SK Channel Modulates Synaptic Plasticity by Tuning CaMKIIalpha/beta Dynamics. Front Synaptic Neurosci. 11, 18.
Simoes, M., et al., 2002. Cysteine mutagenesis and computer modeling of the S6 region of an intermediate conductance IKCa channel. J Gen Physiol. 120, 99-116.
Soden, M. E., et al., 2013. Disruption of dopamine neuron activity pattern regulation through selective expression of a human KCNN3 mutation. Neuron. 80, 997-1009.
Stackman, R. W., et al., 2002. Small conductance Ca2+-activated K+ channels modulate synaptic plasticity and memory encoding. J Neurosci. 22, 10163-71.
Stocker, M., Pedarzani, P., 2000. Differential distribution of three Ca(2+)-activated K(+) channel subunits, SK1, SK2, and SK3, in the adult rat central nervous system. Mol Cell Neurosci. 15, 476-93.
Storm, J. F., 1987. Action potential repolarization and a fast after-hyperpolarization in rat hippocampal pyramidal cells. J Physiol. 385, 733-59.
Sweet, T. B., Cox, D. H., 2008. Measurements of the BKCa channel's high-affinity Ca2+ binding constants: effects of membrane voltage. J Gen Physiol. 132, 491-505.
Szarka, N., et al., 2018. Traumatic Brain Injury Impairs Myogenic Constriction of Cerebral Arteries: Role of Mitochondria-Derived H2O2 and TRPV4-Dependent Activation of BKca Channels. J Neurotrauma. 35, 930-939.
Tabarki, B., et al., 2016. Homozygous KCNMA1 mutation as a cause of cerebellar atrophy, developmental delay and seizures. Hum Genet. 135, 1295-1298.
Tang, Q. Y., et al., 2009. Closed-channel block of BK potassium channels by bbTBA requires partial activation. J Gen Physiol. 134, 409-36.
Tao, X., et al., 2017. Cryo-EM structure of the open high-conductance Ca2+-activated K+ channel. Nature. 541, 46-51.
Tao, X., MacKinnon, R., 2019. Molecular structures of the human Slo1 K(+) channel in complex with beta4. Elife. 8.
Tenma, T., et al., 2018. Small-conductance Ca(2+)-activated K(+) channel activation deteriorates hypoxic ventricular arrhythmias via CaMKII in cardiac hypertrophy. Am J Physiol Heart Circ Physiol. 315, H262-H272.
Thomas, M. V., Gorman, A. L., 1977. Internal calcium changes in a bursting pacemaker neuron measured with arsenazo III. Science. 196, 531-3.
Tian, W. T., et al., 2018. Proline-rich transmembrane protein 2-negative paroxysmal kinesigenic dyskinesia: Clinical and genetic analyses of 163 patients. Mov Disord. 33, 459-467.
Toyama, K., et al., 2008. The intermediate-conductance calcium-activated potassium channel KCa3.1 contributes to atherogenesis in mice and humans. J Clin Invest. 118, 3025-37.
Vivas, O., et al., 2017. Proximal clustering between BK and CaV1.3 channels promotes functional coupling and BK channel activation at low voltage. Elife. 6.
Wallner, M., et al., 1996. Determinant for beta-subunit regulation in high-conductance voltage-activated and Ca(2+)-sensitive K+ channels: an additional transmembrane region at the N terminus. Proc Natl Acad Sci U S A. 93, 14922-7.
Wallner, M., et al., 1999. Molecular basis of fast inactivation in voltage and Ca2+-activated K+ channels: a transmembrane beta-subunit homolog. Proc Natl Acad Sci U S A. 96, 4137-42.
Wang, B., et al., 2016. Knockout of the BK beta4-subunit promotes a functional coupling of BK channels and ryanodine receptors that mediate a fAHP-induced increase in excitability. J Neurophysiol. 116, 456-65.
Wei, A., et al., 1994. Calcium sensitivity of BK-type KCa channels determined by a separable domain. Neuron. 13, 671-81.
Wei, A. D., et al., 2005. International Union of Pharmacology. LII. Nomenclature and molecular relationships of calcium-activated potassium channels. Pharmacol Rev. 57, 463-72.
Whitt, J. P., et al., 2018. Differential contribution of Ca(2+) sources to day and night BK current activation in the circadian clock. J Gen Physiol. 150, 259-275.
Whitt, J. P., et al., 2016. BK channel inactivation gates daytime excitability in the circadian clock. Nat Commun. 7, 10837.

Wilkens, C. M., Aldrich, R. W., 2006. State-independent block of BK channels by an intracellular quaternary ammonium. J Gen Physiol. 128, 347-64.
Womack, M. D., et al., 2004. Calcium-activated potassium channels are selectively coupled to P/Q-type calcium channels in cerebellar Purkinje neurons. J Neurosci. 24, 8818-22.
Wondergem, R., Bartley, J. W., 2009. Menthol increases human glioblastoma intracellular Ca2+, BK channel activity and cell migration. J Biomed Sci. 16, 90.
Wong, R., Schlichter, L. C., 2014. PKA reduces the rat and human KCa3.1 current, CaM binding, and Ca2+ signaling, which requires Ser332/334 in the CaM-binding C terminus. J Neurosci. 34, 13371-83.
Wu, Y., et al., 2013. TRPV1 channels are functionally coupled with BK(mSlo1) channels in rat dorsal root ganglion (DRG) neurons. PLoS One. 8, e78203.
Wu, Y., et al., 2010. Structure of the gating ring from the human large-conductance Ca(2+)-gated K(+) channel. Nature. 466, 393-7.
Xia, X. M., et al., 1998. Mechanism of calcium gating in small-conductance calcium-activated potassium channels. Nature. 395, 503-7.
Xia, X. M., et al., 2002. Multiple regulatory sites in large-conductance calcium-activated potassium channels. Nature. 418, 880-4.
Xia, X. M., et al., 2004. Ligand-dependent activation of Slo family channels is defined by interchangeable cytosolic domains. J Neurosci. 24, 5585-91.
Yamamura, H., et al., 2012. Molecular assembly and dynamics of fluorescent protein-tagged single KCa1.1 channel in expression system and vascular smooth muscle cells. Am J Physiol Cell Physiol. 302, C1257-68.
Yan, J., Aldrich, R., 2012. BK potassium channel modulation by leucine-rich repeat-containing proteins. Proc Natl Acad Sci U S A. 109, 7917-7922.
Yan, J., Aldrich, R. W., 2010. LRRC26 auxiliary protein allows BK channel activation at resting voltage without calcium. Nature. 466, 513-6.
Yang, H., Cui, J., BK channels. In: J. Zheng, M. C. Trudeau, (Eds.), Handbook of Ion Channels. CRC, Boca Raton, FL, 2015.
Yang, J., et al., 2010. An epilepsy/dyskinesia-associated mutation enhances BK channel activation by potentiating Ca2+ sensing. Neuron. 66, 871-83.
Yesil, G., et al., 2018. Expanding the Phenotype of Homozygous KCNMA1 Mutations: Dyskinesia, Epilepsy, Intellectual Disability, Cerebellar and Corticospinal Tract Atrophy. Balkan Med J. 35, 336-339.
Yu, Z., et al., 2014. Targeted inhibition of KCa3.1 attenuates TGF-beta-induced reactive astrogliosis through the Smad2/3 signaling pathway. J Neurochem. 130, 41-49.
Yu, Z. H., et al., 2013. Up-regulation of KCa3.1 promotes human airway smooth muscle cell phenotypic modulation. Pharmacol Res. 77, 30-8.
Yuan, P., et al., 2011. Open structure of the Ca2+ gating ring in the high-conductance Ca2+-activated K+ channel. Nature. 481, 94-7.
Zeng, X. H., et al., 2005. Divalent cation sensitivity of BK channel activation supports the existence of three distinct binding sites. J Gen Physiol. 125, 273-86.
Zhang, F. X., et al., 2018a. BK Potassium Channels Suppress Cavalpha2delta Subunit Function to Reduce Inflammatory and Neuropathic Pain. Cell Rep. 22, 1956-1964.
Zhang, G., et al., 2020. A Gain-of-Function Mutation in KCNMA1 Causes Dystonia Spells Controlled With Stimulant Therapy. Mov Disord. 35, 1868-1873.
Zhang, G., et al., 2010. Ion sensing in the RCK1 domain of BK channels. Proc Natl Acad Sci U S A. 107, 18700-5.
Zhang, J., et al., 2018b. Glutamate-activated BK channel complexes formed with NMDA receptors. Proc Natl Acad Sci U S A. 115, E9006-E9014.
Zhang, L., McBain, C. J., 1995. Potassium conductances underlying repolarization and after-hyperpolarization in rat CA1 hippocampal interneurones. J Physiol. 488 (Pt 3), 661-72.
Zhang, M., et al., 2014. Selective phosphorylation modulates the PIP2 sensitivity of the CaM-SK channel complex. Nat Chem Biol. 10, 753-9.
Zhang, M., et al., 2015a. Molecular overlap in the regulation of SK channels by small molecules and phosphoinositides. Sci Adv. 1, e1500008.
Zhang, M., et al., 2012. Identification of the functional binding pocket for compounds targeting small-conductance Ca(2(+)-activated potassium channels. Nat Commun. 3, 1021.
Zhang, M., et al., 2013. Unstructured to structured transition of an intrisically disordered protein peptide in coupling Ca2+-sensing and SK channel activation. Proc Natl Acad Sci U S A. 110, 4828-4833.
Zhang, Z. B., et al., 2015b. De novo KCNMA1 mutations in children with early-onset paroxysmal dyskinesia and developmental delay. Mov Disord. 30, 1290-2.
Zhao, G., et al., 2010. Type 1 IP3 receptors activate BKCa channels via local molecular coupling in arterial smooth muscle cells. J Gen Physiol. 136, 283-91.
Zhou, Y., et al., 2011. Cysteine scanning and modification reveal major differences between BK channels and Kv channels in the inner pore region. Proc Natl Acad Sci U S A. 108, 12161-6.
Zhou, Y., et al., 2017. Threading the biophysics of mammalian Slo1 channels onto structures of an invertebrate Slo1 channel. J Gen Physiol. 149, 985-1007.
Zhou, Y., et al., 2012. Barium ions selectively activate BK channels via the Ca2+-bowl site. Proc Natl Acad Sci U S A. 109, 11413-8.
Zou, S., et al., 2008. The beta 1 subunit of L-type voltage-gated Ca2+ channels independently binds to and inhibits the gating of large-conductance Ca2+-activated K+ channels. Mol Pharmacol. 73, 369-78.

Notes